NASA TECHNICAL MEMORANDUM NASA TM-77538

REPORT ON THE DEVELOPMENT OF THE ENGINEERING TEST SATELLITE-III (ETS-III) ION ENGINE SYSTEM

S. Kitamura

Translation of Report on the Development of the Engineering Test Satellite-III (ETS-III) Ion Engine System, National Space Development Agency of Japan, Tokyo (Japan), Report DS-114166, March 1983, pp. 1-206

NATIONAL AERONAUTICS AND SPACE ADMINISTRATION
WASHINGTON, D.C. 20546 JULY 1984

STANDARD TITLE PAGE

1. Report No. NASA TM-77538	2. Government Accession No.	3. Recipient's Catalog No.
4. Title and Subtitle REPORT ON THE DEVELOPMENT OF THE ENGINEERING TEST SATELLITE-III (ETS-III) ION ENGINE SYSTEM		5. Report Date July 1984 6. Performing Organization Code
7. Author(s) S. Kitamura		8. Performing Organization Report No. 10. Work Unit No.
9. Performing Organization Name and Address Leo Kanner Associates Redwood City California 94063		11. Contract or Grant No. NASW-3541 13. Type of Report and Period Covered Translation
12. Sponsoring Agency Name and Address National Aeronautics and Space Administration, Washington, D.C. 20546		14. Sponsoring Agency Code

15. Supplementary Notes
Translation of Report on the Development of the Engineering Test Satellite-III (ETS-III) Ion Engine System, National Space Development Agency of Japan, Tokyo (Japan, Report DS-114166, March 1983, pp. 1-206

16. Abstract
The report discusses the ion engine system onboard the ETS-III. The system consists of two electron bombardment type mercury ion engines with 2 mN thrust and 2,000 sec specific impulse and a power conditioner with automatic control functions. The research and development of the system, development of its EM, PM and FM, the system test and the technical achievements leading up to final launch are discussed.

17. Key Words (Selected by Author(s))	18. Distribution Statement
	Unclassified - Unlimited

19. Security Classif. (of this report)	20. Security Classif. (of this page)	21. No. of Pages	22.
Unclassified	Unclassified	384	

Report on Development of ETS-III Ion Engine System

ABSTRACT

The objective of this report is to present the results of research and development of the ion engine system which was boarded on the Engineering Test Satellite III(ETS-III).

The ion engine system was developed to investigate its feasibility for future application of electric propulsion with high specific impulse, through the operation tests under the space environment. The system consists of two electron bombardment type mercury ion engines with 2mN thrust and 2,000 sec specific impulse and a power conditioner with automatic control functions. Having overcome various problems during the developments stage, engines meeting the specifications were finally produced and are currently in orbit, showing fine performance. Discussed in this report are the research and development of this system, development of its EM, PM and FM, the system test and the technical achievement brought by the process leading to the final launching.

Table of Contents

Chapter 1

Foreword

Chapter 1: Foreword

On September 3, 1982, the Engineering Test Satellite III(ETS-III) was launched into an orbit at an altitude of approximately 1,000km by an N-1 rocket from the Tanegashima Space Center. It was given the name of "Kiku No.4."

The ETS-III is an engineering test satellite designed to improve our independent ability to develop common technology for artificial satellites requiring large power, as well as to carry out in space a number of experiments on the functions of the equipments on board. The equipments consisted of the vidicon camera, the ion engine system, the active heat control system and the magnetic attitude control system. This report details the results yielded by the development of the ion engine system. It has been prepared with a view to making a contribution toward future development.

The ion engine system was developed and mounted on the satellite in order to acquire the basic technology for high-specific-thrust electric propulsion systems of the future. The system itself was developed by the National Space Development Agency of Japan(NASDA) and it incorporated the results obtained from research and development efforts of the Electrotechnical Laboratory and the National Aerospace Laboratory, which are national research institutes. Currently on board the satellite in orbit, the ion engine system represents the result of some 12 years of independent research effort by the two institutes. 100-hour sustained jet propulsion experiments and other in-space experiments are being conducted smoothly, yielding valuable data. Japan is the second country to conduct such experiments in space after the United States and it is the first to have successfully conducted experiments on a small-sized ion engine.

This activity has thereby drawn the interest of those engaged in work on future propulsion systems around the world and the achievements of the experiments is thus of great significance.

Work on developing the ion engine system was not necessarily an easy process. In retrospect, it became clear that the standards of design, production and testing which must satisfy the complexity of the equipment involved were not set up sufficiently until immediately before the production of the flight model. It caused many problems. Thanks to the problems, however, the development process has brought forth a greaterwealth of technological knowledge and data. Nevertheless, enquiry should be made as to whether the current success signify clearance of all the problems to be encountered. To do so, it is necessary to put in order all the technical details obtained to date. Further, the development of this ion engine system should be considered as the first step toward the practical application of such a system, providing the basis for future developments. The results obtained in this project must sorted out from this aspect as well.

Thus put together was this "Report on the Development of the ETS-III Ion Engine System." The report covers from the initial research and development at the two research institutes to the actual development and production tests conducted at NASDA, and the subsequent system test, preparation of the launch site and finally, the launching. It was decided to include as much technical information as possible which could serve for reference purposes in the future, even if it did not pertain directly to the main subject matter of this report. In order to make this project complete, some joint reserch was conducted by NASDA and the two institutes. Since their findings have been detailed in a separate report, only the most relevant points have

been extracted here with reference to the original source so as to avoid redundancy. Research engineers from the institutes having participated in writing, this report represents a joint effort by the three establishments involved in the development.

It is intended to prepare a separate report on the evaluation of the in-space experiments conducted on the ion engine system. The authors of this particular report hope that the material provided will lead to the future development of practically applicable ion engine systems and that it will prove worthy of reference for this purpose.

Chapter 2

Background and Objectives of Development

Chapter 2: Background and Objectives of Development

2.1 Principle and Features of Ion Engine

Electric propulsion, a form of propulsion which generates thrust by accelerating particles using electrical energy, is generally capable of yielding a higher particle velocity than conventional chemical propulsion which relies on internal chemical energy to accelerate the particles. This results in a distinct advantage: the impulse per propellant weight, i.e. the specific thrust, is higher, which means that the weight of the propellant required is much less to do the same job. Among the systems of electric propulsion devised are plasma engines and ion engines.[1)]

Fig. 2.1 shows the operative range of all forms of electric propulsion in terms of thrust and specific thrust. The ion engine obtains thrust by ionizing the propellant and by accelerating and injecting the ions thus obtained in a high-potential electrostatic field, and it is characterized by a high specific thrust. In fact, the specific thrust is in the range of 2,000 to 7,000 seconds, which is 7 to 30 times as high as that of a chemical rocket(hydrazine, etc.). The thrust is in the range of 10^{-3} to 10^{-1}N, which is relatively low. Making full use of this feature, ion engines may be employed for maintaining stationary satellites in orbit or as the main propulsion system for spaceships for interplanetary probes or interorbial transporters of large-scale space structures. Its low thrust renders an ion engine suitable also for controlling the attitude of flexible structures with a high degree of precision.

A relatively large power source is required for the ion engine to operate which in turns necessitates a power system. This does not

work out to be an advantage over chemical propulsion in small-scale, short-life satellites. In maintaining a stationary satellite in orbit, for example, an ion engine is on a par with a chemical propulsion system if the satellite has a weight of 500kg and a service life of 2 or 3 years. Above the figures quoted, the heavier the satellite and the longer its service life, the more advantageous it is to employ an ion engine. Fig. 2.2 indicates the weight of each of the propulsion systems which may be used to maintain a 1,000kg stationary satellite in orbit for varying mission durations. On an 8-year mission, for instance, it is possible to increase the payload by 120kg if the conventional catalyst hydrazine is replaced by the ion engine. This is virtually equivalent to a payload placed in stationary orbit by an N-1 rocket.

Consequently, ion engines are suitable as the propulsion systems of large-scale satellites with a large power source and for long-term use, offering a substantial weight advantage.

Three different methods of propellant ionization have been proposed for ion engines so far: contact ionization where cesium or another element with a low ionization potential is passed through a high-temperature metal filter; high-frequency ionization where high-frequency energy is absorbed; and electron bombardment where electrons are bombarded in order to achieve ionization. Each method has its own distinct advantages but in countries such as the United States and Japan it has been the electron bombardment type (which is often referred to as the Kaufmann engine after the name of the man who devised it) that was chosen for development projects.

Fig. 2.3 illustrates the operating principle of the electron bombardment type of ion engine which employs mercury as the propellant.

Liquid mercury sent from the tank is heated and vaporized by the vaporizer and led to the discharge chamber. The electrons emitted from the cathode come under the operation of the electrical field generated by the anode and the magnetic field generated by the permanent magnet. This puts the electrons into a cyclotron motion, with the result that they collide with the mercury atoms and ionize them. The ions in the discharge chamber are electrostatically accelerated by the high voltage applied to the screen grid and they are emitted as an ion beam. If ions alone are taken out, the engine becomes negatively charged and stops accelerating. In order to maintain electrical neutrality, electrons are emitted from the neutralizer into the ion beam. A high negative voltage is applied to the accelerator grid at this time, so that the neutralizing electrongs do not flow backwards toward the engine. Thrust can easily be computed by the beam current and acceleration voltage(current and voltage of PS1), and adjustment may be made by varying the discharge current(current of PS3) or acceleration voltage. Specific thrust is proportionate to the square root of acceleration voltage and is also variable. Such ease in control is one of the characteristics of ion engines. Also, the neutralizer works to maintain a constant electrical neutrality, eliminating the problem of electrification in stationary satellites.

Fig. 2.1 Operative Range of Various Forms of Electric Propulsion

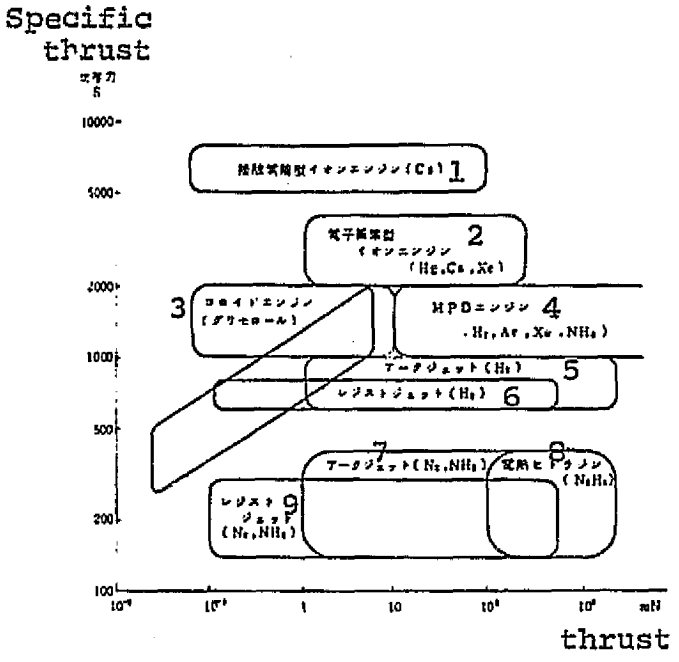

1. Catalyst ionization type ion engine
2. Electron bombardment type ion engine
3. Colloid engine(glycerol)
4. MPD engine
5. Arc jet engine
6. Resist jet
7. Art jet
8. Thermoelectric hydrazine
9. Resist jet

Fig. 2.2 Weight of Systems for Keeping Stationary Satellites in North/south Orbit

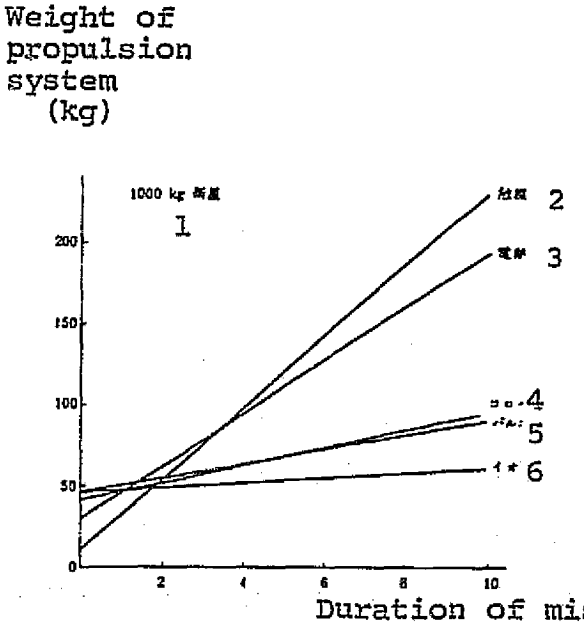

1. 1000kg satellite
2. Catalyst hydrazine
3. Thermoelectric hydrazine
4. Colloid
5. Pulse type plasma
6. Ion

Fig. 2.3 Operating Principle of Electron Bombardment Type Mercury Ion Engine

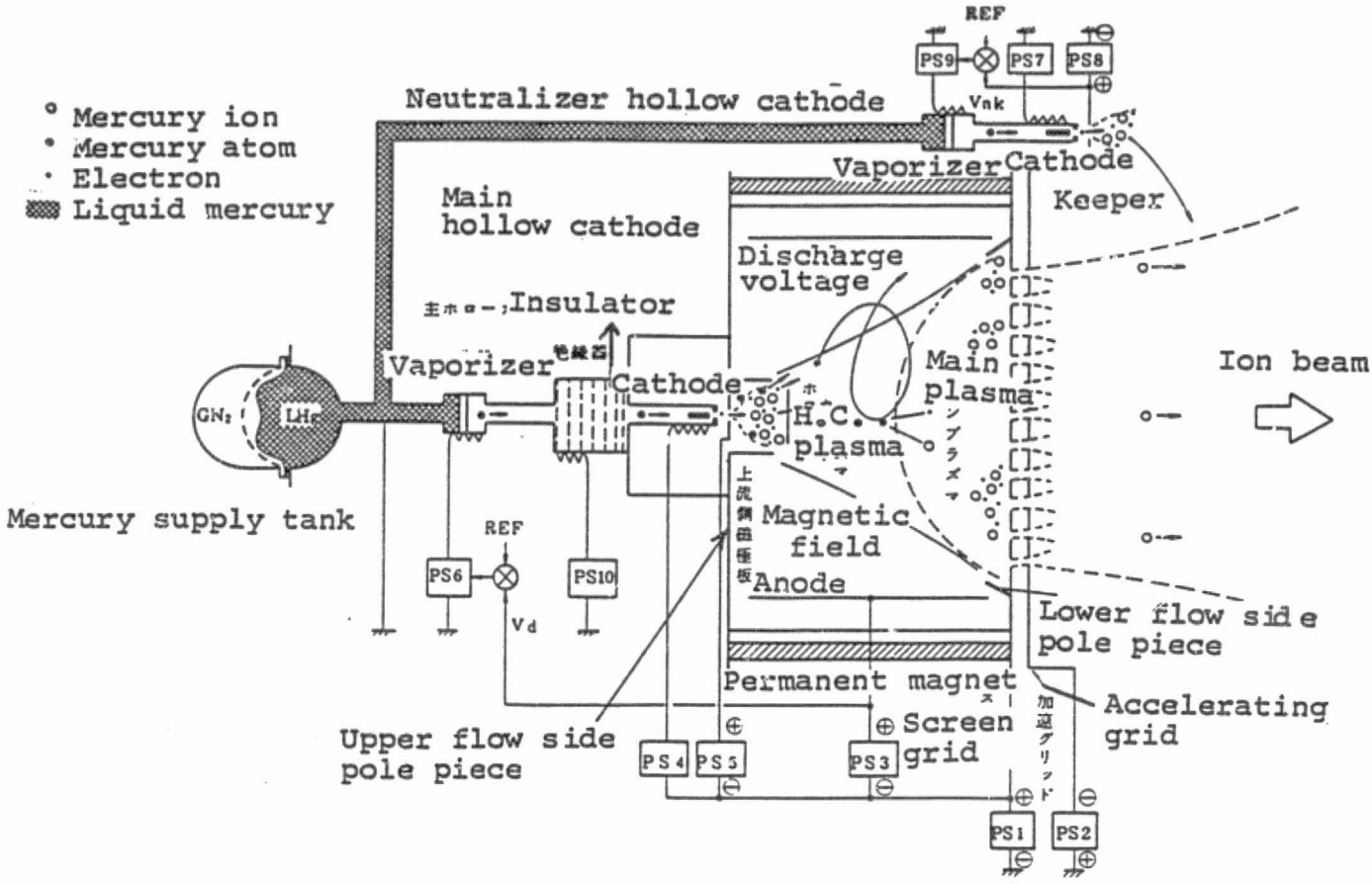

		Voltage	Current
PS1	Screen grid power source	Vn	Jb
	or beam power source	Vb	
PS2	Accelerator grid power source	Va	Ia
PS3	Discharge(anode) power source	Vd	Id
PS4	Main cathode heater power source	Vch	Ich
PS5	Main cathode keeper power source	Vck	Ick
PS6	Main cathode vaporizer power source	Vcv	Icv
	or main vaporizer power source		
PS7	Neutralizer heater power source	Vnh	Inh
PS8	Neutralizer keeper power source	Vnk	Ink
PS9	Neutralizer vaporizer power source	Vnv	Inv
PS10	Insulator heater power source	Vis	Iis

2.2 Current State of Development Overseas

The United States is the leader in the development of ion engines. The first on-board experiments were carried out in 1970 with SERT-II (Space Electric Rocket Test) and the total actual operation time of 7,000 hours was accomplished with a 30mN mercury electron bombardment type engine. Currently, 5mN-class engines are being developed for secondary propulsion, two of which will be boarded on the Satellite P80-1(altitude 740km and angle of inclination 72.5), scheduled to be launched(using space shuttle) in November, 1983, for a flight test mainly of repetitive operations.(See Fig. 2.4.) This is in preparation for the application to North-South orbit control of a 1,000kg-class stationary satellite with a 7-year service life. For main propulsion, basic modules of two each 100mN-class engines, called BIMOD, have been developed. Used in sets of three to six, they are planned to be used for a planet probing space ship, space tug acting as an upper shuttle, etc. Fig. 2.5 illustrates the concept of a space tug(NASA Lewis R. C./ Marshall S.F.C.) in which three stationary satellites are transported from a low orbit to stationary orbit by ten engines in combination with 25kW-solar array. 100mN-class engines have been developed up to EM.

Aside from this development direction that NASA Lewis/Hughes has followed, there is another direction that NASA GSFC/EOS has pursued which used cesium as a propellant. 5mN electron bombardment type was developed for the purpose of testing its use in maintaining North-South orbit, and boarded on ATS-6. Despite the initial success, difficulties in the supply system, peculiar to cesium, have since caused the operation to halt. The technology, however, was taken over by INTELSTAT/EOS and incorporated into the development of mercury MESC

(magnetoelectrostatic containment) ion engines of 15mN-class.

In the West Germany, high-frequency mercury ion engines, which make use of high frequency discharge, are in development. 10mN-class engine, RITA, is planned to be boarded on a television broadcasting satellite TV-SAT and used for North-South orbit control. It has so far been developed to RITA-1 of PM level, whose engine shape and boarding configuration(TV-SAT D3) are shown in Fig. 2.6. Actual boarding on TV-SAT D3, however, seems to have been passed up.

Development is also taking place in England(10mN mercury electron bombardment type), in France(cesium contact ionization type), and more recently in China(5mN mercury electron bombardment type). All are for secondary propulsion, and none has been scheduled for actual flight yet. In the U.S.S.R., although the details are unknown, the emphasis seems to be on plasma engines.

In our country, 2mN mercury bombardment type was developed and boarded on ETS-III. It was the second in-space experiment of ion engines following SERT-II of the U.S., and, as a secondary propulsion system, precedes P80-1. In addition, NAL is leading the research and development of 10mN mercury electron bombardment type engines.

Table 2.1 shows the status of these ion engine system test flights, launched and planned.

Fig. 2.4 Ion Engine System Mounted on P80-1

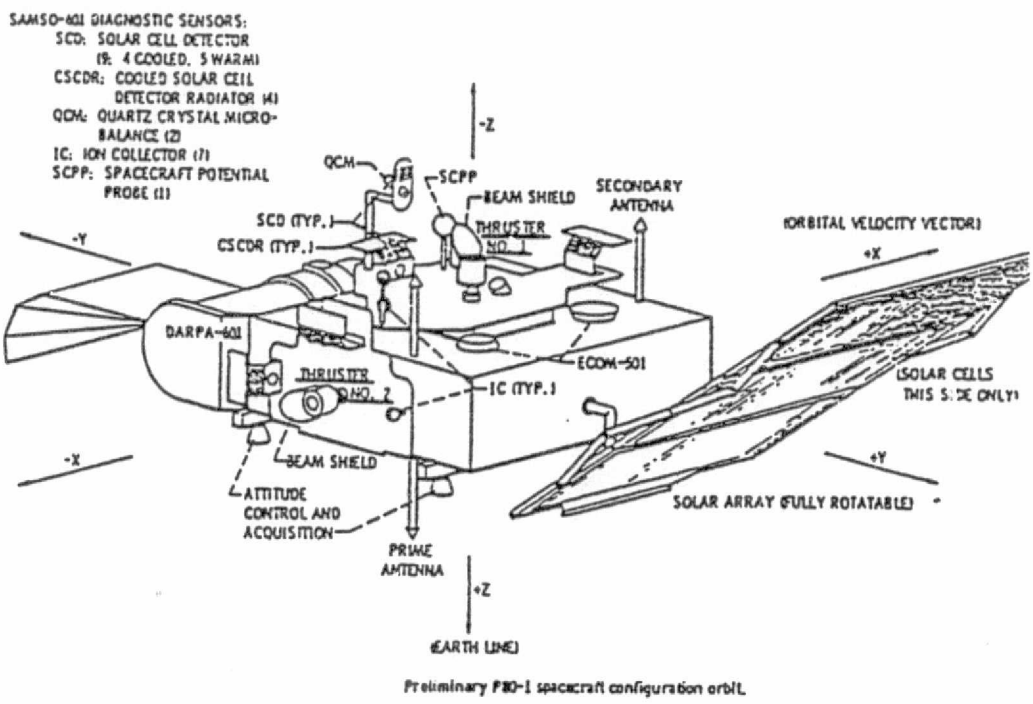

Fig. 2.5 Space Tug Using Electric Propulsion

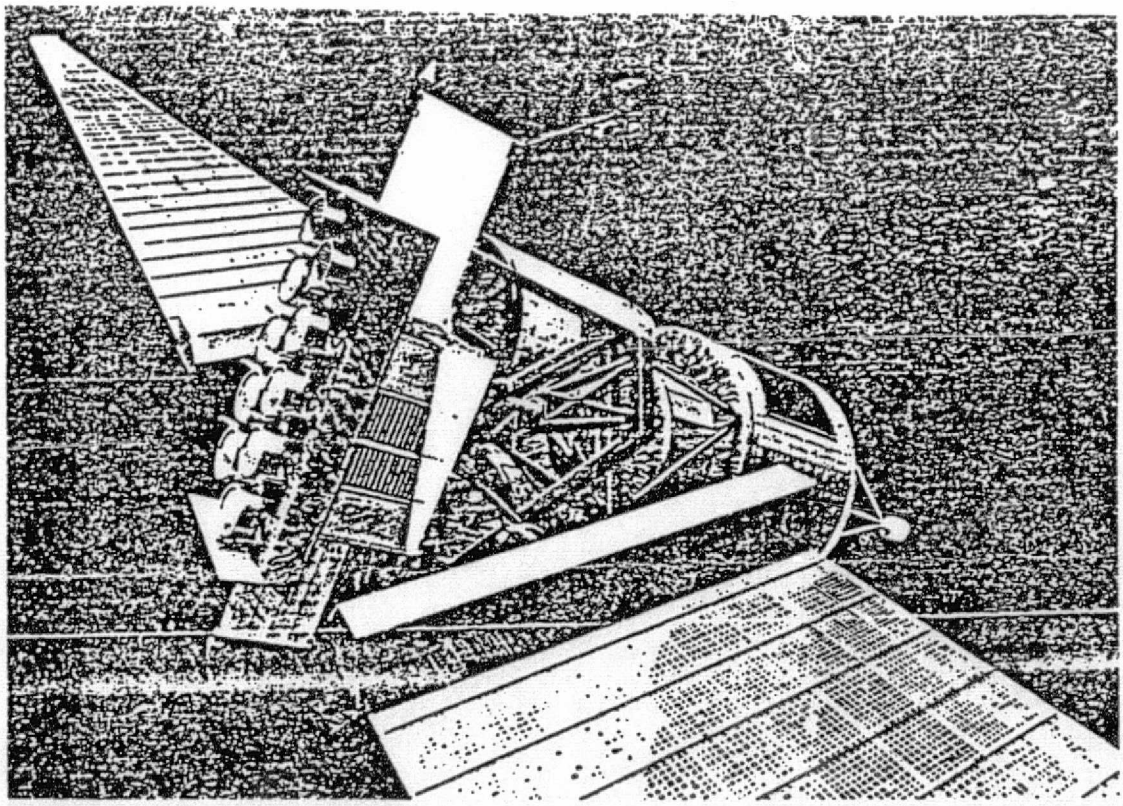

Fig. 2.6 Ion Engine Boarded on TV-SAT D3

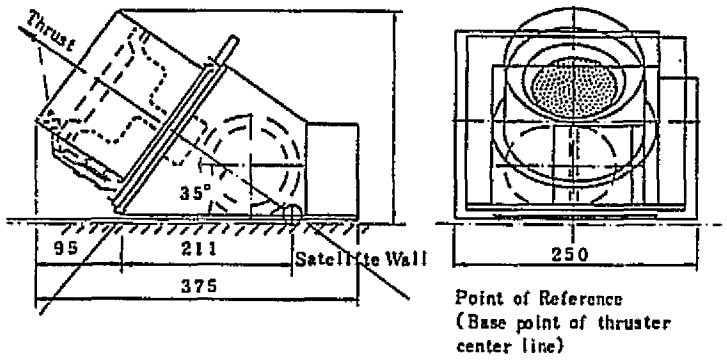

PROPULSION UNIT MAIN DIMENSIONS

Range of thrust:
5-11mN
Input power:
375W
Weight:
39kg per pair
(includes a
3-year supply
of propellant)

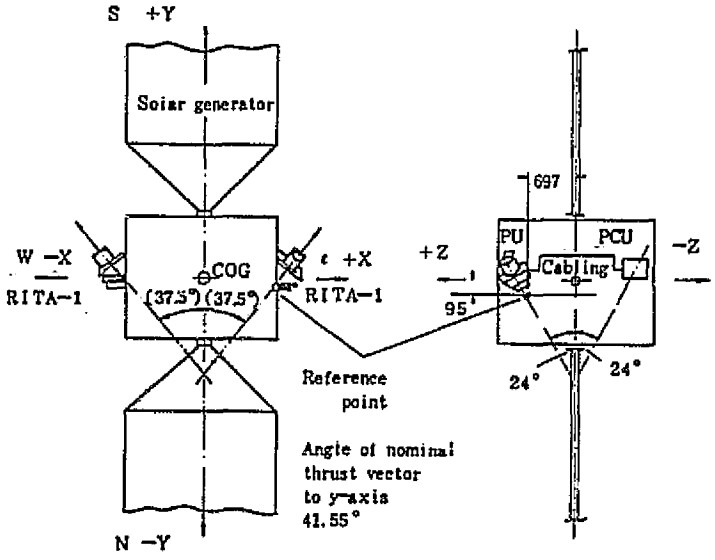

ARRANGEMENT OF E. P. S. HARDWARE ON TV-SAT D 3

Table 2.1 Ion Engine System Tests

Name: Satellite / Engine system	SERT-I	ATS-6	ETS-III IES	P80-I SIT-8	TVSAT RITA-1
Developing organization	NASA Lewis /Hughes	NASA Goddard /EGS	NASDA/NAL/ ETL/MELCO/ Toshiba	NASA Lewis/ Hughes	GFW/Giessen/ MBB
Type	水銀電子衝撃型 A	セシウム電子衝撃型 B	水銀電子衝撃型 A	水銀電子衝撃型 A	水銀高周波電離型 C
Thrust	28	5	2	5	10
Specific thrust	4,200	2,500	2,000	2,600	3,100
Thruster power	860	123	68	120	290
Propellant util. effiency	0.76	0.90	0.70	0.76	0.80
Total power	1,000	145	100	173	375
Launching	1970.2	1974.5	1982.9	1983.11予定*	TBD
Objectives	作動試験 D	南北方向軌道保持運用実験 E	作動試験 D	作動サイクル試験 F	南北方向軌道保持運用実験 E
Results	1号機3,781h 2号機2,011h の累積作動 G	供給系の故障で1度作動後実験不能 H	実験中 I		

A. Mercury electron bombardment type
B. Cecium electron bombardment type
C. Mercury high-frequency ionization type

* planned

D. Operation test
E. Test for maintaining north/south orbit
F. Operation cycle test

G. Accumulated operation of 3,781 hours for No. 1
" " 2,011 hours for No. 2
H. Experiments halted after one operation, due to disorder in supply system.
I. Currently in operation.

2.3 Objective of Development

The objective of developing ion engine system for ETS-III is to study the performance under the space environment of ion engines, a promising secondary propulsion system with high specific impulse for large-scale stationary satellites with long service life, and acquire basic data for such future application.

The engine was mercury bombardment type ion engine of anode diameter 5cm, developed by our national research institutes, the National Aerospace Laboratory(NAL) and Electrotechnical Laboratory (ETL). Based on the stage of development at that time, this type was chosen for its compatibility to the development schedule and to the power and weight distributions of ETS-III.

2.4 Development History

Research and development of ion engine system were started in out country around 1970 by NAL and ETL. Their emphasis was on mercury electron bombardment type with thrust of 2mN and anode diameter of 5cm, to be used for maintaining a satellite orbit. They test-produced a system equivalent of breadboard model and accumulated data from injection and other experiments. By the time the engine became a candidate for equipments to be boarded on Engineering Test Satellite (ETS-III) in 1973, they had indicated a desire to experiment in space, as a preparation for practical application. ETS-III had been planned with the purpose of developing commong technology for satellite requiring large electric power, and at the same time, had been designated to accept "equipments for experiments on-board that are requested by satellite-users. In April, 1974, NAL/ETL and NASDA

started a joint technical study on the possibility of boarding ion engines on ETS-III, and, as a result, a concept design proposal entitled "Ion Engine System: A Study Of An Electronic Equipment Proposed To Be Boarded on ETS-III" was presented to NASDA by NAL/ETL in 1975. In response, NASDA proposed to the Space Activities Commission the boarding of ion engine systems as a promising source of future propulsion system technology. The Commission officially adopted in in August, 1976. A plan for NAL and ETL to develop this system was initially considered, but due to financial limitations and other considerations, it was decided that they would continue through Preliminary Engineering Model and then the project would be taken over by NASDA. Letters of intention to this effect were exchanged between the institudes and NASDA. It was agreed that any tests involving engine injection would be performed using the facilities of the institutes for cost and schedule reasons; that the institutes would provide assistance over the entire period of development, to ensure a smooth transfer of accumulated knowledge, by exchanging the staff and conducting joint studies; and that the three organizations would set up the "Ion Engine Development Communications Committee" for communicating matters concerning development and operation.

It was also decided that based on the strength initially shown, NAL would provide support for the development of engine unit and ETL, that of power conditioner and sub-system integration. For hardware, Mitsubishi Electric was chosen to produce the engine unit and Toshiba, the power conditioner, both based on the past experience. Toshiba, the main contractor for the satellite, was also put in charge of sub-system integration.

Table 2.2 shows the development schedule of ETS-III and ion

engine system. Production and testing of Preliminary Engineering Model were started by the institutes in 1976. Starting 1978, NASDA produced and tested, in order, Engineering Model, Proto-type Model and the Flight Model. With the examinations given after IES Acceptance Test of July 1981, the development of ion engine system was completed.

Table 2.2 Development Schedules of ETS-III and Ion Engine System

ETS-III:

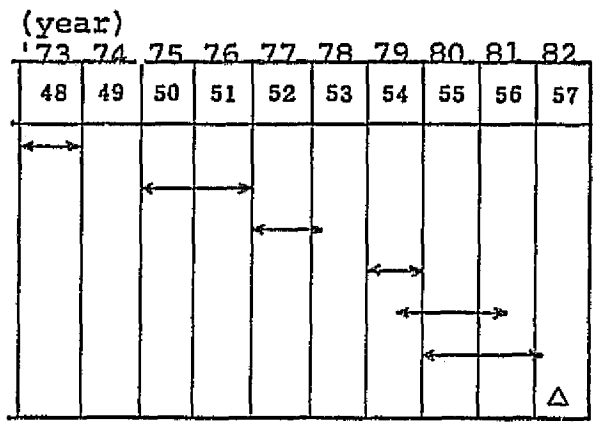

Ion Engine System:

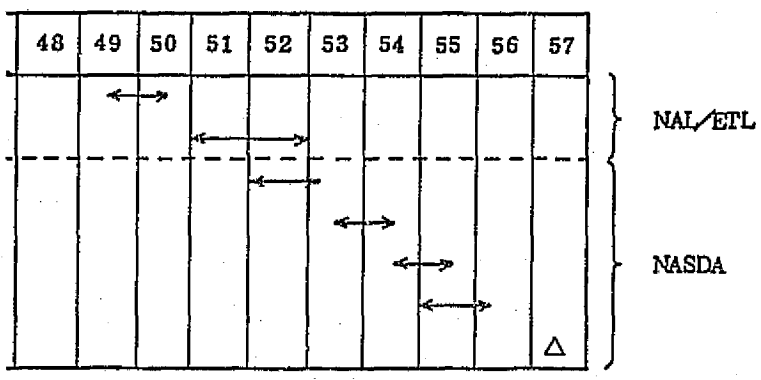

Table 2.3 Actual Development Process of IES and Its Components

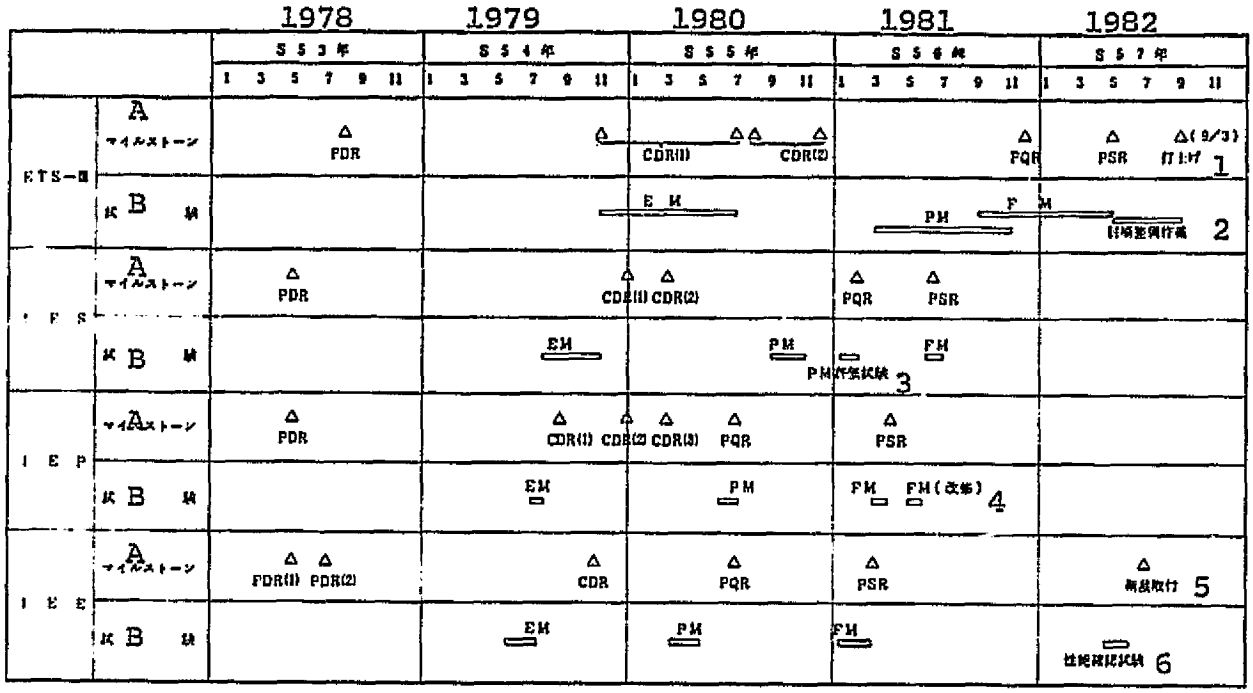

A: Milestone
B: Tests

PDR: Preliminary design review
CDR: Basic design review
PQR: Post-qualifying test review
PSR: Post-acceptance test review

1. Launching
2. Launch site preparation
3. PM evaluation test
4. FM(modified)
5. Installation on satellite
6. Performance check

Chapter 3

Research and Development

Chapter 3: Research and Development

3.1 Outline

It was about 1970 that research work on electron bombardment type ion engines actively began in our country. Already in the United States, NASA Lewis had developed, as part of the SERT-II Plan, electron bombardment type ion engines of 15cm diameter which were being tested for continuous operation in space for over half a year. NAL and ETL designed and test-produced 5cm-diameter filament type ion engines and conducted basic experiments[1-4]. It was in this stage that the basic characteristics of ion engines were studied: discharges using DC magnetic field, the ion source for this type of ion engine; extraction/acceleration of ions from plasma; neutralization of ion beam by electrons and conditions of the beam, etc. Technical problems involved in the major components of ion engine were also studied, while on one hand a vacuum device necessary for experiments was set and various measuring techniques were learned.

The next step was to improve performances, with actual future use in space in mind. Efforts were made to improve the components - vaporizers, insulators and cathodes. Central to the ion engine, these components required special production techniques and care, and much experiences were needed to produce products meeting the requirements. Limited staff and budget did not allow extensive design effort and test production of various structures and specifications, and several years flashed by on trial and error. The U.S., with the development of SERT-II ion engines, had established the technology of today, and the information which gradually became available were extremely helpful. When the qualities of main components reached a reasonably acceptable

level, the concensus was for continuing the efforts into developing an engine system that is operable on board an artificial satellite in space as a goal. For efficiency, NAL took charge of the engine unit (thruster) and ELT, the power conditioner. NAL concentrated on developing a light weight engine of 5cm diameter, as weight reduction was mandatory in space application, while ETL designed, test-produced and test power conditioners. Test products, with some modifications, showed satisfactory performance, and it was agreed that with further improvements they would meet boarding requirements. Thus, On-board Experiment Plan for 5cm-Ion Engine[5] was compiled, requesting operation tests on board Engineering Test Satellite III which was in its initial planning stage. The plan was submitted and accepted.

Up to that point, thruster and power conditioner were test-produced separately, and interfacing as a system had not been complete. In NASDA's taking over and continuing from EM through PM and FM, making major changes in configuration would be difficult, even in the EM stage. Moving straight onto EM, therefore, seemed unreasonable. Further, for actual boarding, ion engines were to be subjected to the same reliability test as other general equipments to ensure that the weight, characteristics, performances, and functions met the requirements. As ion engines required special operating conditions, it seemed necessary to figure out how these tests could be conducted. For this purpose, PreEM(Preliminary Engineering Model) of the thruster and the power conditioner were designed, test-produced and tested completely. The objectives of this process were:

1) to select and design parts and materials and establish production methods based on reliability management;

2) to gather information on structure, weight, characteristics,

performances, etc, in a comprehensive form for input into EM;

3) to establish interface of thruster, power conditioner and the satellite; and

4) to establish test methods for procurement of reliability.

The process also served to summarize the research efforts by the two institutes, to be carried over into the development phase.

In the following, outline of the research done on the ion engine unit and power conditioner from the initial stage to PreEM is presented.

3.2 Ion Engine Unit

3.2.1 Filament-type Ion Engine[1,2)]

Studies on ion engines started with a type using filaments in its electron sources - discharge cathodes and neutralizers. Although filaments as electron sources have limited life and performance, the structure, production and operation are simple and thus suitable for learning the basic technology for ion engines. Magnetic field for the discharge chamber was obtained by sending an electric current through coils wound on the outside of the chamber. Engine size of total beam diameter of 5cm in the cathode and accelerator grid was chosen. This is about the smallest of electron bombardment type engines, and while it lacks in certain performances, it is easier to handle because of its small size, flow and power. It was also applicable to maintaining north-south position of stationary satellites.

Layout of the engine, power sources, wiring and a probe, used for measuring beams, is shown in Fig. 3.1. In this ion engine, mercury was used as a propellant. The engine operates only in a vacuum. A vacuum tank as shown in Fig. 3.2 was set up at NAL

specifically for testing ion engines and gradually equipped for various tests. Diameter of the main tank was 1.5m and length, about 3m, and an ion engine hanger was placed with a gate valve inbetween to facilitate engine installation without breaking the vacuum in the tank. Inside the tank, a shroud was placed for cooling liquid nitrogen. The propellant, mercury, adheres to its surface and helps to increase the degree of vacuum. On the lower flow side, a beam collector was installed. It is electrically insulated from the tank walls and automatically maintains emission current of the ions and electrons from the engine at the same level, simulating movements in space. During engine operation, pressure inside the vacuum tank can be maintained at about 2×10^{-6}Torr. A flat-plate probe for measuing the current density distribution of injected beam and an emission probe for measuring the potential distribution were installed on a moveable device. Of discharge characteristics, the discharge voltage level most suitable for ion production, determined by maintaining a constant discharge power, is shown in Fig. 3.3. Although there are slight differences depending on the amount of flow, the utilization efficiency with mercury reaches the maximum level around 40V. The experiment was conducted at a high specific impulse, and with a high accelerator voltage the holes on the screen and accelerator electrodes were given relatively large diameters of 3mm and 3.5mm. There were 85 holes, 5mm apart(center to center). Examples of ion extraction and acceleration characteristics are shown in Fig. 3.4. It is clear that when the discharge conditions are steady, total acceleration current, the sum of beam current of ions which pass through accelerating electrode holes and shoot out to the lower flow of the engine as a beam and the drain current which flows into accelerating

electrode, is determined by the voltage between the electrodes, i.e. total acceleration voltage. Also, when the net acceleration voltage (beam voltage) which determines the injection speed of ions becomes sufficiently high compared to the accelerating electrode voltage, drain current almost disappears[1]. Taking ion extration, Poisson Equation which determines acceleration, momentum equation and boundary conditions into account, ion flows passing through a pair of holes become similar, provided that 1) size layout of electrodes are similar, 2) ratio R of the total acceleration voltage and net acceleration voltage is maintained constant, and 3) parameter Λ, given below, which binds discharge and acceleration conditions, has equal values[2].

$$\Lambda = (m_i/q)^{1/2} (\pi a_o^2) j_o / V_t^{3/2}$$

where m_i: mass flow of ions
q: electrical load
a_o: distance between accelerating electrodes or a typical length of electrodes - screen hole diameter, etc.
j_o: current density of ions which shoot from the discharge side to acceleration side and become accelerated
V_t: total acceleration voltage

As $\pi a_o^2 j_o$ is the ion current per hole, Λ can be considered a purveyance per hole. Acceleration characteristic noted earlier can also be explained by this relationship, and the results of experiments under various conditions supported that overall ion beam distribution also followed this principle of similarity. Fig. 3.5 shows that two types of purveyance obtained by combinations of beam current and total acceleration voltage give similar distributions. Examples of space potential distribution of beams, obtained by an emission probe, is shown in Fig. 3.6. Beam potential is influenced by the neutralizer's electron emission capability and its position with respect to the beam. Potential of the beam collector is thus an index of the beam potential, i.e. overall neutralization index.

Fig. 3.1 Filament Type Engine and Layout for Experiment

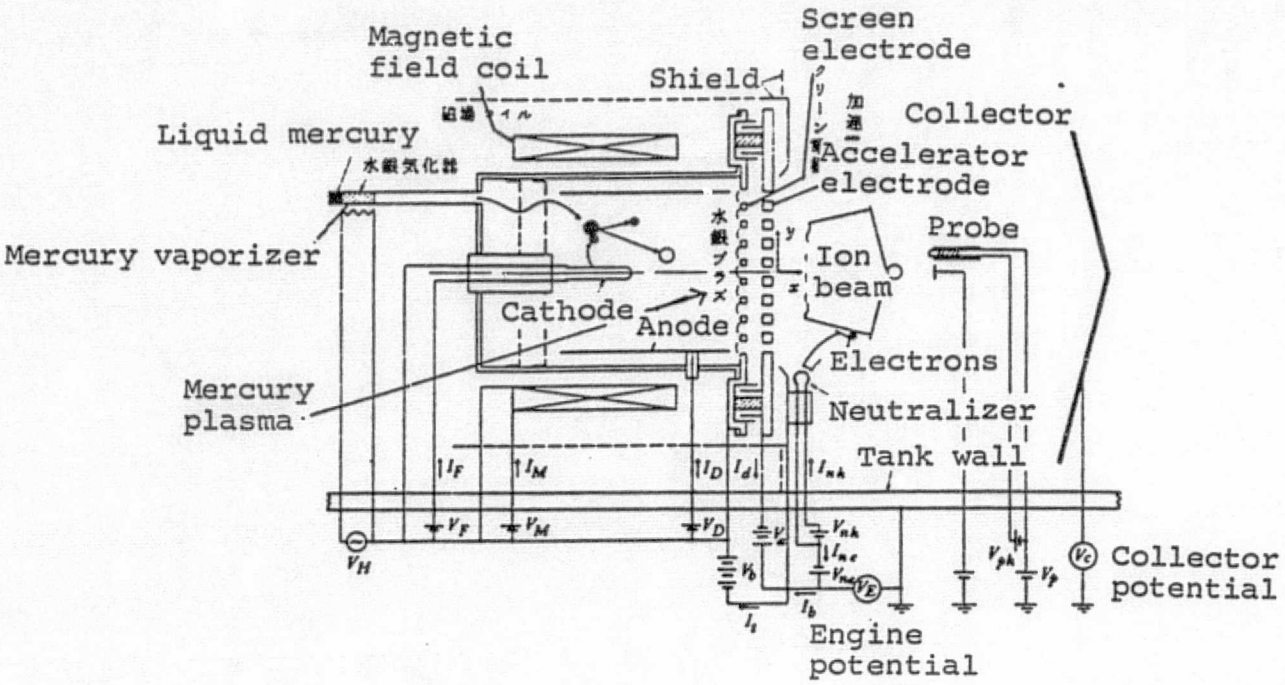

Fig. 3.2 Vacuum Tank for Ion Engine Test

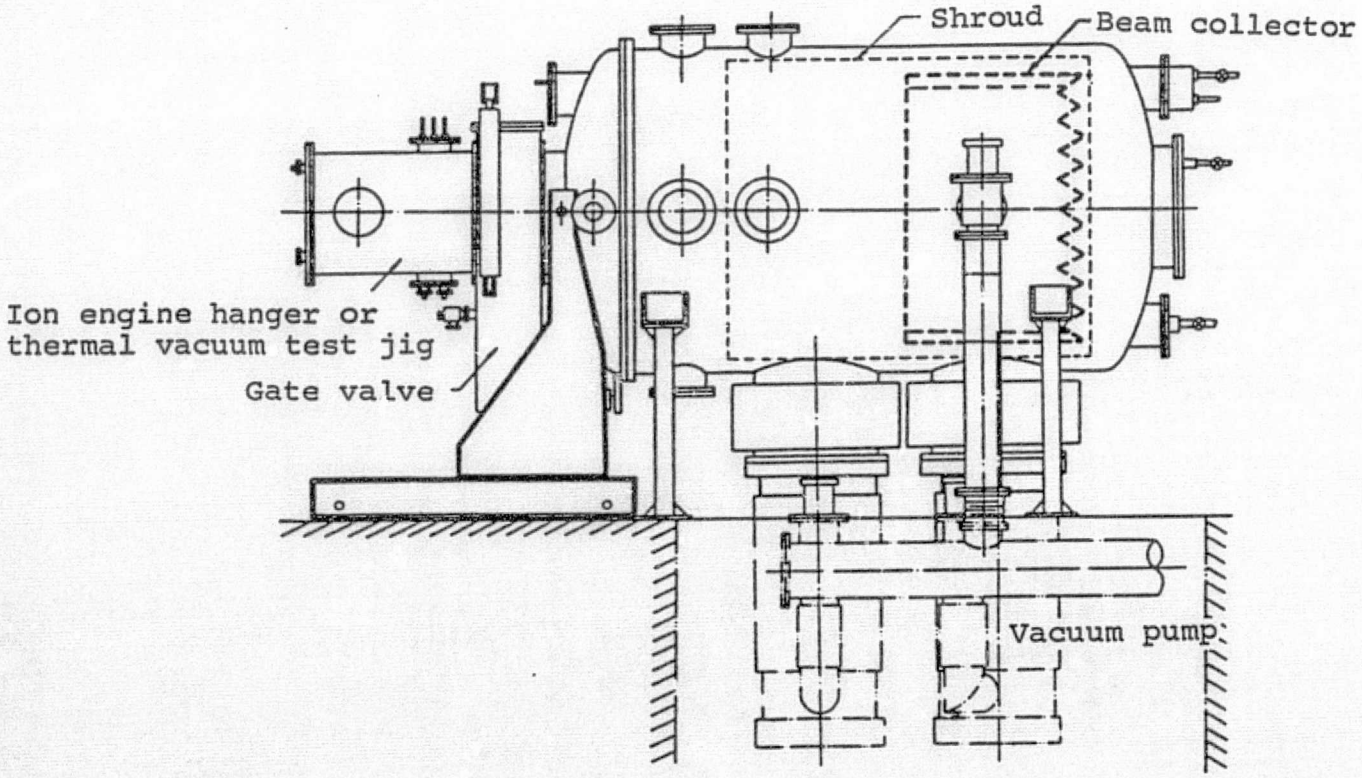

Fig. 3.3 Effects of Discharge Voltage on Ion Production

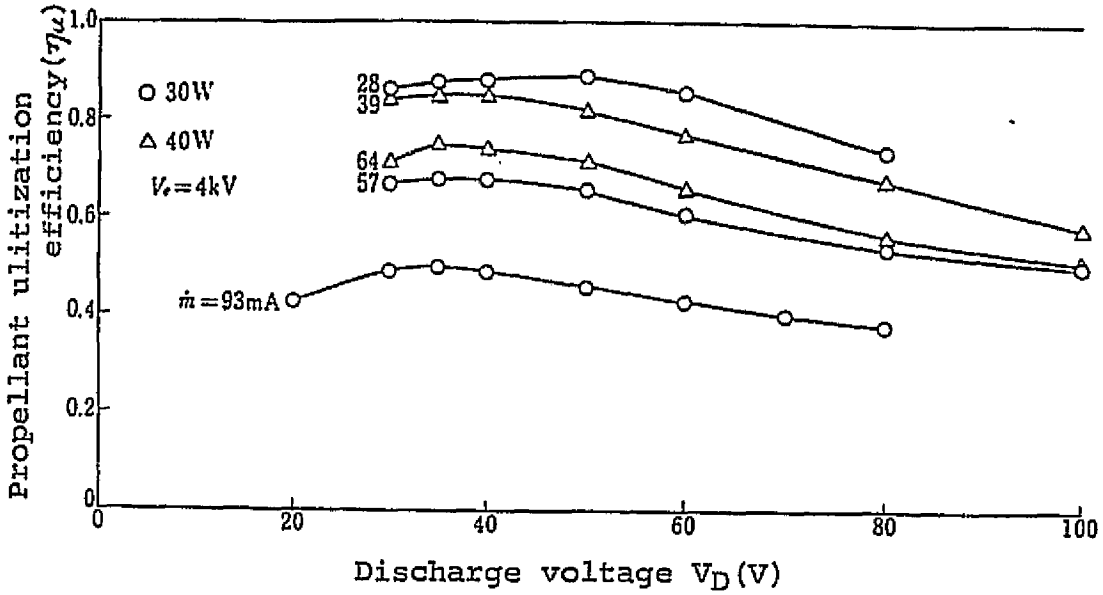

Fig. 3.4 Ion Acceleration Characteristic of Filament-type, 5cm Ion Engine

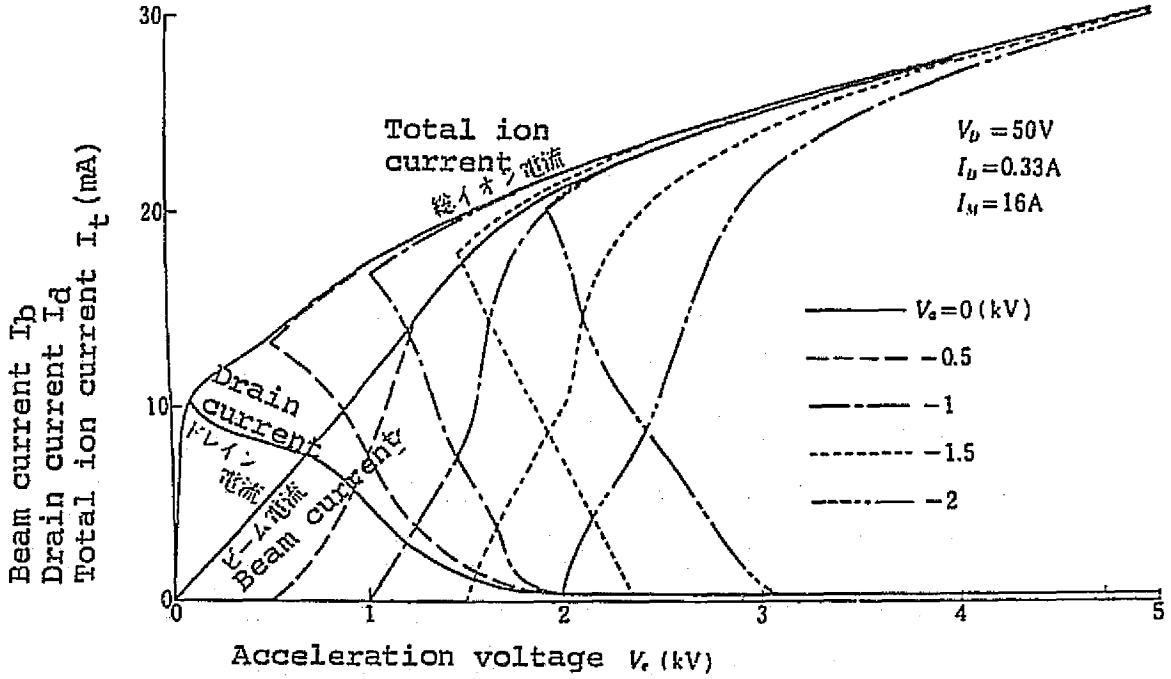

Fig. 3.5 Similarity in the Disctribution of Beam Ion Current Density

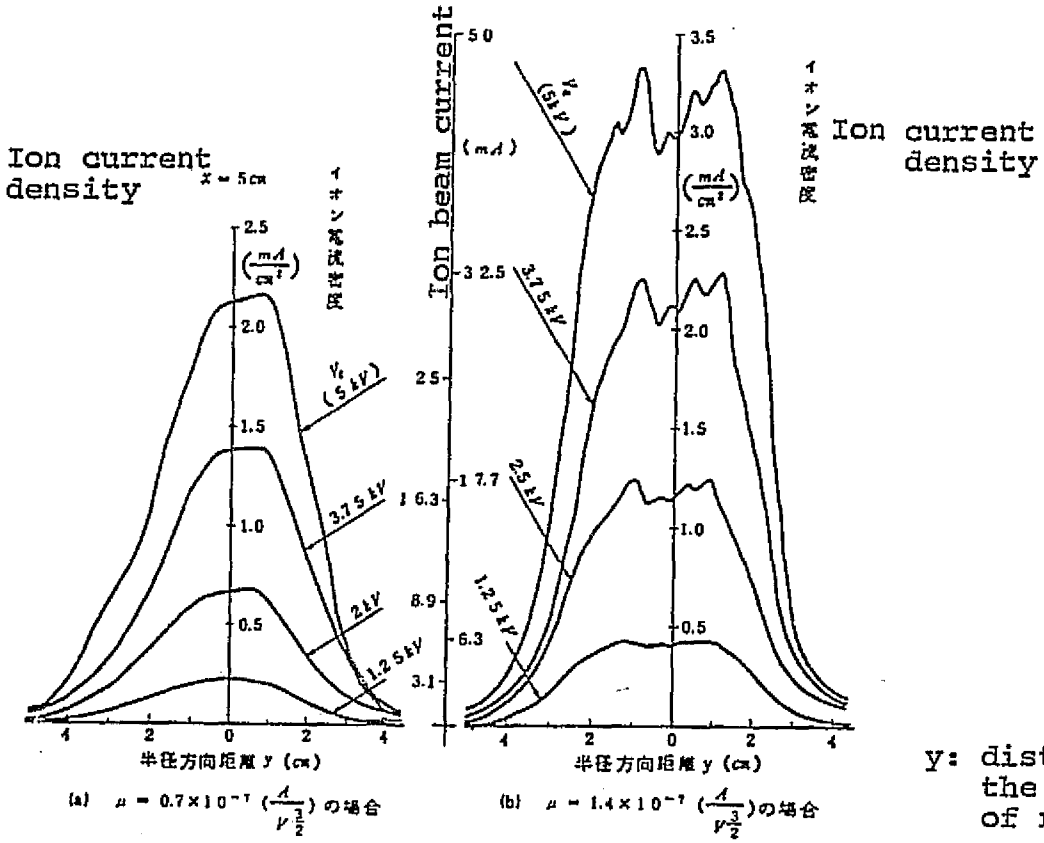

Fig. 3.6 Example of Distribution of Beam Space Potential in the Direction of Radius

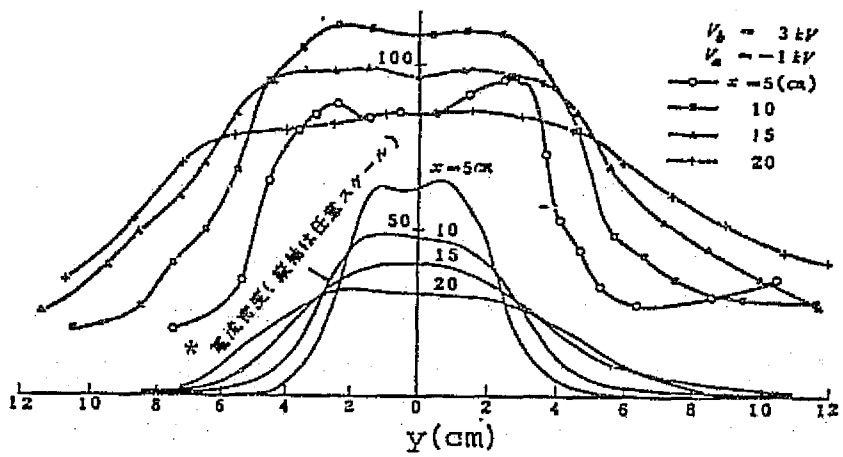

* current density (vertical axis scaled randomly)

3.2.2. Light Weight Ion Engine[6,7]

The next task was to improve those parts that are vital to the performance and life of an ion engine. Test-produced items were: porous vaporizer which provides steady supply of mercury, hollow cathode which replaces filament as an electron source, and insulator using a wire mesh. Production of these parts required special processing techniques such as dry sintering, electric discharge machining, electron beam welding, plasma or flame coating, brazing of metal and insulated materials, etc. for which production conditions were difficult to set. When the mercury vaporizer and hollow cathode reached a reasonable level of quality, it was time to consider their practical use in space. Taking the weight factor as well as performance and life into consideration, a 5cm light-weight ion engine was designed and test-produced. Its structure is shown in Fig. 3.7. Characteristics of this engine are as follows.

1) Light weight structure of thin plates.

2) Entire engine, including a spherical mercury tank, was designed and test-produced.

3) Porous tungsten vaporizer was employed.

4) Grid type insulator was employed.

5) Hollow cathode was used in cathode and neutralizer.

6) Oxidant-coated tantalum foil insert was employed.

7) Independent assembly of accelerating electrode system.

8) Use of alumina insulators, compression-assembled.

9) Length of discharge chamber, strength of magnetic field, size and position of baffle were made variable by replacing in steps.

As the first total design, there were a few problems which required improvements. Originally, the diameter of the orifice at the

tip of the cathode was 0.08-0.2mm. With a small flow of the engine, it was to facilitate easy discharge by increasing the density of vaporized mercury around the orifice. In actual use, however, it was found that discharge ignition was difficult with such a small orifice. The diameter was consequently increased to 0.25mm. Also, the hollow cathode keeper, originally of open type, was modified to a sealed type, as its low density increased the keeper voltage extremely high (over 20V). The discharge chamber had three different length, 40, 50 and 60mm, and the effects of magnetic field strength on performance were studied by placing three permanent magnets around the discharge chamber and changing the diameters to 4.75, 5 and 5.5mm[6,7]. As a typical example, discharge characteristics of the combination of 50mm-long discharge chamber and 5.5mm-diameter magnet for large flows and small flows are shown in Fig. 3.8. It is seen that the discharge voltage lowers as the flow increases. Where the discharge current, i.e. discharge power, is small, increasing the flow does not increase the beam current. As changes in the keeper current hardly affect the beam current, smaller keeper current is more advantageous if a stabel discharge can be maintained. A relatively small keeper voltage of less than 12V was due to the use of a sealed type keeper and oxidant-coated tantalum insert. Performance in terms of discharge loss (ion production cost of discharge) vs. propellant utilization efficiency showed that, in the combinations studied, shorter discharge chamber with thicker magnet gave better results. With magnets of the same diameter, however, shorter discharge chamber produced stronger magnetic field because of shorter distance between magnetic poles, as shown in Fig. 3.9. Fig. 3.10 shows the changes in performance curves for different combinations. In observing actual operation, it

was found that when the discharge chamber was short and the magnetic field became strong, discharge tended to become unstable, causing difficulties in operation, especially with a small flow. The safe combination was that of a 50mm-long discharge chamber and a 5～5.5mm-diameter magnet (alnico-5).

Alumina pipe of the insulator was mechanically pressed, instead of brazed, to the flange for an airtight, linear contact, but a leadage of mercury vapor occurred due to an incomplete contact. To prevent leakage, a thin copper ring was inserted for tighter contact. No ill effect of mercury vapor on copper was observed. In using the same hollow cathode, keeper voltage gradually increased with time, presumably due to deterioration by exposure to air.

Fig. 3.7 Structural Outline of 5cm, Light-weight Ion Engine

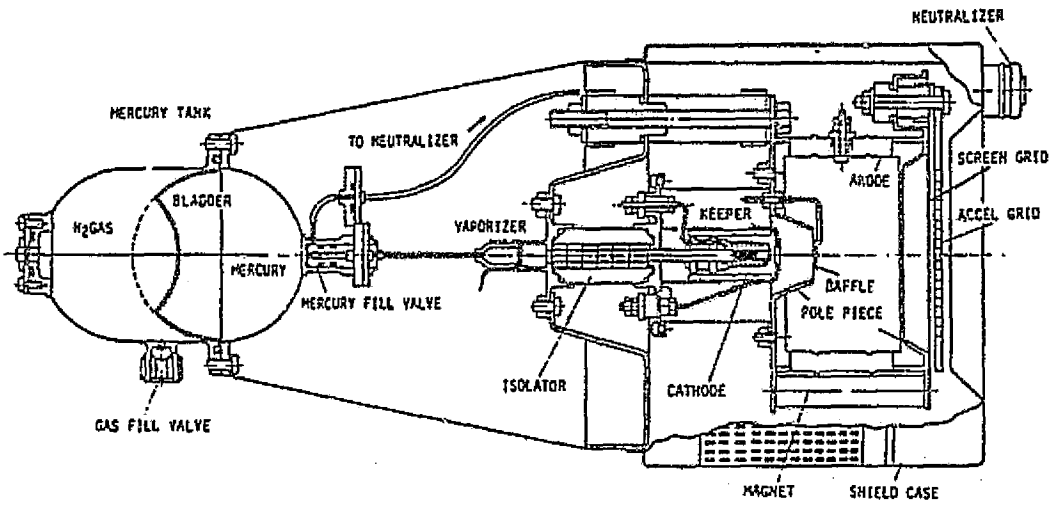

Fig. 3.8 Discharge Characteristics of 5cm, Light-weight Ion Engine

(a) Small flow with varied discharge current

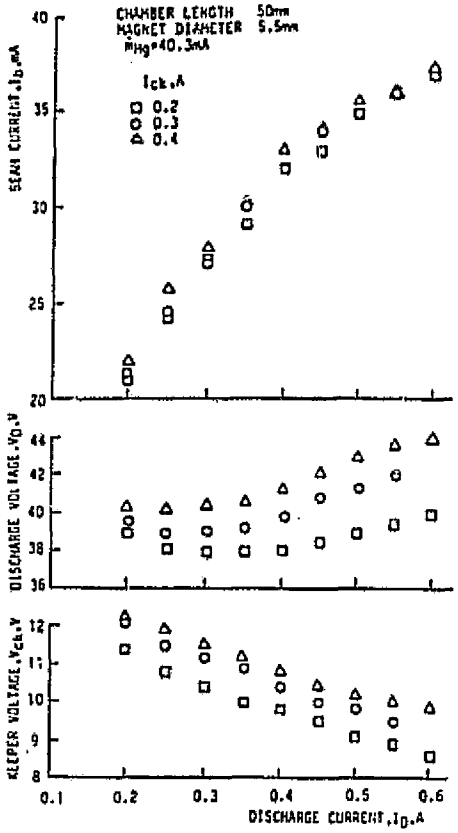

(b) Large flow with varied discharge current

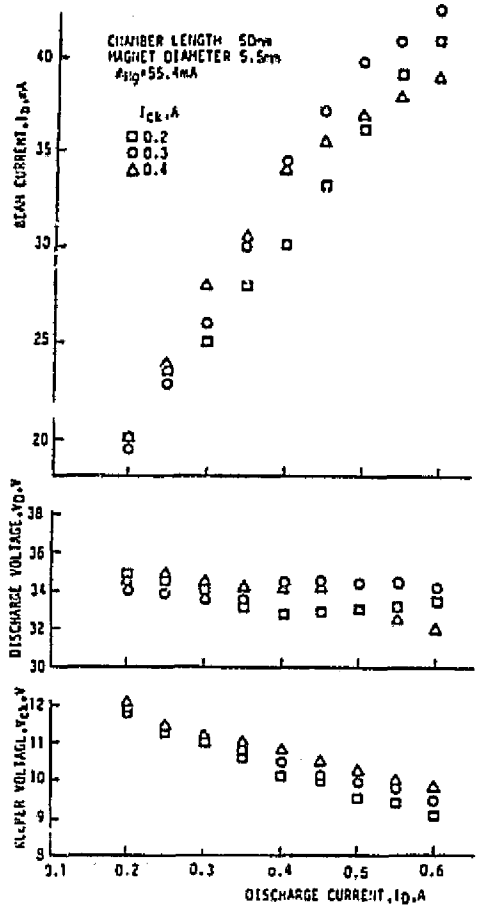

(c) Small flow with varied keeper current

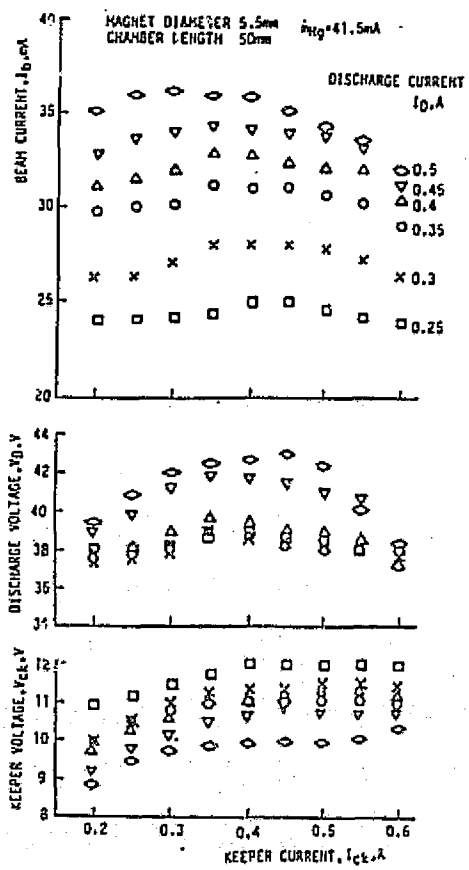

(d) Large flow with varied keeper current

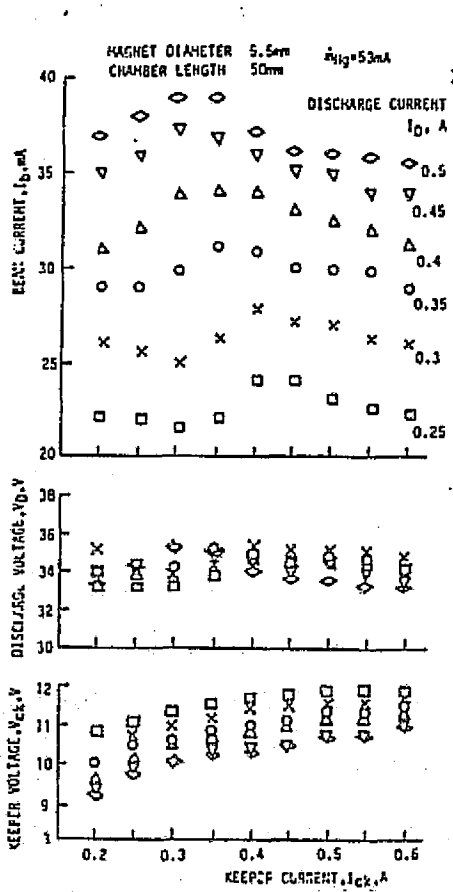

Fig. 3.9 Magnetic Field Strength of Discharge Chamber in 5cm Ion Engine (length of discharge chamber varied)

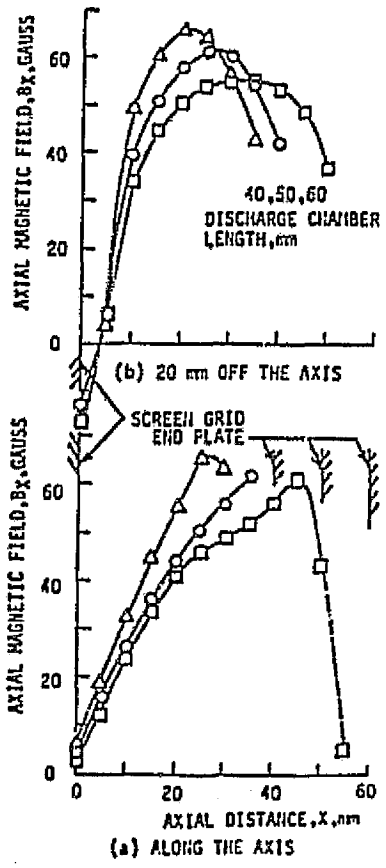

Fig. 3.10 Effects of Discharge Chamber Length and Magnetic Field Strength On the Performance of 5cm Ion Engine

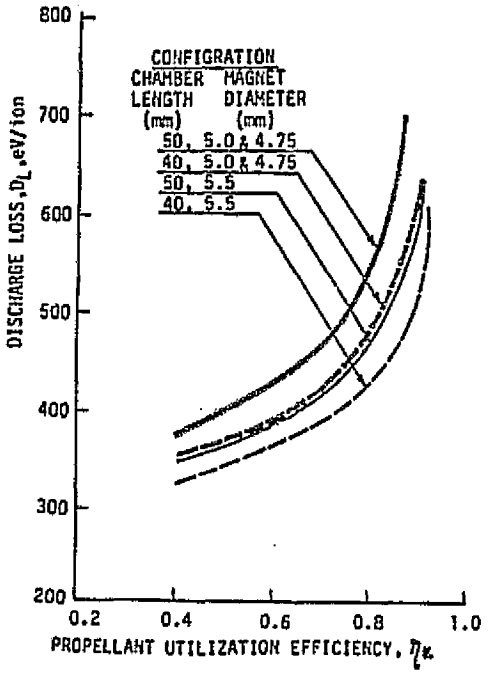

3.2.3 PreEM Ion Engine[8,9]

PreEM ion engine project was planned with the objectives of providing necessary data for designing the subsequent EM, making way for a smooth development of PM, and ultimately producing a reliable FM. Development conditions after EM affect the development plan for the satellite in each phase, and in return, are affected by satellite development. For this viewpoint, a research process was established taking various tests required in the development stage into consideration. For each test, the device and method were planned to be studied and tested. The initial plan is shown in Fig. 3.11. Some minor changes were later made. In the production stage, vital parts were to be tested following the process shown in Fig. 3.12. In actuality, shock test was eliminated as it was replaced by an oscillation test, the results of oscillation test were visually inspected from the outside, and dismantling was eliminated unless a trouble was found. Also, any engine disorder was to be spotted by the performance tests before and after the oscillation test. Diffusion angle of ion beam was also measured during performance tests. Of the tests relating to ETS-III ion engine development, those tests which required techniques specifically developed for ion engines and partial results are discussed later.

Outline of the structure of PreEM is shown in Fig. 3.13. It is an expanded light-weight model. Hollow cathode, insulator and vaporizer were brazed to one piece(CIV assembly), which gave tighter assembly than the light-weight model, eliminating the possibility of mercury leakage. For stainless sheets used for discharge chamber, cathodes, etc., thickness of 0.3mm was chosen for guaranteed reliability, as compared to 0.2mm used in the light-weight model.

Reliability was greatly improved by stricter production conditions set for two of the important parts, vaporizer and hollow cathode. Impregnated type(barium-impregnated porous tungsten) hollow cathode insert was used for the first time. Compared to the oxidant-coated tantalum foil used thus far, it was to give a more stable relationship between the production conditions and the performance. There was also some literature which suggested that it gave better performance. An aluminium flange for assembling onto the satellite was produced for the first time also for the PreEM. Including mercury tank and wiring, the ion engine thus became a complete system, weighing under 3kg per engine including 600gr mercury. Three PreEM were produced, two of which were used mainly for various engine tests at NAL and the other, for testing in combination with PreEM power conditioner at ETL. Photograph of the assembled PreEM engine is shown in Fig. 3.14. Vacuum device used for testing was basically the same as the one used before light-weight models. In order to simulate the power conditioner, test power supply system employed 5kHg short wave for AC and constant current for discharge, and a general power source having a drooping characteristic was employed for keeper along the way. This power source, connected to a mini-computer, automatically controlled the operations of ion engine and helped to increase the efficiency of data processing. For operation under computer(CPU) commands, the keeper power source was also to function as a constant current source.

In the following sections, tests given for research purposes are explained.

Fig. 3.11 Flow of Ion Engine Development Process

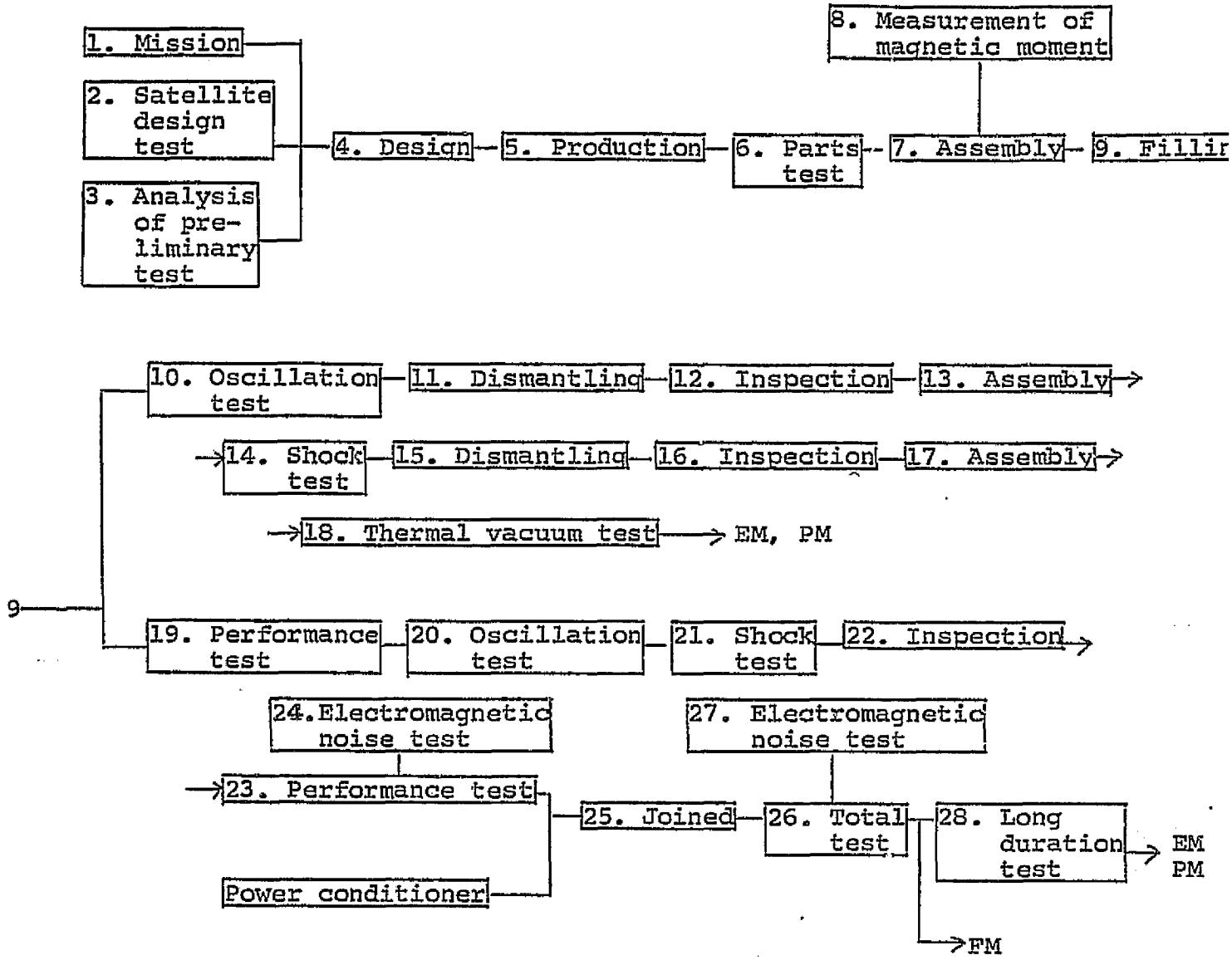

Fig. 3.12 Ion Engine Parts Tests (during production)

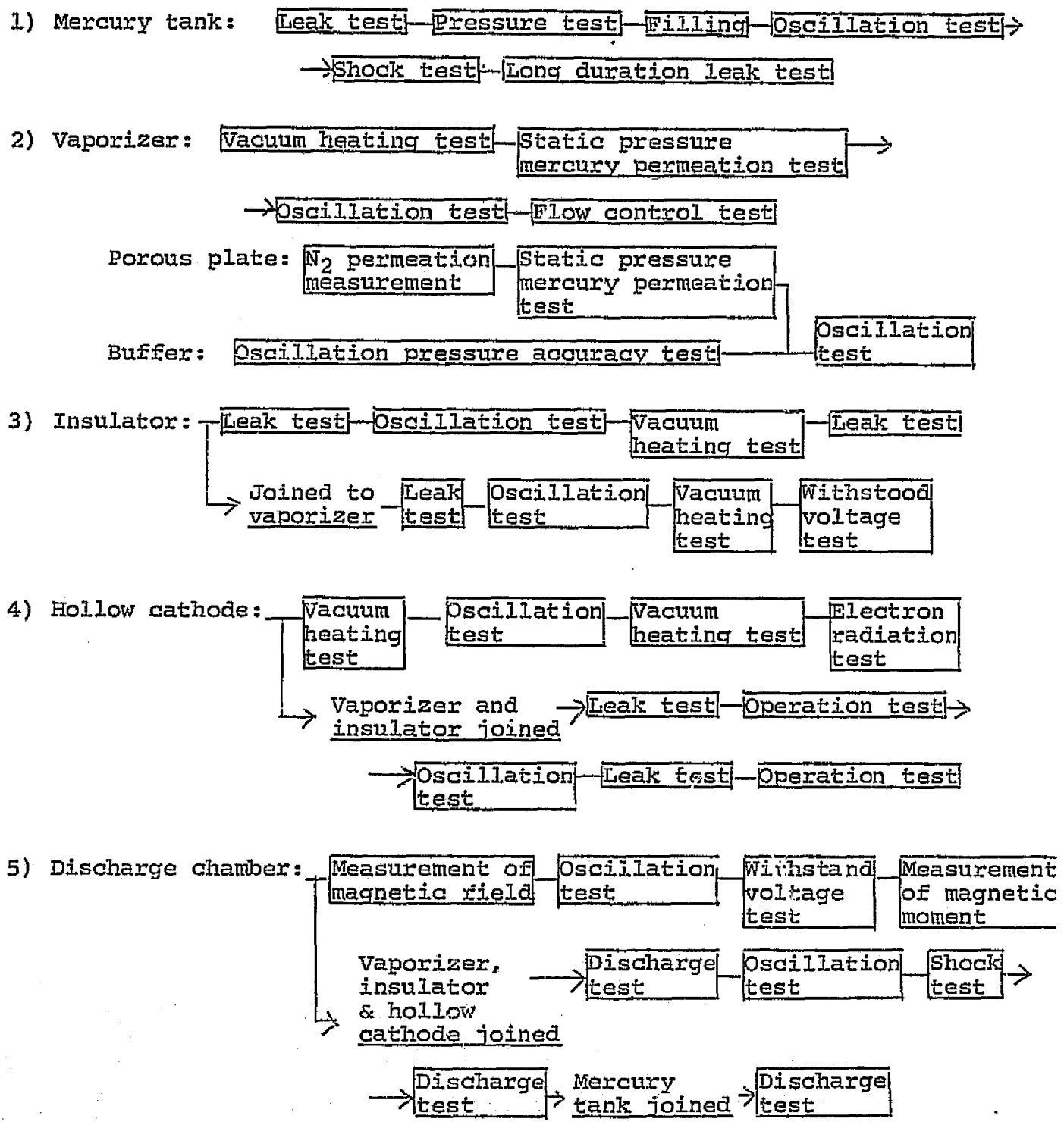

Fig. 3.13 Structure of 5cm PreEM Ion Engine

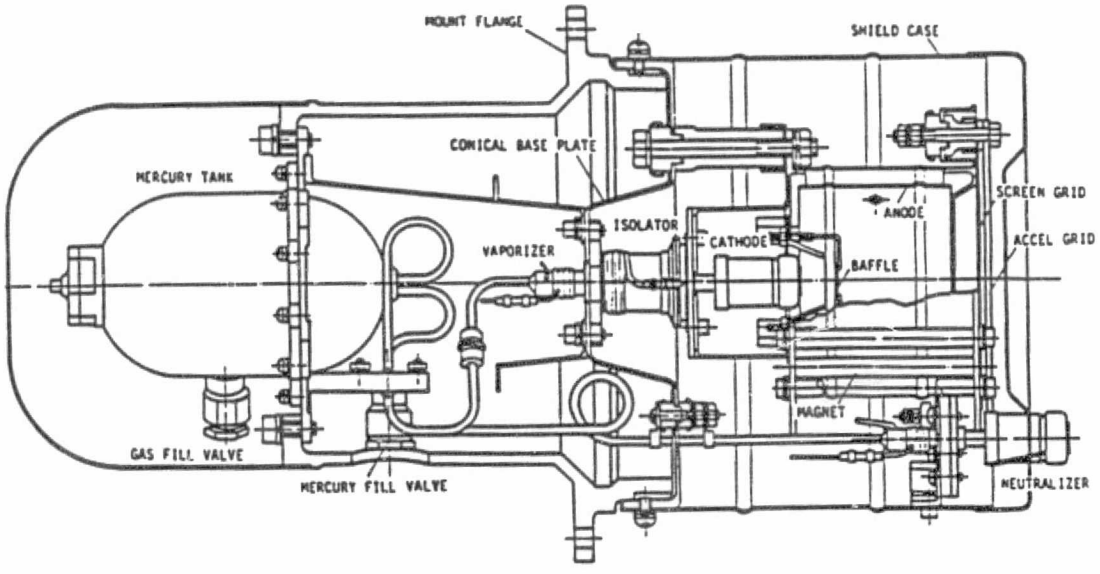

Fig. 3.14 Photograph of 5cm PreEM Ion Engine

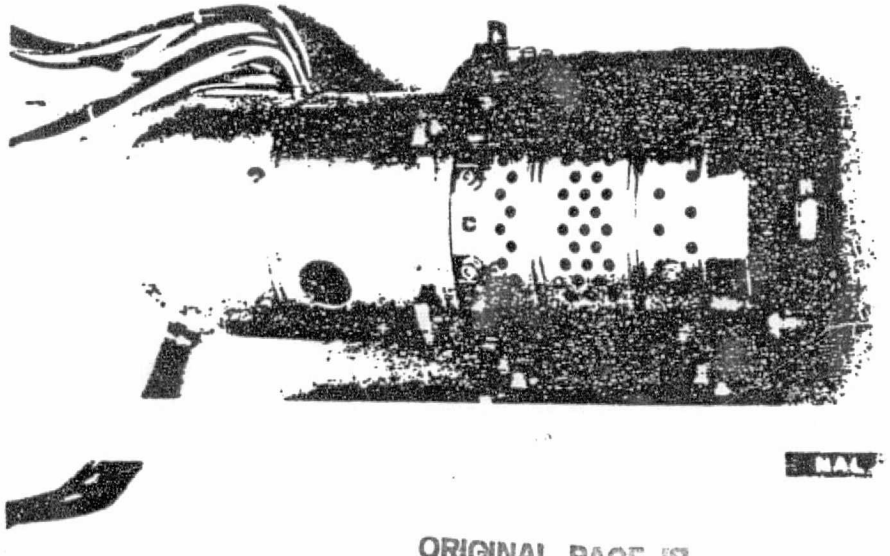

3.2.4 Performance Test[8] of PreEM Ion Engine

Operation parameters were set for PreEM engine using the data obtained from the light-weight model as a reference. However, parameters actually obtained in many cases did not meet the targeted values. The reason, assumably, was that with a different engine, changes in thermal characteristic, in particular, had subtle effects. Table 3.1 shows typical examples of operation parameters obtained under steady-state operation and the targeted values. In obtaining 30mA beam current, there were such differences between parameters and target values as noted below.

(1) Discharge voltage was slightly lower. It is assumably due to to difference in the strength of magnetic fields, but such a slight difference could be caused normally by the position of the baffle.

(2) Cathode and neutralizer keeper voltages were high. This was caused by the change of insert from the foil-wound type to an impregnated type.

(3) Insulator or cathode vaporizer power was large. This was caused by a large heat loss from conduction and radiation due to high operating temperatures of the vaporizer.

(4) Neutralizer vaporizer power was small. As expected, the neutralizer keeper supplied sufficient heat while operating temperatures of the vaporizer were low.

Oscillation test was given between OP1 and OP2 in Table 3.1 at the level specified for EM. A movement was observed in OP2 which suggested that mercury passed through the vaporizer in a liquid form, due to the oscillation test. In other words, OP2 showed a significant change from OP1: discharge was maintained even with drastically reduced power in the vaporizer and insulator, but beam voltage could

not withstand 1,000V. In this regard, importance of parts selection at the production level was recognized. In this particular instance, with a high beginning operation temperature, an unevenness in the vaporizer's porosity, or a crack, was suggested as the cause. As a countermeasure, stricter testing of static pressure mercury transmission was considered.

That there was no difference in operation parameters between the two engines indicated that the production process was satisfactory. It was necessary to study heat characteristics around the insulator vaporizer to cut power consumption. Temperature characteristic of the cathode vaporizer during repeated engine operation in relation to the rated power was as shown in Fig. 3.15. It took over 40 minutes to reach 300C from the ordinary temperature and there was no increase until the hollow cathode was ignited. Once heated, however, the speed of temperature increase rose because of retained heat. Although there was no heat shield around heaters in the early PreEM, operation test of a CIV assembly was performed in order to estimate its effects and heat loss due to conduction. As shown in Fig. 3.16, heat shields were installed around the vaporizer and insulator heaters and a vaporizer flange was installed on a 0.5mm-thick stainless support plate. Vaporizer temperature characteristic during this test is shown in Fig. 3.17. Rate of vaporizer temperature increase with time was about the same regardless of the presence of a shield. This is because there was little heat loss from the flange. It is also evident that the shield not only reduces heat conduction loss but has positive effects on the maximum temperature that the vaporizer reaches. Based on the results, both the installation of heat shields and thermal isolation of the vaporizer were incorporated for reducing power

consumption. In the first EM test, condensation of mercury occurred in the low-temperature part of the vaporizer. It was found that the temperature characteristic around the vaporizer was affected subtly by its rated operation temperature, heating power, position of the heater, size of the heat conduction passage(length and thickness of the pipe between vaporizer and flange), etc. A vaporizer insulator improved upon these observations was used for thermal vacuum test[10] using a PreEM engine. Although there was a slight mercury condensation at the start of the engine due to its operating conditions, a relatively good characteristic was obtained. Operation parameters for this thermally improved vaporizer are shown under OP4 in Table 3.1.

In addition to these improvements on the engine unit itself, redistribution of power was made in the power source device when the EM phase was started, revising the targeted operation parameters for easier engine operation.

Fig. 3.15 Vaporizer Temperature Characteristic at Rated Power

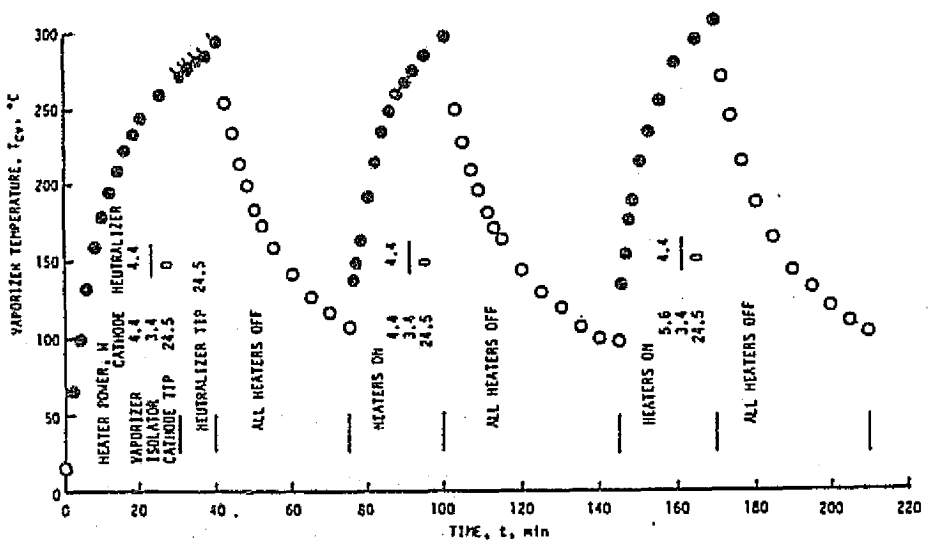

Table 3.1 Examples of PreEM of 5cm Ion Engine

Operation parameter Name:	パラメータ 記号, 単位	Operating values 作動値 OP1	OP2	OP3	OP4	Target value 目標値
Beam voltage (V)	Vb , V	1,000	800	1,000	1,000	1,000
current (C)	Ib , mA	30	30.2	33.9	28.7	30
Accelerator electrode (V)	Va , V	−1,000	−1,200	−1,000	−1,000	−1,000
(C)	Ia , mA	0.28	0.3	0.27	1	0.56
Discharge (V)	V_D , V	40	40	43.5	42	39.8
(C)	I_D , A	0.35	0.35	0.35	0.35	0.35
Cathode heater (V)	Vch, V	0	0	0	0	0
(C)	Ich, A	0	0	0	0	0
Cathode keeper (V)	Vck, V	14.5	15.8	15.9	15.5	12
(C)	Ick, A	0.3	0.3	0.3	0.3	0.3
Cathode vaporizer (V)	Vcv, V	3	2.4	2.9	2.35	2.6
(C)	Icv, A	1.5	1.2	1.35	1.26	1.5
Neutralizer heater (V)	Vnh, V	1.7	0	0	0	2
(C)	Inh, A	2	0	0	0	2
Neutralizer keeper (V)	Vnk, V	20.5	23.2	26	21.1	18
(C)	Ink, A	0.25	0.25	0.25	0.25	0.25
Neutralizer vaporizer (V)	Vnv, V	0.9	1.7	1.5	1.1	2.6
(C)	Inv, A	0.5	1	0.8	0.6	1.5
Insulator heater (V)	Vi , V	6.4	0	5.9	3.4	3
(C)	Ii , A	1.8	0	1.77	1.0	1
Cathode vaporizer temp.	Tcv, ℃	331	201	348	292.5	250
Neut. vaporizer temp.	Tnv, ℃	274	239	265	215.5	250
Ion engine operated		✻ 1	✻ 1	✻ 2	✻ 1	

Fig. 3.16 CIV Assembly Used in Single Unit Temperature Characteristic Test

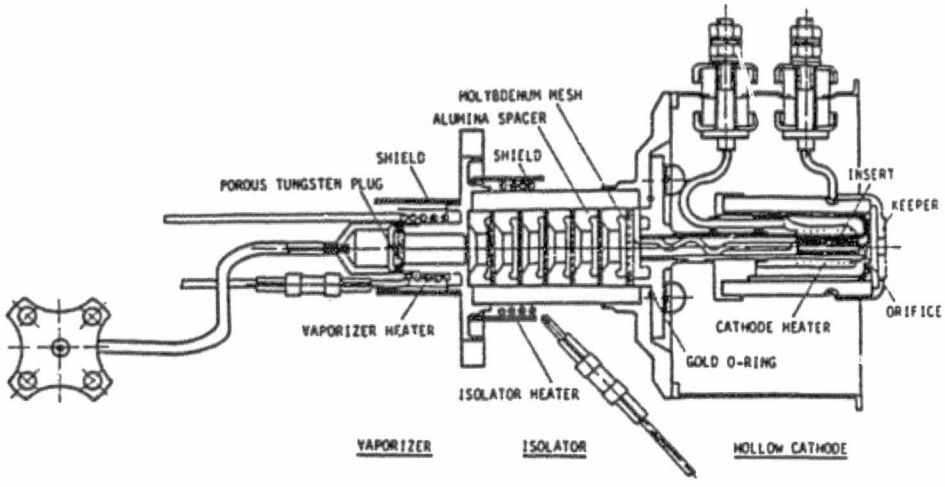

Fig. 3.17 Vaporizer Temperature Characteristic in Single Unit CIV Assembly

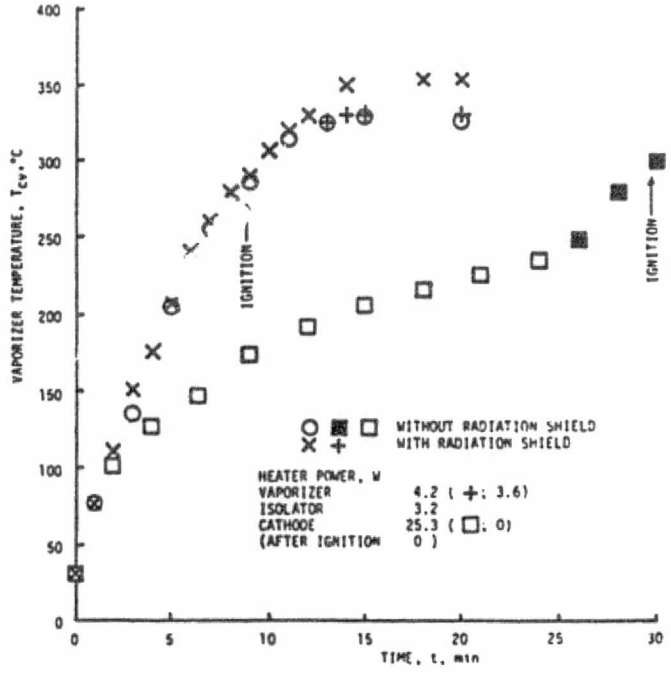

3.2.5 Measurement of Beam Diffusion[11]

Relationship between the satellite and high-speed ion beam is important in the engine operation on the satellite. In maintaining the north-south direction of a stationary satellite, its effect on the solar cell paddle extending north-south must be taken into consideration. Thrust loss due to a diffusion of the beam with respect to its central axis should be estimated. Diffusion angles are also measured in order to obtain basic data necessary for selecting an installation method having no negative effect on the satellite and other equipments. For this purpose, smaller diffusion angle is more desirable. Effects of grid systems and accelerating conditions on diffusion angles were studies as an expansion of the studies on beams already done in the filament type engines. As a beam diffuses almost linearly from the engine outlet, ion current density was measured by moving a flat plate probe horizontally to the axis through the center of the beam, mainly in the area where the distance in the axial direction is 30cm. Effects of different grid distances and hole sizes, and of ratio R between the net accelerating voltage(roughly equal to the beam voltage) and gross accelerating voltage(roughly equal to the voltage between screen and accelerating electrodes) were also studied for the cases where ions were accelerated in a two-grid system of screen and accelerating grids and where a third grid(for decelerating) was installed. Fig. 3.18 shows the typical distribution of current density. From this distribution, diffusion angle α is obtained by

$$\alpha = \mathrm{Arctan}(rb - 2.5) / 30)$$

with the radius rb cm which is 5% of the maximum value as the diffusion of the beam. Beam diffusion is smaller when R is larger, and also smaller with a three-grid system than with a two-grid system. Although

its support structure is complex, a three grid system is more advantageous in view of smaller diffusion and less spattering by exchange ions. Beam diffusion can be decreased by reducing the size of grid holes and space between grids and increasing R while maintaining the same beam voltage. When R is large, difference of diffusion angles between two grid and three grid systems is smaller.

Fig. 3.18 Example of How Accelerating Conditions and Grid System Affect Beam Distribution

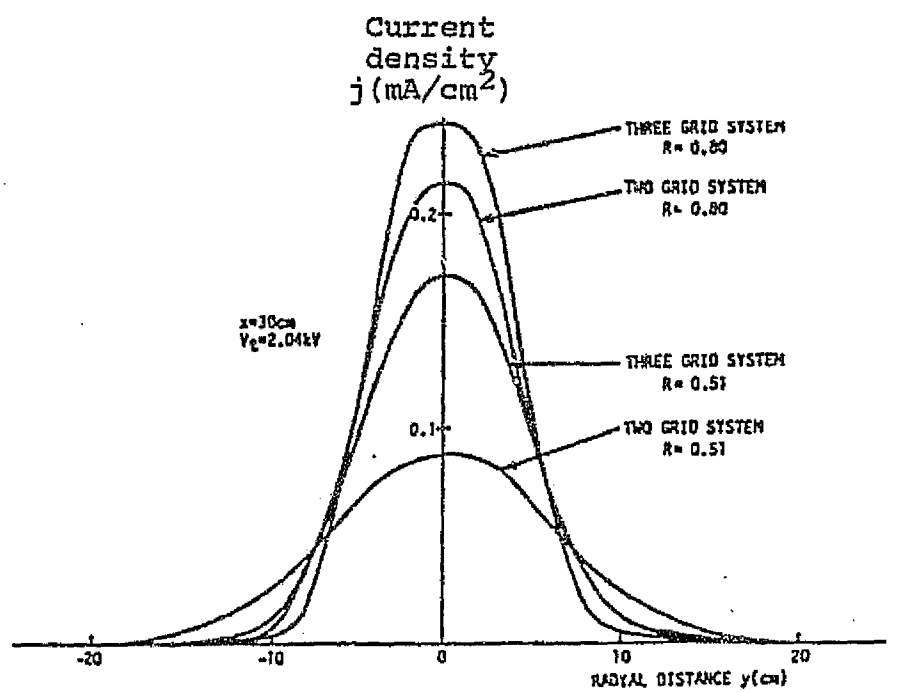

3.2.6 Measurement of Thrust

Thrust is the most important performance value in any engine. In an ion engine, injected particles contributing to the generation of thrust are mostly univalent ions, and the amount of flow is determined by the beam voltage(to be exact, plasma potential of discharge chamber close to the discharge voltage is added) as a beam current of uniform speed. In the ideal case where each ion speed is parallel to the beam axis and the ratio of univalent and bivalent ions is known, thrust can be determined by the beam current and voltage. As mentioned in the previous section, there is a thrust loss caused by ions' speed component perpendicular to the beam axis and the presence of bivalent ions, and thus, the actual thrust is smaller than the computed value. It is therefore meaningful to measure the thrust directly as a power. With an ion engine, however, thrust is small for its weight and it must be operated in a vacuum, which makes accurate measurement somewhat difficult. In this section, a measurement method using a twist type balance and the measured results are discussed. As shown in Fig. 3.19, the arm of the balance is hung by a piano wire. An ion engine placed on one end is balanced with a counterweight on the other end. Power is supplied by soaking a power terminal in a mercury pot, placed for each channel, for allowing for free movements by thrust. The piano wire is twisted by thrust perpendicular to the arm, in the horizontal direction, turning the arm. The displacement of this arm thus caused is detected by a differential transformer. The displacement is cancelled by a reverse torque given by a magnet placed on the arm. By using such a zero displacement method, thrust can be determined by the electric current in the magnet. Coil current was adjusted using accurately measured weights instead of thrust. This was first done in the air.

However, in order to eliminate the effects of air current and errors caused by slipping of the balance in a vacuum, a method of hanging a weight by a fine thread which allows gravitational force to go towards the direction of thrust, shown in Fig. 3.20, was eventually employed. Three 100mg weights were chained by a thread and sent out by turning the thread rod from the outside. By using this method, making adjustments during operation in a vacuum became possible and the measurement accuracy increased. Accuracy in adjustment is most affected by the angle of the thread slipping from 45-angle, but corrections were made by measuring the actual angle using tran-jet(?). Fig. 3.21 shows the thrust, measured with an actual engine, plotted with respect to beam voltage. Smaller thrust at lower voltage is assumed to be largely due to diffused beams.

It is also possible to indirectly measure thrust by placing a target instead of an engine on the balance. This method eliminates the problem of exposing the engine to air during adjustment of the balance. The target must be able to receive the entire beam, without any reflection, which resulted in a shape of a large cone. As the target was smaller than the diffused beam in the measurement of a light-weight engine, its size was increased for the EM test so that the entire beam would be received. The results with a light-weight engine are shown in Fig. 3.22. Measured values are smaller especially at lower beam voltage because the target did not receive all of the beam. Improved results were obtained with EM, with measured values being 90-95% of the ideal at the beam voltage of 80-1,400V.

Fig. 3.19 Twist-type Balance for Measurement of Thrust

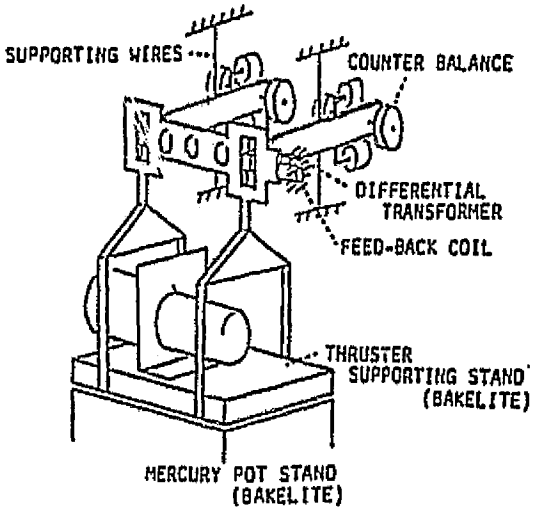

Fig. 3.20 Thurst Adjustment Method

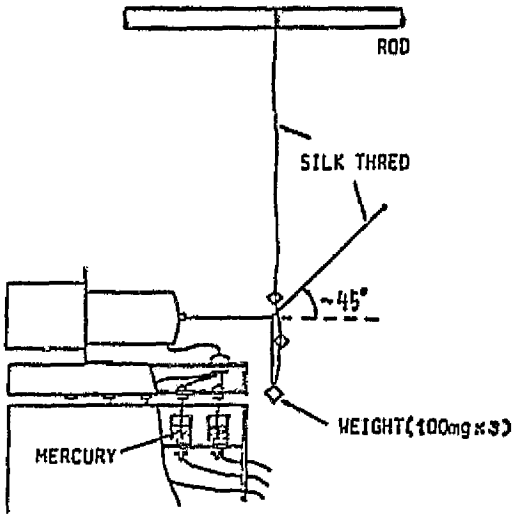

Fig. 3.21 Relationship Between Thrust and Beam Voltage Measured With An Engine

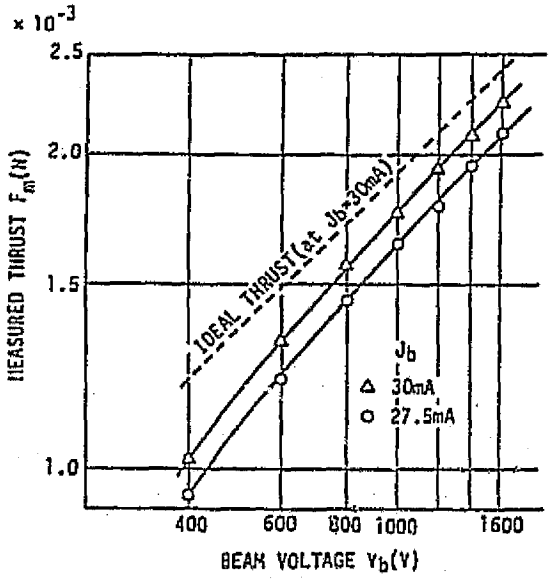

Fig. 3.22 Relationship Between Ratio of Thrust Measured With A Target And Computed Thrust And Beam Voltage

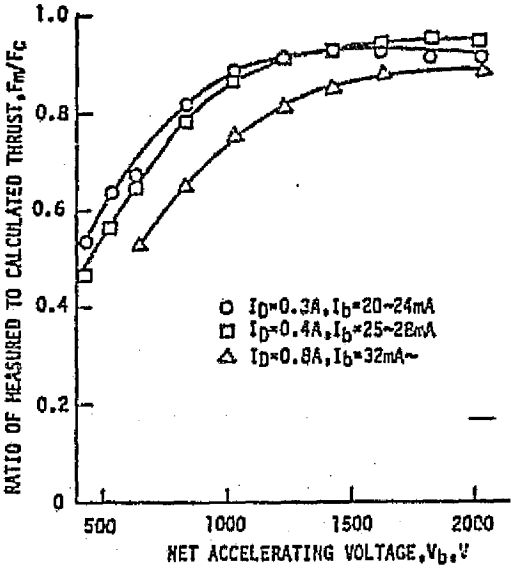

3.2.7 Measurement of Electromagnetic Interference[9)]

Ion engine, because of discharging, has a possibility of radiating electromagnetic waves. Intense radiation can cause faulty actions in other equipments on board and communication interference. However, hardly any measurements had been made thus far of electromagnetic interference of ion engines, especially those of electromagnetic radiation, and thus, there was no substantial reference data. It was therefore necessary to measure the electromagnetic interference and to establish the measuring method, as well as to make comparison with reference limit values and locate the source of electromagnetic waves before further development of the engines for ETS-III.

Measuring instrument and its position, limit values and measuring method for electromagnetic interference are established in MIL-STD 461A and 462. Although it is not possible to strictly observe the MIL standards, as ion engines are operable only in a vacuum(in a vacuum tank on the groun), they should be followed as much as possible to obtain data which can be compared against reference limit values.

Two methods were considered. One used an antenna placed inside a vacuum tank, and the other was measurement from the outside, by placing an ion engine inside a vacuum tank which permeates electromagnetic waves. The latter was chosen for the following reasons: the vacuum tank currently in use was too small to accommodate the antenna specified under the MIL standards; exchanging antennas inside the tank was inconvenient; and reflection of electromagnetic waves on the inner walls of the tank affected measurement.

Conduction interference is not a problem for an ion engine itself, as it is electrically connected to the satellite via power source device. Also, there is no possibility that the engine itself receives

interference from electromagnetic waves. Therefore, electromagnetic radiation alone was measured.

(1) Test device and measuring method

Test device consists of an ion engine system test antenna, amplifier and spectrum analyzer. The device is outlined in Fig. 3.23. The engine system is a combination of PreEM ion engine unit and power conditioner. The engine is placed inside a sub vacuum tank of cylindrical glass, connected to the main vacuum tank. Inner diameter of the sub-tank is 30cm, length 50cm and the thickness of glass is 7.5mm. Glass walls assumably absorbing almost no electromagnetic waves, measurement can be made with placed outside the tank.

Measurement was for the frequency range of 0.15MHz to 1GHz, using a rod antenna, biconical antenna and log spiral antenna. Preparatory measurement had confirmed that electromagnetic radiation between 1GHz to 10GHz was sufficiently weak compared to the limit values under MIL-STD 461A. The three antennas were placed, one at a time, 1m from the engine to the side. Signals received by the antenna were amplified and the frequency was analyzed by the spectrum analyzer. Maximum values of electromagnetic radiation obtained by CRT's residual light storage function were taken as the measured values.

An ion engine generally goes through a pre-heating state and a state of maintaining discharge before it reaches a beam acceleration state. In order to study electromagnetic radiation characteristics and to estimate the radiation source for each state, measurements were made in each operating condition. Power conditioner was placed in an aluminium shield box to reduce the effects of its own electromagnetic radiation. Power line between the power conditioner and the engine unit was covered with shield tapes, also to reduce radiation. These

measures were taken so that the radiation from the ion engine unit alone could be measured.

In measuring interference, electromagnetic radiation is classified into a narrow band(continuous sine wave) and a broad band (contains many waves in a set band area). Broad band radiation is further divided into impulse type(phases of waves contained are even) and random type(phases are not even). The classification is based on the changes in power reception with the changes in the band width analyzed by the spectrum analyzer. To a 10-fold increase in the analyzed band width, power reception increased by 0dB, 10dB and 20dB respectively in the narrow band, random type broad band and impulse type broad band.

As measurements were made without using a wave shield room, the antenna received electromagnetic waves from the outside along with the radiation from the ion engine. Radiation from the engine was identified by comparing the distribution of electromagnetic radiation spectrum during operation and that during non-operation of the engine. Radiation from the engine was mostly of broad band random type, with no strong, narrow band radiation detected.

(2) Measurement results

Radiation distribution in the broad band during beam acceleration is shown in Fig. 3.24. marks indicate data obtained by increasing the spectrum-analyzed band width by 10 times that indicated by asteriks. Limit values of electromagnetic radiation according to the MIL-STD 461A are indicated by a real line as a reference. Except for slight differences under 1MHz, they mostly coincide. This indicates that electromagnetic radiation is actually of random type at over 1MHz and partially impulse type at under 1MHz. Peaks occur at around 4MHz,

6MHz and 15MHz. Outside these peaks, the strength of radiation is below the limit values of MIL standards. It exceeds the limit by about 10kB around 6MHz and 15MHz.

Fig. 3.25 shows the distribution of radiation in the broad band during pre-heating of the engine. Symbols used are the same as in Fig. 3.24. An ion engine is pre-heated with main cathode and neutralizer heater currents and insulator heater current, both at a low level. Discharge does not occur in pre-heating, which means that in radiating electromagnetic waves, the engine acts as a passive antenna that converts conduction radiation from the power conditioner into electromagnetic radiation. At under 10MHz, values indicated in the figure for the wider analyzed band width are about 10dB higher than the rest. This suggests that electromagnetic radiation in this frequency range is not a random type but actually an impulse type. Normalized as an impulse type, the actual strength of electromagnetic radiation is about 90-100dBMV/m/MHz. That heater current is a 5kHz rectangular wave alternate current and that radiation measured with narrower width of spectrum-analyzed band contained impulses at 10KHz intervals indicate that this radiation is due to the heater current supplied by the power conditioner. Peak in the radiation strength appears around 6MHz also in pre-heat condition, suggesting the influence of the power conditioner.

Fig. 3.26 shows the distribution of radiation strength during discharge. The peak around 15MHz, observed during beam acceleration, appears here also and is assumed to be caused by the discharge phenomenon.

Fig. 3.23 Layout of Electromagnetic Interference Measurement Device

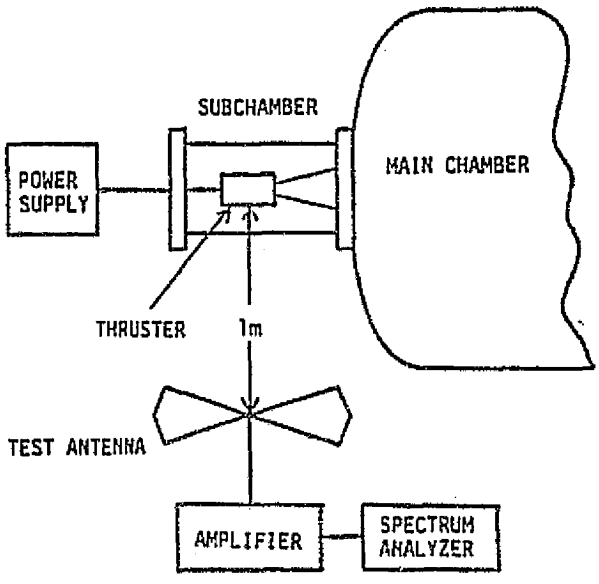

Fig. 3.24 Electromagnetic Radiation in The Broad Band During Acceleration

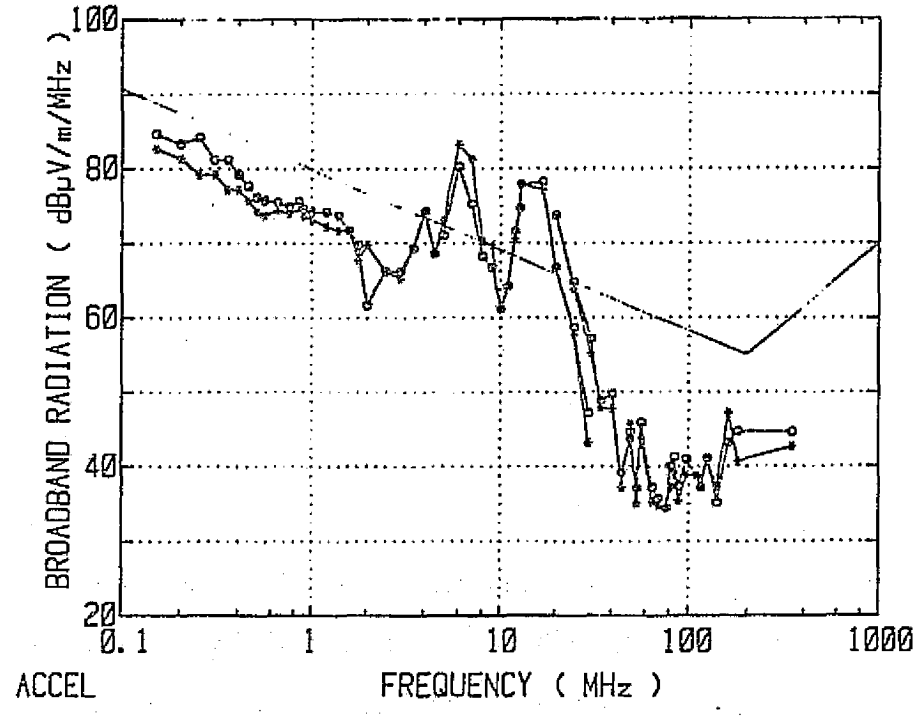

Fig. 3.25 Electromagnetic Radiation in The Broad Band During Pre-heating

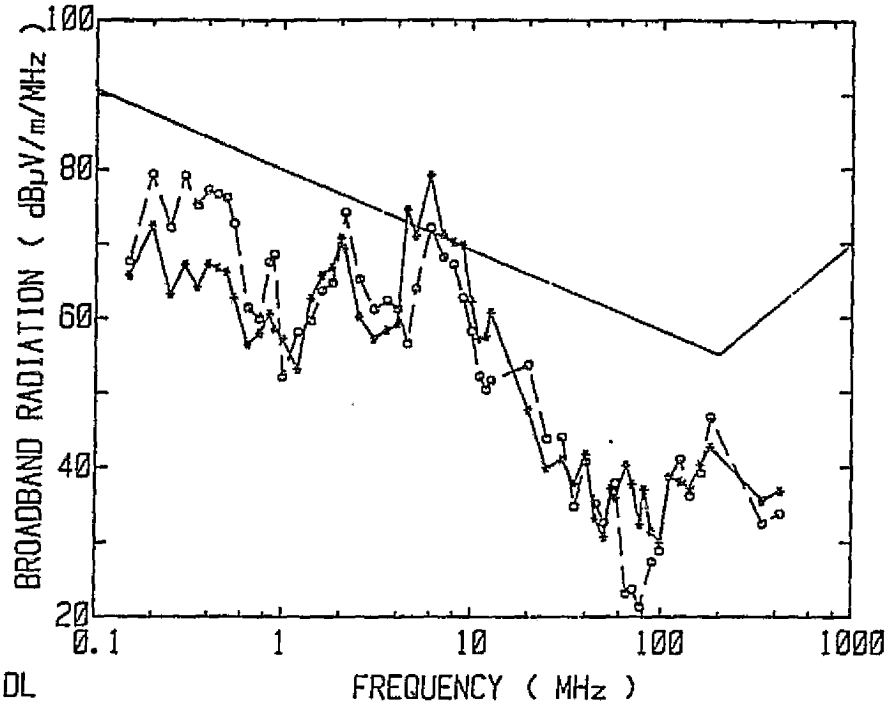

Fig. 3.26 Electromagnetic Radiation in The Broad Band During The Time Discharge Is Maintained

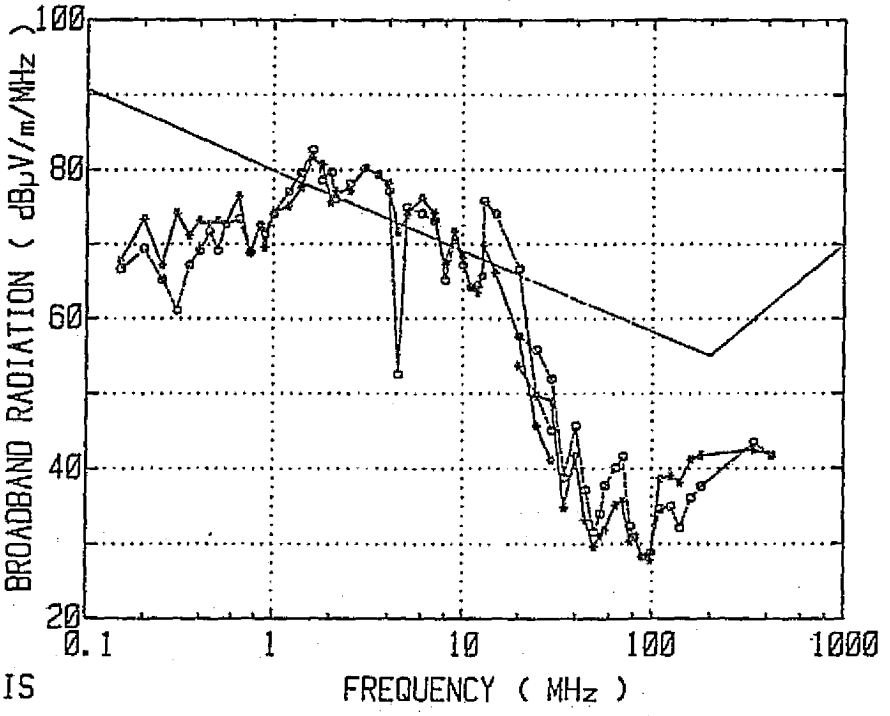

Reference materials

1) Nakamura, Azuma and Miyazaki, NAL TR-326, 1973.
2) " " " " TR-398, 1975.
3) Kudo, Murakami, Kozeki, Nakayama, Journal of Aeronautics & Space, Japan, 19, P43, 1970.
4) I. Kudo, H. Murakami and K. Nakayama, Proc. of 9th ISTS, P99, 1971.
5) NAL and ETL, Study on Electronic Equipments for Engineering Test Satellite III, 1975.
6) Y. Nakamura, AIAA Paper No. 76-1046, 1976.
7) Y. Nakamura, K. Ishihara and K. Miyazaki, Proc. of 12th ISTS, P433, 1977.
8) Y. Nakamura, K. Ishihara, K. Kitamura and K. Miyazaki, AIAA Paper No. 78-680, 1978.
9) Y. Nakamura and K. Kitamura, Acta Astronautica Vo. 7, P1, 075, 1980.
10) NAL/NASDA, Report on Joint Research: Studies on Testing and Evaluation of Ion Engine System(I), 1981.
11) Y. Nakamura, K. Ishihara, K. Miyazaki and Y. Yamagiwa, IAF-80-G313, 1980.
12) H. Azuma, Y. Nakamura, K. Ishihara and K. Miyazaki, AIAA Paper No. 78-700, 1978.

3.3 Power Conditioner

Power conditioner receives power from the power source system of a satellite, and generates, supplies and controls current and voltage required by the engine unit. In this section, necessary functions of a power conditioner and its test production in the research and development stage are discussed.

3.3.1 Functions of Power Conditioner

Power conditioner must receive DC power from the power source system of an artificial satellite, and generate and supply currents having various AC and DC voltage/current characteristics required by the engine unit. Fig. 3.27 is the block diagram showing the connections between the power supply and the engine unit. Table 3.2 shows voltage/current characteristics of each power source.

3.3.2 Pre-Engineering Model

PreEM was developed as a way of summarizing all the studies done on the power conditioner thus far. Objectives of the development were for the power conditioner to 1) completely control the engine unit and 2) satisfy interface conditions with the satellite. From the actual design point of view, the objectives were as follows.

1) For each power source to have necessary and satisfactory functions.

2) To reduce power consumption.

3) To reduce weight while taking various mechanical environments expected on board into consideration.

4) To prevent errors by taking countermeasures for noise, while taking electromagnetic compatibility on board into consideration.

5) To improve engine starting characteristics so that steady-state condition can be achieved in as little time as possible.

Mainly out of noise consideration, the power conditioner was separated into a power source device which is a collective unit of power sources and a power source control device which is the sequence logic unit. Appearance of the PreEM power conditioner is shown in Fig. 3.28.

Fig. 3.27 Connections Between Ion Engine and Power Conditioner

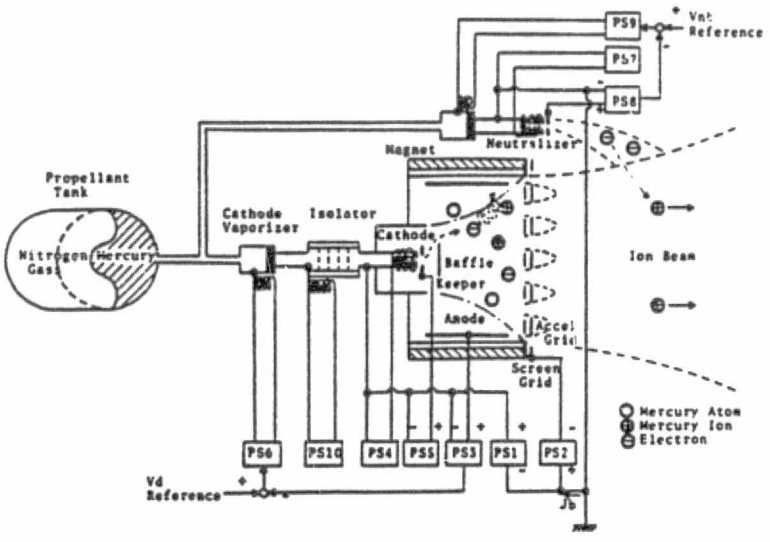

Fig. 3.28 PreEM Ion Engine System (From left, power source control device, power source device and ion engine)

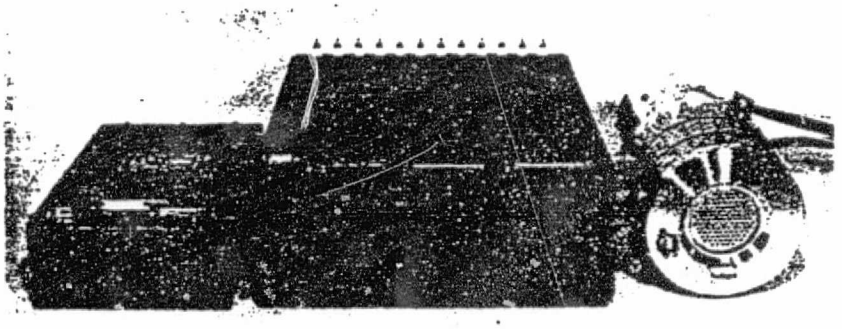

Table 3.2 Electrical Specifications of Power Source Device

PEM Rated Values

Rated output

Power source #		Name	定格出力 レベル	電圧 Voltage Level	電流 Current	電力 Power	ピーク リップル Peak ripple	レギュレーション Regulation	
PS 1	PS hv	Beam	N. L	1KV	30mA	30W	3%	2%	800~1400V constant voltage
			M. L	1.4KV	35mA	49W			50mA limiter
PS 2		Accel	N. L	−1KV	1mA	1W	3%		PS1と連動 Linked to PS1
			M. L	−1.4KV	3mA	4.2W			
PS 3	PS d	Disharge	N. L	42V	0.35A	14.7W	2%	1%	0.3~0.5A
			M. L	45V	0.5A	22.5W			F. G. 短絡時60W at no load
PS 4	PS ch	Cathode heater	N. L	5V	5A	25W	AC		F. G
			H. L	6V	6A	36W			
			I. L	1.6V	2.5A	4W			
PS 5	PS ck	Cathode keeper	N. L	12V	0.3A	3.6W	2%		Drooping characteristic
			S. L	300V	5mA	1.5W			F. G
PS 6*	PS cv	Cathode vaporizer	M. L	2.6V	1.5A	3.9W	AC	5%	Proportional control with closed loop limiter of 0.4-1.5A.
PS 7	PS nh	Neutralizer heater	N. L F. L	5V	5A	25W	AC		N. L, F. L — output terminal switched by a relay.
			I. L	1.6V	2.5A	4W			
PS 8	PS nk	Neutralizer keeper	N. L	24V	0.25A	6W	2%		Drooping characteristic
			S. L	300V	5mA	1.5W			
PS 9	PS nv	Neutralizer vaporizer	M. L	2.6V	1.5A	3.9W	AC	5%	Proportional control with closed loop limiter of 0.4-1.5A.
PS 10	PS is	Isolator	N. L	3V	1A	3W	AC		F. G
			M. L	5V	1.6A	8W			

N. L ; Nominal Level
I. L ; Idling Level
M. L ; Maxium Level
H. L ; High Level
S. L ; Start Level
F. L ; Filament Level
F. G ; Floating Ground

*Changed to 3.5V, 2A, 7W in the improved PEM.

3.3.3 Power Source Device

To obtain the voltage/current characteristics as shown in Table 3.2, power conditioner is consisted of 4 DC-DC converters and 5 DC-AC converters. As each power source uses a switching regulator, a master oscillator is used to integrate oscillation circuits for all power sources so that they do not interfere with one another. Design of the power source device is shown in Fig. 3.29. Each power source is explained below.

(1) High voltage power source

Once separated into a beam power source and accelerator power source, high voltage power sources were incorporated into one regulator generating power for both, in order to reduce weight. It is a DC constant voltage power source and variable on command. Variable range is between 800V and 1,400V. Being a high voltage constant voltage power source, it has a protective circuit against beam current. It is a drooping characteristic whereby the voltage lowers when the beam current exceeds 50mA. Accelerator current has 50kΩ resistance connected in series which provides excess current protection. For protection against high voltage dielectric breakdowns which are thought to be caused by unstable plasma, it has a logic circuit which switches off high voltage and vaporizer power sources. As a similar phenomenon occurs when the high voltage power source is on, a time constant is set so that it does not function in such a case.

(2) Discharge power source

Various methods for stabilizing had been studied for this power source which directly controls plasma formed inside the engine. Constant current DC power source was employed, with its current variable on command for control of plasma density. Variable range is

0.3-0.5A. With mercury as a propellant, voltage was set at 60V at no load. Also, feedback signals were sent to ground level via VF-FV converter in order to be on the high voltage power source. This insulator amplifier circuit sometimes made errors depending on the discharge current waveform, and was later changed to an AM modulation method. It incorporates a feedback loop which controls the main cathode vaporizer power source in such a way that the discharge voltage stays constant, using the characteristic that this potential decreases when the flow increases. Control method is that of proportional control, with upper and lower limiters. Setting of the discharge voltage is variable on command. Fig. 3.30 shows the characteristics of the feedback loop.

(3) Main cathode heater power source

This power source is for heating the tip of hollow cathode to cause an emission of heat electron which becomes the starter of a keeper discharge. It has an idling level for pre-heating the engine unit, heating while discharge is being stabilized and for draining excess mercury inside the cathode when stopped. Its high level is for assisting the cathode when its characteristic deteriorates. The power source is a 5KHz, DC-AC inverter of unstable type constant voltage with a current limiter. For efficiency purposes, it operates at a 50% duty at a steady load. Originally designed with a constant current, the power source incorporated these changed in order to simplify the circuit and to avoid use of unapproved parts. With the elimination of a complex control loop, structure was simplified and its weight was reduced.

(4) Main cathode keeper power source

This power source is for maintaining the keeper discharge of

hollow cathode. It is a DC power source of 300V at no load and 12V, 300mA, at the rated load. Its voltage/current characteristic is shown in Fig. 3.31. This power source also switches to 50% duty for maximizing efficiency. In order to produce the desired characteristic, the power source uses a transistor switch for selecting between the two different output both having a drooping characteristic. The switch replaced two sets of choke coils originally used, for efficiency and weight reduction purposes.

(5) Insulator heater power source

This is the power source for heating the insulator, to prevent mercury condensation around it. It is a 5KHz AC power source of unstable type constant voltage output, and it has a high level output for countering high voltage dielectric breakdowns in the insulator.

(6) Main cathode vaporizer power source

This is a heater power source for vaporizing liquid mercury. Flow of the propellant is controlled here. As mentioned earlier, it is an AC constant current power source with a limiter, controlled by the discharge voltage. Feedback loop for constant current is formed by squaring the current transformer signals by RMS/DC converter and taking the average value.

(7) Neutralizer heater power source

This power source is similar to the main cathode heater power source. The difference is that it has a filament mode instead of high level output. In this model, the ion engine has a hot filament in addition to the hollow cathode neutralizer for neutralizing beams. For this reason, it has a relay for switching to large current. The filament was eliminated from EM on.

(9) Neutralizer vaporizer power source

This is a heater power source which controls the flow of mercury to the neutralizer. It is basically the same as the main cathode vaporizer power source except that its feedback signal is the neutralizer keeper voltage and the set values cannot be changed on command.

Fig. 3.29 Structure of Power Source Device

1. Bus line
2. Auxiliary power source unit
3. Master oscillator unit
4. Standard voltage
5. Level control signal
6. Protective logical circuit unit
7. Telemetry exchange unit
8. Monitor circuit unit

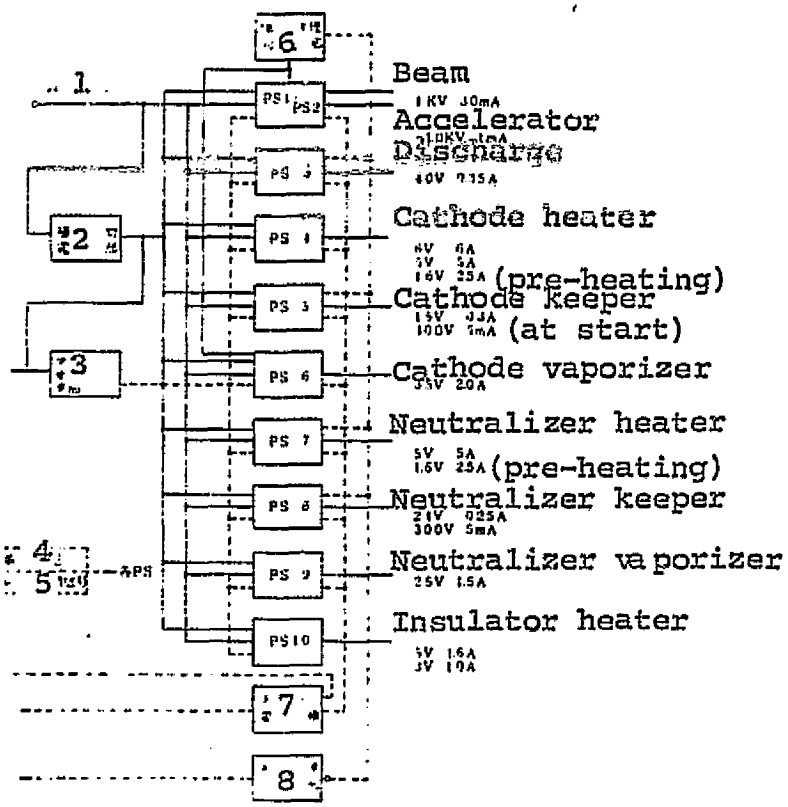

Fig. 3.30 Discharge Voltage Control Loop

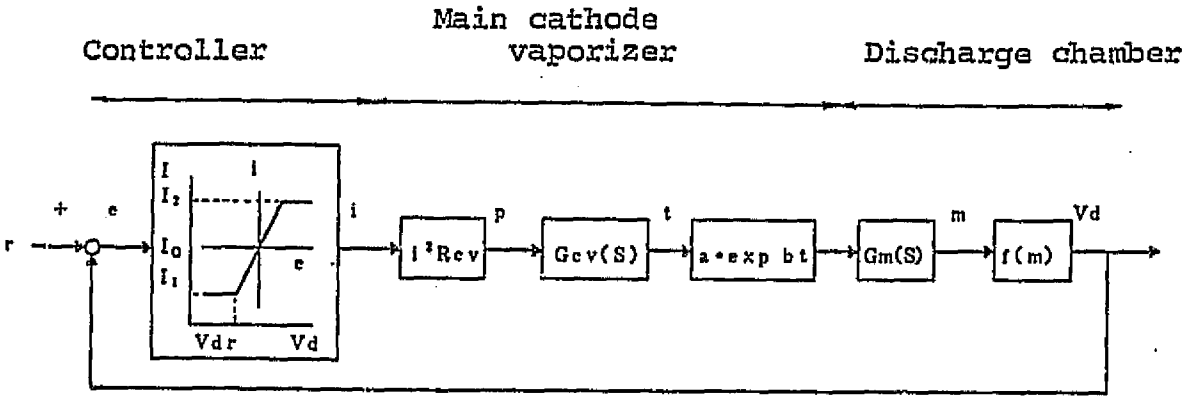

$I_1 = 0.4$ A, $I_2 = 2.0$ A
ゲイン 0.5 A/V gain

Fig. 3.31 Characteristic of Main Cathode Keeper Power Source

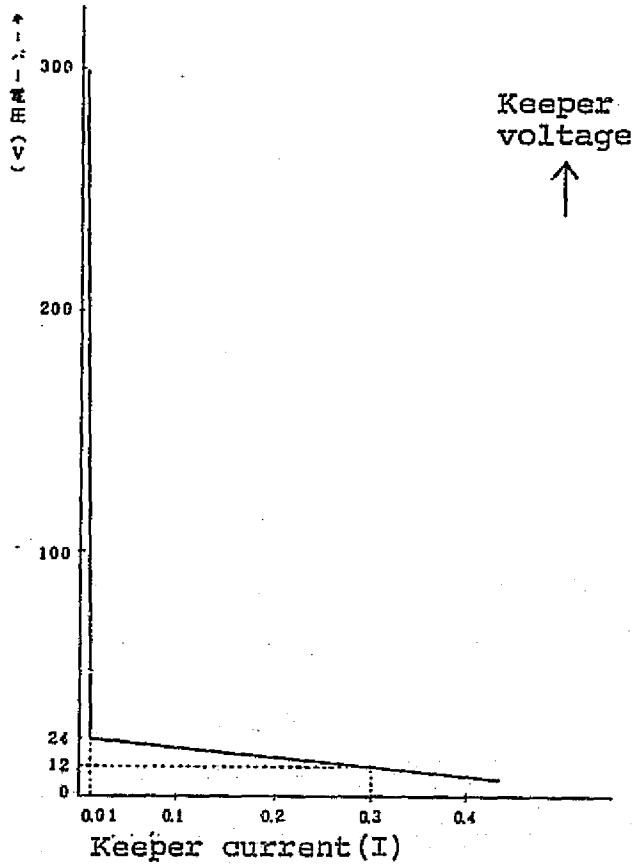

Fig. 3.32 Characteristic of Neutralizer Keeper Power Source

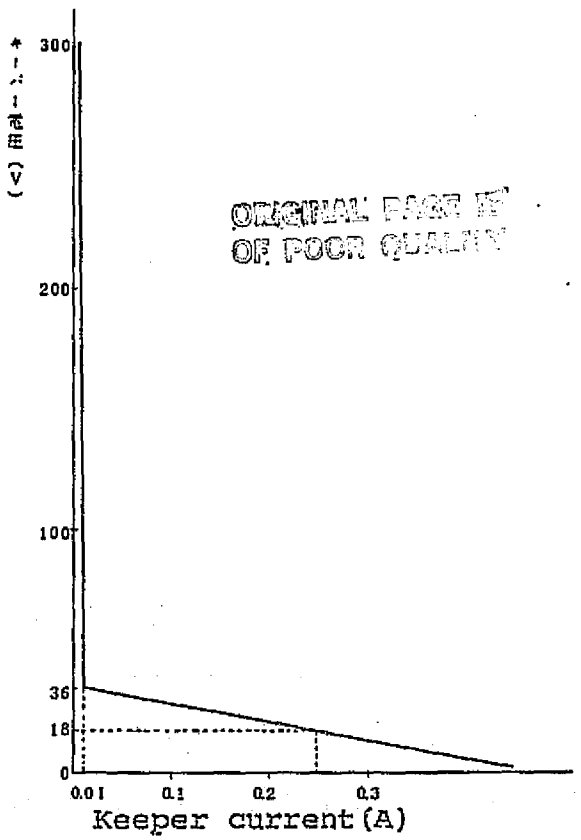

3.3.4 Power source control device

Power source control device has the function of controlling the power source device on command from the satellite. In this device, necessary power is internally generated, rather than received from the power source device. Min functions are:1) to receive commands from the satellite; 2) to generate the sequence flow which switches on/off each power source inside the power source device necessary for engine operation; and 3) to communicate sequence conditions to the satellite.

Each function is explained below.

(1) Command interface unit

This unit receives 4 discrete and 4 magnitude commands and generates signals required by the power source control device. Discrete commands are 28V DC signals which activate a latching relay. Magnitude commands are 16-bit TTL serial signals, and one of the commands is for selecting the engine operation mode. The unit also receives solar modulation signals. Commands are listed in Table 3.3.

(2) Power source control unit

Power source control unit switches on/off each power source inside the power source device by running a sequence flow in response to each signal received in the command interface unit and the action of each power source in the power source device. The sequence flow is shown in Fig. 3.33. This complex flow was produced by incorporating a logic IC. The flow is modulated by clock pulses, but the clock stops during 'timer wait' and steady-state conditions to prevent errors by the engine noise. It is possible to use a VLSI such as micro CPU, but there was no appropriate flight-proven product available at that time and thus an ordinary logic IC was used.

(3) Sequence status unit

This unit converts ST signals which show the progress of the sequence flow and dielectric breakdown circuit from the power source device into binary signals of 8-bit each and sends them out as serial binary codes each totalling 16 bits.

Table 3.3 PEM Commands

Type	Item	Command	
Mode selection*	NH Mode	Hollow cathode used in neutralizer	NR=0
	NF Mode	Filament used in neutralizer	NR=1
	OB Mode	Beam injection	OR=0
	OH Mode	Hollow cathode operation test	OR=1
	CN Mode	Nominal level of cathode heater	CR=0
	CH Mode	High level of cathode heater	CR=1
	IN Mode	Nominal level for insulator heater	IR=0
	IH Mode	High Level of insulator heater	IR=1
	SN	Prohibit solar tuning	SR=0
	SS	Solar tuning mode	SR=1
	FC	Automatic continuation of sequence flow	FR=0
	FH	Stop sequence flow	FR=1
Execution commands**	Start 1	Start engine	
	Shut Off	Stop Engine	
	Idling	Pre-heat engine	
	Continue	Continue sequence (Start beam injection)	
Reference*	Vn	Beam voltage	
	Id	Discharge current	
	Vd	Discharge voltage	

* Magnitude commands
** Discrete commands

Fig. 3.33 Sequence Flow

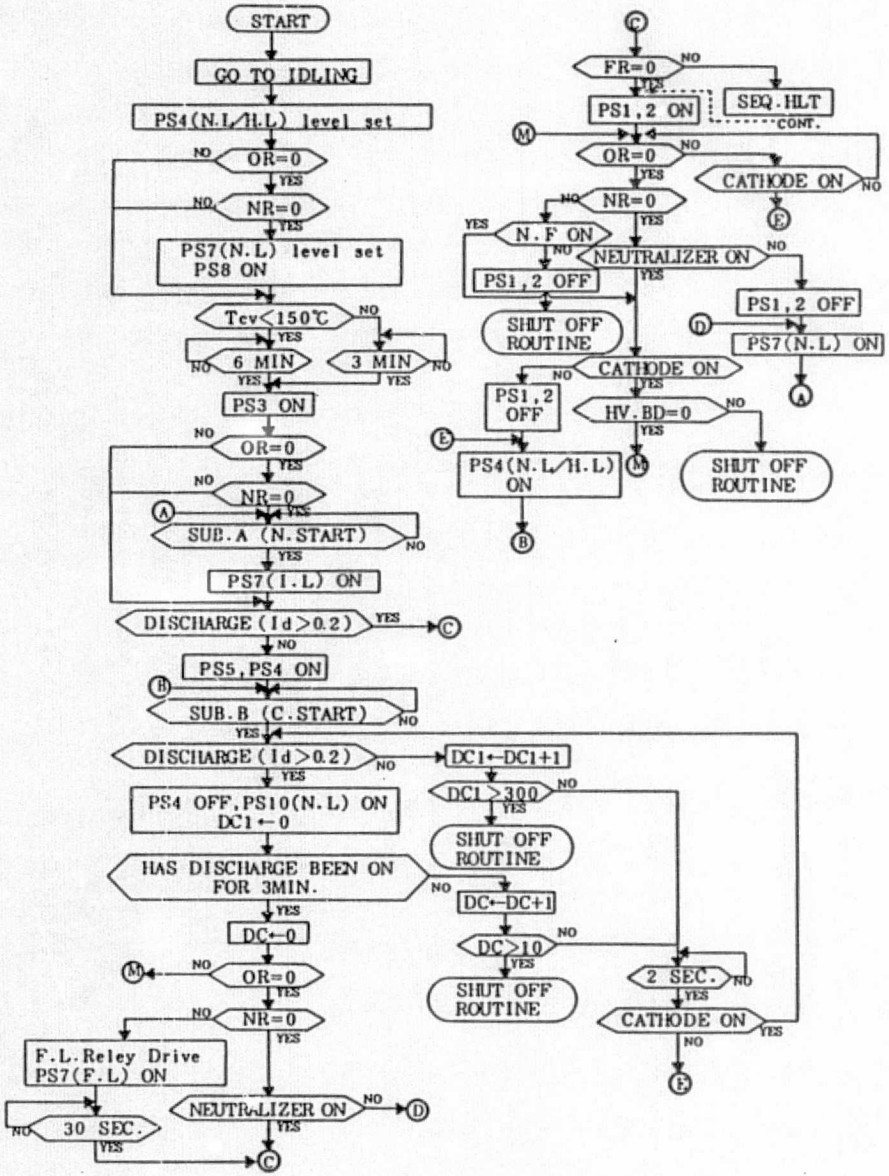

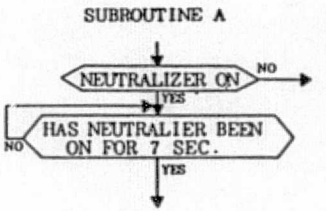

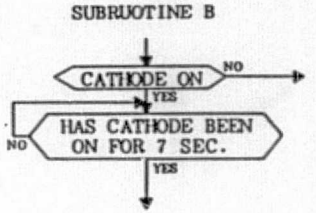

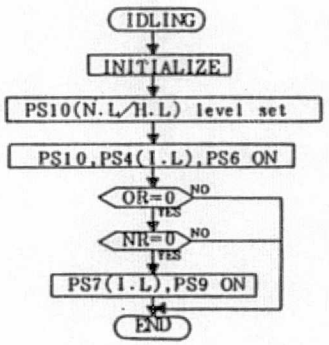

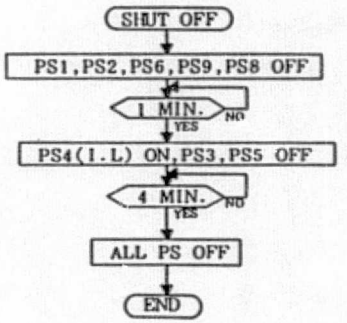

3.3.5 Measures for Thermal Vacuum

High voltage area and other areas inside the power source device which are floated by high voltage were potted with epoxy material. Potting material was light weight, containing micro-balloons and with a specific gravity of 0.78. The switching transistor for large power source was installed on a heat sink which was thermally connected to the base plate, and other ICs with large calorific values were also thermally connected to the base plate. The frame was coated with black paint on both sides, the back side especially for absorbing heat radiated from the substrate. In the absence of a suitable connector for the output source of high voltage power source and those power sources which become floated, a flying lead wire was soldered to the high voltage terminal.

3.3.6 Countermeasures for Noise

Emphasis was placed on lowering transmitted noise. Ripples, caused by switching, were reduced in the power line, except in AC, from the power source device to the engine unit. This was done by adding a condenser and choke coil to the output, a task requiring caution due to weight factor. In the power line from the satellite, a filter was placed at the entrance to the frame to prevent reverse flow of noise. As mentioned earlier, the sequence flow was modulated with the clock, with stops during timer wait and monitor modes to avoid errors in the power conditioner.

3.3.7 Mechanical Structure

Mechanical structure was not given major emphasis. A simple structural analysis was made.

3.4 Sub-system[1)]

In an ion engine system, interface between the engine unit and the power conditioner and between the satellite and the engine system are the major consideration. Here, improvements made on each interface and tests performed are discussed. PreEMs of the engine unit and power conditioner were used.

3.4.1 Heat Design Around Main Cathode Vaporizer

The problem here was that due to an insufficient temperature increase in the main cathode vaporizer, engine did not operate within the rated heater power. As countermeasures, 1) lower flow pipe in the vaporizer was extended in attempt to gain as much heat resistance as possible, and 2) a heat shield was installed around the vaporizer and insulator in order to cut the loss due to heat radiation. On the power source side, maximum rated power of the vaporizer heater power source was increased from 4W to 7W. These measures successfully eliminated the problem. In addition, some modifications were planned inthe sequence flow at the start of the engine for the development models.

3.4.2 Stabilization of Main Discharge

There were two problems. One was that discharge sometimes became intermittent, causing much difficulty in beam injection. The other was that this caused errors in the discharge power source. For the latter, it was discovered that errors occurred in the feedback signals for converting the power source into a constant current power source which are insulated by VF-FV converter, especially when the frequency of discharge waveform approached the modulation frequency, and incorrect output was resulted. To eliminate this problem, AM

modulation was employed instead. Cause for the former problem was estimated to be that the plasma impedance in the discharge chamber became a negative resistance at the beginning of discharge, which resonated with a smoothing capacitor in the power source output. To prevent it, output impedance need only to be changed from capacitive type to inductive type. For this purpose, capacity of the smoothing capacitor was reduced from 50μF to 1.5μF and choke coil was increased from 1.2mH to 15mH. Main discharge was completely stabilized by these measures. Main discharge power source consumes much power, and its stabilization without power loss was a significant accomplishment, contributing greatly to the subsequent development efforts.

3.4.3 Improvements on Transient Response

The problem was two-fold. First, transient response characteristic of PS1 made the engine inoperable. Next, there was a possibility that the current rise characteristic and peak current expected to be required by the ETS-III power source system were exceeded.

Inoperable engine conditions occurred at the closing time of high voltage. It was because regulator characteristics caused the maximum voltage to be applied, and it was applied too fast, causing a high voltage dielectric breakdown or disappearance of main discharge. Beam injection was impossible under these conditions. Improvements were therefore made in the way high voltage was applied, so that it would rise rapidly until it reached 800V where plasma around the grid stabilized and then slowly increased to the desired level. The rise was set also not to exceed the input current increase characteristics required by the satellite. Discussed next are the current rise characteristic (about 100,000 A/sec) and the peak current (5A) expected to be required by the satellite. Possible situations

in which they may be exceeded are during bus line closing time and main discharge ignition. Both were exceeded at the bus line closing time, as capacitors on the primary side of each power source were charged. In order to correct the situation, it was necessary to install a choke in the input unit as well as to send the current via a limiting resistance during input. As this was structurally difficult in the EM, it was planned to be incorporated into design from the development model on. At the time of main discharge ignition, the problem phenomenon was that of the peak current exceeding 5A when the main cathode keeper ignition and main discharge occurred at the same time. Especially in the PreEM engine, elimination of this phenomenon was absolutely necessary because all ignitions were simultaneous. The answer was to limit the main discharge current. For this purpose, high-speed current-limiting circuit was added to the primary side of discharge power source to maintain the peak current under 5A. However, depending on the time constant chosen, this circuit sometimes caused a parasitic oscillation in the switching regulator, creating a condition where control was impossible(PM). At this point, however, it did not become a problem.

3.4.4 Protective Logic

Neutralization failure due to a high voltage dielectric breakdown or neutralizer failure could become a serious problem not only in the engine alone but for the satellite. Protective logical circuit was necessary for this reason. Its useage, however, involves some difficulties. High voltage dielectric breakdowns can occur between grids by unstable plasma, a short-circuit due to flakes generated inside the engine, or by an internal breakdown of the insulator. A common countermeasure for these occurrence is to drop the high

voltage power supply. However, transient excess current flows at the closing time of high voltage power source, at which time such protective logic need to be prohibited. In view of the flow rate, prohibition time was set to be one second. Neutralizer breakdown mode, incorporated into the logical sequence inside the power source control device, could also be effective in the hardware inside the power source device. Although not realistic in PreEM, it was planned to be incorporated in the EM and subsequent models.

3.4.5 Countermeasures for Noinse in the Logical Control Circuit

Despite the measures taken, errors occurred in the logical sequence circuit inside the power source control device. They occurred during ignitions of neutralizer hollow cathode, main cathode hollow cathode and main discharge, and high voltage dielectric breakdown. The cause is the large amount of energy released at the start of discharge. To reduce the energy, it would be sensible to reduce the capacity of the output capacitors of power sources involved in the discharge so that not as much energy would be released. The parts having been potted, the PreEM could not accommodate such a measure. Also, insulating the power source and signal lines would prevent noise in the power source line from interfering with signals, which was another measure difficult to be taken at this time. Thus, both were planned to be reflected in the designs of later models. What was possible in PreEM was to add a resistance and capacitor in the signal line as a filter in the power source control device. This accomplished a fair result, reducing errors by noise.

Table 3.4 shows a summary of problems in the PreEM and countermeasures taken.

Table 3.4 Problems in PreEM and Countermeasures

Problem		Countermeasure
Heat design around CIV	•Engine inoperable within the rating due to insufficient temperature increase in vaporizer.	1) Pipe on the lower flow side of vaporizer extended and heat shields installed on vaporizer and insulator. 2) Maximum rated power of PS6 changed from 4W to 7W. 3) Sequence control flow changed (electrical and thermal matching)
Stability of main discharge	•PS3 sometimes caused errors when discharge was unstable. •Occasional intermittent discharge caused impossible beam injection.	4) Insulator amplifier circuit changed (from VF/FV exchange method to AM modulation method). 5) Output filters of PS3 matched (L=1.2mH, C=50μ , F→L=15mH, C=1.5μF).
Transient response	•Iin > 5A, dIin/dt > 10^5A/S when IES power supply thrown in. •Iin > 5A at main discharge ignition. •Dielectric breakdown when high voltage is thrown in.	6) Choke and switch-type dumping resistance added to bus line. 7) Fast-response type current limiting circuit added to the primary side of PS3. 8) PS1/2 thrown in slowly.
Protective logic	•High voltage dielectric breakdown protective logic and grid system transient response incompatible. •Reliability of protection of neutralizer breakdown mode.	9) Recycle protective logic prohibited at PS1/2 closing time only and setting value between current limiters changed. 10) Protective logic for fast-response added, to result in a redundant system.
Logical control circuit	•Faulty actions at ignition of neutralizer, cathode and main discharge, and at dielectric breakdown.	11) Capacity of output condensers in PS3, 5 and 8 reduced (1/3 to 1/30). 12) R and C added to signal lines of command interface to counter noise. 13) Clock stop circuit added (after high voltage thrown in). 14) Power source line and signal line insulated.

Table 3.5 Typical Performance Values of PreEM Ion Engine System

		Nominal	Maximum
Beam Voltage	Vn(kV)	1.0	1.4
Beam Current	Jb(mA)	28.4	36.8
Accelerator Voltage	Va(kV)	1.0	1.4
Accelerator Current	Ia(mA)	0.3	0.4
Discharge Voltage	Vd(V)	40.4	40.0
Discharge Current	Id(A)	0.380	0.500
Cathode Keeper Voltage	Vck(V)	13.5	13.2
Cathode Keeper Current	Ick(A)	0.320	0.330
Cathode Vaporizer Voltage	Vcv(V)	2.35	2.25
Cathode Vaporizer Current	Icv(A)	1.36	1.30
Neutralizer Keeper Voltage	Vnk(V)	21.5	21.5
Neutralizer Keeper Current	Ink(A)	0.275	0.275
Neutralizer Vaporizer Voltage	Vnv(V)	0.7	0.7
Neutralizer Vaporizer Current	Inv(A)	0.4	0.4
Isolater Voltage	Vis(V)	3.0	3.0
Isolator Current	Iis(A)	1.0	1.0
Thruster Input Power	Pth(W)	60.8	88.8
IES Input Power	Pin(W)	92	128
Thrust	F(g)	0.186	0.287
Specific Impulse	Isp(s)	≈1866	≈1831
Mass Flow Rate	ṁ(g/h)	≈0.36	≈0.34
Propellant Utilization Factor	η_m	≈0.59	≈0.81
Ion Production Cost	D(ev/ion)	540	543
Energy Efficiency Jb·Vn/Pin	η_e	0.51	0.40
Overall Efficiency	η_T	≈0.18	≈0.33

Fig. 3.34 Operating Time History(PreEM)

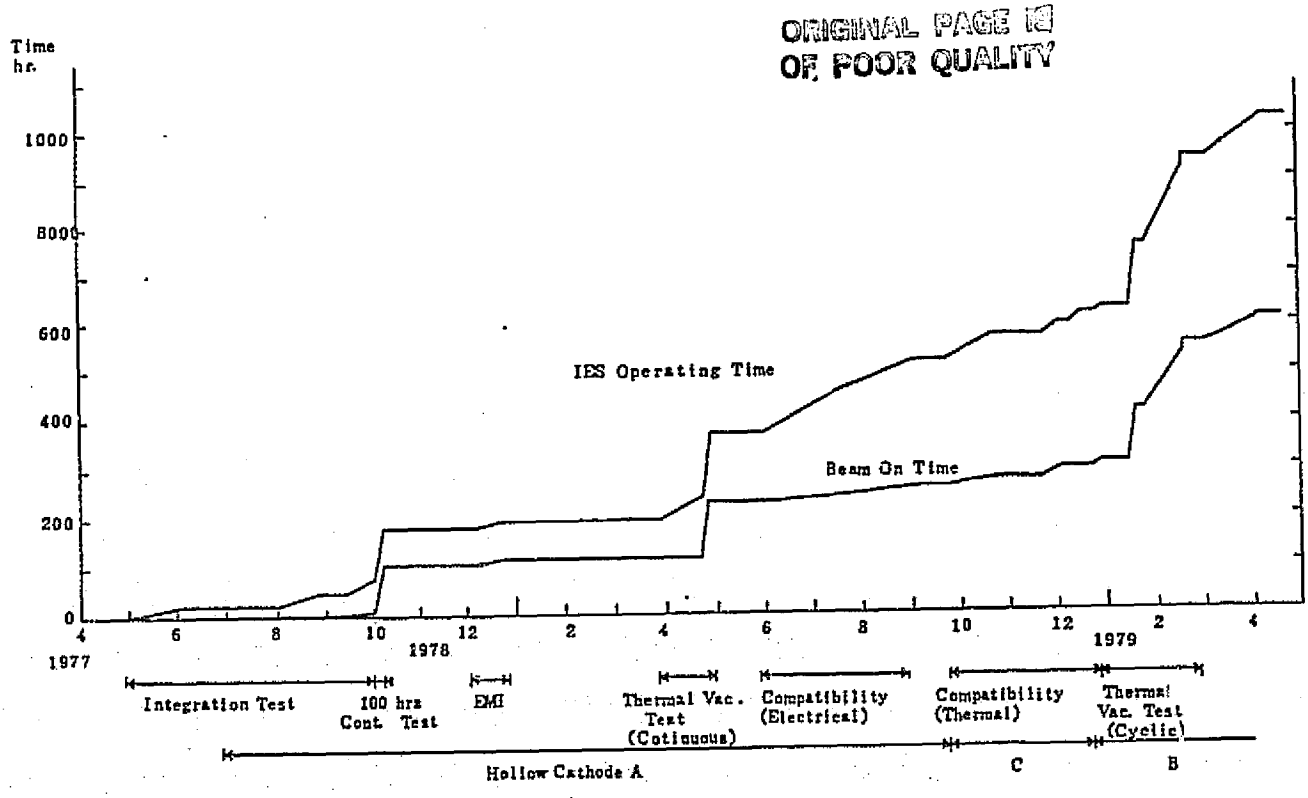

3.4.6 PreEM Tests

With improvements described in the preceding sections made, PreEM reached a fairly satisfactory performance level.[5] Thermal vacuum test, 100-hour continuous test and 100 repetition test[1] were given. Fig. 3.34 shows the operating time history under these tests. Accumulated test hours reached over 1,000 hours. Typical characteristics and performances are shown in Table 3.5.

(1) Thermal vacuum test

This test was given at the mount surface temperature of 20-55C. The reason was not only the limitation of the test device but also to find out how each internal part in the power conditioner held out at high temperature. The temperature was increased to the maximum of 55C, and stability was maintained without such problems as breaking.

(2) 100-hour continuous test

The test was given on the assumption that the satellite was on the full sunshine orbit. Operation was continued after 100hours, but halted after 120 hours due to problems in the test device. Ion engine system itself was stable, with no signs of trouble.

(3) 100 repetition test

On the assumption that the satellite rotates around on a 1,000km orbit, repetitions of 70-minute operation under sunshine each followed by a 35-minute rest were performed. A fuse was blown on the primary side of the neutralizer vaporizer power source in the early stage, but the heat input from the neutralizer cathode was large enough that operation was continued. With one time exposure of the engine to air for inspection after 76 cycles, 100 repetitions were completed successfully.

As a result, it was found that there were some problems in the heat design around the neutralizer.

3.4.7 Development Support Systems

With operation in a vacuum so central to ion engines, a vacuum chamber was a mandatory test device. Especially in the system test, both the engine and the power supply system needed to be placed in a vacuum, requiring the device to be so equipped. However, operating the engine for the purpose of checking the power source system not only increases turnaround time but makes it difficult to concentrate on either the engine or power system. Here, an ion engine simulator used for this reason, as well as the vacuum chamber for system tests and the test monitor system, are explained.

(1) Ion engine simulator[3)]

Ion engine has two principal characteristics based on its operating principles: one is the plasma characteristic and the other is thermal characteristic which affects the engine's propellant supply. Because of its response speed, plasma cannot be simulated by ordinary electronic ciruits. However, a model load could be used for simulating a steady-state condition, and simulation of transient response seemed possible to an extent by use of a discharge pipe. Also, thermal response, model of which was easily made, because of a long time constant, was used in determining the steady-state plasma load. A micro-computer was used for calculation and the resulted load was a dynamic load with a transistor. This greatly shortened the power source development process and also played an important role in determining a heat model of the engine.

(2) Vacuum chamber[4)]

Vacuum chamber is shown in Fig. 3.35. With the system test requirements in mind, a shield room was installed around the sub-chamber to facilitate measurement of magnetic noise. The sub-chamber

also had many ports to facilitate installation of various feed-through items. The chamber itself had an effective inner diameter of 800mm and effective length of 2,500mm, and 2 liquid nitrogen shrouds, and its target part, with a fin planted at 45C, formed a molecular sink. Exhaust speed was 2,500t/sec. in the sub-chamber, and the degree of vacuum reached using liquid nitrogen shrouds was 10^{-6} Pa. The same device was later used in the subsystem tests of ion engine systems developed after EM.

(3) Monitor system[4)]

As mentioned earlier, an ion engine system has a complex sequence control and protective logic, and thus it is possible to operate as a completely independent system. When the whole system is in a vacuum, its conditions can only be known by telemetry data. A monitor system was therefore developed to obtain data and observe the engine system. With this system, unmanned operations over long periods of time became possible for the first time.

These support systems played important roles in the later development. The vacuum chamber, in particular, was used all the way to the sub-system testing of the flight model.

Reference materials

1) K. Machida., Y. Toda, H. Murakami, I. Kudo, AIAA Paper 81-0691.
2) Y. Toda, K. Machida, M. Hirata, H. Murakami, S. Goseki, I. Kudo, AIAA Paper 81-0755.
3) Machida, Toda, Murakami, and Kudo, Journal of Aeronautics & Space, Japan, 29, P488, 1981.
4) Toda, Machida, Murakami, Goseki and Ono, Proc. of 22th ISTS, P124, 1978.
5) Machida, Toda, Murakami and Kudo, Proc. of 23rd ISTS, P288, 1979.

Fig. 3.35 Vacuum Device for Ion Engine System Test

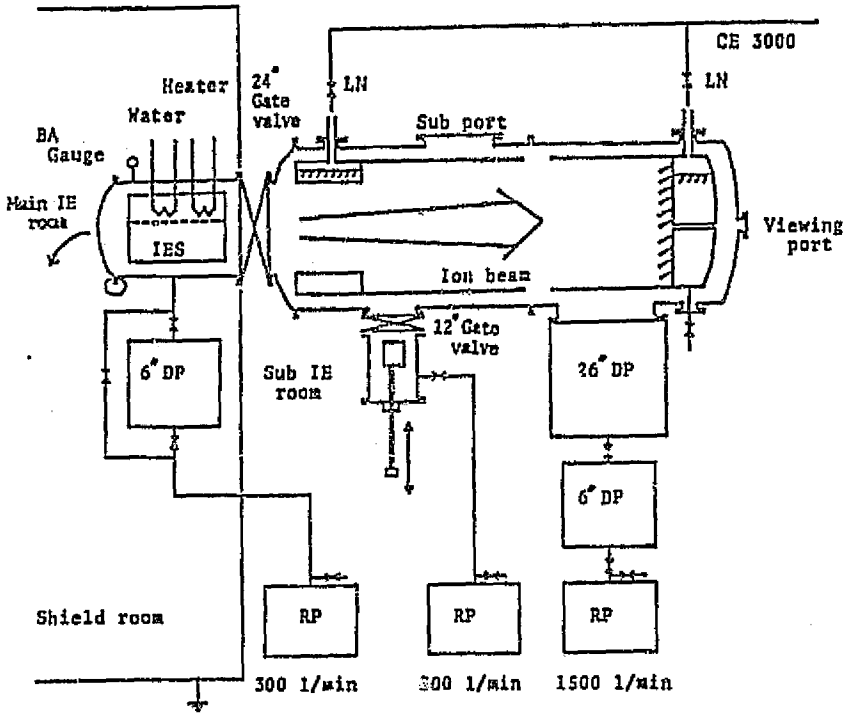

Chapter 4

Design and Development Tests

Chapter 4: Design and Development Tests

4.1 Specifications

Design specifications of ion engine system are given in the Development Specifications (NASDA-ESPC-41) and in the Specifications for Engineering Test Satellite III Interface Management (NASDA-ESPC-71). In these specifications, efforts were made to avoid duplications in order to simplify revisions after enactment: Development Specifications emphasize performances of ion engine system itself; and Specifications for Interface Management contain all necessary interface information while allowing satellite technicians to treat ion engine system as a black box. Development Specifications were written to serve as a reference guide for possible future use of ion engine system in the subsequent satellites as well.

Although technical management of the system was provided by the National Space Development Agency, ion engine unit was produced by Mitsubishi Electric Co. and Tokyo Shibaura Electric Co. (Toshiba) was in charge of power conditioner as well as incorporating the system. Therefore, in order to clarify the scopes of specifications, ion engine unit specification was treated as a supplement to the Development Specifications.

Designing ion engine was based on this Development Specifications, incorporating, for details, the test results of development models for finalization.

Summary of finalized specifications is given below.

4.1.1 Ion Engine System

Ion engine system(hereafter referred to as IES) will consist of engine unit(hereafter referred to as IEE) and power conditioner

(hereafter referred to as IEP). IEP will consist of power source device(IP) and power source control device(IR). The structural concept is shown in Fig. 4.1. IES, in other words, consists of 2 IEEs, 2 IPs which supply power to each IEE and 1 IR which controls IPs.

Components of IES and their functions are shown in Table 4.1 and Fig. 4.2.

Required performances of IES are given in Table 4.2. Weight distribution is shown in Table 4.3.

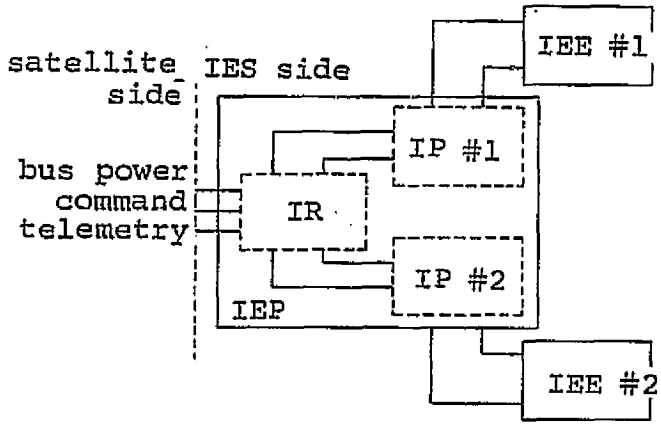

Fig. 4.1 Structure of Ion Engine System

Table 4.1 Diagram of IES Components

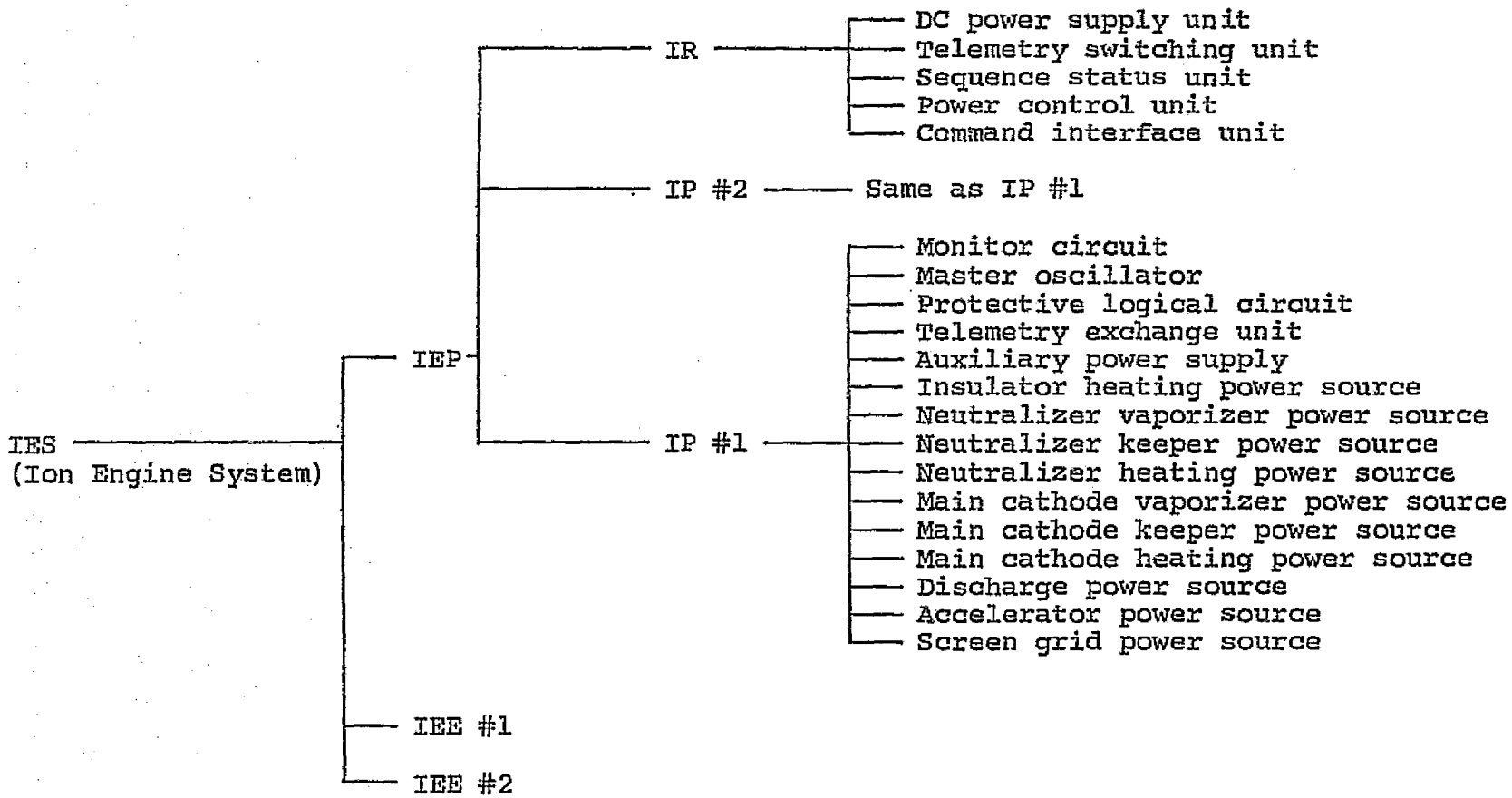

Fig. 4.2 Diagram of IES Functions

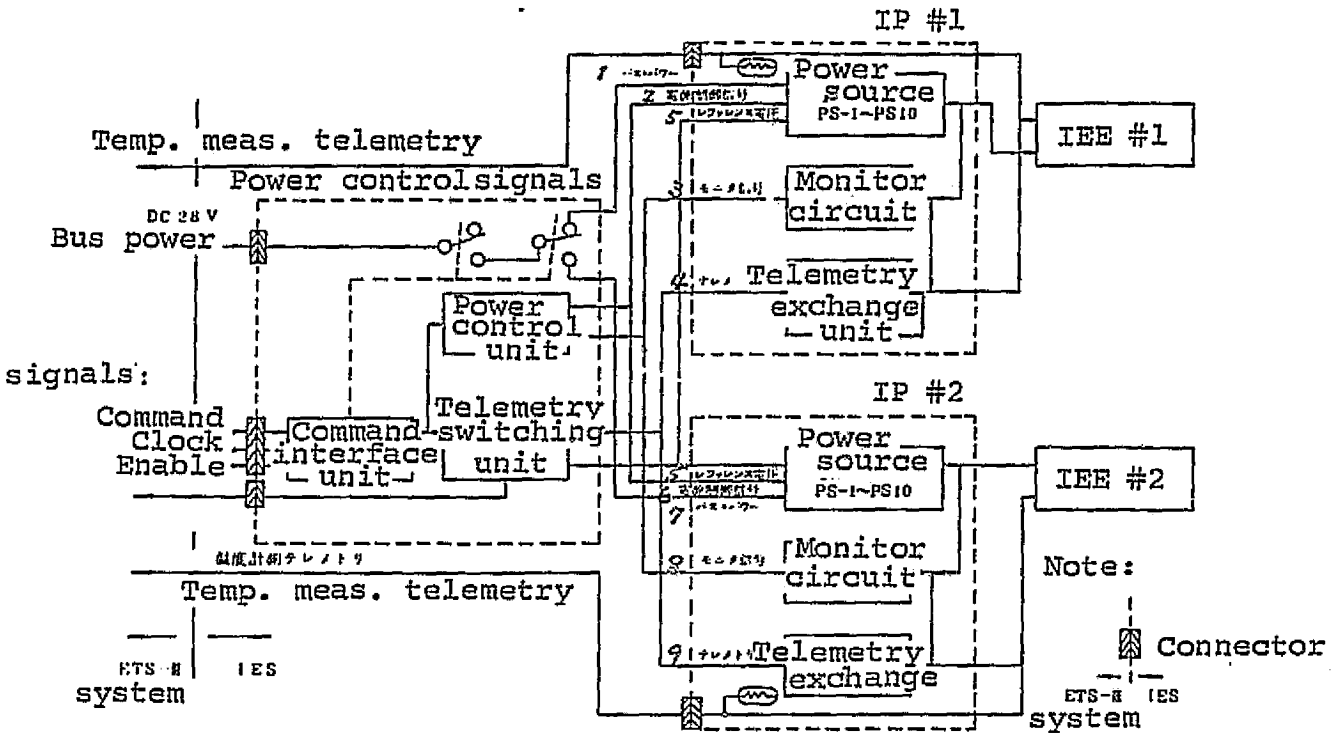

1. Bus power
2. Power control signals
3. Monitor signals
4. Telemetry
5. Reference voltage
6. Power control signals
7. Bus power
8. Monitor signals
9. Telemetry

Table 4.2 Required Performance of IES

Item		Required value
Thrust	推力	0.18±0.03 g
Specific impulse	比推力	2000±200 sec
Mass flow	流量	(1±0.25)×10^{-4} gr/sec
Propellant efficiency	推進剤効率	70±10%
Propeller power efficiency	推進機電力効率	44±5%
Power consumption:	消費電力	≦100W以下
engine unit	エンジン本体	≦68W以下
power control device	電源制御装置	≦5W以下
power source device	電源装置	≦27W以下

Table 4.3 Weight Specification of IES

Item	Quantity	Maximum wt. (kg)	Remarks
1. IEE	2台	3×2=6	Includes wire harness & 600g mercury
2. IEP	1式	17.06	Consists of 2.1 & 2.2
2.1 IP	1台	3.66	Includes wire harness
2.2 IR	2台	6.70×2=13.40	Includes wire harness
	Total	23.06	

4.1.2 Engine Unit

The shape and the center of gravity of IEE Unit #1 are shown in Fig. 4.3. Unit #2 will of the same structure, with the wire harness and permanent magnet inverted. This is because the two are installed symmetrically on the satellite. It also serves to offset residual magnetism.

Overall performance requirements will be as shown in Table 4.2. Item-by-item requirements are shown in Table 4.4.

Table 4.4 Engine Unit Item-by-Item Specification

* Weight (per unit) Less than 3kg (including 600±60g mercury weight)
* Shape & dimensions See Fig. 4.3
* Capacity of vaporizers of main hollow cathode and neutralizer hollow cathode for holding liquid mercury
  1×10^{-6} g/sec (10kg/cm^2 pressure and under ordinary temperature
* Leakage
  - Tank assembly: Less than 1×10^{-9} atm cc/sec He
  - Vaporizer joint: Less than 1×10^{-9} atm cc/sec He
* Withstand voltage
  - Insulator: Over 3 kVDC (in vacuum)
  - Electrode assembly: Over 3 kVDC (in vacuum)
  - Main hollow cathode keeper: Over 1 kVDC (in vacuum)
  - Neutralizer hollow cathode keeper: Over 1 kVDC (in vacuum)
* Temperature measurement - Temperature should be measurable at the following locations.
  - Tank: -40℃ ~ +150℃
  - Engine unit: -40℃ ~ +150℃
  - Main hollow cathod vaporizer: 0℃ ~ +400℃
  - Neutralizer hollow cathode vaporizer: 0℃ ~ +400℃
* Heater characteristics

Heater	DC resistance at 20℃	Temp.Coefficient
Main cathode heating heater	0.425±0.05 (Ω)	4.9×10^{-4} (Ω/deg)
Main cathode vaporizer heater	1.62±0.15	3.5×10^{-4}
Insulator heater	2.84±0.2	5.7×10^{-4}
Neutralizer vaporizer heater	1.62±0.15	3.5×10^{-4}
Neutralizer heating heater	0.425±0.05	4.9×10^{-4}

*Values of temperature coefficient are the nominal values.

Fig. 4.3 Shape and Dimensions of IEE(1)

Center of gravity

$X_G = 0.5 \pm 1\,0$

$Y_G = 8.4 \pm 1\,0$

$Z_G = -16.5 \pm 1\,0$

Connector pin layout

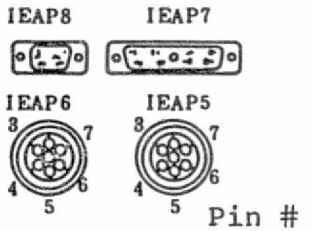

Seen from C

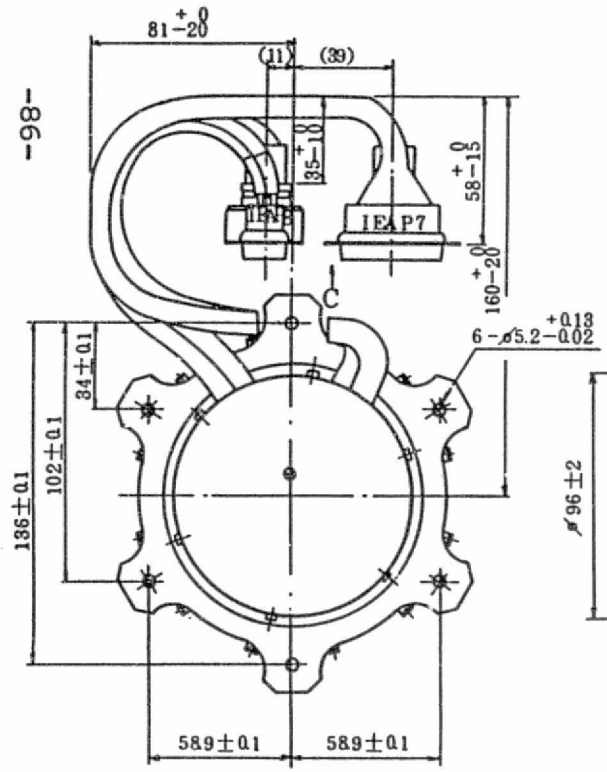

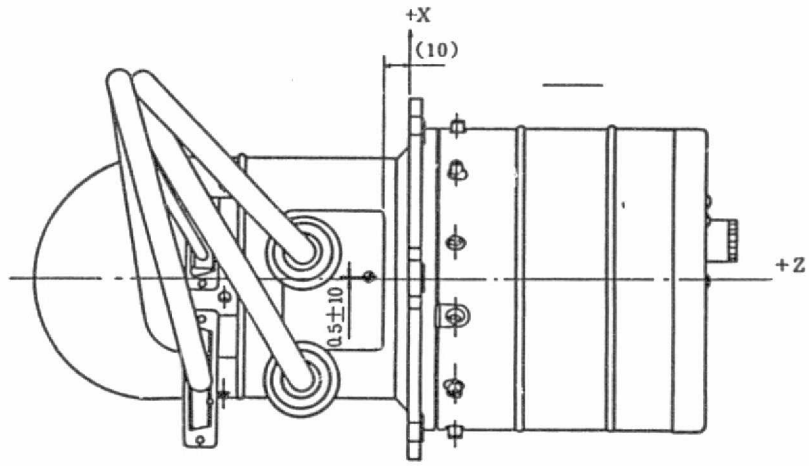

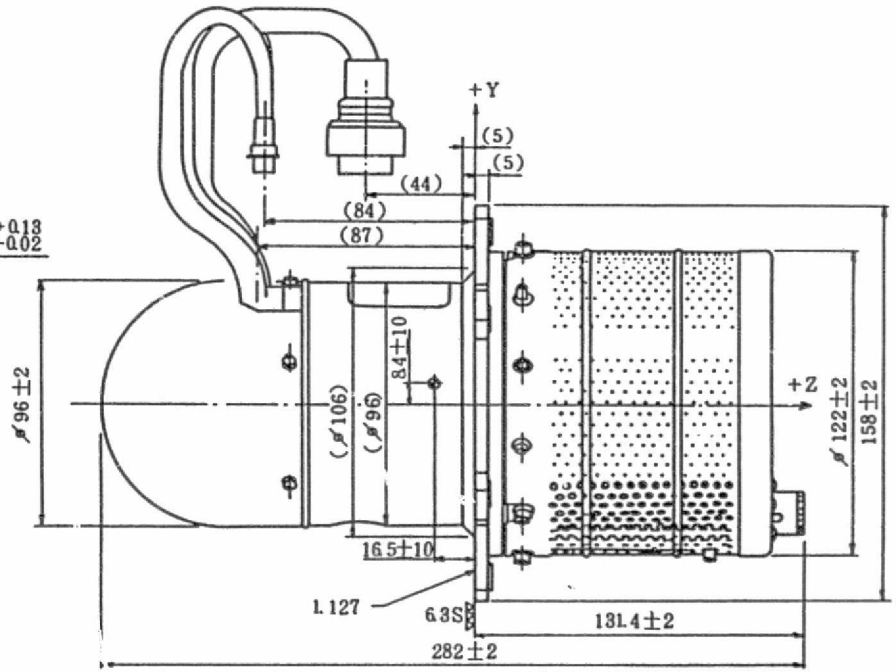

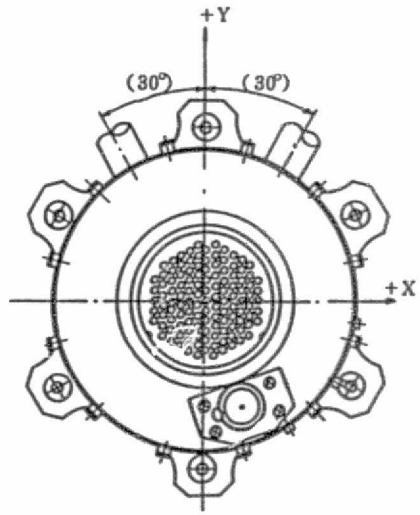

4.1.3 Power Source Control Device

Power source control device is the interface of satellite and IES: It receives commands to run and control power source device, and sends telemetry signals to the satellite telemetry encoder.

(1) Shape

Shape and the center of gravity of the power source control device will be as shown in Fig. 4.4.

(2) Input

i) Input voltage: $28\ ^{+0.22}_{-0.78}\ V_{DC}$

ii) Signals:

9 discrete commands and 4 magnitude commands, shown in Table 4.5, will be received. Commands will be as specified in Section 4.1.5.

Clock signals and enable signals will be as specified in Section 4.1.5.

The device will also receive monitor signals shown in Table 4.6 and determine load conditions of the power source device, i.e. engine conditions.

Telemetry signal input will be as specified in Table 4.7.

(3) Output

i) Power:

Connections to bus lines will be controlled by discrete commands IES ON, IES OFF, ION1 and ION2.

ii) Power source control signals:

ON/OFF signals, level signals and reference signals shown in Table 4.8 will be sent to power source device to control each power source module.

Output of telemetry signals to the satellite encoder will be as specified in Table 4.9.

iii) Sequence control program:

In response to each command, control signals will be sent to power source device according to the logical flow shown in Fig. 4.5 and Fig. 4.6.

Table 4.5 Commands

No.		Code	Type
1	Bus line to ion engine system ON	IES ON	Discreet commands
2	Bus line to ion engine system OFF	IES OFF	
3	Bus line to power source device in engine unit #1 ON	ION 1	
4	Bus line to power source device in engine unit #2 ON	ION 2	
5	Start ion engine system	START	
6	Shut off ion engine system	SHUT	
7	Run ion engine system idle	IDL	
8	Activate hollow cathode	ACT	
9	Continue sequence flow	CONT	
10	Change accelerating voltage	X1 V_N	Magnitude commands
11	Change discharge current	X2 I_D	
12	Change mercury flow	X3 V_D	
13	*Select mode	X4	

*Mode selections are shown below.

Code	Mode	Code	Meaning
OR	Selection of IES operation mode	OB	Beam injection
		OH	Hollow cathode operation
CR	Selection of main cathode heating level	CN	Nominal level
		CH	High level
IR	Selection of insulator heating level	IN	Nominal level
		IH	High level
FR	Selection of sequence flow	FN	Automatic continuation
		FH	Stop sequence flow

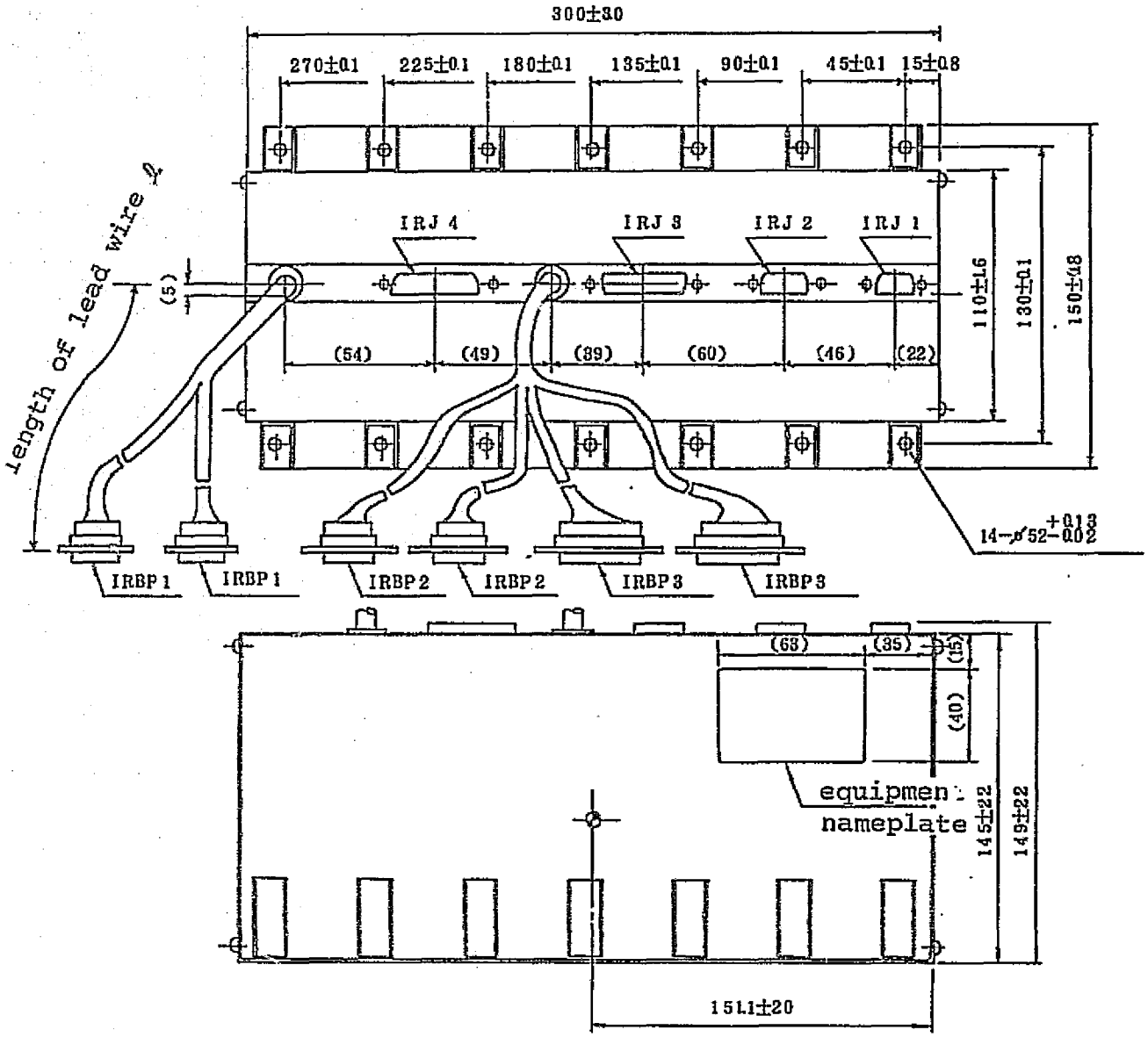

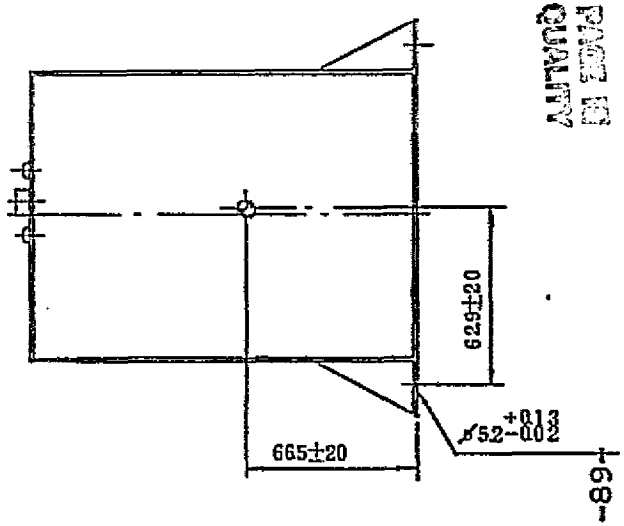

注Note:

記　号 Symbol	リード線の長さ（公　称　値） Length of lead wire (nominal value)
IRAP 1	650
IRBP 1	500
IRAP 2	700
IRBP 2	650
IRAP 3	650
IRBP 3	700

（　）内の数字は参考値である。

Numbers in (　) are reference values.

Fig. 4.4 Shape and Dimensions of Power Control Device

Tabe 4.6 Monitor Signals

	Monitor signal		Standard	Level
	Signal	Name		
Main cathode keeper current monitor	Ickm	主陰極キーパ電流モニタ	IcK>0.1A IcK<0.1A	L H
Neutralizer keeper current monitor	Inkm	中和器キーパ電流モニタ	InK>0.12A InK<0.12A	L H
Discharge current monitor	Idm	放電電流モニタ	Id >0.2A Id <0.2A	L H
Dielectric breakdown monitor	HVBDm	絶縁破壊モニタ	HVBD=0 HVBD≠0	L H

Note) ±10% error is tolerated in current values.

Table 4.7 Telemetry Input Signals

Beam voltage
Beam current
Discharge voltage
Discharge current
Accelerator current
Main cathode keeper current
Neutralizer keeper current
Main cathode vaporizer current
Neutralizer vaporizer current
Input current
Main cathode heater power
Neutralizer heater power
Main cathode vaporizer temperature
Neutralizer vaporizer temperature
Power device heat sink temperature
Vaporizer standard temperature
Number of dielectric breakdowns

No.	Item	Code	Range of output voltage	Remarks
1	ビーム電圧	Vb	0~5V	
2	ビーム電流	Jb	0~5V	
3	放電電圧	Vd	0~5V	
4	放電電流	Id	0~5V	
5	アクセラレータ電流	Ia	0~5V	
6	主陰極キーパ電流	Ick	0~5V	
7	中和器キーパ電流	Ink	0~5V	
8	主陰極気化器電流	Icv	0~5V	Analog
9	中和器気化器電流	Inv	0~5V	
10	入力電流	Iin	0~5V	
11	主陰極加熱電力	Pch	0~5V	
12	中和器加熱電力	Pnh	0~5V	
13	主陰極気化器温度	Tcv	0~5V	
14	中和器気化器温度	Tnv	0~5V	
15	電源装置ヒートシンク温度	Ths	0~5V	
16	気化器基準温度	Tref	0~5V	
17	絶縁破壊回数	HVCNTR	L:0.5V±0.5V H:10V±1.5V	Digital

Table 4.8 Power Source Control Signals

Signal level

ON/OFF signal

Symbol	Name	Level signal レベル信号 Level	ON/OFF	ON/OFF		Remarks
PS1 / PS2	スクリーングリッド電流 / アクセラレータグリッド電流	-	-	ON OFF	H L	Voltage level L: 0±0.2V H: 5 +0V −2V
PS3	Discharge	-	-	ON OFF	H L	
PS4	Main cathode heater	L.L N.L/H.L	H H/L	ON OFF	H L	
PS5	Main cathode keeper	-	-	ON OFF	H L	
PS6	Main cathode vaporizer	-	-	ON OFF	H L	
PS7	Neutralizer heater	I.L/ N.L	H/L	ON OFF	H L	
PS8	Neutralizer keeper	-	-	ON OFF	H L	
PS9	Neutralizer vaporizer	-	-	ON OFF	H L	
PS10	Insulator heater	N.L/ H.L	H/L	ON OFF	H L	

Screen grid current
Accelerator grid current

N.L(Nominal Level)
H.L(High Level) L.L(Idling Level)

(a) Level signals, ON/OFF signals

Symbol	Name	Voltage range
V_n	Accelerator	Less than 5.5VDC
I_d	Discharge current	Less than 5.5VDC
V_d	Mercury flow (discharge voltage)	Less than 5.5VDC

(c) Reference signals

Table 4.9 Telemetry Output Signals

No.	Item	Symbol	Output voltage range	Sampling speed
1.	Beam voltage	Vn	0~5V	1/1
2.	Beam current	JB	0~5V	1/1
3.	Discharge voltage	Vd	0~5V	1/1
4.	Discharge current	Id	0~5V	1/1
5.	Accelerator current	Ia	0~5V	1/8
6.	Main cathode keeper current	Ick	0~5V	1/1
7.	Nuetralizer keeper current	Ink	0~5V	1/1
8.	Main cathode vaporizer current	Icv	0~5V	1/1
9.	Neutralizer vaporizer current	Inv	0~5V	1/8
10.	Input current	Iin	0~5V	1/1
11.	Main cathode heater power	Pch	0~5V	1/8
12.	Neutralizer heater power	Pnh	0~5V	1/8
13.	Main cathode vaporizer temperature	Tcv	0~5V	1/8
14.	Neutralizer vaporizer temperature	Tnv	0~5V	1/8
15.	Power device heat sink temperature	Ths	0~5V	1/8
16.	Vaporizer standard temperature	Tref	0~5V	1/8
17.	Accelerator voltage set value	RVn	0~5V	1/8
18.	Discharge voltage set value	RVd	0~5V	1/8
19.	Discharge current set value	RId	0~5V	1/8

(a) Analog

1.	Status telemetry	ST	L: 0.5±0.5V H: 10±1.5V	1/1
2.	Number of dielectric breakdowns	HVCNTR	(same)	1/1

(b) Serial digital

No.	Telemetry item	Signal form	Determining value
1.	Bus line ON/OFF	Bi-level	1/0
2.	Engine Unit #1 ON/ engine Unit #2 ON	"	"
3.	Beam injection/hollow cathode operation	"	"
4.	Main cathode heater nominal/high levels	"	"
5.	Insulator heater nominal/high levels	"	"
6.	Sequence flow automatic continuation/shut	"	"

(c) Bi-level

C-2

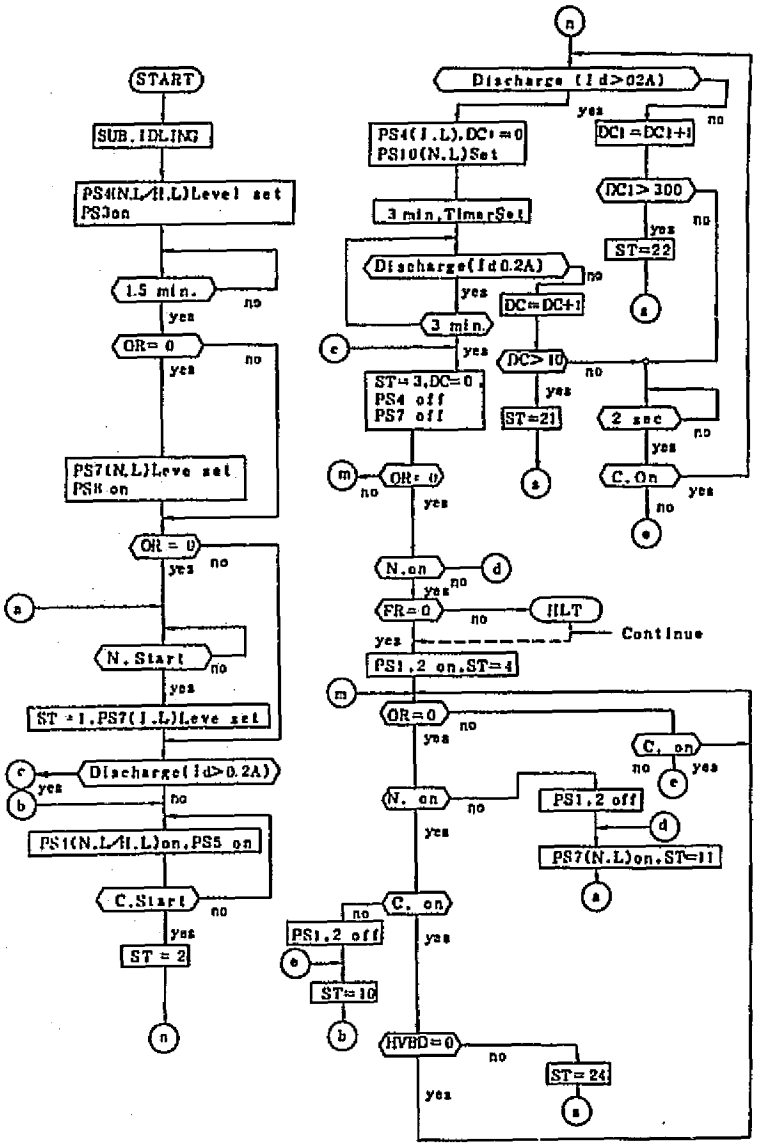

Fig. 4.5 Logical Flow of START

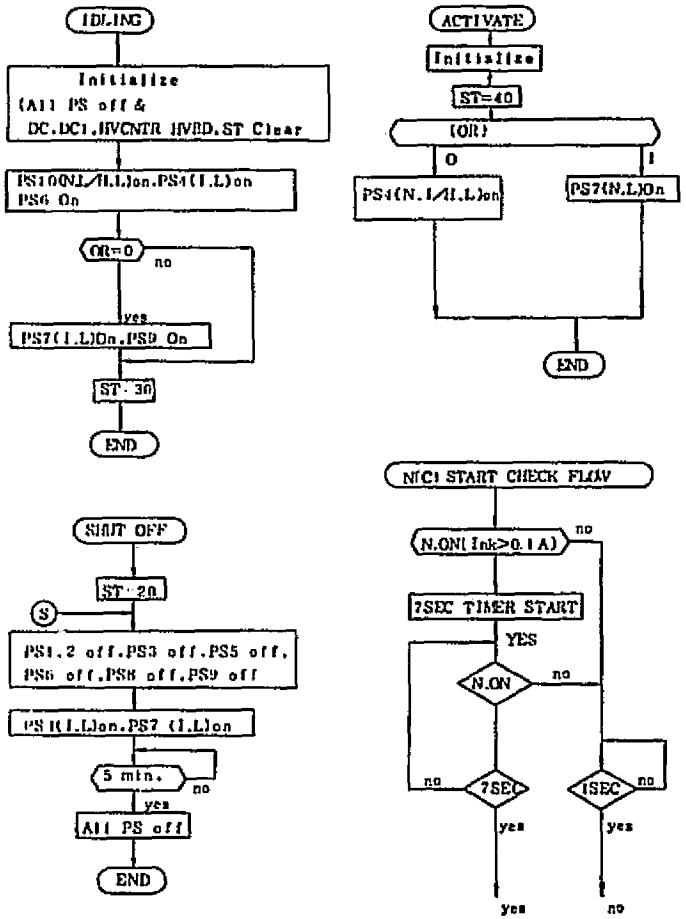

Fig. 4.6 Logical Flow of IDLING, ACTIVATE, SHUTT OFF, N(C) START

4.1.4. Power Source Device

Power source device supplies 10 power systems to the engine unit.

(1) Shape

Shape and the center of gravity of the power source device will be as shown in Fig. 4.7.

(2) Input

i) Input voltage: $28\ ^{+0.22}_{-0.78}\ V_{DC}$

ii) Signals:

ON/OFF signals, level signals and reference signals from power source control device (see Table 4.8) will be received.

(3) Output

i) Output voltage, current, output stability and ripple:

As shown in Table 4.10.

ii) Response properties and set values for excess current protection:

As shown in Table 4.11.

iii) Monitor output:

As shown in Table 4.6.

iv) Dielectric strength and insulation resistance:

Dielectric strength of output transformer will be over AC 2.1kV, with the exception of over AC 2.83kV for PS1 and PS2. Also, insulation resistance of output transformer will be over 20MΩ (measured by DC1KV megger) for PS1 and PS2.

v) High voltage dielectric breakdown protection circuit:

As shown in Fig. 4.8. Number of dielectric breakdowns will be sent to power source control device.

(4) Temperature telemetry

Temperature telemetry, shown in Table 4.12, will be sent to the telemetry encoder via power source device.

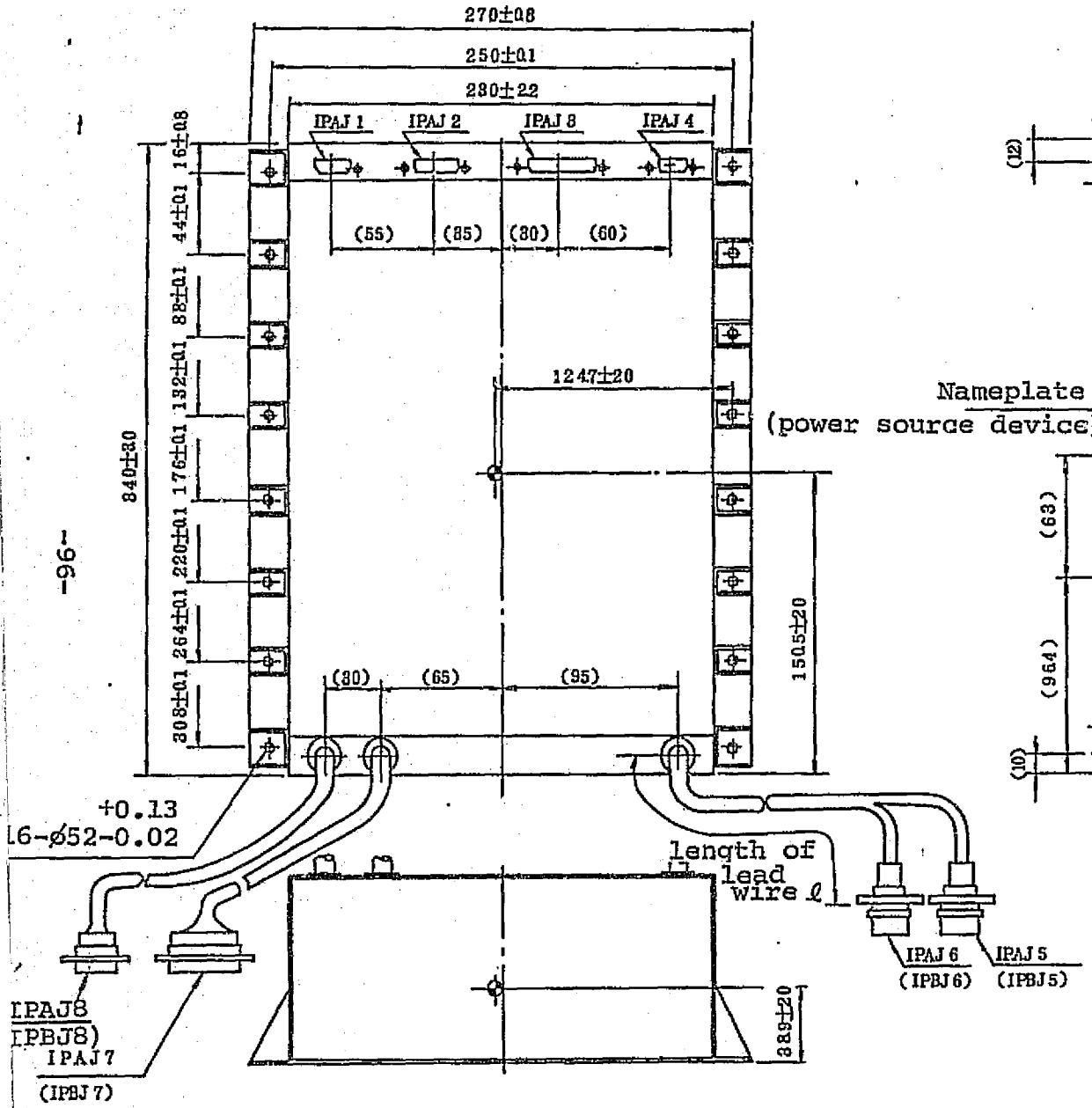

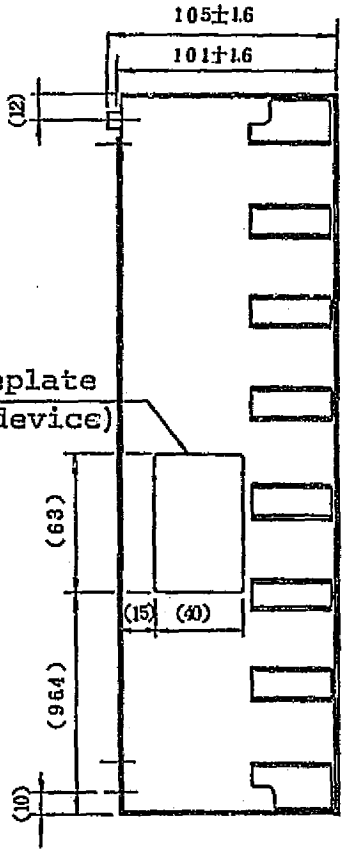

IP (1)	
Connector symbol	Length of lead wire (nominal value)
IPAJ5	640
IPAJ6	600
IPAJ7	480
IPAJ8	400

IP (2)	
Connector symbol	Length of lead wire (nominal value)
IPBJ5	510
IPBJ6	460
IPBJ7	820
IPBJ8	600

Note: Values in ( )are reference values.

Fig. 4.7 Shape and Dimensions of Power Source Device

Table 4.10 Power Source Specifications (1)

Power source				Level	Voltage	Current	Power	Type	Peak ripple (%)	Regulation (%)	Control range	Remarks
Screen grid	PS1	PSHv	スクリーングリッド電源	N.L	1 kV	30mA	30W	DC	3	±2	800 ~ 1,400 V	Regulation applied for beam current of 20-35mA. Ripple at rated load.
				H.L	1.4kV	35mA	49W					
Accelerator grid	PS2		アクセラレータグリッド電源	N.L	-1kV	1mA	1W	DC	3	-		Changes with set voltage of PS1. Ripple at rated load.
				H.L	-1.4kV	3mA	4.2W					
Discharge	PS3	PSd	放電電源	N.L	40V	0.35A	14.0W	DC	2	±2	0.3~0.5A	Ripple at rated load.
				H.L	45V	0.5 A	22.5W					
Main cathode heater	PS4	PSch	主陰極加熱電源	N.L	5V	5A	25W	AC	-	-		
				H.L	6V	6A	36W					
				I.L	1.6V	2.5A	4W					
Main cathode keeper	PS5	PSck	主陰極キーパ電源	N.L	15V	0.3A	4.5W	DC	3.5	-		Output characteristics shown in Fig.3-5. Ripple at rated load.
				S.L	300V	5mA	1.5					
Main cathode vaporizer	PS6	PScv	主陰極気化器電源	H.L	3.5V	2A	7W	AC	-	±5	0.5~2A 制御	Output characteristics shown in Fig. 3-5. Gain: 0.5A/V; Discharge voltage: 35-45V.
Neutralizer heater	PS7	PSnh	中和器加熱電源	N.L	5V	5A	25W	AC	-	-		
				I.L	1.6V	2.5A	4W					
Neutralizer keeper	PS8	PSnk	中和器キーパ電源	N.L	24V	0.25A	6W	DC	3.5	-		Output characteristics shown in Fig. 3-5. Ripple at rated load.
				S.L	300V	5mA	1.5W					
Neutralizer vaporizer	PS9	PSnv	中和器気化器電源	H.L	2.6V	1.5A	3.9W	AC	-	±5	0.5~1.2A 制御	Output characteristics shown in Fig. 3-5. Gain: 0.2A/V; keeper voltage set at 22-24V.
Insulator heater	PS10	PSis	絶縁筒加熱電源	N.L	3V	1A	3W	AC	-	-		
				H.L	5V	1.6A	8W					

* N.L.(NOMINAL LEVEL) M.L(MAXIUM LEVEL) H.L(HIGH LEVEL) I.L(IDLING LEVEL) S.L(START LEVEL)

Table 4.11 Power Source Specifications (2)

Voltage or current fluctuation

Response time

Condition

Power source	Symbol		名称	Response			Excess current set value
				応答時間	電圧または電流変動	条件	
Screen grid	PS 1	PSHv	スクリーングリッド電源	≦50ms以下	voltage, ノイズ含む	無負荷から定格まで 1.	50±5mA
Accelerator	PS 2		アクセラレータ電源	−	〃	〃	7±0.7mA
Discharge	PS 3	PSd	放電電源	≦15ms以下	−	電流設定値を±20%変動させたとき 2.	−
Main cathode heater	PS 4	PSch	主陰極加熱電源	−	−	−	8±0.8A
Main cathode keeper	PS 5	PSck	主陰極キーパ電源	≦10μs以下		無負荷から定格まで 1.	−
Main cathode vaporizer	PS 6	PScv	主陰極気化器電源	−	−	−	−
Neutralizer heater	PS 7	PSnh	中和器加熱電源	−	−	−	6±0.6A
Neutralizer keeper	PS 8	PSnk	中和器キーパ電源	≦10μs以下	−	無負荷から定格まで 1.	−
Neutralizer keeper	PS 9	PSnv	中和器キーパ電源	−	−	−	−
Insulator heater	PS10	PSis	絶縁器加熱電源	−	−	−	−

1. No load to rated load
2. Current set value fluctuated by ±20%

Table 4.12 Temperature Measurement Telemetry

No.	Item to be measured	Code
1	Temperature of Engine Unit #1	TE1
2	Temperature of Engine Unit #2	TE2
3	Temperature of mercury tank #1	TTANK1
4	Temperature of mercury tank #2	TTANK2
5	Temperature of base plate in power source device #1	Tbs 1
6	Temperature of base plate in power source device #2	Tbs 2

Fig. 4.8 Logical Flow of Dielectric Breakdown Protection

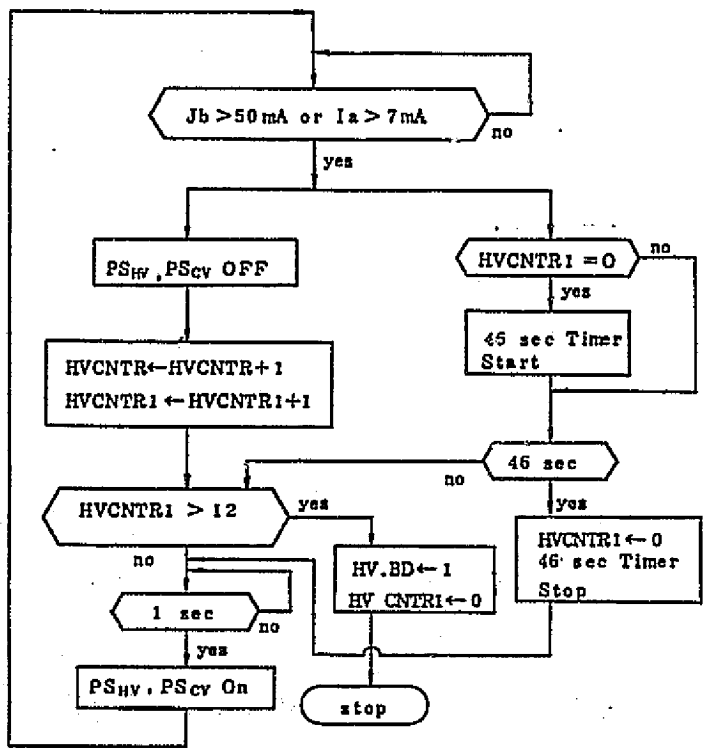

*HVCNTR is sent as telemetry signal.

4.1.5 Interface With Satellite

Basic components having interface with ion engine system are the structural system, power source system, telemetry/command system, heat control system, attitude control system and gas jet system. Field separation points are established as follows.

a. Mechanical separation points: mounting surface of each component. Weight of mounting hardware will not be included in IES.

b. Electrical separation points: 6 connectors - bus power line, discrete command line, magnitude command line, analog telemetry line and temperature measurement line - shown in Fig. 4.9.

(1) Structural system interface

Boarding position of each component is shown in Fig. 4.10. It is a roll surface called mission panel II. Alignment of engine unit will be determined by an alignment mirror which is mounted on a grid. Accuracy will be set to be within 0.24°.

(2) Power source system interface

i) Supplied voltage: $28\ ^{+0.22}_{-0.78}\ V_{DC}$ (IEP input terminal)

ii) Ripple: Less than 100mV

iii) Disturbance voltage resistivity:

Resistivity to stabilized bus disturbance voltage (single peak) of +5V, 250μV sec and -10V, 600μV sec will be required.

iv) Load current:

di/dt $\leq$ 100,000A/sec

Overshoot $\leq$ 5A

Overshoot total energy $\leq$ 160 x 10^{-4}A·sec/(per steady load current of 1A)

v) Other:

Diodes requiring series arrangement should not be used in the power source line which prevents reverse voltage. Also, care must be taken so that IES will not be in short-circuit mode to bus power.

(3) Telemetry/command system interface

Commands shown in Table 4.5 are sent and telemetry signals shown in Table 4.9 are received.

i) Discrete commands:

Sent according to the command matrix below.

At execution; X line 27.0±1.5V 10Ω

Y line 1.2±1.2V 10Ω

At non-execution; X line Open, transistor OFF

Y line Open, transistor OFF

Pulse width; 55±5ms

ii) Magnitude commands:

Data format will be as shown in Fig. 4.11 and timing as shown in Fig. 4.12. Clock bit speed of data transmission will be 128 bps.

iii) Analog telemetry:

Analog telemetry will be coded to 8 bit (1 bit, 20mV; total accuracy, ±0.6% F.S.) by telemetry encoder.

iv) Serial digital telemetry

8 bit-long and bit speed of 2048 bps. Timing will be as shown in Fig. 4.13.

(4) Heat control system interface

Heat environment of each component at the time of launching and in orbit is 0 ~ 40C (estimated) and design temperature will be -15~55C.

Power consumption of each component is shown in Table 4.2. Heat density of each component will be as shown in Table 4.13. Items whose temperature are measured, types of sensors and their locations are shown in Table 4.14.

(5) Attitude control system

Nominal torque arm length of each axis of IEE will be 232.5mm for pitch axis, 0mm for roll axis and 100mm for yaw axis. Thrust will be the nominal 0.18gr wt. and its cumulative operating time will be over 150 hours.

(6) Gas jet system

N/A.

Fig. 4.9 Connector Numbers of Ion Engine System Components

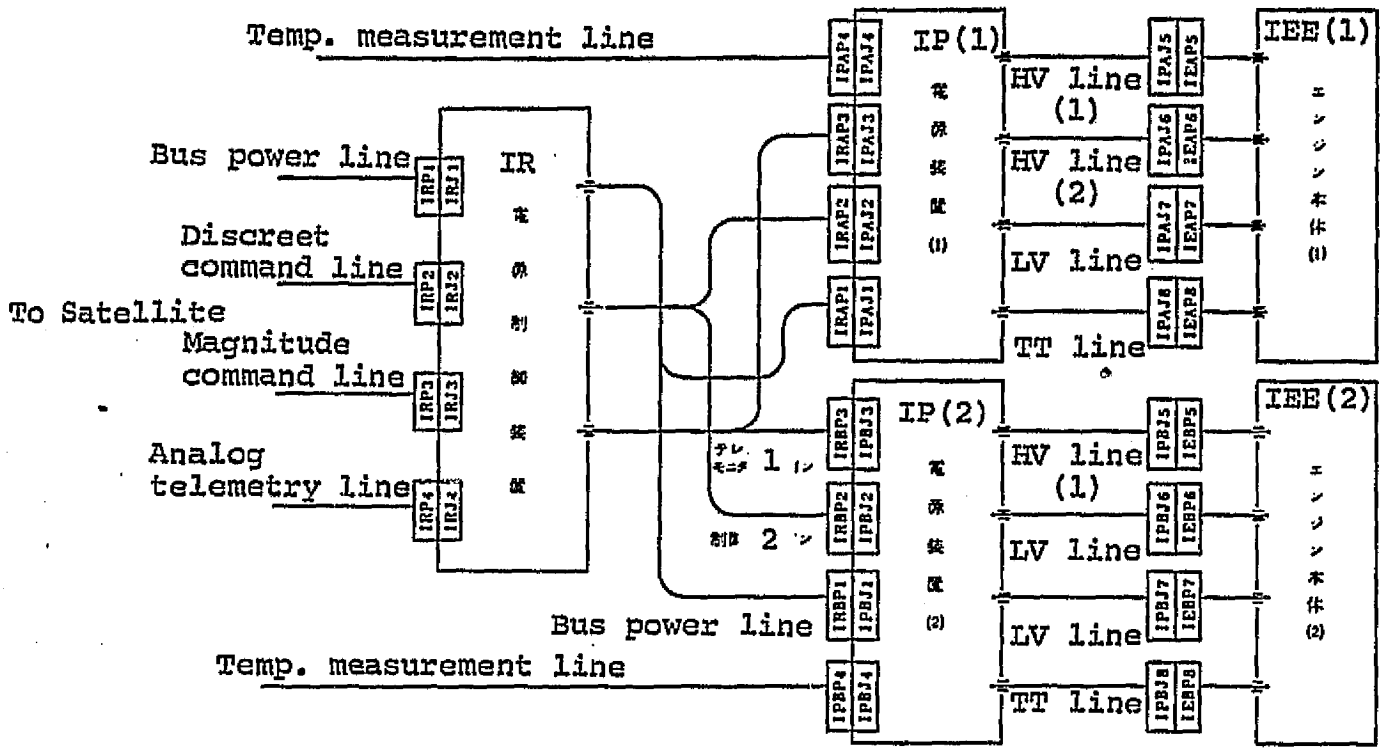

1. Telemetry monitor signal line
2. Control signal line

HV: High voltage output
LV: Low voltage output
TT: Temperature telemetry

Fig. 4.10 IEE/IEP Boarding Positions

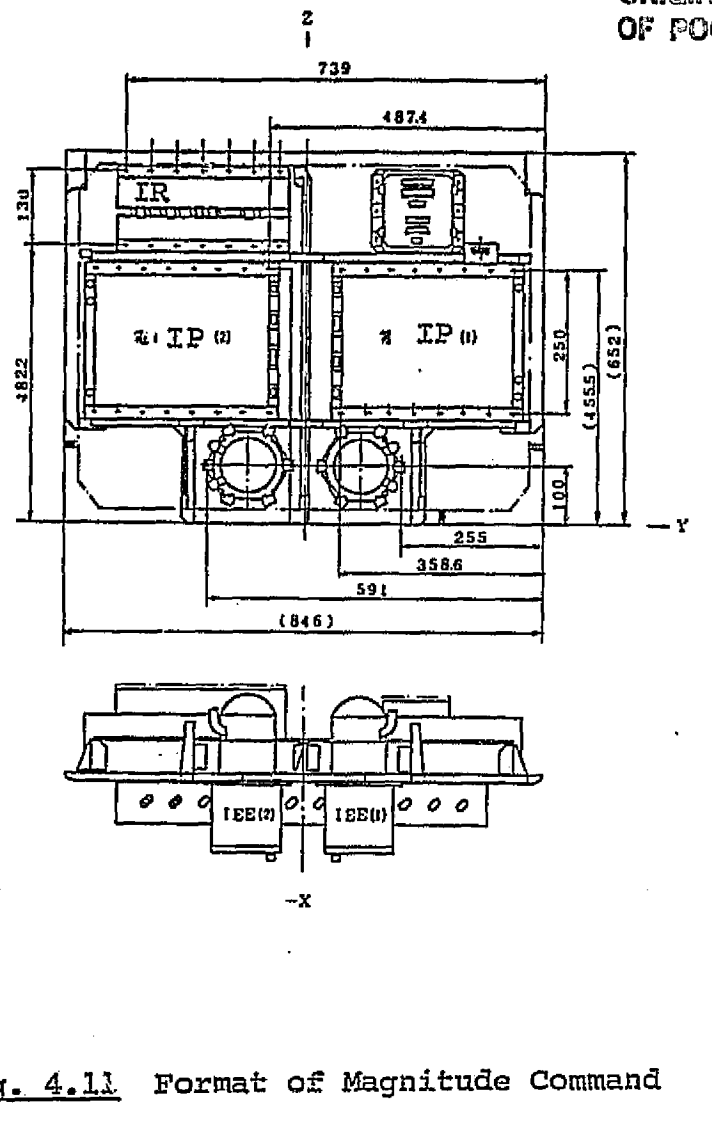

Fig. 4.11 Format of Magnitude Command

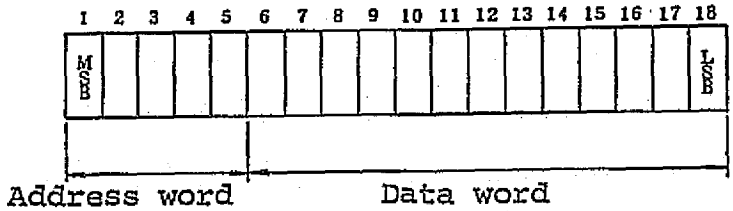

Fig. 4.12 Timing Chart of Magnitude Command

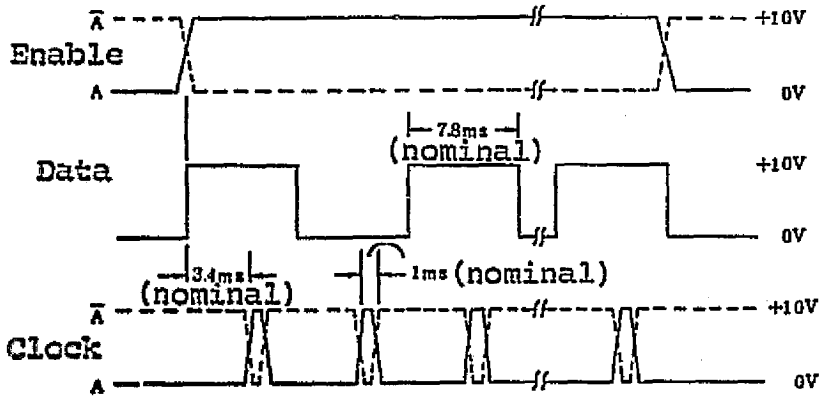

Enable and clock signals are sent as differential signals, and agreement of signals is within 2 μs.

Fig. 4.13 Timing of Serial Digital Data

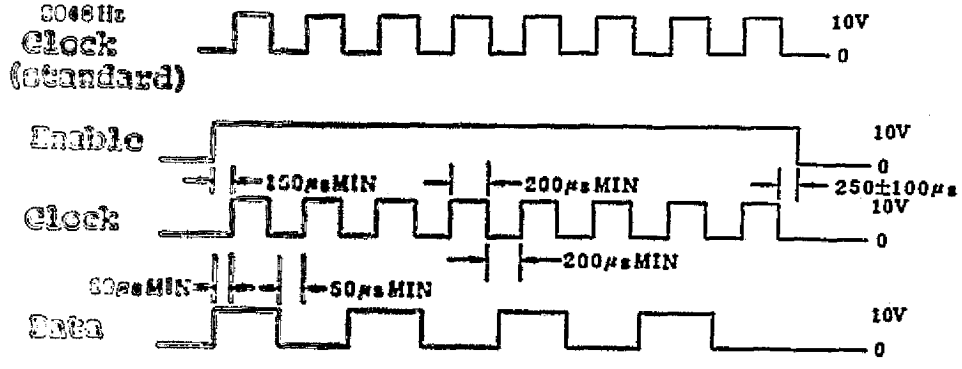

Rise time(tr) and fall time(tf) of each signal: tr≤10μs
tf≤10μs

Table 4.13 Heat Density

IR	IP	IEE
≦0.011W/cm以下	≦0.030W/cm以下	≦1W/cm以下

Table 4.14 Temperature Measurement Items, Sensor Types and Location

Item	Sensor type	Location
Engine Unit #1 temperature	Platinum resistance wire R9256P3	Engine Unit #1
Engine Unit #2 "	Platinum resistance wire R9256P3	Engine Unit #2
Mercury tank #1 "	Thermistor S311P18-07T15R	Mercury tank #1
Mercury tank #2 "	Thermistor S311P18-07T15R	Mercury tank #2
Power source device #1 "	Thermistor 47C247072	IP #1 base plate
Power source device #2 "	Thermistor 47C247072	IP #2 base plate

4.1.6 Design Standards

Only the main subject matters will be outlined in this section. Details are given in the Interface Management Specifications and the Common Specifications.

(1) Mechanical design standards

i) Natural oscillation:

Less than 100 H_Z for each component.

ii) Load limit:

Strength and stiffness to produce permanent deformation of no more than 0.2% of load limit (estimated load x 1.5 = approved test load. See Table 4.17) will be required.

iii) Ultimate load:

No failure or breakdown will occur at the ultimate load(load limit x 1.25).

iv) Safety coefficient:

IEE employing liquid or air will be designed with the safety coefficients given in Table 4.15.

(2) Electrical design standards

Grounding of each component will be electrically insulated from the satellite frame. Insulation between bus power return and (illegible) will be DC resistance of over 1MΩ.

Insulation between secondary power line returns, primary power lines and cases will be DC resistance of over 1MΩ each.

(3) Electromagnetic radiation

IES will follow the electromagnetic compatibility requirements given below. Between IES and ETS-III system, compatibility tests will be performed successively and standards will be set by the EMC

management plan, test specifications, test execution plan and test procedure manual.

i) Transmission interference noise in power lines:

In IES and IEP, transmission interference in power source lines will not exceed the tolerance levels set below.

Frequency band	Tolerated transmission noise interference
30Hz ~160Hz	107mAP—P, 20dB/decade
160Hz ~1.6KHz	20mAP—P, 20dB/decade
1.6KHz ~100KHz	200mAP—P
100KHz~10MHz	30mAP—P

trasient response 100,000A/sec (loat current > 1A)

Satisfaction of the standards will determined by oscilloscope(50MH_Z) and electric current probe.

ii) Transmission interference sensitivity of power lines:

a) Sine wave voltage

Sine wave voltage of levels set below, when charged to power source input, should not cause any abnormal action in IES and IEP.

Amplitude	Source impedance	Frequency
01Vp-p	05Ω	1Hz
01Vp-p	05Ω	60Hz
01Vp-p~05Vp-p	05Ω	60Hz~800Hz
(Linear increase)		(linear increase)
05Vp-p	05Ω	800Hz
05Vp-p	05Ω	800Hz~50KHz
05Vp-p	05Ω	50KHz~10MHz

Test method will be based on MIL-STD-462.

b) Transient

Pulse voltage of 60PPS, 25V_O-p, 10 μs for a maximum

of 10 minutes, applied to power bus line in either positive or negative direction should not cause any significant deterioration in performance of IES and IEP. Test method will be in accordance with MIL-STD-462-CS06.

ii) Magnetic field interference:

a) Radiation interference noise

IEP must not radiate more than 0.1 Gauss($30H_Z \sim 1KH_Z$) and 0.01 Gauss($1KH_Z \sim 30KH_Z$). Measuring distance is 7cm from the component surface. Test method will be based on MIL-STD-462, RE01.

b) Radiation interference sensitivity

IEP must satisfy performance requirements in the tests based on the requirements and testing methods of MIL-STD-461A and 462, RS02. Applicable tests and test standards must be indicated in each test specifications, test execution plan and test procedure manual. Testing frequency of RS02 will be $400H_Z$ and amplitude of current source will be 2A.

c) Magnetic dipole moment

Residual magnetic dipole moment of IEP component must not exceed 0.8μwbm for each axis. As MAC has a maximum of 8.16μwbm magnetic dipole moment, IEP component must be designed so that a magnetic field having a flux density of $1.62 \times 10^{-4} wb/m^2$ (estimated to be 20cm based on MAC) will not be affected at all.

iii) Electric field interference

a) Radiation interference noise

Radioactive interference of 14KHz to 10GHz, radiated from components, must not exceed the limits set by MIL-STD-461A, Notice 3, Fig. 21 and 22. In the frequency band of 147 - 149MHz, however, narrow band radiation limit is 31 dB V/m. Radioactive interference by radiation from IES must not exceed the set limits.

b) Radiation interference sensitivity

Normal operation of IEP in the frequency band of 14KHz - 10GHz and exposed to the electric field of 1V/m must be verified. For the frequency bands of 135 - 137MHz and 1700 - 1710MHz, IEP is exposed to the electric field of 5V/m for measurement.

Table 4.15 Safety Coefficient

Load class / Structural division	Proof load (Note 1)	Burst load (Note 2)
Pressure tank	1.50	2.30
Pressure pipings and others	1.50	2.30

(Note 1) Proof load is the pressure load applied to check production technique and material quality of pressure container.

(Note 2) Burst load is the pressure load under which pressure container must withstand without breaking down.

4.1.7 Tests

Test subject matrix is shown in Table 4.16. Oscillation test levels are shown in Table 4.17 and impact test levels are shown in Fig. 4.14. Heat vacuum test will be given with the heat cycle shown in Fig. 4.15. Electromagnetic compatibility test was explained in the preceding section.

Fig. 4.14 Impact Spectrum

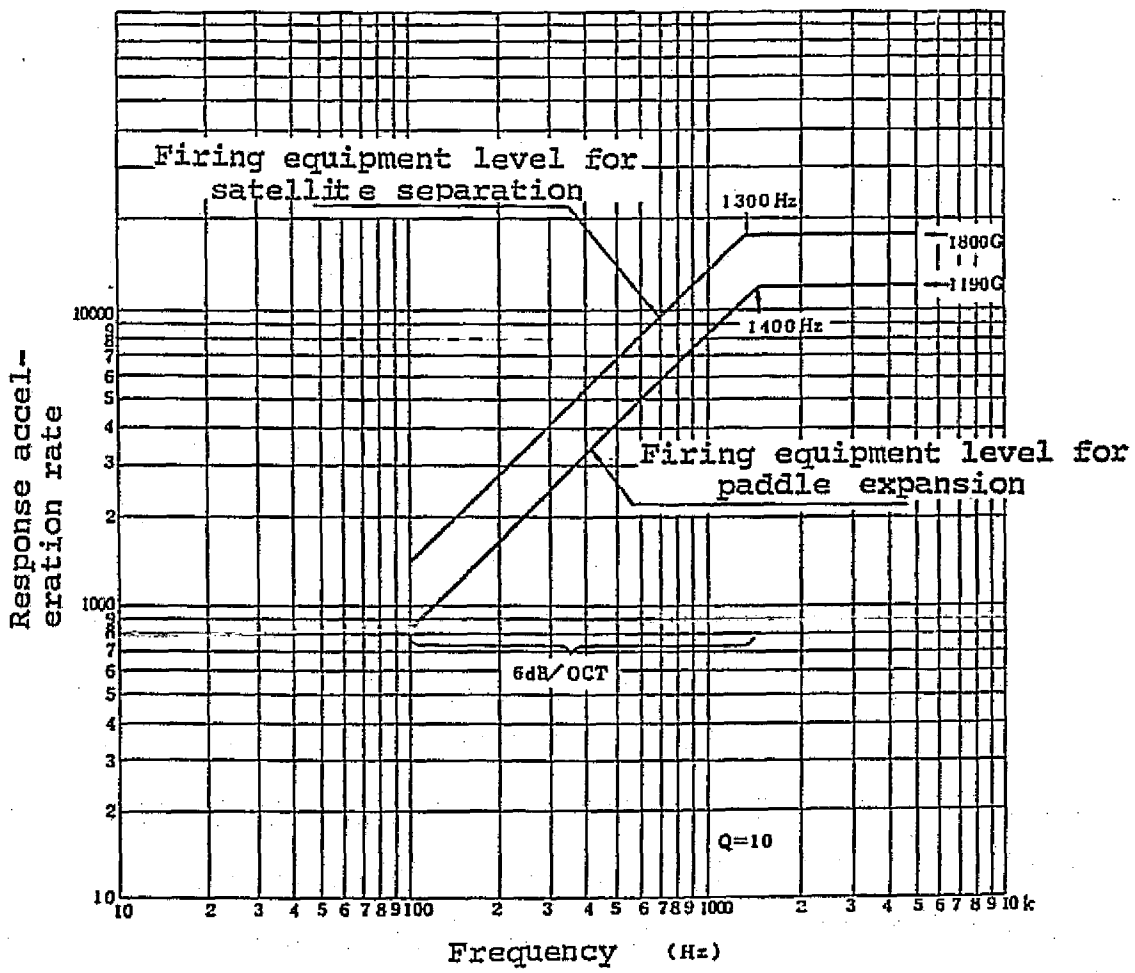

Table 4.16 Test Matrix

Test subject	Model PM	FM	Remarks
Appearance and dimension inspection	O	O	
Weight and position of center of gravity inspection	O	O	
Charge and resistance inspection	O	O	
Performance test	O	O	Electromagnetic compatibility test given for PM.
Oscillation test	O QT	O AT	QT level test for PM. AT level test for FM. Random oscillation test only for FM.
Impact test	N/A	N/A	
Heat vacuum test	O QT	O AT	QT level test for PM. AT level test for FM.
Measurement of residual magnetic moment	O	O	

(a) IEE

PM: prototype model
FM: flight model
QT: qualifying test
AT: acceptance test

Test subject	Model PM	FM
Appearance and dimension inspection	O	O
Weight and center of gravity inspection	O	O
Performance test	O	O
Electromagnetic compatibility test	O	N/A
Oscillation test	O QT	O
Heat vacuum test	O	O
Measurement of residual magnetic moment	O	N/A
Impact test	O	N/A

Oscillation test - QT level for PM and AT level for FM.

(b) IEP

Test subject	Model PM	FM
Function and performance test	O	O
Measurement of thrust	N/A	N/A
Measurement of beam diffusion angle	N/A	N/A
Electromagnetic compatibility test	O	N/A
Heat vacuum test	O	O
Long-mode test	O	N/A

(c) IES

Table 4.17 Oscillation Test Levels

Sine wave oscillation level for Qualifying Test:

Direction of axis of thrust

Rt. angle to axis of thrust

Range of frequency (Hz)	Level (G : O-P) 推力軸方向	推力軸に直交する方向
5-200	12.0*	15.0*
200-2000	5.0	5.0
Sweep rate 2 oct/min		

Random oscillation level for Qualifying Test:

Range of frequency — Accel. density — Av. level

周波数範囲 (Hz)	加速度密度 (g^2/Hz)	平均レベル (Grms)
20-230	0.09	15.64
230-350	+6dB/oct	
350-900	0.2	
900-2000	-6dB/oct	

Test duration: 2 min. for each direction

Sine wave oscillation level for Acceptance Test:

Direction of axis of thrust

Rt. angle to axis of thrust

Range of frequency Hz	レベル (G O-P) 推力軸方向	推力軸に直交する方向
5-200	8.0*	10.0*
200-2000	3.3	3.3
Sweep rate: 4 oct/min		

Random oscillation level for Acceptance Test:

Range of frequency — Accel. density — Av. level

周波数範囲 (Hz)	加速度密度 (g^2/Hz)	平均レベル (Grms)
20-230	0.04	10.4
230-350	+6dB/oct	
350-900	0.089	
900-2000	-6dB/oct	

Test duration: 1 min. each direction

Fig. 4.15 Heat Vacuum Test Cycle

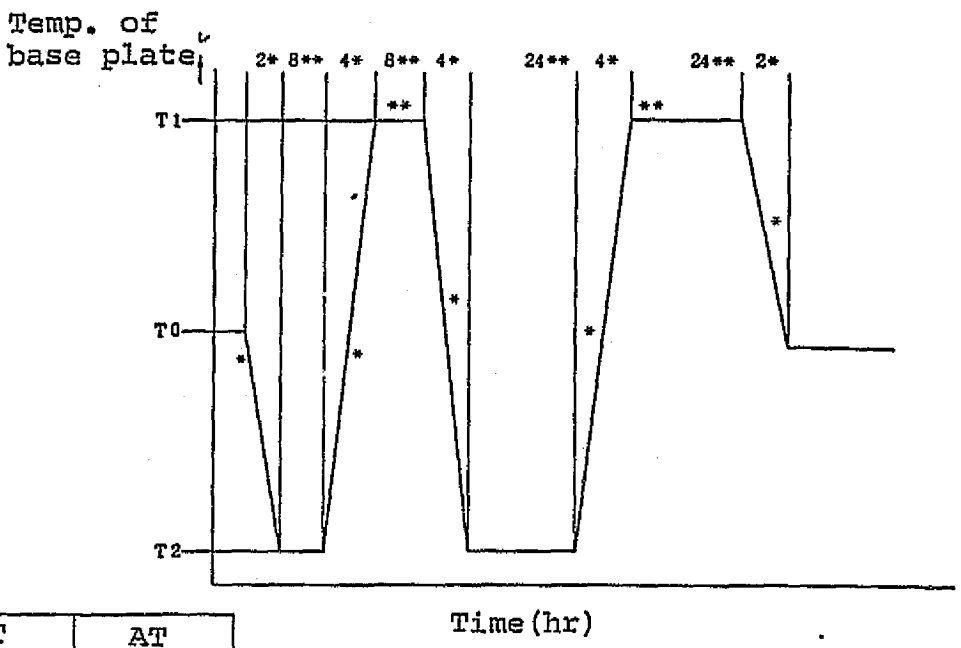

	QT	AT
T1	+55℃	+45℃
T0	≅20℃	≅20℃
T2	−15℃	−5℃

T_1：高温側 T_2：低温側
high temp. low temp.

*From high temperature to low temperature, or a reverse process, over 4 hours and less than 8 hours should be spent. Rate of temperature change depends on temperature difference.

**Temperature stability during this period, measured by temperature sensor which controls testing device, should be within ±3C.

4.1.8 Operation requirements

Plan shown in Table 4.18 will be the reference in operating the ion engine system on the satellite.

Table 4.18 Operation Plan for IES

Phase	Subject	Duration	No. of engine unit used	Experiment conditions	Orbit and operation conditions
Early phase	IDLING	2 rotations/unit, total 4 rotations	2	IN mode: 1 rotation/unit IH mode: 1 rotation/unit	2-orbit continuous operation in the visible range.
	Hollow cathode activation	2 rotations/unit, total 4 rotations	2	Activation of main cathode: 1 rotat/unit Activation of neutralizer cathode: 1 rotation/unit	30-minute continuous operation in an orbit.
Steady phase	Hollow cathode test	(8+2) rotat./unit, total 20 rotations	2	(per rotat) N+1 rotat. orbit IDLING 105 min. N+2 " Hollow cathode test 20 " N+3 " I_d reference change (3 min x3) 20 " N+4 " " 20 " N+5 " SHUT OFF 30 " P+1 " IDLING 105 " P+2 " Hollow cathode test 40 " P+3 " V_d reference change 40 " P+4 " " 40 " P+5 " SHUT OFF 30 "	IEE operated 20 min. before entering visible area by stored command, for testing in the visible area.
	Neutralizer movement check	(2+1) rotations/unit, total 6 rotations	2	1st orbit IDLING 105 min. 2nd " OB, FH mode START 40 " 3rd " " 40 "	"
	Varied parameter test	(12+3) rotat./unit, total 30 rotations		1st orbit IDLING 105 min. 2nd " OB, FH mode START, CONT 40 " 3rd " CONT, I_d change 40 " 4th " " 40 " 5th " " SHUT OFF 30 " Varied V_d and V_n test at the same time.	"
	Repetition test	100 rorations/unit	1	Parameters for stable IEE conditions set from above data. Beam radiation: 10 min.	First 10 rotat. in visible area.
	Long mode test	Over 100 accum.hrs/unit; over 10 cont. hrs.	1	Parameters for stable IEE conditions set from above data.	Beginning and end in visible area.

4.2 Engine Unit

4.2.1 Design Values

Design values of Engineering Model(EM) with respect to the required design values in the development specifications of the preceding section are shown in Table 4.19.

Table 4.19 Design Values of Main Parts

Hollow cathode

	Main	Neutralizer
Orifice diameter, mm	0.25	0.25
Keeper aperture diameter, mm	2	2

Accelerating grid system

	Screen	Accelerator
Thickness, mm	0.5	1.5
Hole diameter, mm	3.0	2.2
Number of holes	121	
Grid separation, mm	1.5	

Discharge chamber

Chamber length, mm	60
diameter, mm	60
Anode diameter, mm	50
Buffle diameter, mm	9
Distributer pole piece inner diameter, mm	12
Buffle to pole piece separation, mm	1.2

4.2.2 Structure, Functions and Designs

Components, functions and designs of the engine unit are given below. Cross section of the engine unit is shown in Fig. 4.16.

(1) Tank assembly

Cross section is shown in Fig. 4.17. It has a function of supplying propellant(mercury), and consists of liquid mercury tank and force(nitrogen) tank, separated by fluorofubber bladder. Liquid mercury tank has flanges for joining the tank with main hollow cathode assembly and neutralizer hollow cathode assembly. Each is connected through O-ring. Force gas pressure is 25±0.2kg/cm^{2}abs.

(2) Main hollow cathode assembly

Cross section is shown in Fig. 4.18. The assembly consists of vaporizer which holds liquid mercury and controls the flow of mercury vapor, hollow cathode which is the electron emission source, and insulator which insulates back flow of hollow cathode and the front flow of vaporizer under high voltage.

Vaporizer: Porous tungsten plug of sintered tungsten powder having particle diameter of μm is joined with tantalum cylinder by electron beam welding. Sheath heater, mounted on the outside of the cylinder, heats and vaporizes mercury held by the tungsten plug, controlling its flow. Particle density of tungsten plug is 70%(75% for neutralizer). Sheath heater terminal, composed of ceramic seal and tantalum cap, converts into nickel lead wire.

Insulator: 6 molybdenum meshes are placed at equal distances inside an alumina ceramic pipe. Voltage between the meshes is kept at less than 300V to prevent discharge under a wide range of mercury vapor pressure. Molybdenum meshes are supported by alumina spacers with rippled surface, so that short circuit is not likely to occur between

the meshes in the event liquid mercury freezes. Sheath heater is placed over the ceramic pipe on the vaporizer side to heat mercury vaporized and prevent it from freezing.

Cathode is a cylindrical tantalum pipe, one end of which is blocked by a thorium tungsten chip. Vaporized mercury passes through the pipe and is supplied to the discharge chamber through a narrow hole in the center of the thorium tangsten chip. For a cathode insert, porous tungsten impregnated with barium compound is placed in the front of thorium tungsten chip, which, by heat, turns into oxide cathode having an electron discharge ability. Outside of the tantalum cylinder is coated with alumina, over which rhenium tungsten heater is wound. The heater has one end spot-welded to the cylindrical pipe and the other end to the tantalum lead wire, and is further coated with alumina. Keeper electrode is placed on the downstream side of the thorium tungsten chip. The keeper is mounted on the alumina ceramic surface and welded by electron beam.

(3) Neutralizer hollow cathode assembly

Cross section is shown in Fig. 4.19. Its components are similar to those of main hollow cathode, except that it does not have an insulator. During oscillation test of the development test, breaking of keeper lead wire and slipping of cathode insert occurred, necessitating addition of another point of support for the keeper lead wire and use of tantalum foil cylinder for supporting the cathode insert. Also, control of keeper voltage/vaporizer current failed during IES combination test, which prompted increasing the keeper diameter from 1ø to 2ø.

(4) Discharge chamber assembly

Cross section is shown in Fig. 4.20. The assembly has soft steel

pole pieces on the upper- and down-stream sides with discharge chamber in-between, and a permanent magnet of alnico 5 is inserted and fixed between them. Discharge chamber has a cylindrical anode which insulates the chamber with alumina ceramic (insulator). Grid assembly, consisted of screen grid, accelerating grid and alumina ceramic insulator, is mounted on the pole piece of the downstream side. Discharge chamber, anode, screen grid, accelerating grid, etc. are made of stainless steel.

(5) Housing

Housing, the interface of above assemblies, comprises various support materials, base plate for mounting on satellite, support materials for wire harness , etc. SUS304, aluminum alloy, is used as structural material.

Fig. 4.16 Structure of Ion Engine

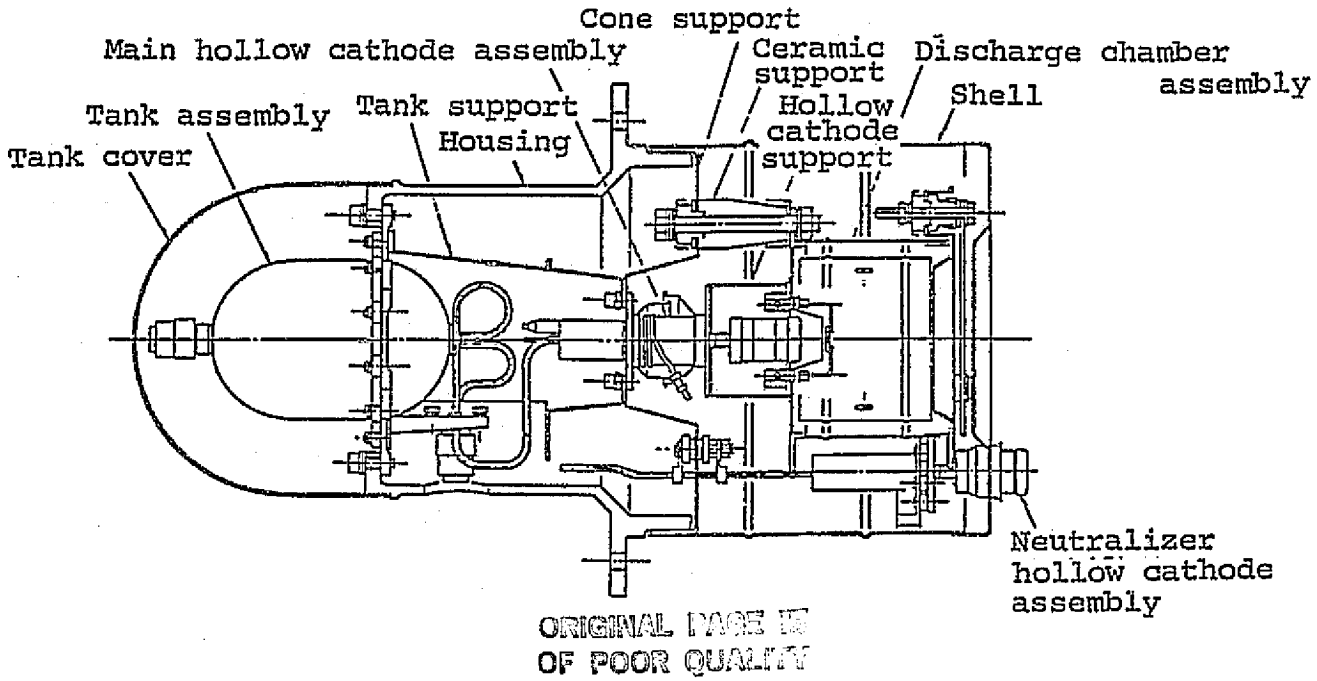

Fig. 4.17 Tank Assembly

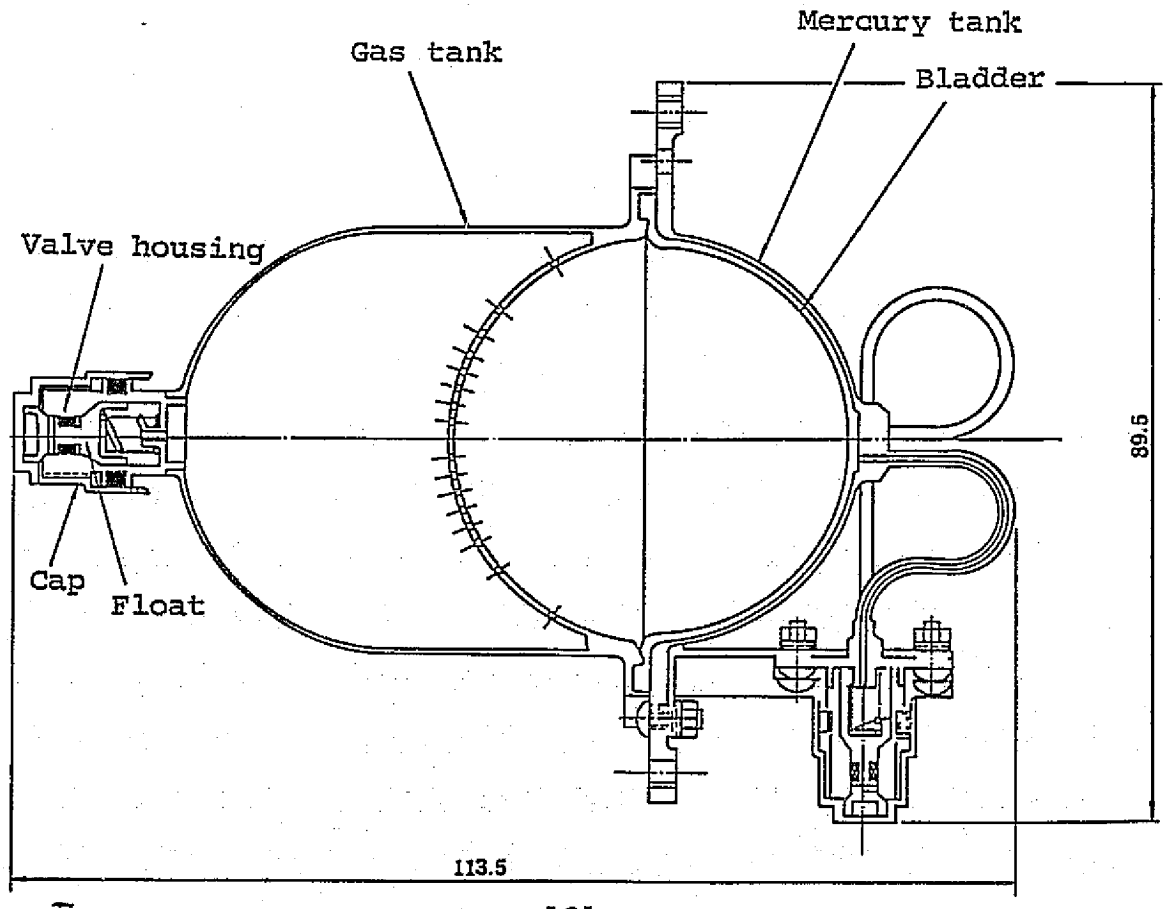

Fig. 4.18 Main Hollow Cathode Assembly(EM) (Slight change from PM on)

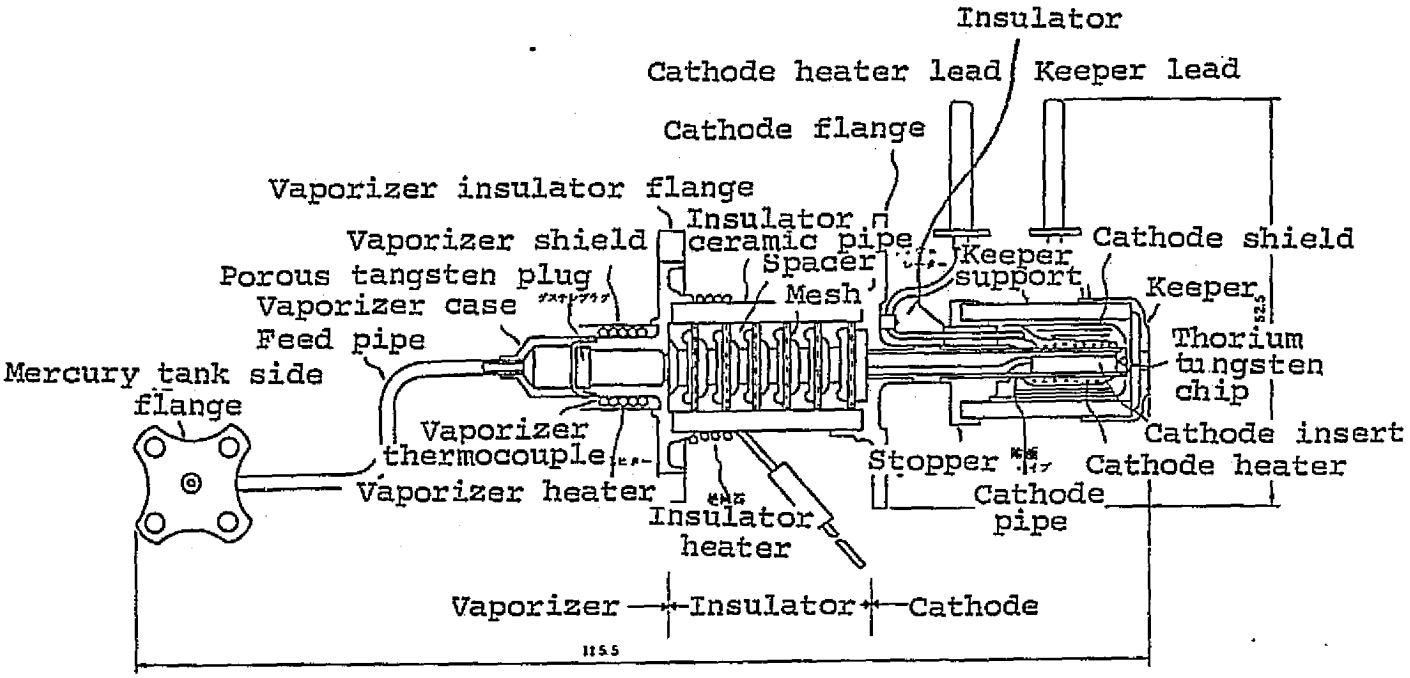

Fig. 4.19 Neutralizer Hollow Cathode Assemby(EM) (Slight change from PM on)

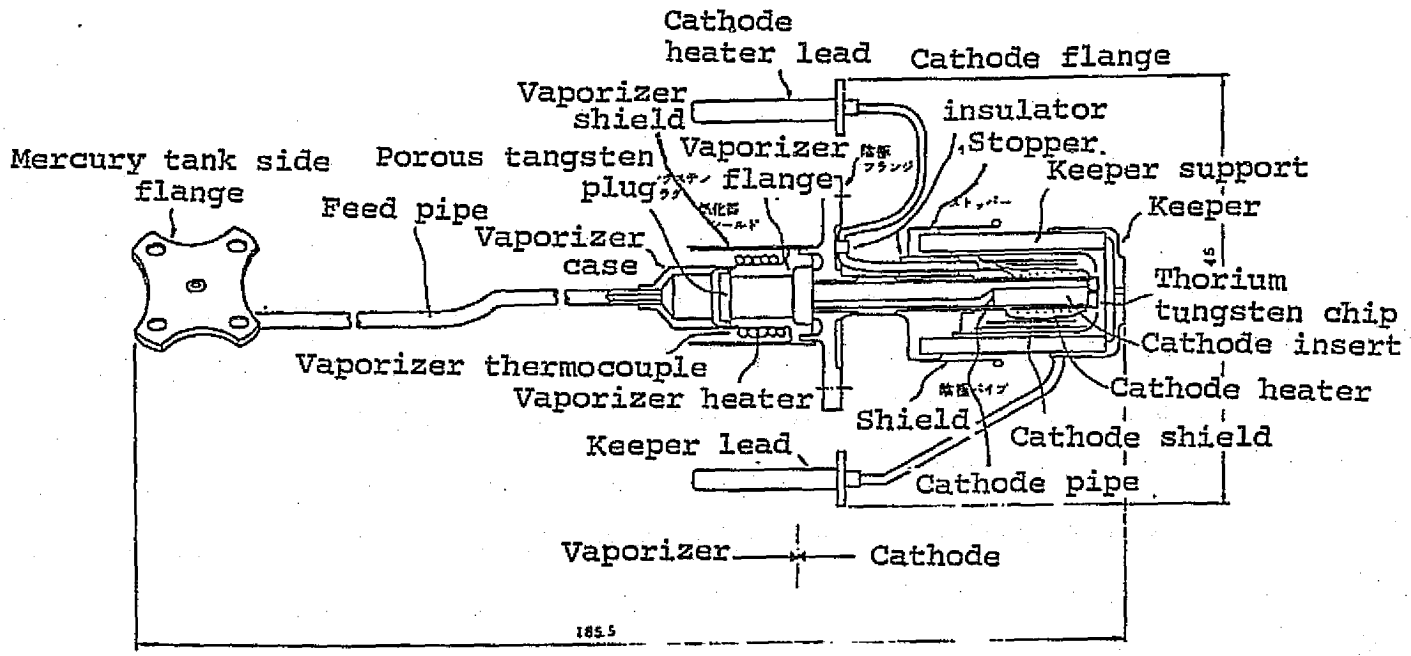

Fig. 4.20 Discharge Chamber Assembly

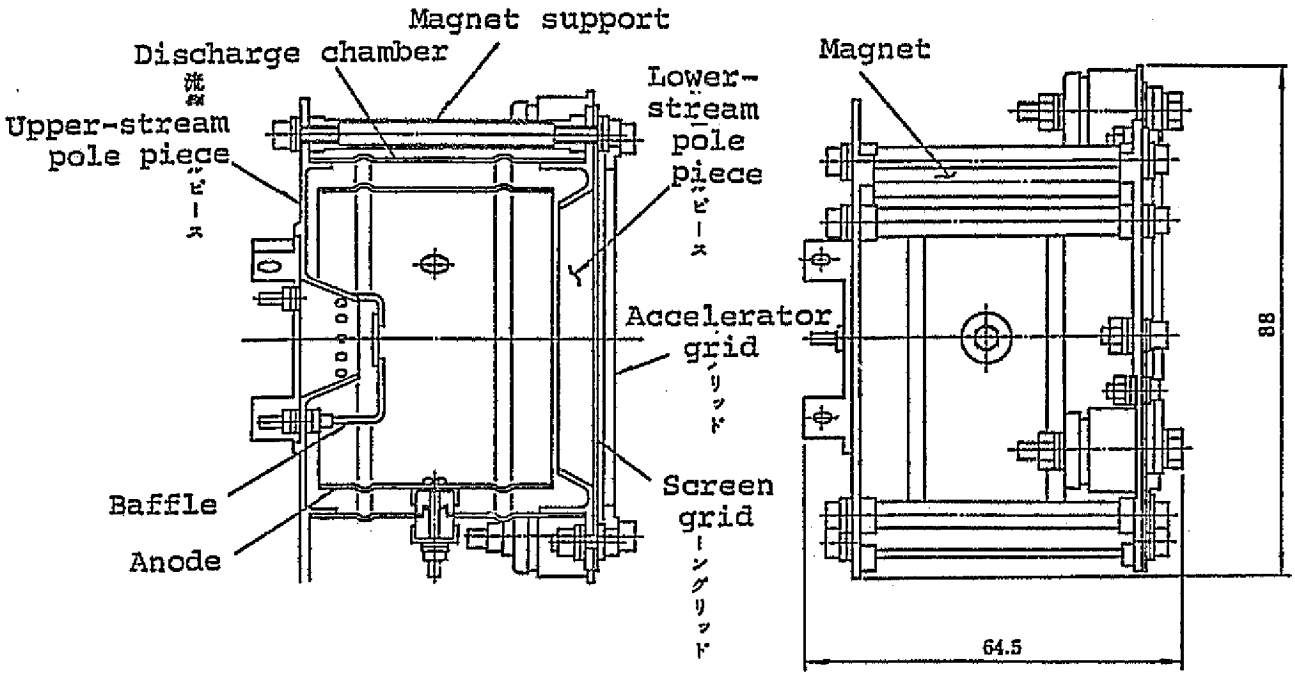

4.2.3 Structural Design

Feasibility of structural design was evaluated by structural analysis. Oscillation analysis results and test results are compared in Table 4.20. Load and stress analysis were made under the following conditions.

(a) Sine wave oscillation load conditions:

Controlled load 5G input
Ultimate load 6.25G input
Q=30

(b) Random oscillation load:

To horizontal direction of engine,
$f=350$ Hz, $So=0.2\ G^2/Hz$, $Q=30$
Ultimate coefficient 1.25
$Gmax=3\left(Q2\pi f\ So/4\right)^{\frac{1}{2}}=215$ G
To vertical direction of engine,
$f=900$ Hz
$Gmax=345$ G

(c) Steady acceleration:

Controlled load - 25G each to the direction of satellite axis and vertical direction
Ultimate load - 25G x 1.25

Safety factor, load and estimated stress of discharge chamber, determined by the load conditions (a), (b) and (c) are shown in Table 4.21. Safety factors calculated were all positive.

Table 4.20 Natural Oscillation of Discharge Chamber/Hollow Cathode

	Without tank support		With tank support	
	Test results	Analysis results	Test results	Analysis results
X-direction	-	197.22Hz	-	276.01Hz
Y "	200Hz	193.45Hz	275Hz	272.80Hz
Z "	340Hz	262.57Hz	560Hz	595.73Hz

Table 4.21 Analysis Values of Structural Design

(a) Safety Factor

Parts	Critical mode		Safety factor
Discharge chamber strut	Random oscillation,	yield	+0.1
Pole piece	"	"	+0.15
Main support screw(#2)	"	breaking	+2.0
Flange MCA	"	"	+0.02
Main support	"	buckling	>5.0
Discharge chamber	"	"	>5.0
Mounting screw(traction)*	"		+5.4
Mounting screw(shear)*	"		+10.4

*#10 steel bolts of Ftu=125000Lb , Fsu=75000Lb

(b) Load

Parts	部材名称		Rated acceleration* 定常加速度*	Sine wave oscillation** 正弦波振動**
Case IOS	ケースISO	P	0.4 Kg	–
		V	3.7 Kg	11.0 Kg
		M	55.0 Kg-mm	178.9 Kg-mm
Main support	メインサポート	P	0.6 Kg	–
		V	2.7 Kg	17.0 Kg
		M	130.0 Kg-mm	414.7 Kg-mm
Discharge chamber	放電室	P	4.3 Kg	–
		V	4.3 Kg	17.2 Kg
		M	180.8 Kg-mm	808.4 Kg-mm
Discharge chamber strut	放電室支柱	P	6.8 Kg	–
		V	1.6 Kg	5.2 Kg
		M	36.5 Kg-mm	121.9 Kg-mm

P: injection axial force
V: shearing force meeting P at right angle
M: moment
*Rated acceleration falls at right angles with injection axis. 25G, simultaneous.
**Q=20, input 5G. Oscillation at right angles to injection axis.

(c) Stress (unit: kg/mm^2)

Parts	部材名称	Rated Acceleration 定常加速度	Sine wave Oscillation 正弦波振動	
Discharge chamber strut	放電室支柱	2.20	25.0	
Main support screw(#2)	メインサポートネジ(#2)	3.8Kg(剪断)	9.2Kg(剪断)	——(shear)
Pole piece	ポールピース	3.0	7.1	
Flange MCA	フランジMCA	2.4	4.7	
Main support	メインサポート	0.3	0.9	
Discharge chamber	放電室	0.16	0.3*	

*For this value only, oscillation in the direction of injection axis.

4.2.4 Heat Design

(1) Thermal interface with satellite

In order to determine the thermal interface, a thermomathematical model of approximately 50 nodes was created and calculator simulation was made of 16 cases. For parameters, several combinations of (a) conduction heat resistance between the engine unit mounting panel on the satellite and the housing of the engine unit, (b) coefficient of radiation heat exchange between the satellite interior and the part of engine unit which faces the interior (this sentence's meaning unclear - translator) and (c)α/ε of screen shell which protrudes to the outside of satellite, were taken. Compatibility was determined using the following as allowable temperature conditions for the engine unit.

i) Minimum temperature of liquid mercury holding part during non-operation to be over -25C.

ii) Maximum temperature of mercury supply tank during operation to be under 150C.

iii) Heater power, which maintains the rated temperature in the main hollow cathode vaporizer and neutralizer hollow cathode vaporizer during operation to be over 1W and less than 4W.

Each case of simulation and the results are shown in Table 4.22. Following conclusions, satisfying the above conditions, were obtained.

(I) Conduction heat resistance between the satellite side engine unit mounting panel and the engine unit side housing should be over 1/0.58(deg/W).

(II) Radiation rate of the part which faces the satellite interior should be over 0.9.

(III) α/ε of screen shell should be over 0.9/0.5.

If the internal heat generated by the engine unit under rated operation is 38.6W, the heat balance when the temperature reaches balance level is as shown in Fig. 4.21.

(2) Heat design of engine unit

Engine unit, because of its functional requirements, is designed to have strong thermal isolation from the system comprising discharge chamber assembly and main hollow cathode assembly; and the neutralizer hollow cathode assembly, from the housing. Especially with the main hollow cathode assembly and vaporizer and cathode in the neutralizer ho hollow cathode assembly, improvements have been made on heat conduction pass, heat shield, etc. to secure their rated operation characteristics during operation and the transient temperature increase curve at the beginning of operation.

Fig. 4.21 Heat Balance of Engine Unit

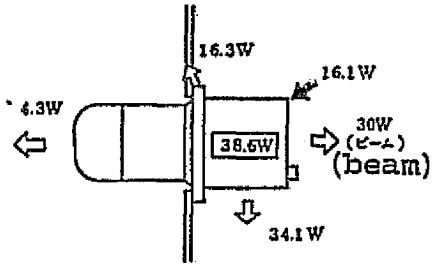

HC: hollow cathode
T_t: tank temperature
T_e: engine unit temp.
T_v: vaporizer temp.
All temp.& power approx.

Table 4.22 Results of Thermal Interface Trade-off Study

Case No.	R	Ein	α/ε	Twall	Ts/c	External heat Input	Engine unit	Required conditions for engine unit and compatibility		Heat density
ケース 1	1/0.03	0.9	1	−15℃	−15℃	Low	non-operation	T_t=15C; T_e=17C; T_v(min.): main HC=17C; neut. HC=39C	×	
ケース 2	〃	〃	〃	+55℃	+55℃	High	operation	T_t=95C; T_e=153C; To maintain rated T_v, main HC=1.4W and neut. HC=2.6W	×	ヒートデンシティ ~0.1W/㎠
ケース 3	1/0.58	0.02	1	−15℃	−15℃	Low	non-operation	T_t=15C; T_e=17C; T_v(min.): main HC=17C; neut.=HC 39C	×	
ケース 4	〃	〃	〃	+55℃	+55℃	High	operation	T_t=80C; T_e=136C; To maintain rated T_v, main HC=1.7W and neut. HC=2.7W	○	ヒートデンシティ ~0.7W/㎠
ケース 5	1/0.03	0.02	1	−15℃	−15℃	Low	non-operation	T_t=10C; T_e=13C; T_v(min.): main HC=12C; neut. HC=30C	×	
ケース 6	〃	〃	〃	+55℃	+55℃	High	operation	T_t > 200C; T_e > 200C; Control failure due to excessive increase in main HC T_v.	×	ヒートデンシティ ~0.2W/㎠
ケース 7	1/0.58	0.9	1	−15℃	−15℃	Low	non-operation	T_t=15C; T_e=17C; T_v(min.): main HC=17C; neut. HC=40C	×	
ケース 8	〃	〃	〃	+55℃	+55℃	High	operation	T_t=75C; T_e=130C; To maintain rated T_v, main HC=1.8W and neut. HC=2.8W	○	ヒートデンシティ ~0.5W/㎠
ケース 9	1/0.58	0.9	0.9/0.5	−15℃	−15℃	Low	non-operation	T_t=14C; T_e=15C; T_v(min.): main HC=14C; neut. HC=22C	○	
ケース10	〃	〃	〃	+55℃	+15℃	High	operation	T_t=75C; T_e=134C; To maintain rated T_v, main HC=1.7W and neut. HC=1.9W	○	ヒートデンシティ ~0.6W/㎠
ケース11	1/0.03	0.9	0.9/0.5	−15℃	−15℃	Low	non-operation	T_t=11C; T_e=11C; T_v(min.): main HC=10C; neut. HC=20C	○	
ケース12	〃	〃	〃	+55℃	+55℃	High	operation	T_t=101C; T_e=160C; To maintain rated T_v, main HC=1.3W and neut. HC=1.7W	×	ヒートデンシティ ~0.1W/㎠
ケース13	1/0.58	0.02	0.9/0.5	−15℃	−15℃	Low	non-operation	T_t=14C; T_e=15C, T_v(min.): main HC=14C; neut. HC=22C	○	
ケース14	〃	〃	〃	+55℃	+55℃	High	operation	T_t=89C; T_e=140C; To maintain rated T_v, main HC=1.6W and neut. HC=1.8W	○	ヒートデンシティ ~0.3W/㎠
ケース15	1/0.03	0.02	0.9/0.5	−15℃	−15℃	Low	non-operation	T_t=14C; T_e=1C T_v(min.): main HC=2C; neut. HC=14C	○	
ケース16	〃	〃	〃	+55℃	+55℃	High	operation	T_t > 200C; T_e > 200C; Control failure due toexcessive increase in main HC T_v.	×	ヒートデンシティ ~0.3W/㎠

R: conduction resistance(deg/w) between engine unit side mounting base plate and satellite side engine unit mounting panel. T_{wall}: temp. of engine unit mounting panel(constant). Ein:radiation rate in the satellite interior. α/ε: absorption rate/radiation rate anticipating space. T_s/c: temp. of satellite interior(constant). External heat input: full sunshine, High; high noon, Low. Heat density: heat input to mission panel II/contact area where contact area=22cm^2.

4.2.5. Electrical Design

Electrical design of the engine unit can be summed up in the design of its wire harness. The harness is designed under the following standards.

(a) In order to keep the temperature increase under 10C, allowable electric current is set as follows:

Wire size(AWG)	Allowable current
#20	3.7A
#22	2.5A
#24	2.0A

(b) Withstand voltage: under 50% of rated voltage.

(c) Environment(temperature): under 70% of rated temperature.

(d) EMC countermeasure: As a principle, RTN uses an exclusive circuit, and twists and shields are provided as necessary.

(e) Voltage and electric current of connectors: Under 50% of rated values(under 25% for voltage).

(f) Materials that do not degas are selected.

Performance requirements and parts used are given below.

(1) Circuit design

i) Wire harness from power conditioner to engine unit

a) Connectors to the power conditioner

For high voltage(over 6kV withstand voltage): AMP multi-pin LGH(7-pin, withstand voltage of 15kV)
For low voltage: Nikko Denki DBM-21W1(cannon)
Temperature monitor line: AMP HD-22 series

b) Wires

For high voltage: withstand voltage of over 3kV and temperature of up to 260C
For low voltage: temperature of up to 260C; MIL-W-16878 standard product(withstand voltage of 600V and temperature of less than 260C)
Temperature monitors:
Engine unit temperature(T_e) and tank temperature(T_{tank})
Shield twist pair wire, Raychem 44, A112-24

Cathode vaporizer temperature(T_{cv}) and
neutralizer vaporizer temperature (T_{nv})
Max 180C
MIL-W-16878, standard product

As an EMC countermeasure, wire harness uses 2-strand spiral wires which are shielded with copper tape (Scotch #1245).

ii) Inside of engine unit

a) Terminal

Repeating point of wire harness from the power conditioner and connections inside the engine unit is designed as shown in Fig. 4.22, repeating through a caulking terminal.

b) Internal connections

As the temperature inside the engine reaches about 300C, anoxia copper wire(EOF CuWJIS H3503 0.8ø) of 0.8ø-diameter(equivalent of #22AWG) is used.

(2) Wiring

Instrumentation wiring diagram covering the connectors to power conditioner to the inside of the engine unit is shown in Fig. 4.23.

Fig. 4.22 Structure of Engine Unit Terminal

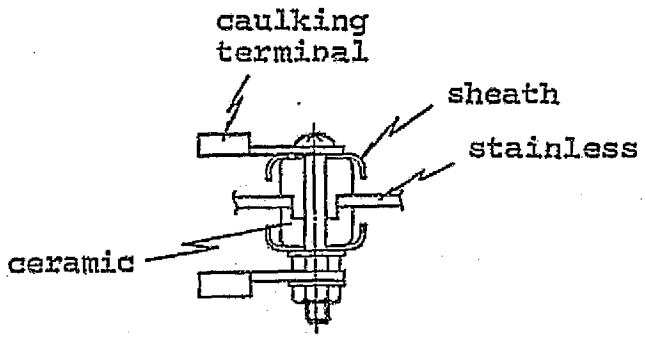

Fig. 4.23 Engine Unit Instrumentation Wiring Diagram

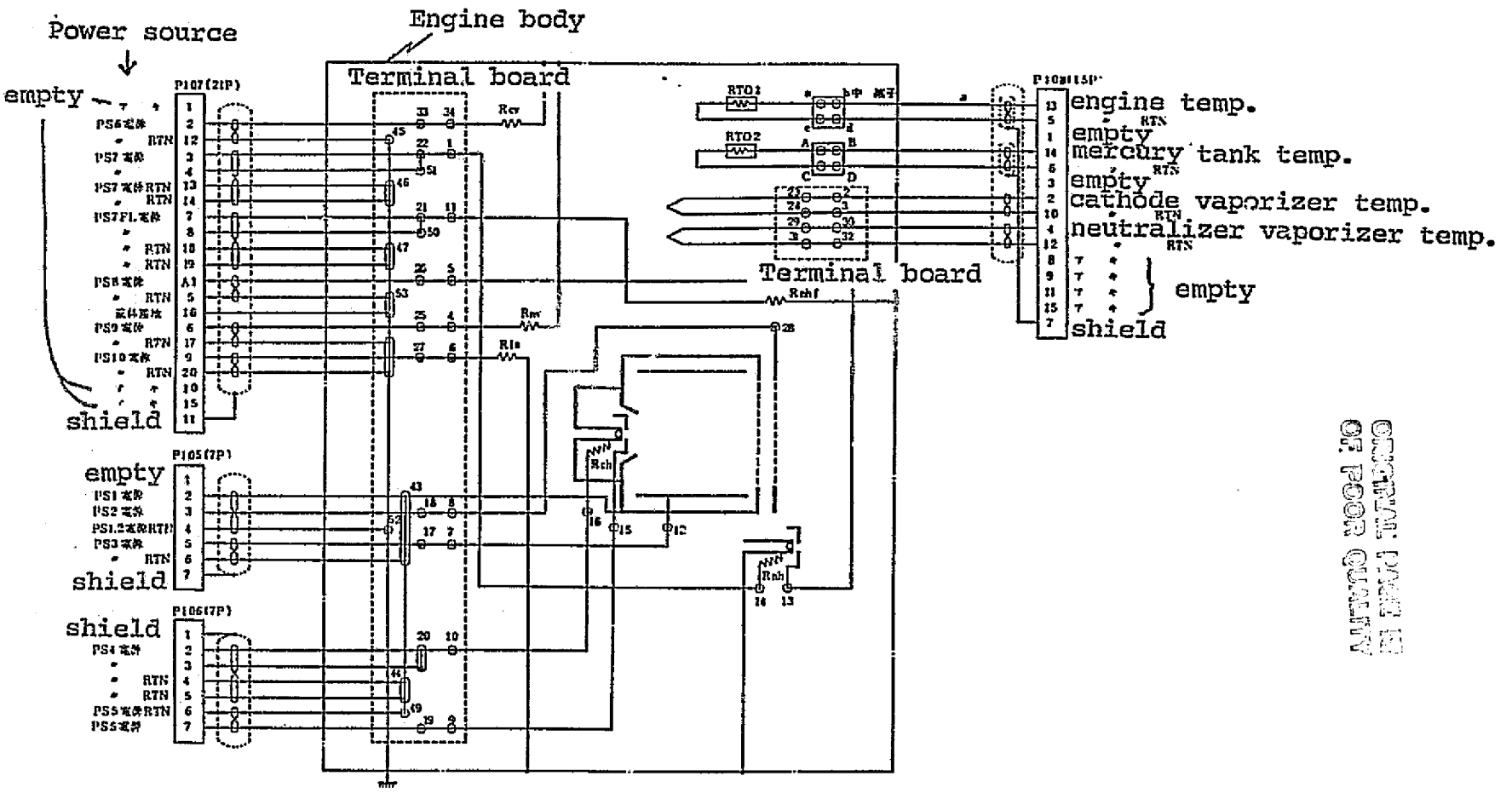

4.2.6 Reliability Design

Engine unit reliability was estimated by the following methods.

a. Analytical estimation

1) Calculation of structural reliability by stress/strength model.

2) Calculation using accidental breakdown model, if the breakdown rate is known or the breakdown rate of a similar hardware is available.

b. Estimation by test

$$MTBF = \frac{T}{X^2_{2r+2,\alpha}}$$, where T: total operation time
r: # of breakdowns
α: reliability standard of 50%.

Reliability calculation method for each assembly is shown in Table 4.23. Reliability block diagram and the results of calculations of breakdown rates and reliability levels are shown in Table 4.24. For the breakdown rate of main hollow cathode, it was assumed that tests could substantiate MTBF 500 hours and the breakdown rate of neutralizer hollow cathode was assumed to be 2/3 of the main hollow cathode based on its complexity.

Table 4.23 Classification of Reliability Calculation Methods

No.	Assembly	Analysis: stress/strength	Analysis: accidental breakdown	Test	Remarks
1	Tank		O		
2	Main hollow cathode			O	
3	Discharge chamber		O		
4	Neutralizer hollow cathode			O	Based on similaries to main hollow cathode.
5	Wire harness		O		Breakdown rate of connectors & thirmister
6	Structure	O			
7	Neutralizer filament	N/A	N/A	N/A	Eliminated, as it is for back-up.

Table 4.24 Block Diagram of Ion Engine Unit Reliability

Block diagram of reliability

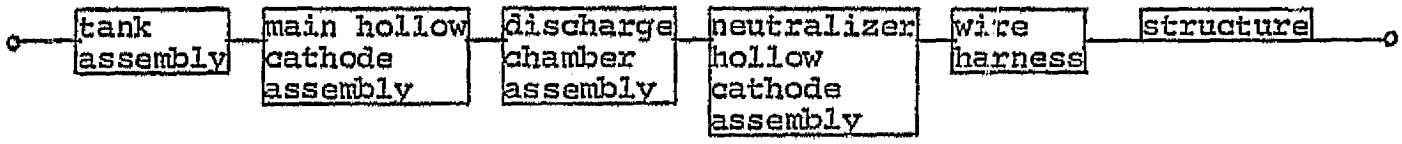

(Neutralizer filament is for back-up and thus not included in the reliability estimation model.)

Breakdown rate and reliability

	1	2	3	4	5	6
Assembly	tank	main hollow cathode	discharge chamber	neutralizer hollow cathode	wire harness	structure
Breakdown rate ($\times 10^{-6}$/hr)	0.467	2000	0.030	1333	0.082	-
Reliability (R_1)	0.9959	0.7408	0.9097	0.8188	0.9993	0.9999
Operation time		150 hrs.		150 hrs.		

Mathematical model

$$R_{IEE} = R_1 \times R_2 \times R_3 \times R_4 \times R_5 \times R_6 = 0.6034$$

Table 4.25 Development Test Flow(Engine Unit)

Test subject	Test items	Execution date
charge·insulation resistance test	I E E(1), I E E(2)	1 9 7 9 4 / 1 5
wt. & cntr. of gravity check(I)	I E E(1), I E E(2)	4 / 1 5 ~ 4 / 1 7
performance test(I)	I E E(1), I E E(2)	4 / 2 0 ~ 5 / 1
wt. & cntr. of gravity check(II)	I E E(1), I E E(2)	5 / 7 ~ 5 / 1 0
oscillation test	I E E(1)	5 / 2 5, 2 6, 2 7
heat vacuum test	I E E(1)	6 / 5, 6, 7
performance test(II)	I E E(1)	6 / 7 ~ 6 / 1 3
thrust measurement	I E E(2)	6 / 1 4 ~ 6 / 2 2
electromagnetic compatibility test	I E E(2)	7 / 3 ~ 7 / 5
residual magnetic moment measurement	I E E(1), I E E(2)	7 / 1 0 ~ 7 / 1 3

Table 4.26 Characteristics at Rated Flow

Parameter		Nominal value 公称値*	IEE(1)	IEE(2)
Beam voltage	(KV)	1	0.99	0.99
Beam current	(mA)	30	30.0	29.0
Accelerator grid voltage	(KV)	−1	−1.02	−1.02
Accelerator grid current	(mA)	∠1以下	∠1以下	∠1以下
Discharge voltage	(V)	40	49.7	41.2
Discharge current	(A)	0.35	0.35	0.35
Main hollow cathode: cathode heater power	(W)	0	0	0
Main hollow cathode: keeper voltage	(V)	15	14.7	16.0
Main hollow cathode: keeper current	(A)	0.3	0.30	0.3
Main hollow cathode: vaporizer heater power	(W)	∠7以下	3.3	3.9
Neutralizer hollow cathode: cathode heater power	(W)	0	0	0
Neutralizer hollow cathode: keeper voltage		24	22.2	18.6
Neutralizer hollow cathode: keeper current		0.25	0.245	0.245
Neutralizer hollow cathode: vaporizer heater power		∠39以下	0.6	0.8
Insulator heater power		3	3.1	3.1
Main hol. cathode vaporizer temp.		−	320	316
Neut. hol. cathode vaporizer temp.		−	226	222
Engine potential	(V)	−	−234	−19.6
Target potential	(V)	−	11.5	13.8
Total power consumption	(W)	∠683以下	650	615
Mercury flow (main hollow cathode)	$\times 10^{-1}$(g/sec)	9	9.11	9.35
" " (neut. hollow cathode)	$\times 10^{-1}$(g/sec)	1	1.06	1.07
Propellent util. efficiency(main HC)	(%)	70	69	65
Thrust	(g重)	0.18	0.197	0.191
Specific impulse	(秒)	2200	2153	2032
Power efficiency	(%)	44	45.6	46.8
Propulsive efficiency	(%)	−	31.3	30.2
Beam diffusion angle	(°)	30	approx. 約30	approx. 約30

*Nominal values are based on NASDA-ESPC-41 "Development Specifications for Ion Engine System."

4.2.7. Development Tests

Objectives of Development Tests were to verify the engine unit (IEE) design and to spot any problems in design and manufacturing processes by performance and environment tests with an engineering model(EM) as a sample. Another objective was to establish test methods for Qualifying and Acceptance Tests.

In order to accomplish these objective, tests and inspections shown in Table 4.25 were carried out. Because of an incident in which discharge voltage rose abnormally at the time of IEE(1) beam injection, test to find the cause were added to the initial list of tests.

Below are the results which require explanations. Although most test results satisfied specifications, heat design was reevaluated due to an abnormal increase in discharge voltage at beam injection and structural changes were made due to problems in oscillation test.

(1) Performance test(I)

Following tests were given.

IEE(1): operation check and measurement of beam diffusion angle

IEE(2): operation check, testing with varied parameter and measurement of beam diffusion angle

(1-a) Operation check

The test was for checking that main discharge and beam injection were maintained stable. Table 4.26 shows the comparison of operation characteristics at the rated flow between nominal values, IEE(1) and IEE(2). In both IEE(1) and IEE(2) discharge and beam injection were maintained stable. It was found, however, that discharge voltage of IEE(1) reached an abnormally high V_D immediately after beam injection. Details of investigation of the cause and the consequent design change

are discussed in Section 6.1. As a result, improvement was made in the heat design of main hollow cathode.

(1-6) Test with varied parameter

This was performed for IEE(2). Fig. 4.24 shows the changes in keeper voltage and discharge voltage and Fig. 4.25 shows the changes in beam current, drain current, engine potential(between engine and grounding) and target potential(between collector and grounding), in relation to main hollow cathode keeper current. Discharge current is used as a parameter, with 4 variations. Fig. 4.26 shows the changes in keeper voltage and Fig. 4.27, changes in engine potential, target potential and drain current, in relation to neutralizer keeper current. Here, 3 variations of neutralizer vaporization temperature as a parameter are shown.

(2) Oscillation test

Results of modal survey of IEE(1) preceding oscillation test are as follows. They satisfied the required natural oscillation of over 100Hz.

Axis	Primary resonance pt.	Secondary resonance pt.
X	280Hz	900Hz
Y	258Hz	812Hz
Z	580Hz	1100Hz

For IEE(1), sine wave oscillation test and random oscillation test were given at QT level for each of X, Y and Z axis.

During the oscillation test, following problems occurred.

i) Breaking of lead wire in the neutralizer hollow cathode keeper area during Y-axis random oscillation test.

ii) Slipping of cathode insert in the neutralizer hollow cathode.

Problem 1

Neutralizer keeper lead wire broke off at random Y-axis after sine wave oscillation of random X-axis. Location of break-off is shown in Fig. 4.28(a). Following conclusions were obtained by analysis.

i) Y-direction primary resonance mode was excited and caused the break-off. This resonance point is estimated to have been slightly less than the maximum oscillation frequency 2000 Hz.

ii) As a countermeasure, there, Y-direction resonance point should be moved to over 2000Hz.

A design change based on the conclusions was made to secure the lead wire between A and B, as shown in Fig. 4.28(b).

Problem 2

During performance check after oscillation test, malfunctioning of neutralizer hollow cathode occurred: plasma heat from keeper discharge did not reach cathode insert, resulting in a phenomenon indicating an insufficient electron emission. Observation of the inside, by cutting the hollow cathode, showed that welded part of the cathode insert support wire lifted off, causing the cathode insert to slip. As the problem was thought to be caused by the welding structure rather than welding conditions, supporting tantalum wire was replaced by a pipe made of tantalum foil. Fig. 4.29 shows a cross-section of the hollow cathode before and after the change.

(3) Heat vacuum test

The test was given to IEE(1) after replacing the neutralizer hollow cathode which caused problems in the oscillation test.

Operating conditions of the engine under the conditions given below were satisfactory, and data on temperature changes in each part of IEE was obtained.

- Constant temperature (+20C) operation.....operation check (once)
- Low-temperature (-5C) non-operation.....heat balance in non-motion at low temperature (once)
- Low-temperature (-5C) ~ high-temperature (+45C) motion.....motion under extreme temperature condition (once)
- High-temperature (+45C) motion.....heat balance in motion at high temperature (once)
- Low-temperature (-15C) operation.....operation check under low temperature condition (4 times)
- High-temperature (+55C) operation.....operation check under high temperature conditions (once)
- High temperature (+55C) ~ constant temperature (+20C) motion..... motion under extreme temperature conditions (once)

Note: temperatures in ( ) are the base plate temperatures.

(4) Performance Test (II)

For IEE(1), similar tests with varied parameter as given to IEE(2) in the performance test (I) was given.

(5) Measurement of thrust

The test was given to IEE(2), using two methods (see Section 3.2.6) direct measurement by hanging the ion engine on a thrust measuring balance; and indirect measurement by catching ion beam in a cone hang from thrust measuring balance. Results are shown in Table 4.27. "Calculated values" were obtained assuming that all ions are univalent and that beam does not diffuse.

(6) Electromagnetic compatibility test

The following subjects were tested.

Electric field radiation interference noise (RE02)

Magnetic field radiation interference noise(RE01)

Conduction interference noise(CE04)

(7) Measurement of remanence moment

Results are shown in Table 4.28. In the combination of IEE(1) and IEE(2), slope of axis of thrust of the engine units was both 1.1°.

Fig. 4.24 Main Hollow Cathode Keeper Voltage vs. Main Hollow Cathode Keeper Voltage and Discharge Voltage

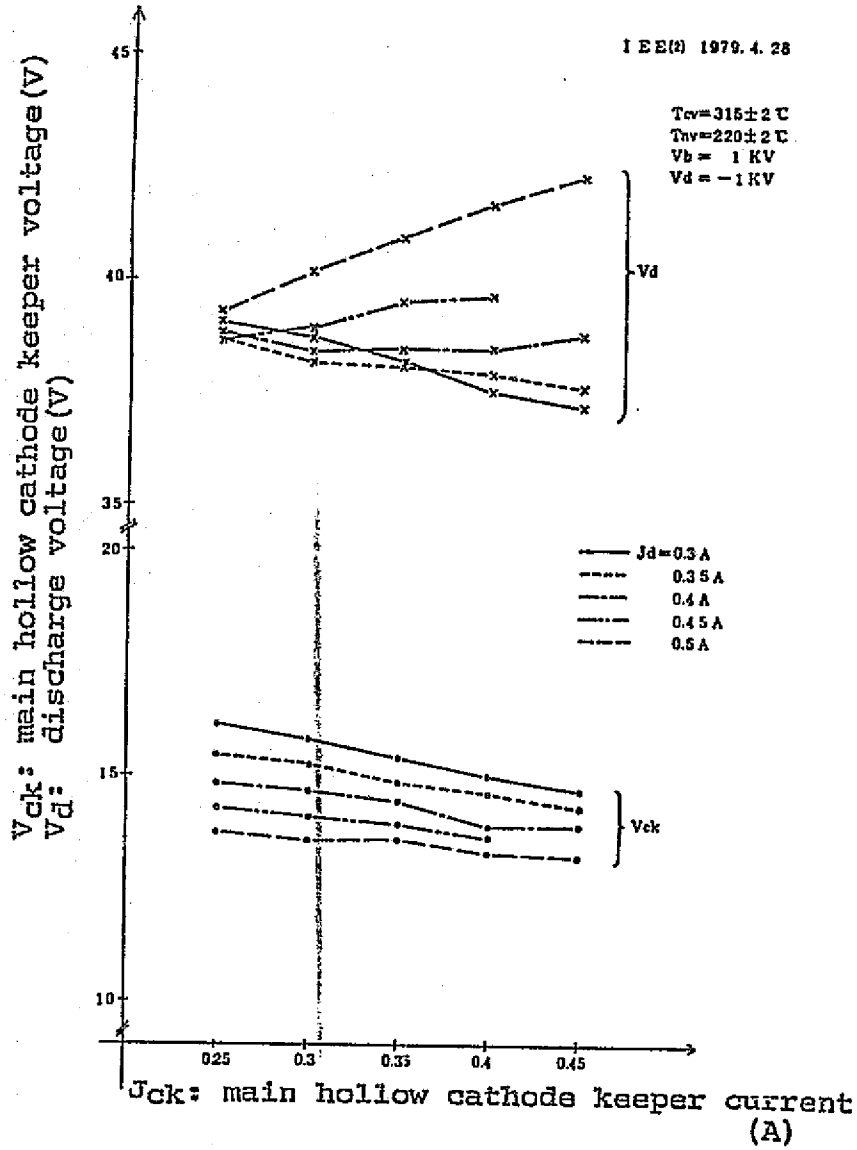

Fig. 4.25 Main Hollow Cathode Keeper Current vs. Beam Current, Drain Current, Engine Potential and Target Potential

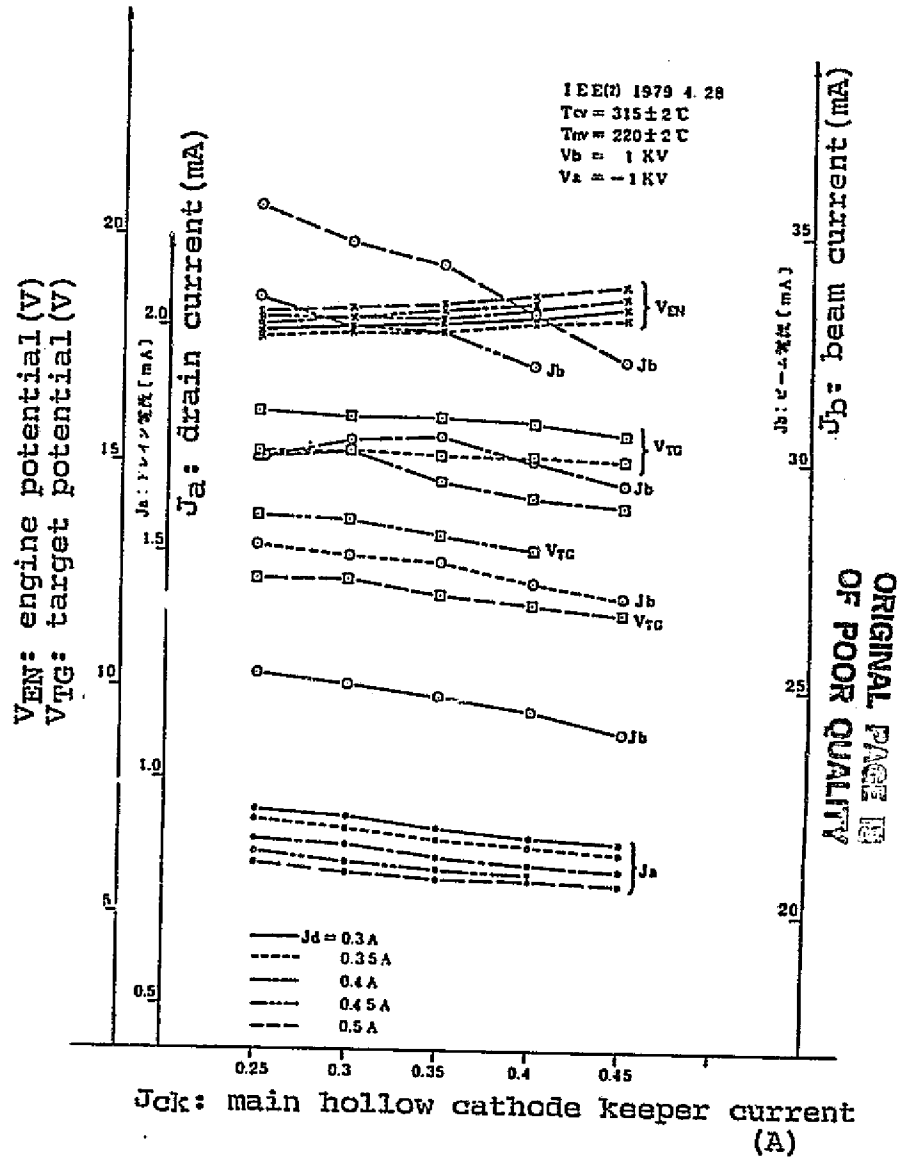

Fig. 4.26 Neutralizer Hollow Cathode Keeper Current vs. Keeper Voltage

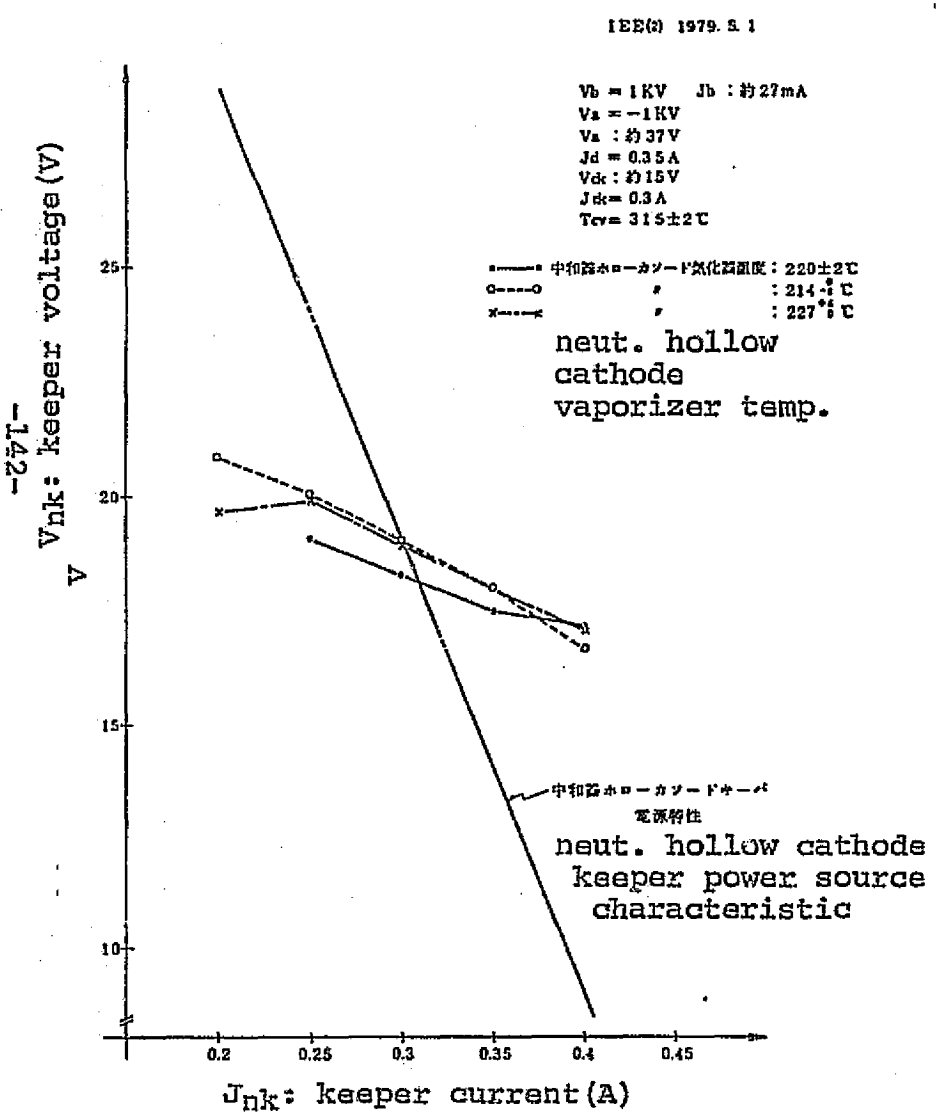

Fig. 4.27 Neutralizer Hollow Cathode Keeper Current vs. Engine Potential, Target Potential and Drain Current

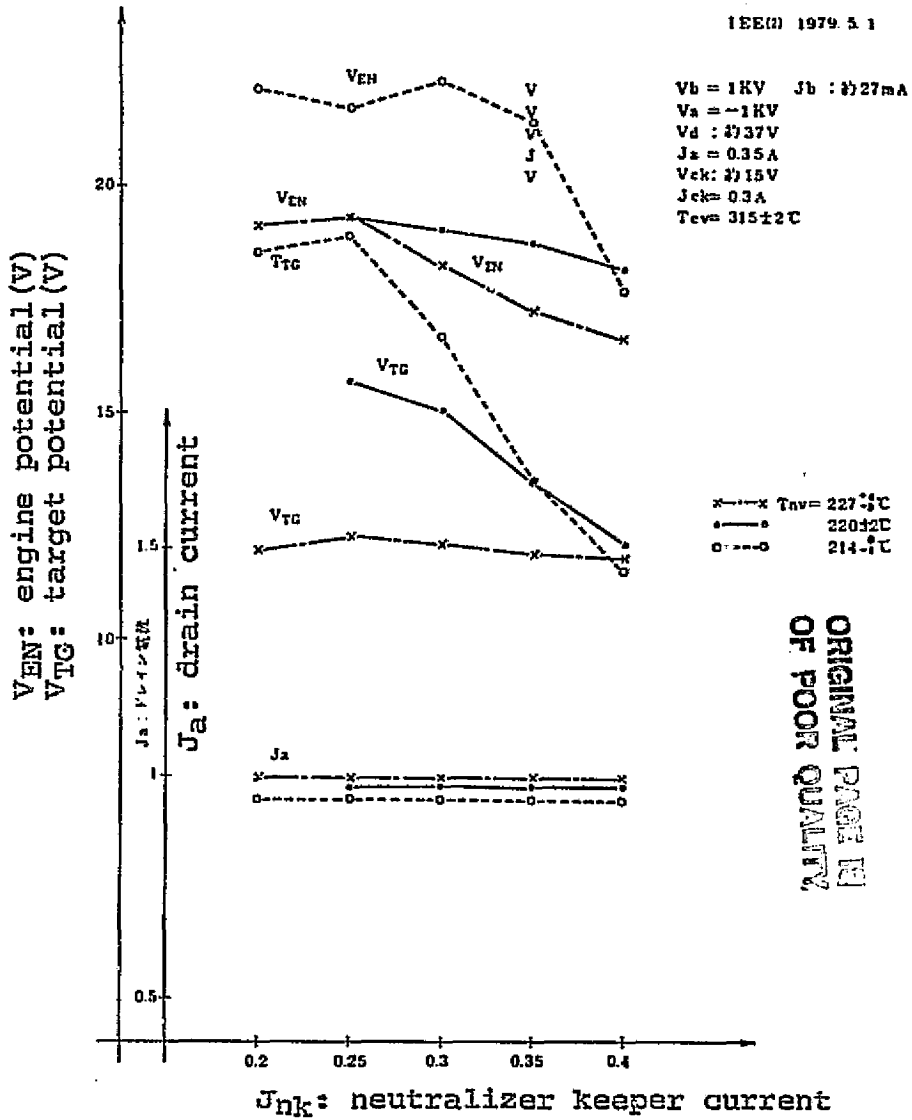

Fig. 4.28 Neutralizer Keeper Lead Wire Support Method

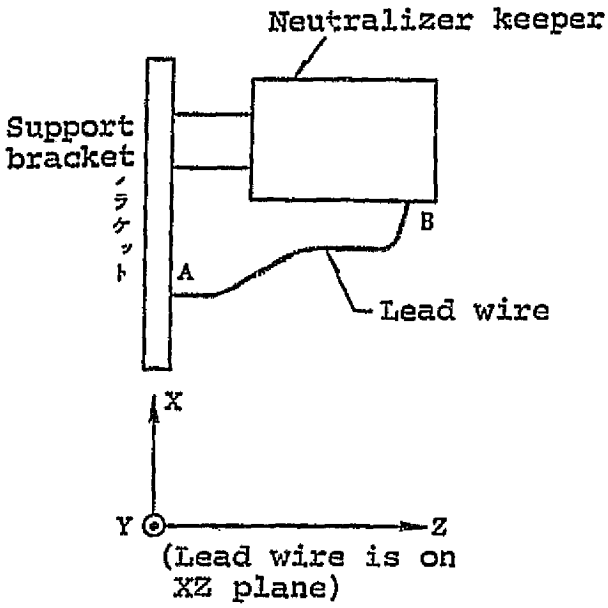

(a) EM

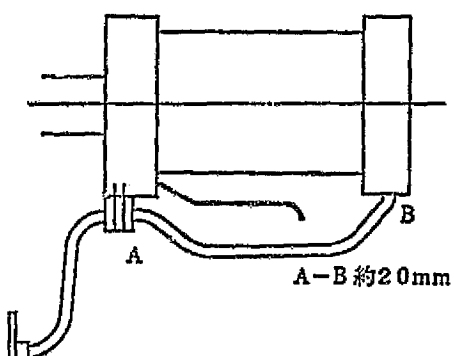

(b) after improvement

Fig. 4.29 Neutralizer Hollow Cathode Insert Support Method

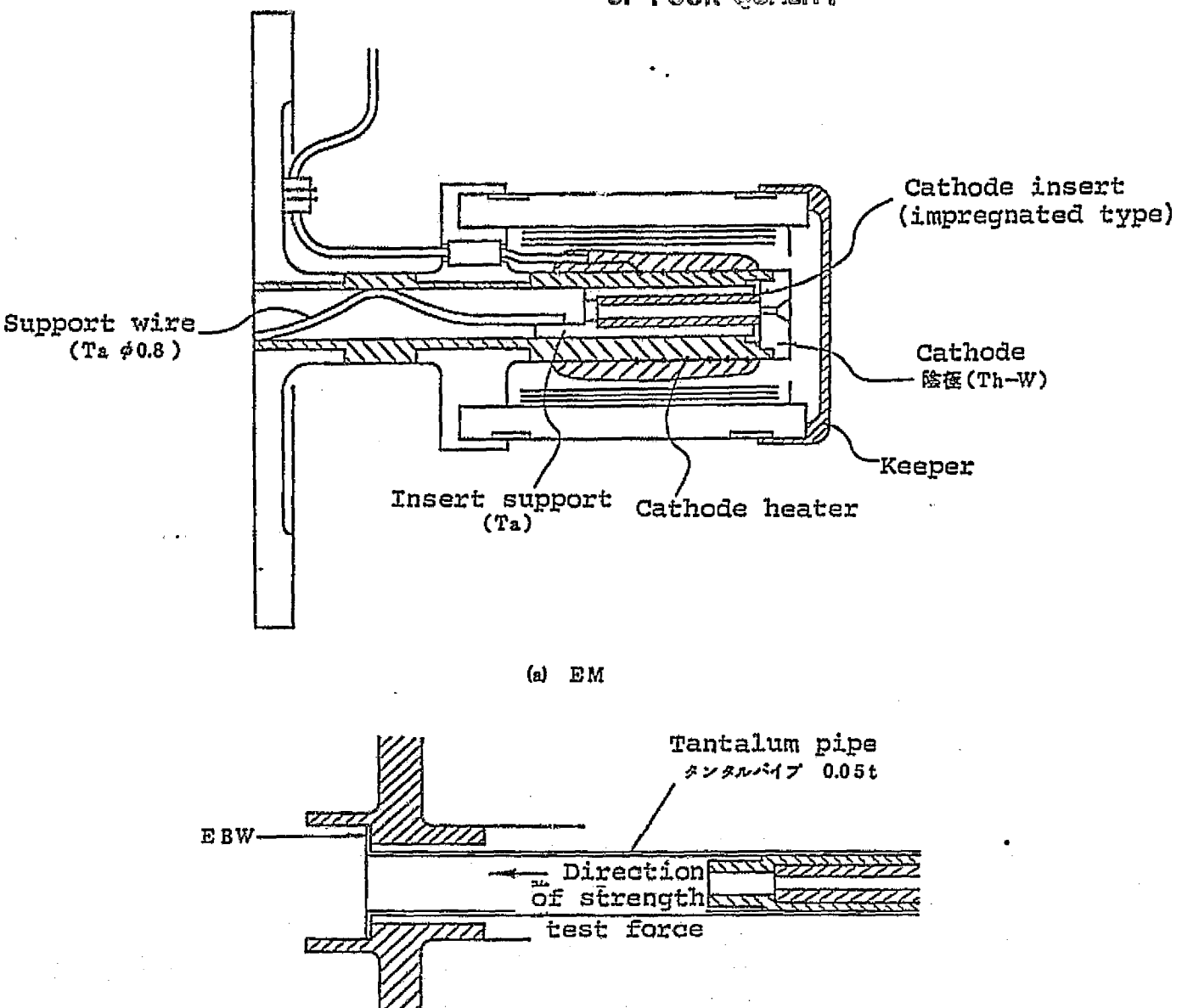

(a) EM

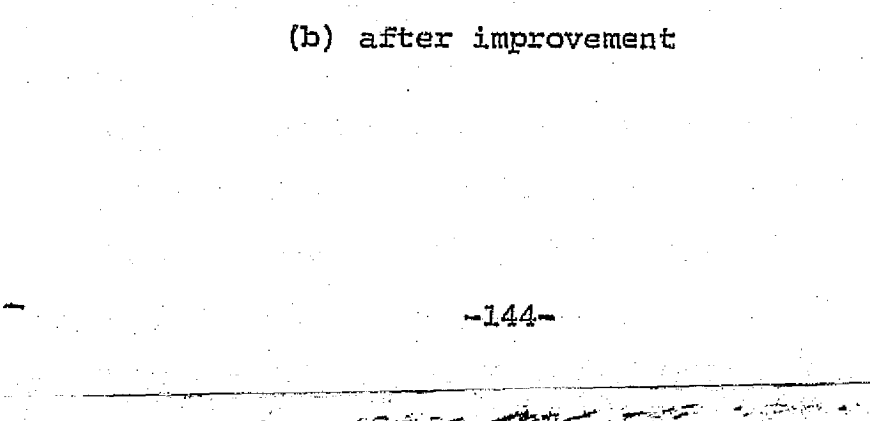

(b) after improvement

4.3 Power Conditioner

Basic design of power conditioner which satisfies the specifications in Section 4.1 and the results of development tests on EM which was produced based on this basic design are discussed in this section.

4.3.1 Electrical Design of Power Source Device

Block diagram of the power source device is the same as that given in Fig. 3.29. The device consists of power sources PS1 ~ PS10 which supply power to the engine, auxiliary power source, master oscillator, telemetry exchange unit, monitor circuit and protective logical(AND/OR) circuit.

(1) Screen grid power source and accelerator grid power source

These are the power sources which prevent acceleration of ion beam and reverse current of neutralized electrons. Power supply of the former(screen grid power source) reaches 50% of the total power, and its contribution to the weight and efficiency is accordingly large. This is achieved by a combination of a fixed pulse width converter and a booster-type chopper regulator for pulse width control. Output voltage is variable with commands. This power source receives ON/OFF signals from protective logical circuit(described later) and is protected from excess load. Structure is shown in Fig. 4.30. Excess current protection circuit(limits current), because of its tedious composition, has been omitted after PM.

(2) Discharge power source

This is a power source used for plasma formation in the discharge chamber and employs a constant-current system. It is characterized by that its input power floats at the above-described screen grid voltage with respect to the satellite potential, and it is necessary to detect output voltage and current at the screen grid potential and to

insulate and amplify to the satellite potential having a control circuit. Power sources whose output float at the screen potential are also used in other power source systems described later, and insulation of such control monitor circuits employs AM modulation method(fixed modulation frequency). Block diagram of insulation circuit is shown. It includes a circuit for delivering output voltage from the satellite potential which varies output current with magnitude commands from the discharge power source itself and controls closed loop for main cathode vaporizer power source. The composition is shown in Fig. 4.31.

(3) Main cathode heater power source

This is for heating cathode hollow cathode in the discharge chember at start, and supplies the maximum of 36W AC power to heater wire at the hollow cathode chip. Actual circuit is of push/pull type inverter which is not stable and controls electric current only when cold-starting the heater. Composition is shown in Fig. 4.32.

(4) Main cathode keeper power source

This power source is for starting and maintaining discharge in the main cathode. As shown in the specifications, it supplies power of 300V and 5mA at start and 15V and 0.3A during steady operation. Drooping characteristic of load is also required. The circuit uses a push-pull converter and the drooping characteristic of output is obtained by combined use of choke coil and transistor constant current switch circuit. Circuit composition is shown in Fig. 4.33.

(5) Main cathode vaporizer power source

This power source is for producing necessary amount of gas mercury from liquid mercury for engine operation. It needs to be able to control a closed loop for stabilizing the amount of mercury vapor in

the main cathode. The circuit employs a push-pull inverter which controls pulse width and the closed loop control can be set by magnitude commands in the constant current AC power source. Composition is shown in Fig. 4.34.

(6) Neutralizer heaer power source

This is for heating neutralizer hollow cathode, supplying maximum of 25W-AC output to heater wires. Circuit composition is similar to that of main cathoder heater power source: a push/pull type inverter with unstable output voltage.

(7) Neutralizer keeper power source

Power source for starting and maintaining discharge in the neutralizer, it supplies power of 300V and 5mA at start and 24V and 0.25A during steady operation of ion engine. As with main cathode keeper power source, drooping characteristic of load current is required. Circuit composition is also similar to that of main cathode keeper power source(See Fig. 4.33).

(8) Neutralizer vaporizer power source

This circuit controls the amount of gas mercury passing through neutralizer and its composition is quite similar to that of the vaporizer power source for main cathode(See Fig. 4.34).

(9) Insulator heater power source

This power source prevents liquefaction of mercury vaporized in the cathode vaporizer. Circuit system is that of unstable push/pull inverter.

(10) Auxiliary power source

This power source supplys power to the 10 power drive cuicuit control circuits described earlier and logical circuit. Composition is shown in Fig. 4.35.

As described above, the power source device consists of 10 power source circuits, auxiliary power source, master oscillator, telemetry circuit, monitor circuit, etc. In order to reduce power consumption, CMOS-IC is used in pulse width control and varying elements in the converter/inverter units; and screen grid/accelerator grid power source and discharge power source, because of their large output, use drive transformer for higher efficiency.

Following points were considered in designing.

(11) Insulator circuits

Insulator circuits are required in the current telemetry circuit of discharge power source and cathode keeper power source, because their output are floated at the screen grid potential. Discharge current, discharge voltage and main cathode keeper current are detected at the screen grid potential, accurately converted to the satellite grounding potential and sent out as output control or telemetry signals. A combination of pulse transformer and V/F-F/V converter was planned in the preliminary design stage, but it was discovered, during a combined test of engine and power source device, that faulty movements could occur when the load change and V/F converter output cycle reached the same level in the semi-stable condition theoretically held by the engine unit. Therefore, AM modulation method was employed despite its added weight. The composition of the circuit is shown in Fig. 4.36.

(12) Primary and secondary power source insulation

While it is necessary to insulate primary and secondary power sources with insulation resistance of over 1MΩ, all power source groups in the device are secondary and the entire control system is grounded with secondary power source. Thus, as the primary side of the push/pull

converter is grounded with primary power source and the control system of above-described output detection, error amplification, etc. is grounded with secondary power source, it is necessary to place a circuit having a resistance of over 1MΩ and which transmits signals somewhere in the power source circuit. Such a system can be that of transmitting analog amount or transmitting digital amount. In this power source device, the latter proves superior both in accuracy and stability, due to the use of switching regulator. As a transmission element, pulse transformer and photo coupler were considered. Photo coupler was chosen because of its power consumption. The circuit is shown in Fig. 4.37.

(13) Telemetry exchange circuit

Telemetry required by the specifications can be classified into:

i) DC current and voltage telemetry

ii) Power telemetry

iii) AC current telemetry

iv) Temperature telemetry, and

v) Dielectric breakdown telemetry.

Design points are as follows.

i) DC current and voltage telemetry

They are either at the satellite potential, such as beam current and beam voltage, or floating at the screen potential, such as discharge current and voltage. Discharge voltage and current share the insulator circuit used for control, but the main cathode keeper current requires an exclusive insulator circuit. Linear IC was employed for current telemetry, as resistance was required for current detection and the size of detection resistance

greatly affected the power source efficiency, and to secure an appropriate output impedance. Amplifier was also used for measuring voltage.

ii) Power telemetry

This applies to main cathode heater power and neutralizer heater power. It uses primary side current, detected and adjusted, and a circuit system which amplifies current telemetry signals with auxiliary power source which has been insulated from signal return and primary power source return. Advantages of this system is that the isolation between the primary power source return and signal return is complete and that voltage drop due to primary power source return is not added to the current telemetry signals.

iii) AC current telemetry exchange circuit

This applies to the main cathode and neutralizer vaporizer current telemetry. AC current is detected and insulated by current transformer, exchanged to DC voltage by an effective AC - DC voltage converter and then sent by IC having a required amplification.

iv) Temperature telemetry

In a temperature measuring circuit, temperature measuring element is determined by the temperature of the point to be measured or by the shape of the mounting area. The element then becomes a factor in determining a circuit. Main cathode vaporizer and neutralizer vaporizer temperatures are measured by a thermocouple, and heat sink(?) and the standard vaporizer temperature are

measured by a thermister. Thermocouple requires a cold junction compensator which requires an exclusive power source and is also heavy in weight. Instead, the cold junction side of thermocouple was measured with thermister and thermocouple output was adjected by its output.

v) Dielectric breakdown number telemetry circuit

Beam current and accelerator current are detected inside the power source device and sent to sequence status area of the power source control device through Schumit trigger circuit of CMOS-IC having a set threshold.

(14) Monitor circuit

This circuit monitors movements of the engine unit by the output of its power source device, converts it to binary signals of HIGH/LOW by the threshold value and sends them to power source control device. The circuit uses a comparator circuit of linear IC and its threshold value is determined by the standard voltage of constant voltage diode. Each telemetry output is used as an input for the monitor circuit, and, for the transient state peculiar to ion engine, excessive response is prevented by inserting a primary delay element in the input side of the circuit.

(15) Protective circuit

This circuit detects beam current and accelerator current and shuts off screen grid/accelerator power source and main cathode vaporizer power source when excessive current comes in. It turns them back on again after a certain time. In consideration to the slow start function of output voltage of both high voltage power sources, it permanently shuts off the sequence when the overload reaches 12 times per 46 seconds. Circuit composition is shown in Fig. 4.38.

(16) Master oscillator

Generally, reduction in weight can be expected as switching frequency of power source is increased, but its efficiency lowers due to increased switching loss of diode and transistor against the total loss. In each DC power source, frequency of 20kHz from the oscillator is divided in two by flip-flop to drive the push/pull converter. The same 20kHz is divided in two and the requlting 10kHz is sent to each AC power source and divided again in two by flip-flop to drive a push/pull converter. Oscillation frequency of the 10 power sources, auxiliary power source, insulation circuit and power source in the power source control device was all singularized in order to prevent interference between power sources and to simplify EMI countermeasures. Each frequency of 160kHz, 40kHz, 20kHz and 10Hz, used in the basic oscillation circuit, is devided from the main source oscillation of 160kHz by CMOS flip-flop, or (missing word) and sent out. Its composition is shown in Fig. 4.39. Accuracy of oscillation frequency can be evaluated mainly by its temperature characteristics which depend on threshold value of CMO-IC, power source voltage, protective diode of gate, resistance, temperature characteristics of condenser, etc., and is kept at ±3% in consideration to average temperature increase within the baseboard and design temperature range.

Table 4.27 Thrust

Case No.	Jd (A)	Va, Vb (KV)	Jb (mA)	Calculated value (g wt)	Measured value (gwt)	Measured/calculated value (%)	
1	0.35	0.8	25	0.15	0.14	93	*
2			24	0.15	0.14	93	**
3	0.35	1	27	0.18	0.16	89	*
4			26	0.17		94	**
5	0.35	1.2	34	0.24	0.19	79	*
6			27	0.20	0.19	95	**
7	0.35	1.4	32	0.25	0.21	84	*
8			29	0.22	0.21	95	**
9	0.35	1.6	39	0.32	0.24	75	*
10			30	0.25	0.23	92	**
11	0.4	0.8	27	0.16	0.16	100	*
12			26	0.16	0.15	94	**
13	0.4	1	28	0.19	0.18	95	*
14			28	0.19	0.18	95	**
15	0.4	1.2	30	0.22	0.21	95	*
16			29	0.21	0.20	95	**
17	0.45	1.4	31	0.25	0.23	92	*
18			31	0.24	0.23	96	**
19	0.45	0.8	28	0.17	0.16	94	*
20			29	0.17	0.16	94	**
21	0.45	1	29	0.19	0.19	100	*
22			30	0.20	0.19	95	**
23	0.45	1.2	31	0.23	0.22	96	*
24			32	0.23	0.22	96	**
25	0.45	1.4	33	0.26	0.25	96	*
26			33	0.26	0.25	96	**

*Directly measured by hanging engine from thrust measuring balance.
**Indirectly measured by catching ion beam in a cone.

Table 4.28 Remanence Moment

	first time (μwb·m)	second time (μwb·m)	average (μwb·m)
IEE(1) component	3.47	3.59	3.53
IEE(2) component	3.63	3.60	3.62
IEE(1)/IEE(2) combinat'n	0.33	—	—

Fig. 4.30 Block Diagram of Screen Grid and Accelerator Grid Power Source

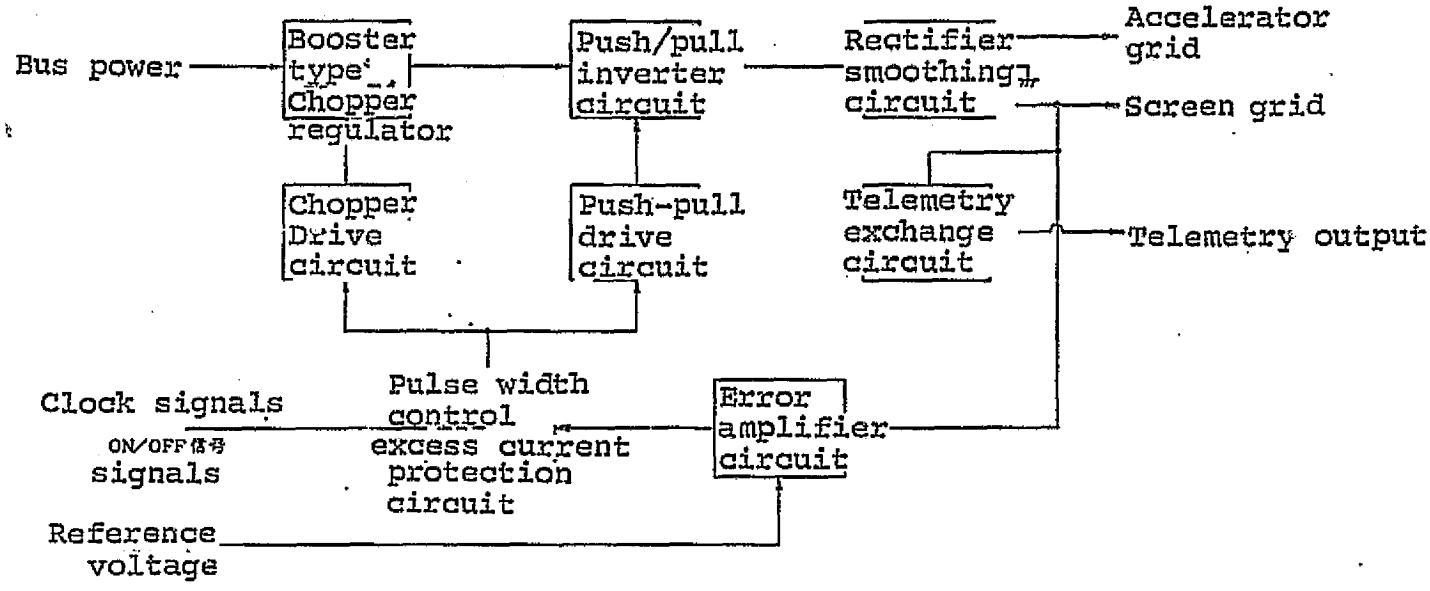

Fig. 4.31 Block Diagram of Discharge Power Source

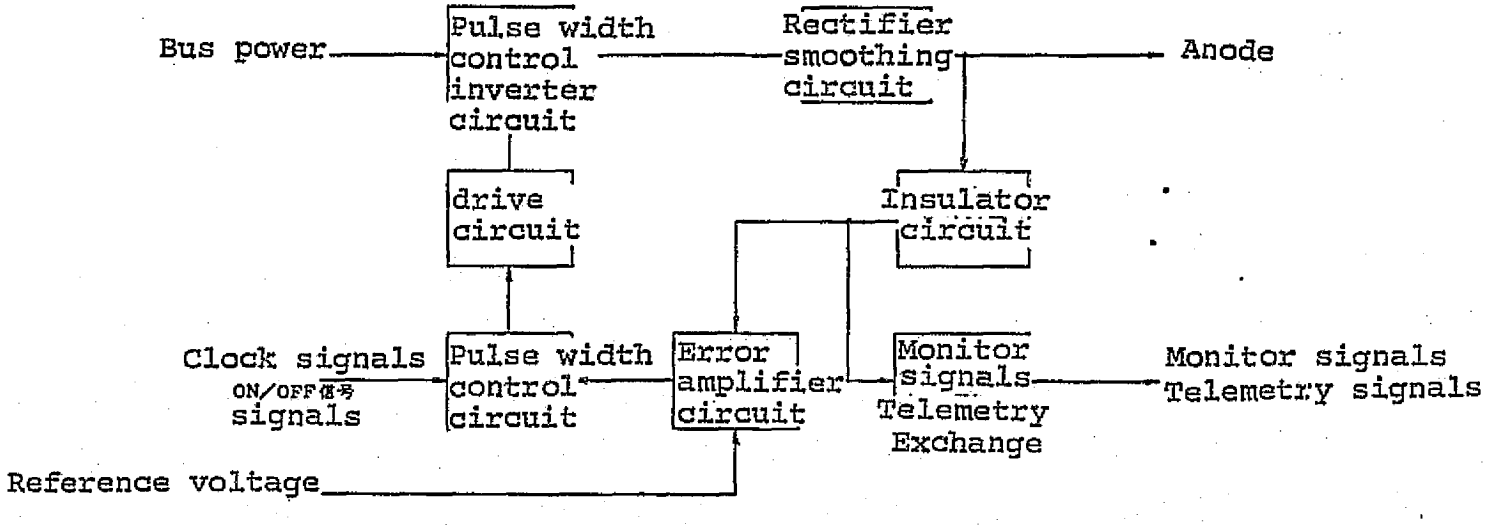

Fig. 4.32 Block Diagram of Cathode and Neutralizer Heater Power Source

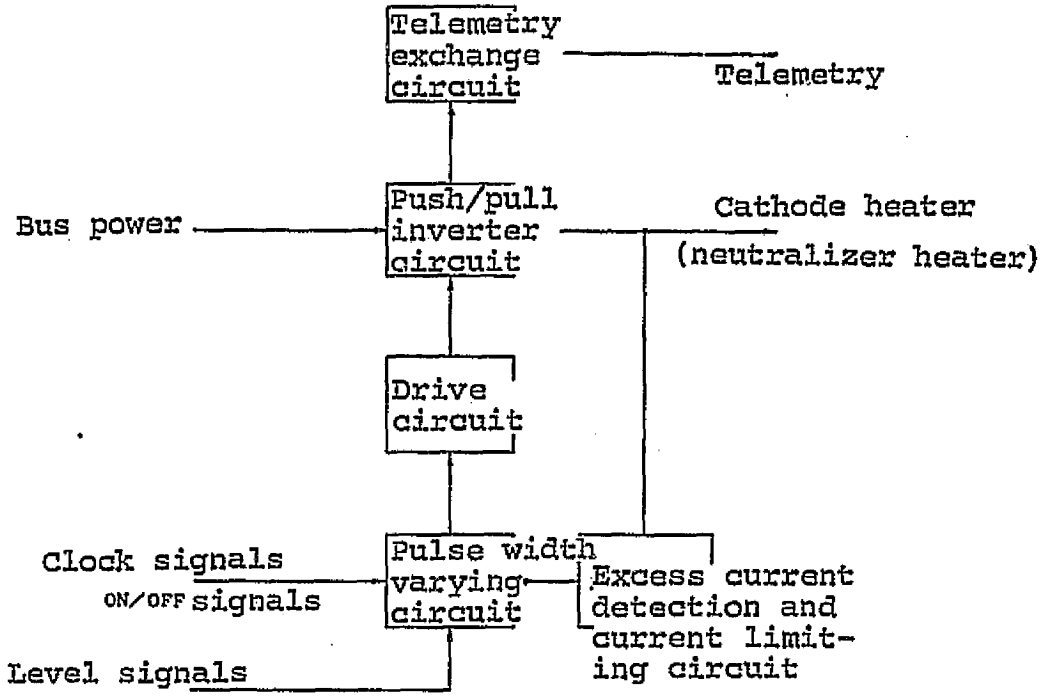

Fig. 4.33 Block Diagram of Cathode and Neutralizer Keeper Power Source

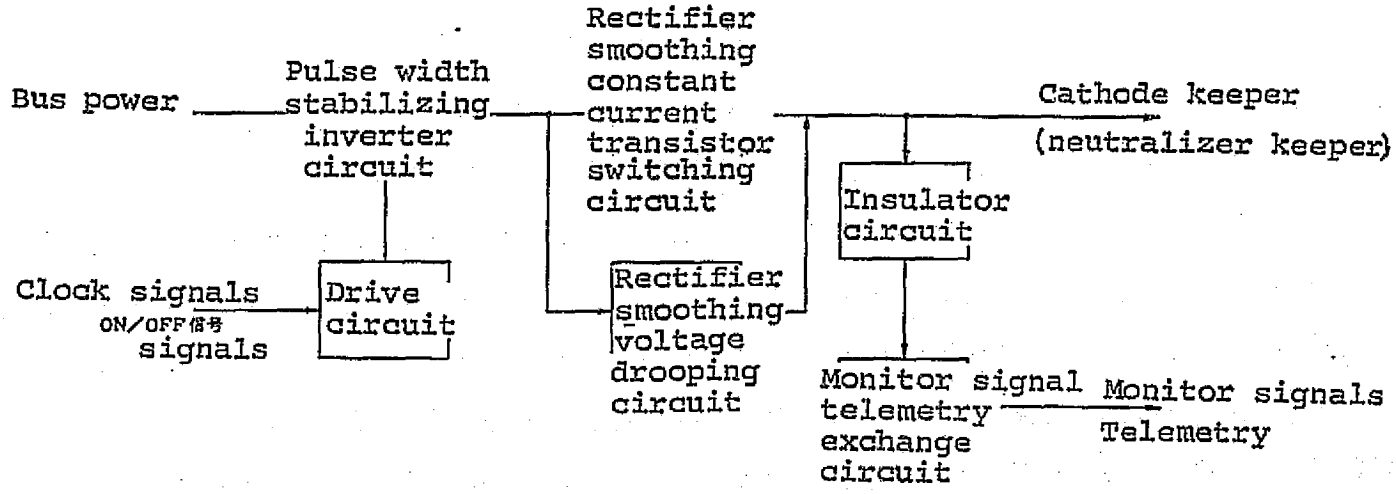

Fig. 4.34 Block Diagram of Cathode and Neutralizer Keeper Power Sources

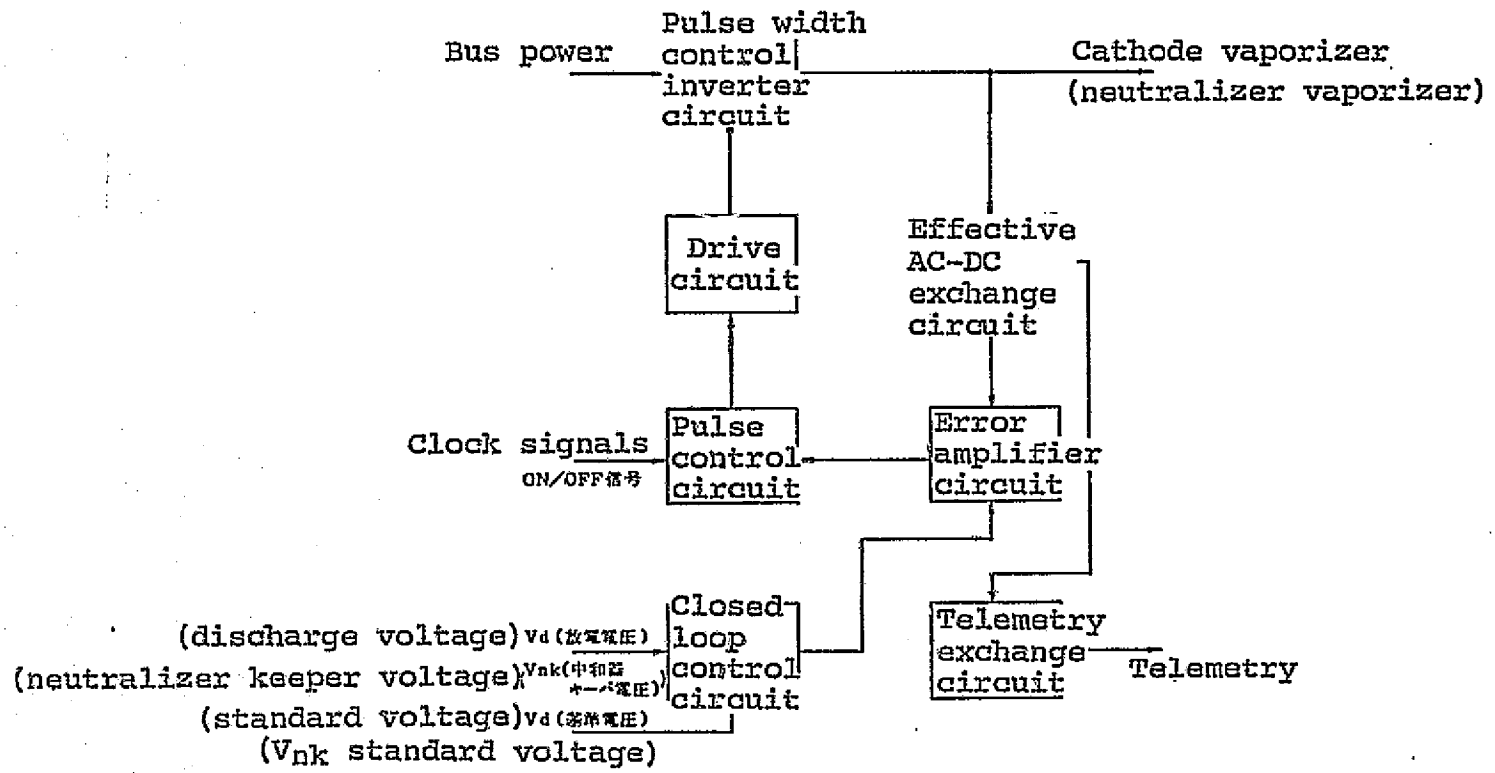

Fig. 4.35 Block Diagram of Auxiliary Power Source

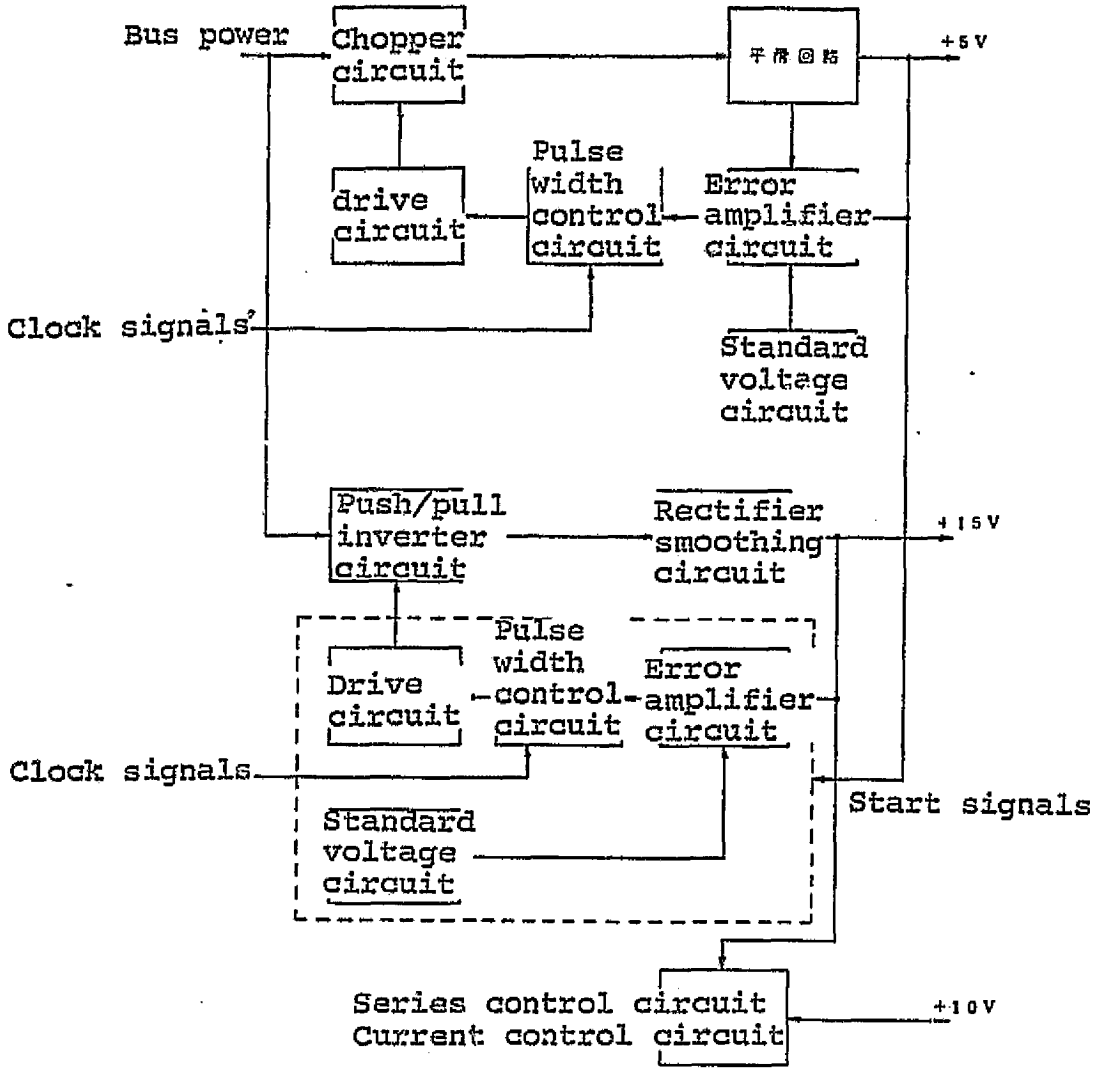

Fig. 4.36 Block Diagram of Insulator Circuit

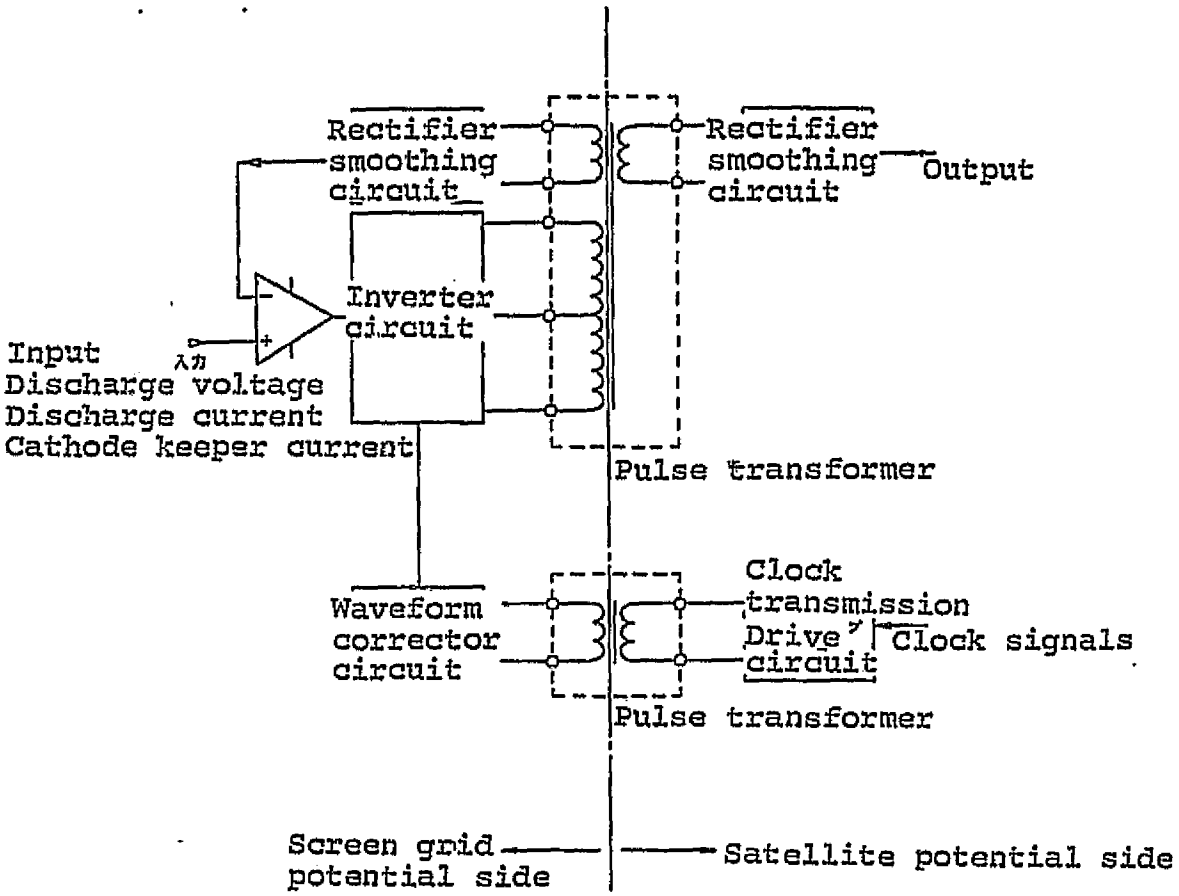

Fig. 4.37 Insulation of Primary and Secondary Power Source

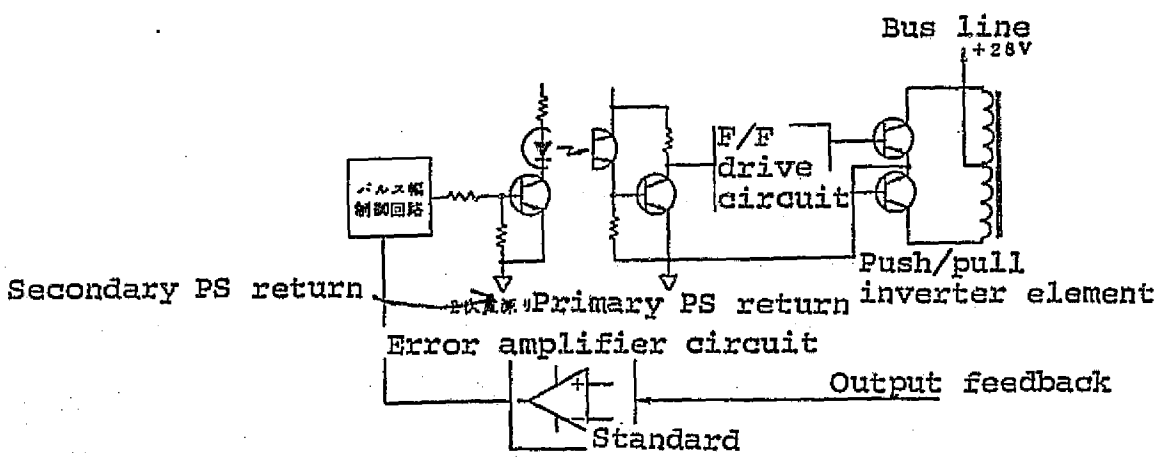

Fig. 4.38 Block Diagram of High-voltage Dielectric Breakdown Protective Logic Circuit

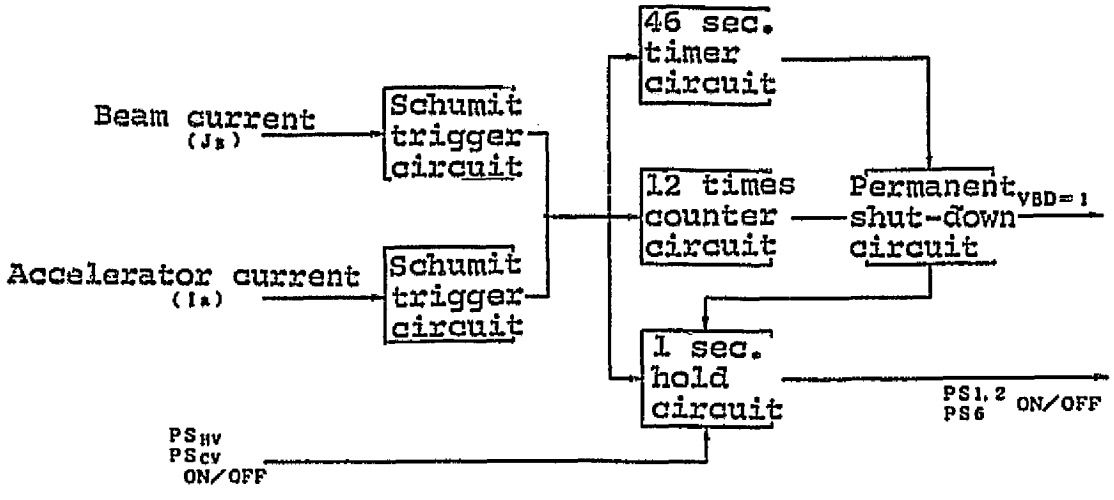

4.3.2 Electrical Design of Power Source Control Device

Block diagram of power source control device is shown in Fig. 4.40.

(1) Command interface unit

This unit has 4 selector commands and 5 executing commands as discrete commands; and one action command and 3 reference value set commands as magnitude commands. Selector commands send the engine unit selector signals to power control unit and telemetry switch unit by memorizing contents with a latching relay and supplying DC+28V bus power to the power source unit and the specified power sources in the power source device. Execution commands send the contents to the power source control unit.

(2) Power source control unit

This unit receives command signals from the command interface and monitor signals from the power source unit, and controls the 10 systems in the power source device according to the set sequence flow. It also sends status telemetry for monitoring progress of sequence flow to the sequence status unit. Block diagram of the power source control device is as shown in Fig. 4.40. Control circuit receives command signals, monitor signals, sequence counter signals, etc., determines where in the split sequence flow they should go and sends the corresponding sequence signals. Upon receiving such signals, sequence counter circuit sends corresponding split sequence counter signals. Control circuit sends timer set signals to the timer circuit, which sets time to stop the progress of sequence flow. Control circuit also sends power source control signals of the 10 systems to ON/OFF level signal register.

Power source control unit, under a tuning system, resets sequence counter, ON/OFF level signal register, etc. in tune with the clock

to control the sequence in power source device. Thus, by stopping the clock, the counter and register cannot be reset, consequently stopping the sequence control. This enables to prevent faulty movements due to noise when high voltage power source is applied by stopping the clock. When the conditions for high voltage application are no longer satisfied, monitor signals from the power source device detect it and restart the clock to control the device according to a set flow. Fig. 4.41 is a basic timing chart of the power source control unit whose actions are summarized as follows. Monitor signal (signal e) is received at a certain point and sequence counter set signal(signal f) is sent. Upon receiving signal c, timer circuit stops clock b by sending a clock stop signal(signal d) to clock stopping circuit for a set duration. Signal d is withdrawn after the set duration, and with the start of the clock the sequence counter, circuit sends a set counter signal(signal g) to the control circuit which in turn sends control signals(signal h) to the ON/OFF level register. Upon receiving signal h, the register sends out power source control signal i at the fall of clock b.

(3) Telemetry switching unit

The unit selects analog telemetry signals from the two power source devices with selector signals of the engine unit and sends them to the telemetry encoder.

Analog signals can be switched by either a relay system or analog switch system. Latching relay shown in Fig. 4.42 was used for cathode heater power telemetry and analog switch, shown in Fig. 4.43, was used for others.

Switch circuit for digital signals uses CMOS-IC and its composition is shown in Fig. 4.44.

Fig. 4.39 Master Oscillator

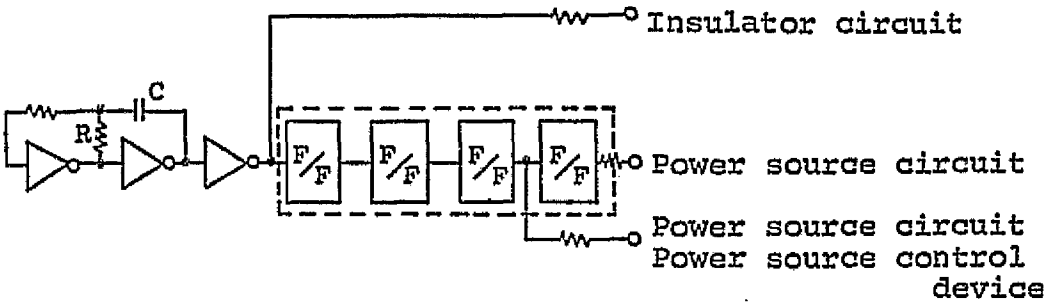

Fig. 4.40 Block Diagram of Power Source Control Device

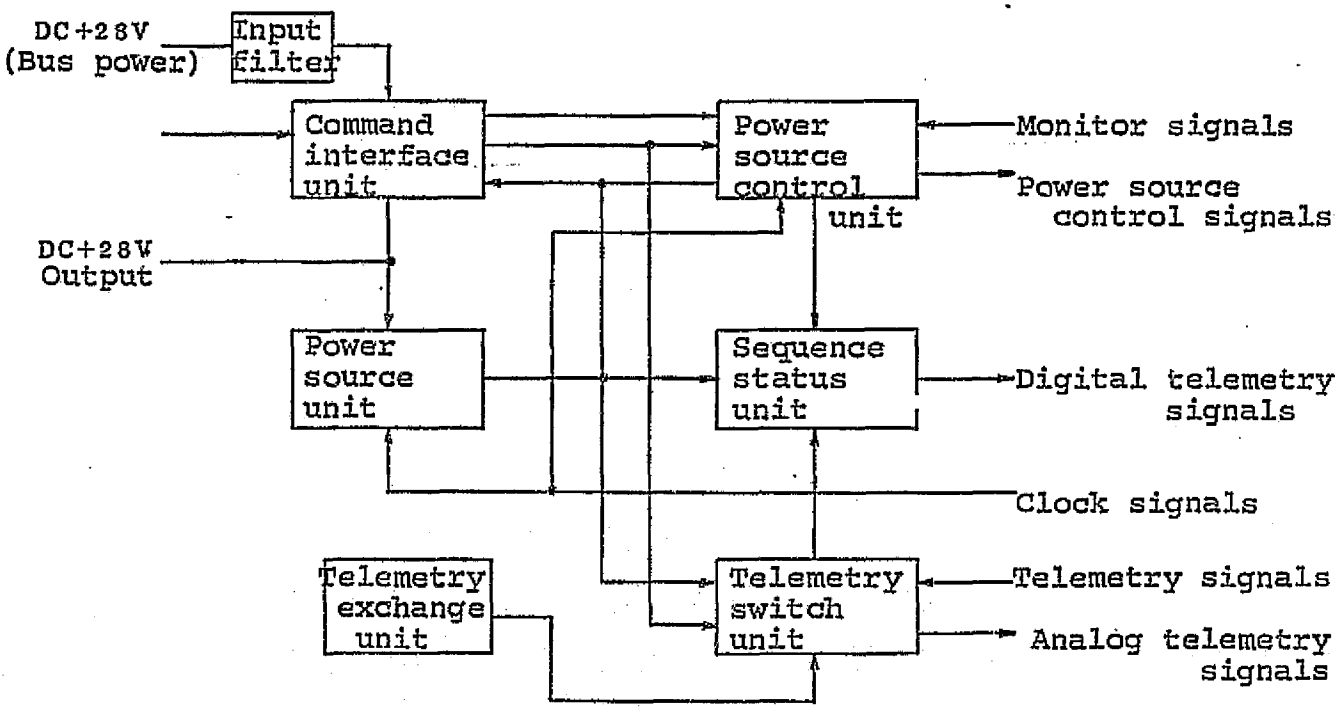

Fig. 4.41 Basic Timing Chart of Power Source Control Unit

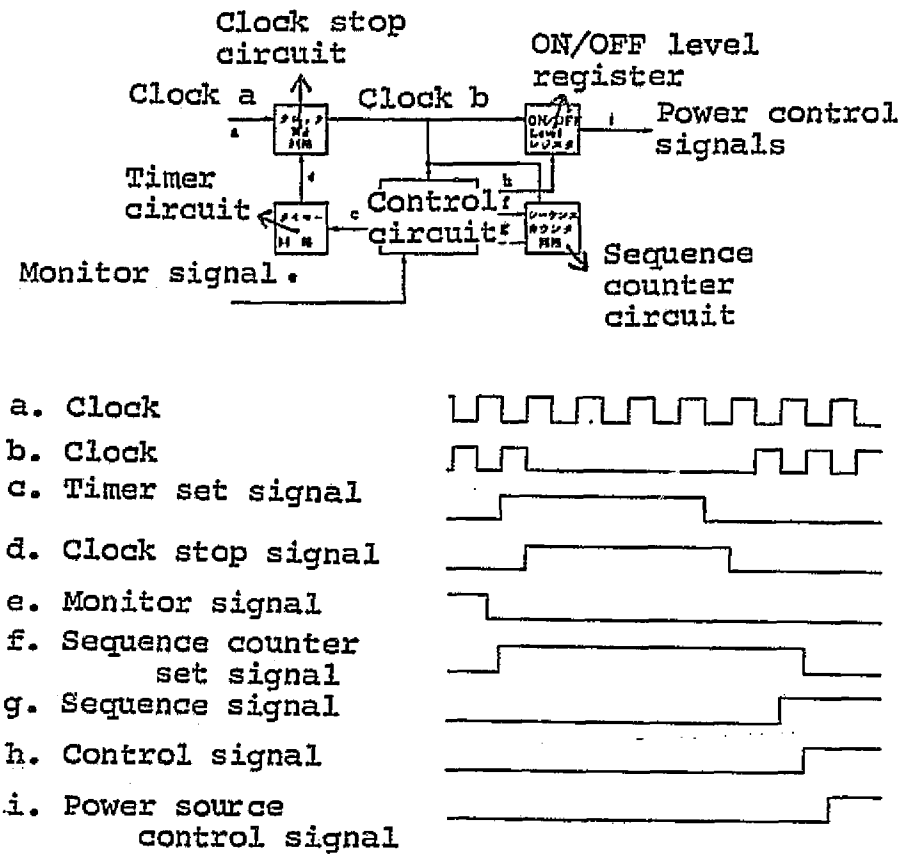

Fig. 4.42 Switch Circuit for Analog Telemetry(Pch, Pnh)

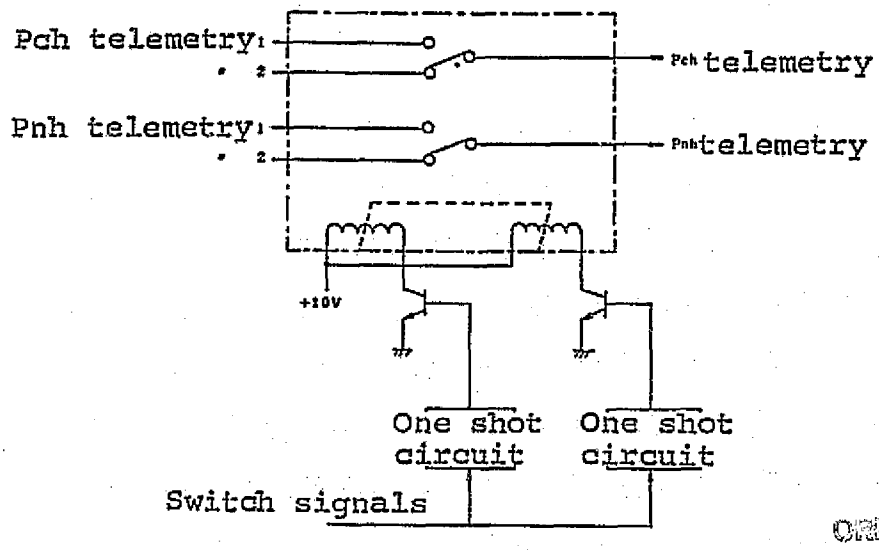

Fig. 4.43 Switch Circuit for Analog Telemetry

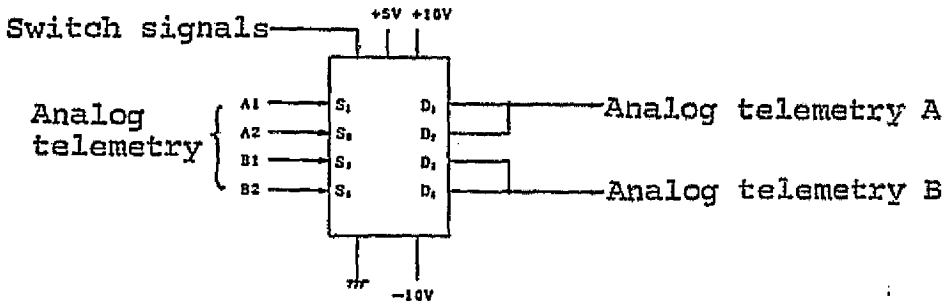

Fig. 4.44 Switch Circuit for Digital Telemetry

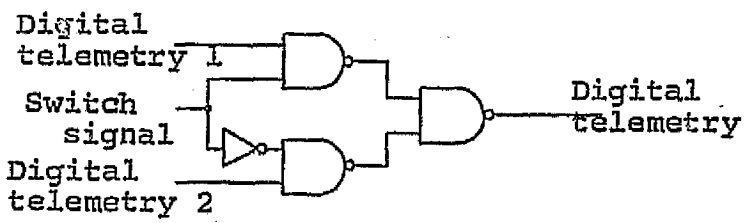

4.3.3 Structural Design

Thickness of structural materials was reduced for less weight and the number of parts was reduced for less number of screws. Also, monologue construction was employed in view of problems with EMI and reduction of weight was aimed by the use of thin printed substrate and by simplifying supporting structure.

Internal structures of power source device and power source control device are shown in Fig. 4.45 and Fig. 4.46, respectively.

Dead analysis and oscillation analysis were made for the structures designed according to the conditions required by the specifications.

Analysis values of natural oscillation of the power source device are given in Table 4.29 and those of power source control device are given in Table 4.30.

Load conditions of stress analysis and the analysis results are given in Tables 4.31 and 4.32. Required safety factor is over 0.

Results of analysis of printed unit for the power source control device and power source device are as shown in Table 4.33.

In the power source device, a potted insulator amplifier was placed in the center and used as a strength member, which increased the rigidness of the device. In the power source control device a highly rigid material was also placed in the center. Electrical parts were fixed on this material and further, the printed substrate was connected by a spacer. By doing so, primary natural oscillation increased to 4111 Hz.

Fig. 4.45 Internal Structure of Power Source Device

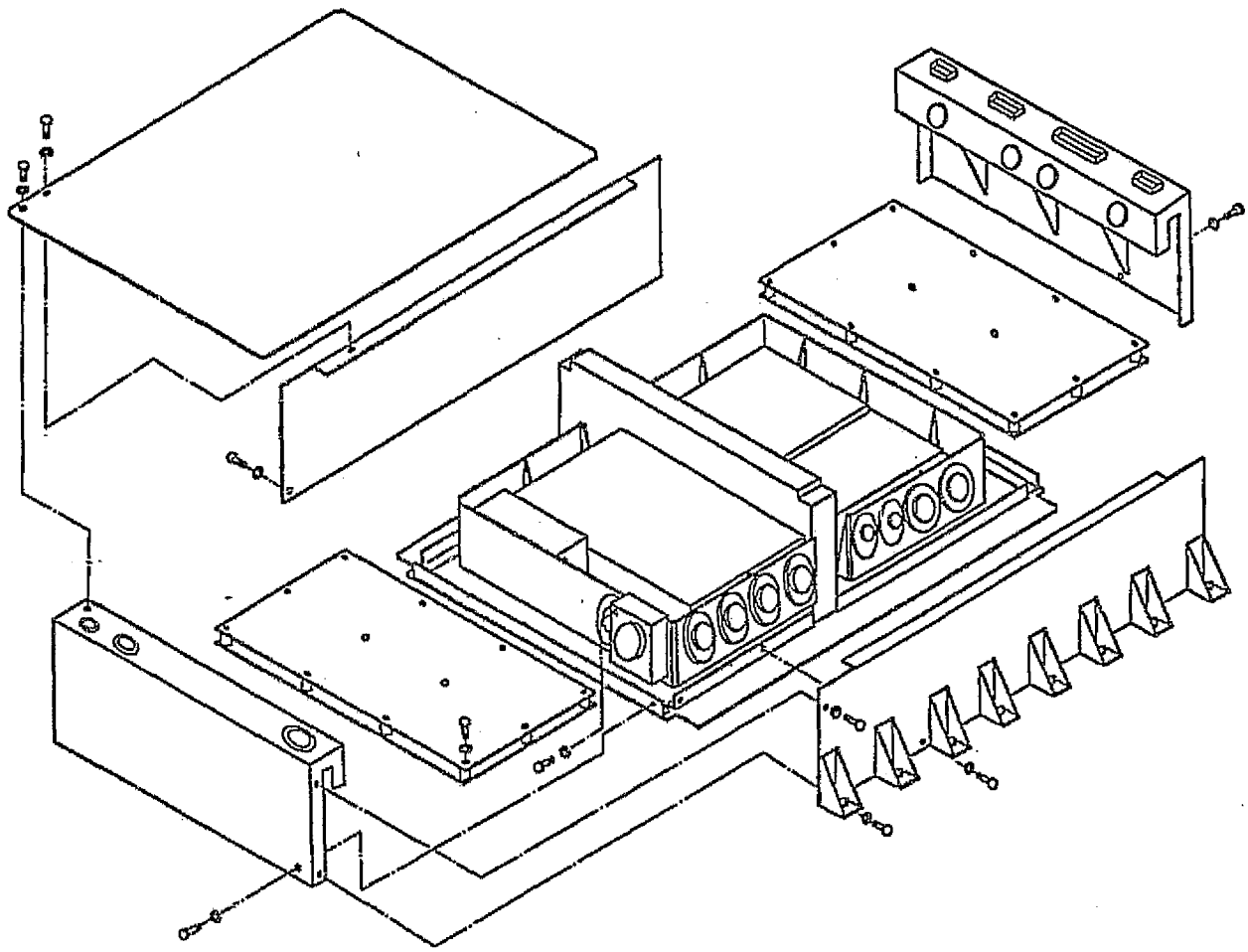

Fig. 4.46 Internal Structure of Power Source Control Device

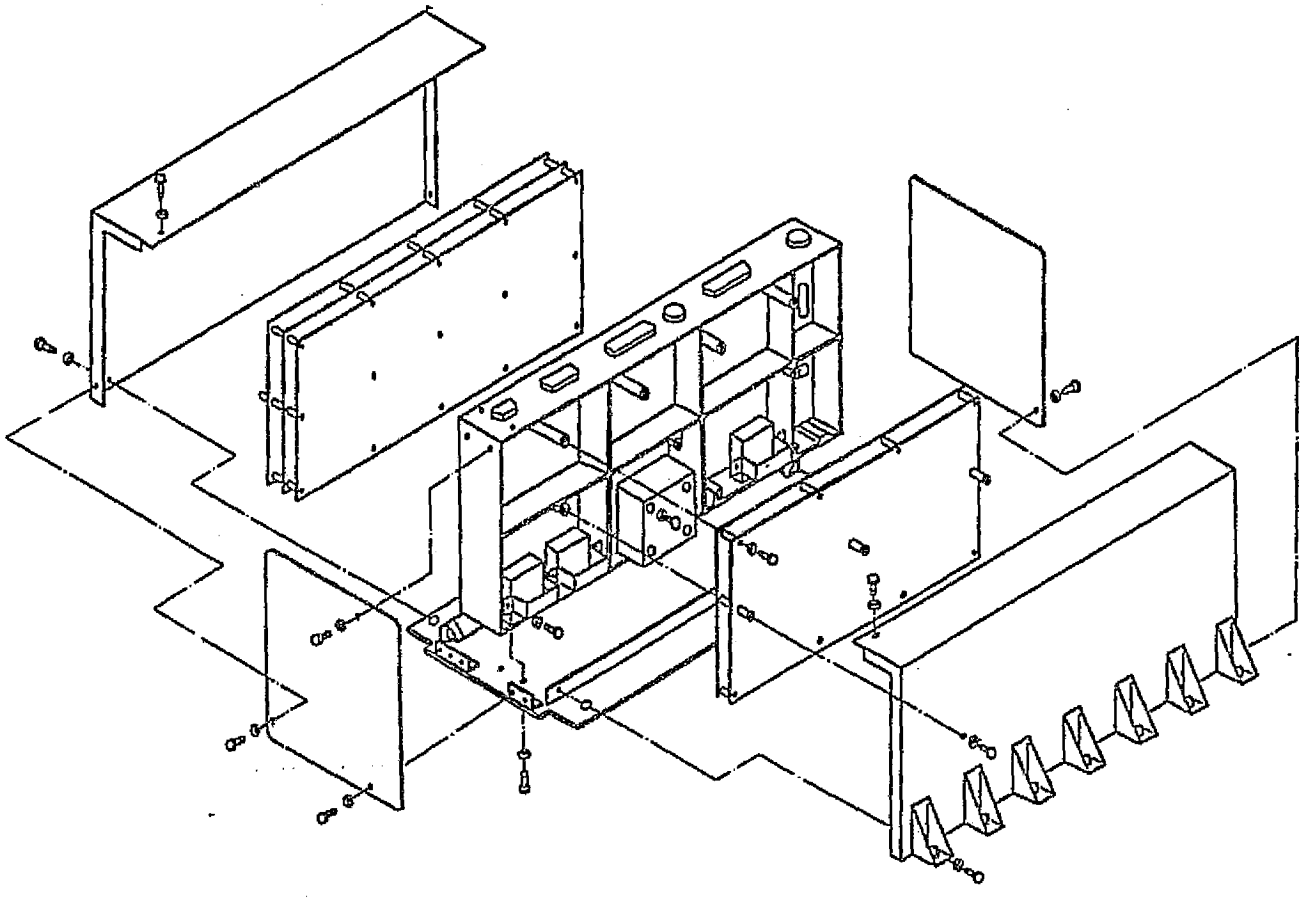

Table 4.29

No.	Basic design		Detailed design	
	Natural oscillation	Oscillation mode	Natural oscillation	Oscillation mode
1	160 Hz	Unsymmetrical bending of connector and side plate	180 Hz	Unsymmetrical bending of overhead plate.
2	166	Symmetrical bending " "	213	" " "
3	191	Unsymmetrical bending of connector	243	Unsymmetrical bending of base plate and heat sink
4	195	Symmetrical bending Unsymmetrical bending of overhead plate	281	" "
5	235	Bending of connector, overhead plate and base plate	398	Unsymmetrical bending of heat sink

Table 4.30 Natural Oscillation of Power Source Control Device

No	Basic design		Detailed design	
	Natural oscillation	Oscillation mode	Natural oscillation	Oscillation mode
1	125 Hz	Unsymm..bending of connector	411 Hz	
2	138	Symm. bending of connector	469	Unsymm. bending of cover A & B hardware(support) and lid A & B
3	344	Unsymm. bending of overhead plate	544	
4	371	Symm. bending of overhead plate	638	
5	510	Unsymm. bending of side plate	674	

Table 4.31 Safety Factor of Power Source Control Device

Name	Material	Load cond.	Allowable stress (kg/mm²)	Breakdown mode	Safety factor
Hardware(support)	A5052P-H	Z axis	1600	tension	
Cover A	A5052P-H34	50G			>10
" B					
Lid A					
" B					
Base		X軸50G			

Table 4.32 Safety Factor of Power Source Device

Overhead plate.	A5052P-H34	X軸150G	1600	tension	
Side plate A		Y軸150G			>10
" " B					
" " C		Z軸120G			
Base		X軸150G			29
Block 1 & 3 fixed screw	SUS303	X軸150G	2100	引張り	3.7

Table 4.33 Results of Printed Unit Structural Analysis

	Shape (mm)	Wt. (f)	Primary natural oscillation (Hz)	Load cond	Allowable stress (kg/cm²)	Breakdown mode	Safety factor
Power source device printed unit	230×155×1.2	1953	200	150G	1400	引張 tension	9.1
Power source control device printed unit	255×120×1.6	1863	411	50G	1400	引張	>10

NASDA-QTS-1005 (material)

4.3.4 Heat Design

Temperature of mission panel II, onto which power conditioner is mounted, is controlled to 0 - 40C.

Power conditioner is heat-controlled by a passive method where heat is dispensed from the base plate to the mounting face of the satellite, as shown in Fig. 4.47 and Fig. 4.48.

In the power source device, transformers, choke coils, etc. which are heavy and consume large amounts of electric power are blocked by potting and glued to the base plate, instructural consideration to vibration and shock. Power transistor is placed as close as possible to the base plate. RMS/DC converter generates a large amount of heat and, when used thermally unprotected, exceeds allowable temperature of parts. Therefore, RMS/DC converts were mounted in such a way that the back was in tight contact with the chassis' side plate to release heat, as shown in Fig. 4.49. Inside the printer unit, parts were arranged on the base plate in the way that heat could not concentrate.

Power source control device was designed for efficient radiation, by placing choke coil and transistor whose power consumptions are relatively large close to the base plate. By using a 4-ply multi-base plate for printed substrate, temperature is uniform and those parts with large calorific values do not turn into heat spots.

Arrangements of main electronic parts which make up the power source device and power source control device are shown in Fig. 4.50. and Fig. 4.51, respectively. Heat generated by those electronic parts during operation and the analyzed temperature of each nodal point are given in Table 4.34 and Table 4.35.

Fig. 4.47 Heat Design of Power Source Device

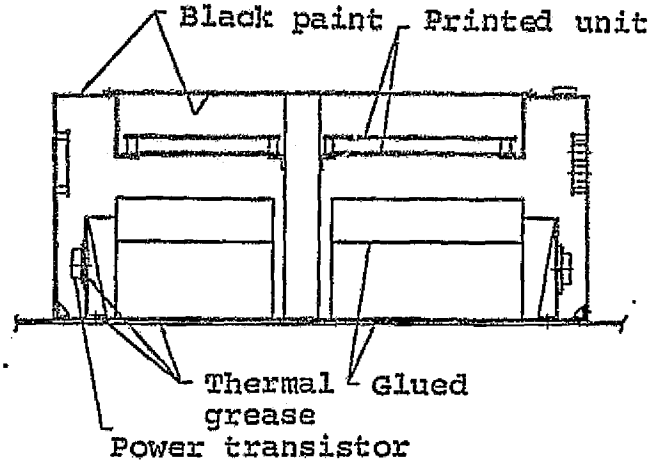

Fig. 4.48 Heat Design of Power Source Control Device(Outline)

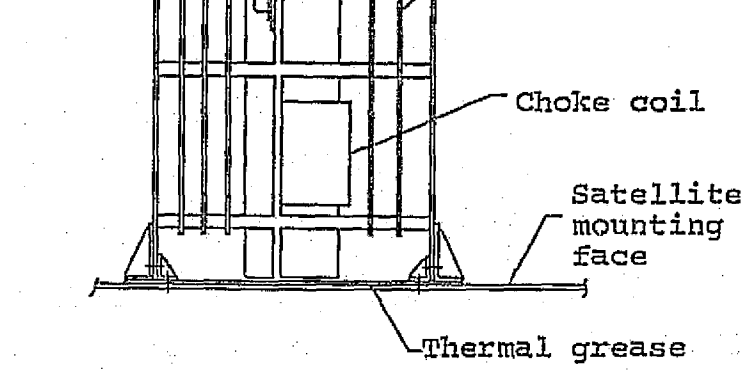

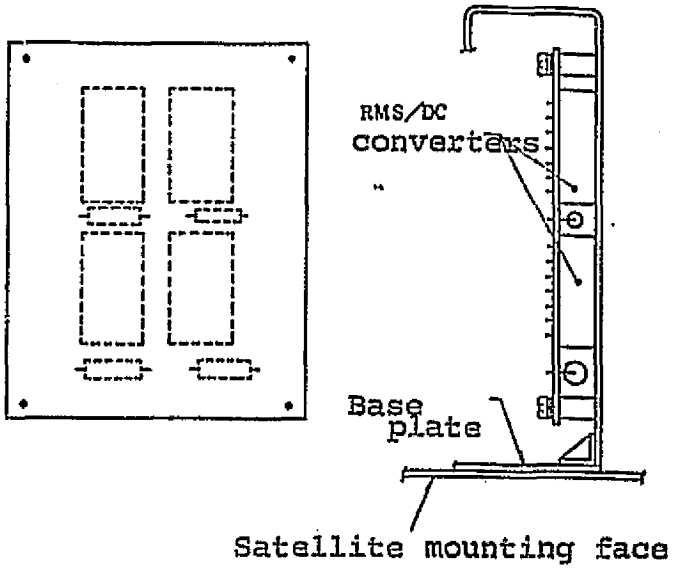

Fig. 4.49 Mounting Method of RMS/DC Converters

Table 4.34 Power Source Device Analysis Results

Nodal point No	Definition	Heat gen. 発生熱量(W)	Temp. dist. 温度分布(℃)
1	potting block (A2)	0.74	64
2	" (A2)	1.2	64
3	" (U5)	1.6	76
4	" (A5)	1.0	76
5	transistor mounting hardware	0.44	57
6		0.7	57
7		0.4	57
8	printed unit (U4)	24	97
9	" (U3)	22	95
10	overhead board	—	76
11	potting block (A1)	3.74	66
12	" (A3)	28	80
13	transistor mounting hardware	1.62	60
14		2.69	60
15		0.3	57
16	printed unit (U2)	24	91
17	" (U1)	1.6	85
18	potting block (A4)	0.7	74
19	overhead board	—	73
20	"	—	72
21		1.0	57
22		1.5	72
23	printed unit mounting hardware	—	66
24	side plate	—	62
25	"	—	62
26	"	—	62
27	(same as 23)	—	64
28	side plate	—	62
29	"	—	62
30	"	—	62
31	base plate	—	56
32	"	—	55
33	"	—	55
34	(same as 23)	—	66
35	"	—	68
36	satellite mounting face	—	55

Table 4.35 Power Source Control Device Analysis Results

Nodal point No	Definition	Heat gen. 発生熱量(W)	Temp. dist. 温度分布(℃)
1	printed unit (U4)	0.807	66
2	" (U5)	0.9	68
3	" (U3)	0.966	67
4	" (U2)	0.084	65
5	" (U1)	0.05	62
6	cover (upper part)	—	61
7	support hardware	—	60
8	cover (upper part)	—	61
9	side plate	—	59
10	"	—	59
11	cover	—	60
12	strut	—	—
13	"	—	—
14	"	—	—
21	"	—	—
22	"	—	—
23	"	—	—
24	sup.hdwr (upper pt)	—	65
25	" (lower pt)	—	57
26	cover	—	59
28	base plate	—	55
29	resistance (R2)	0.32	80
30	" (R1)	0.32	80
31	transistor (Q3)	0.64	78
32	" (Q2)	0.059	63
33	" (Q1)	0.059	63
34	choke coil (U6)	0.765	85
35	transformer (U7)	0.067	63
36	satellite mounting face	—	55

Fig. 4.50 Heat Model for Power Source Device

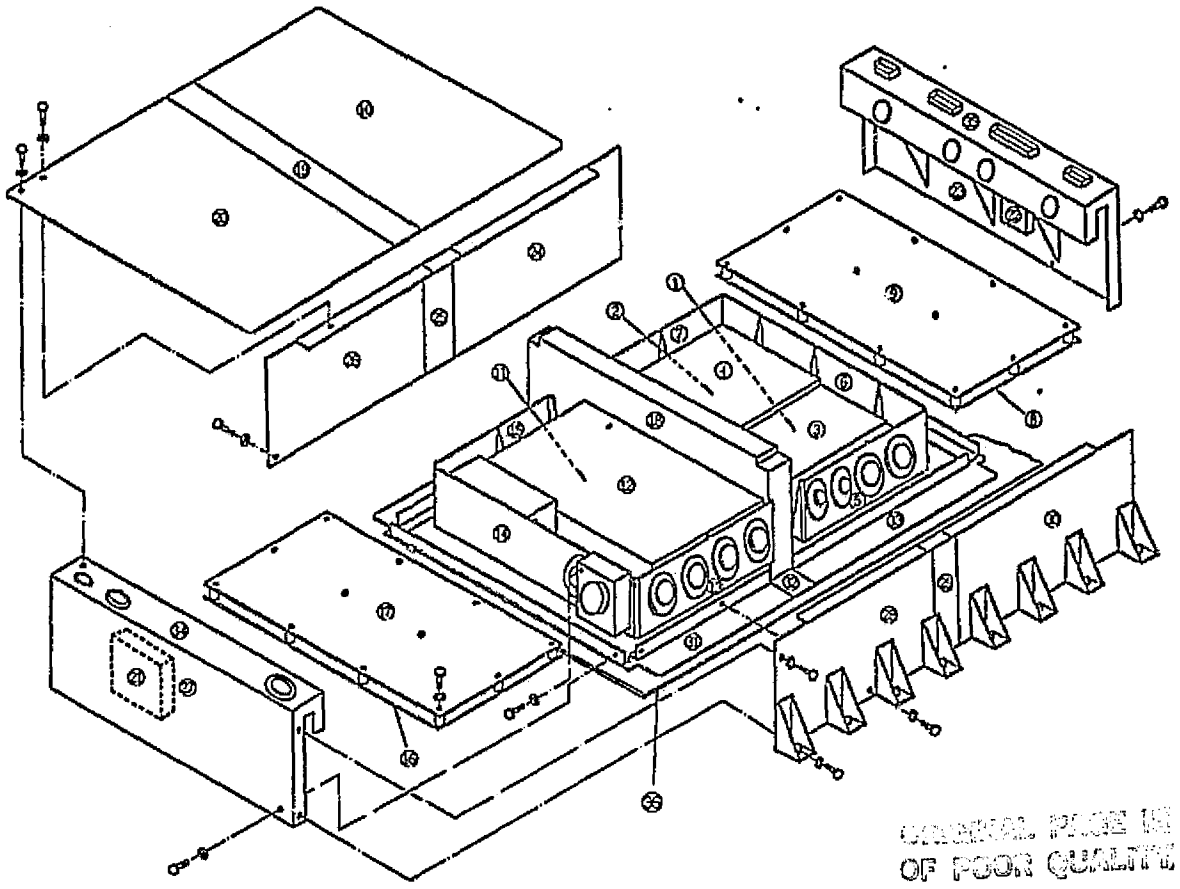

Fig. 4.51 Heat Model for Power Source Control Device

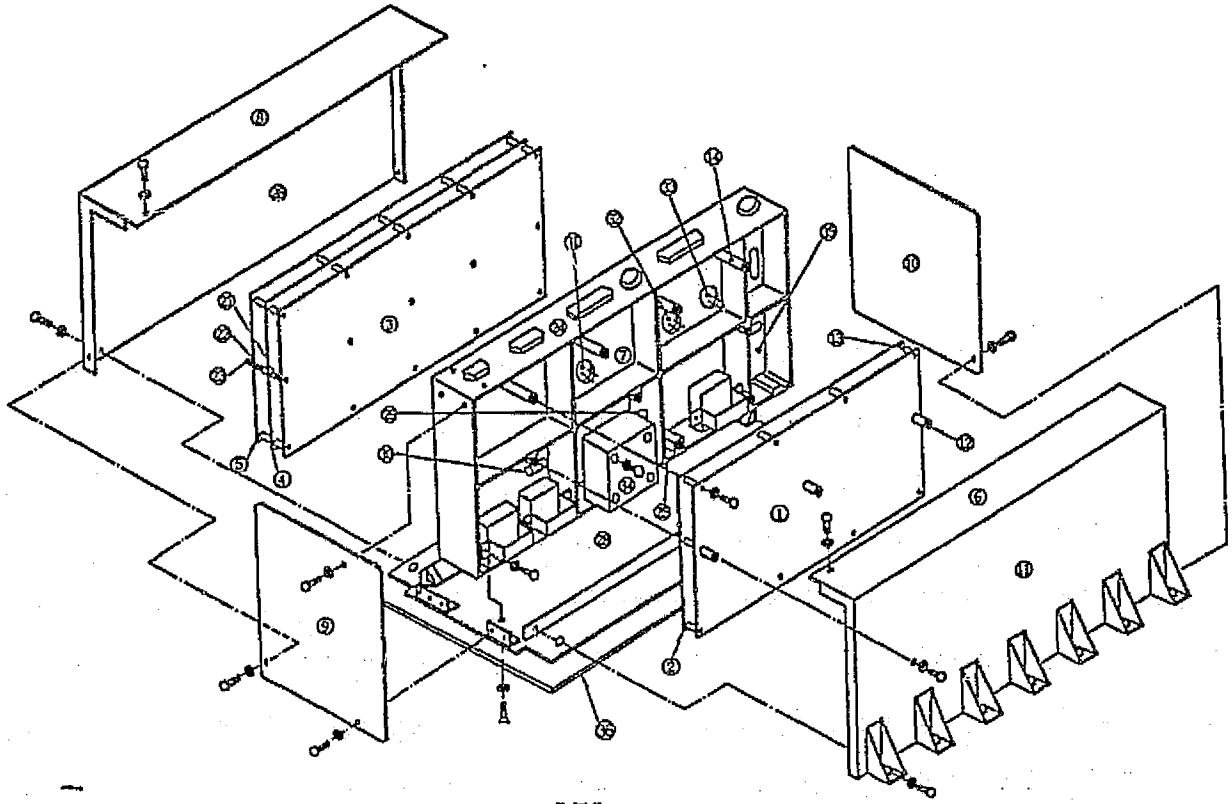

4.3.5 Reliability Analysis

Reliability block diagram, reliability estimation model and reliability block diagram of power source device are shown in Fig. 4.52. Power source device block can be divided into 17, all of which are series connected.

Power source control device block is divided into 8 which are also series connected. Reliability block diagram of the power conditioner is as shown in Fig. 4.54.

Estimated reliability values are given in the block diagrams. In accordance with NASDA SPC-1318, operating time was 150 hours, stand-by time was 8610 hours, and breakdown rate during stand-by period was set at 1/10 of that during operation. MIL-HDBK-217B data was used in calculating breakdown rates of parts. As parameters, surrounding temperatures were set at 60C around heat sink, 75C around potted area, and 85C for other parts, based on the results of heat analysis.

Fig. 4.52 Power Source Device Reliability Estimation Block Diagram

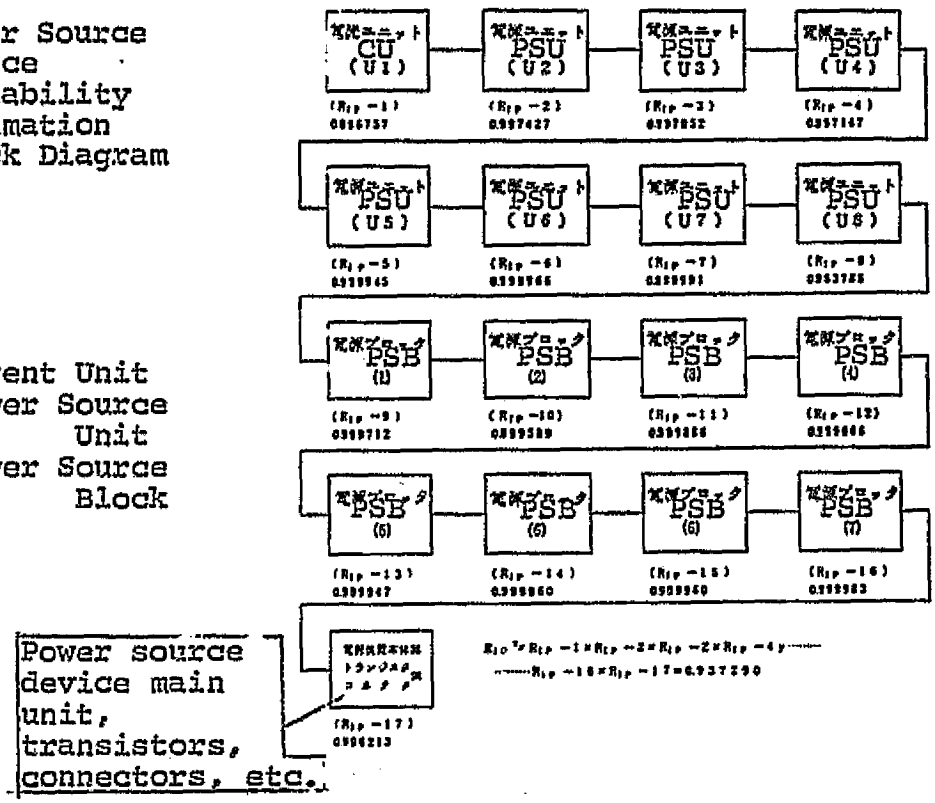

CU: Current Unit
PSU: Power Source Unit
PSB: Power Source Block

Fig. 4.53 Power Source Control Device Reliability Estimation Block Diagram

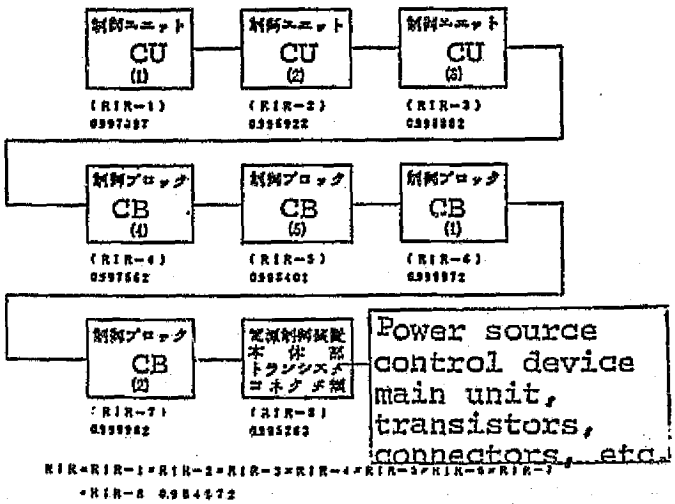

CU: Control Unit
CB: Control Block

Fig. 4.54 Power Conditioner Reliability Block Diagram

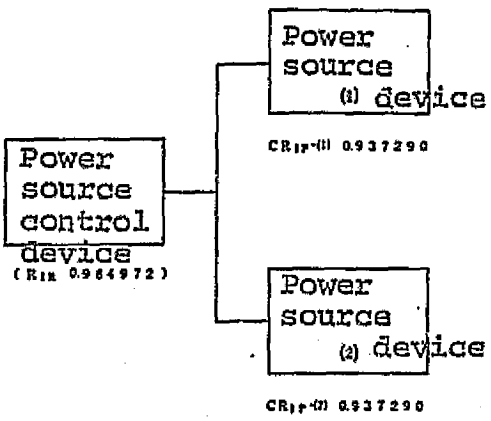

4.3.6. Development Tests

Engineering model was tested in order to check the functions and performances required by the development specifications, to be reflected in design details. Following tests were given.

- Function/performance test
- Electromagnetic compatibility test
- Temperature test and vacuum test
- Vibration and shock test

Some problems which came up are explained below.

(1) Efficiency of screen grid/ accelerator grid power source was low.

Efficiency drop was caused by a low self-resonance frequency of converter transformer which created capacitive impedance at the frequency used, causing excessive charge current to flow when the switching transistor was ON. As a measure, self-resonance frequency was specified in the transformer specifications for subcontractor. The circuit was also test-produced separately to check its efficiency and to confirm that there was no impact after PM(meaning unclear - translator).

(2) Faulty movement of sequence flow occurred during short-circuit test of high voltage circuit.

Noise mixed into discrete command signal line during short-circuit of power source was thought to be the cause. Integrating circuit was added for signal input.

(3) Measured values were above the specified values in the 100KHz - 10KHz range during transmission interference noise test of power source line.

Faulty design of power source line filter was the cause. Choke

coil was added to the power source line.

(4) Ripple voltages of PS5 and PS8 did not meet the standards.

Ripple values were 2% over the specified values, due to reduced output capacity for suppressing rush current at keeper ignition. Studies confirmed that this would not present any technical problems when incorporated into the engine unit, and thus, ECP(?) suggestion was made.

(5) In response to the axial directional shock during shock test, relay transferred by 0.3ms. It returned immediately, however.

Point of relay contact transferred(1800G, 0.3ms applied) for a split second due to shock. No transfer occurred at under 1216G when relay alone was tested and there was no problem at the shock level of 900G, 0.3ms, in PM. Thus no action was taken.

(6) Faulty action of discrete command

Relay in receiving circuit acted faulty to discrete command signal. Diode was added to the receiving circuit in a tedious system.

All other test results satisfied the required conditions. As a reference, measurements of radiation noise made during electromagnetic compatibility test of power source device are given in Fig. 4.55.

Fig. 4.55 Radiation Noise of Power Conditioner

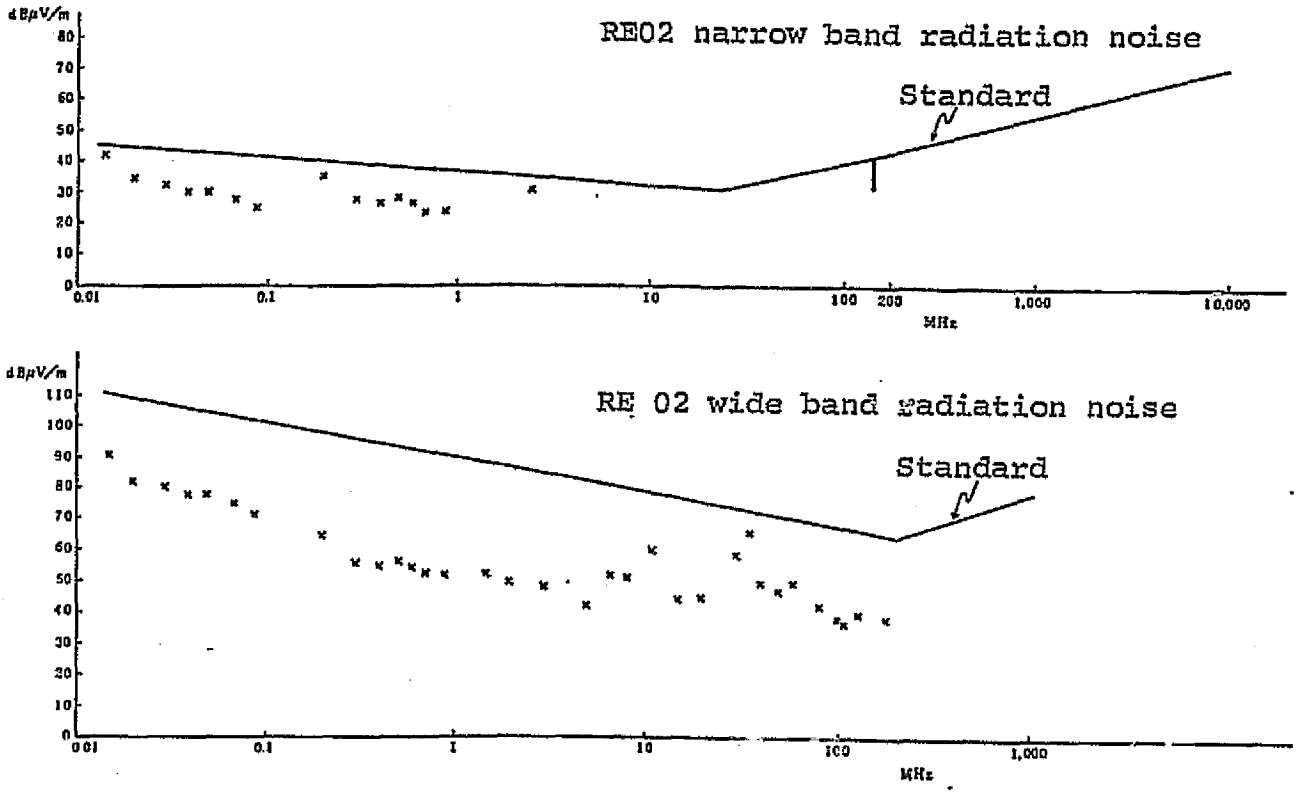

4.4 Sub-systems

For the two components of ion engine system - power conditioner and the ion engine unit - independent component tests were performed using artificial loads and power sources. Here, results of tests given to the combination of the two components to check their compatibility and the overall performance of ion engine, as well as to establish testing methods, are discussed.

Following tests were given.

- Electrical compatibility test
- Measurement of thrust
- Measurement of beam diffusion angle
- Heat vacuum test
- Electromagnetic compatibility test

4.4.1 Electrical Compatibility Test

Electrical compatibility between the ion engine unit and power conditioner was checked under the configuration shown in Fig. 4.56. An example of the results of varied parameter test is shown in Fig. 4.57. Also, main characteristics of different combinations of ion engine and power conditioner tested are shown in Table 4.36.

Compatibility test brought out the following two points to be reflected upon PM.

i) Control of closed loop to neutralizer vaporizer power source for controlling neutralizer keeper voltage was not compatible with the characteristics of the neutralizer, causing a positive feedback which stopped neutralizer discharge.
Changes in neutralizer keeper diameter(1ø - 2ø) and output range(0.4-1.5A - 0.5-1.2A) of the neutralizer vaporizer power source were made. Details are given in Section 6.2.

Fig. 4.57 Characteristics of IES

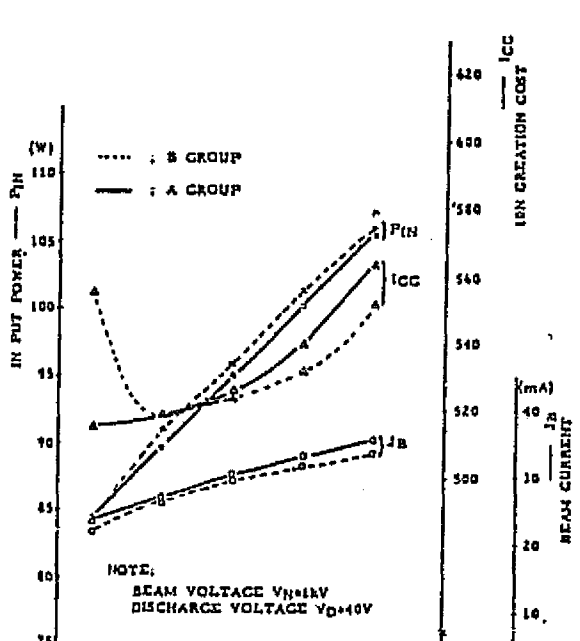

Table 4.36 Comparison of Main Characteristics of IES

Symbol	Main characteristic	Unit	IEE2 IEP1	IEE1 IEP1	IEE1 IEP2
P_{IN}	Input power	W	95.2	93.8	92
V_b	Beam voltage	KV	1.0	1.0	1.0
I_b	Beam current	mA	28	27.5	27.2
I_a	Accelerator current	mA	0.2	0.3	0.35
V_d	Discharge voltage	V	42	42	42
I_d	Discharge current	mA	350	350	350
I_{ck}	Main cathode keeper current	mA	250	242	225
I_{cv}	Main cathode vaporizer current	A	1.41	1.7	1.74
P_{cv}	Main cathode vaporizer power	W	4.8	6.2	6.2
I_{nk}	Neutralizer keeper current	mA	320	252	230
$\frac{V_d \times I_d}{J_B}$	Cost of ion production	eV/ion	507	535	540
$\frac{V_b \times I_b}{P_{IN}}$	Ion engine system power efficiency	%	30.4	29.3	29.5

ii) In some cases, excess current protection of IEP beam power source and accelerator power source was too sensitive and the transient caused protective logic to act. Time constants were therefore reviewed, and, as a result, unserviceable time of protective logic when high voltage was thrown was changed to 1.6 sec. and the protective logic monitor time constant for PS2 in steady state was changed to 100ms.

Fig. 4.56 Configuration of Function/performance Test

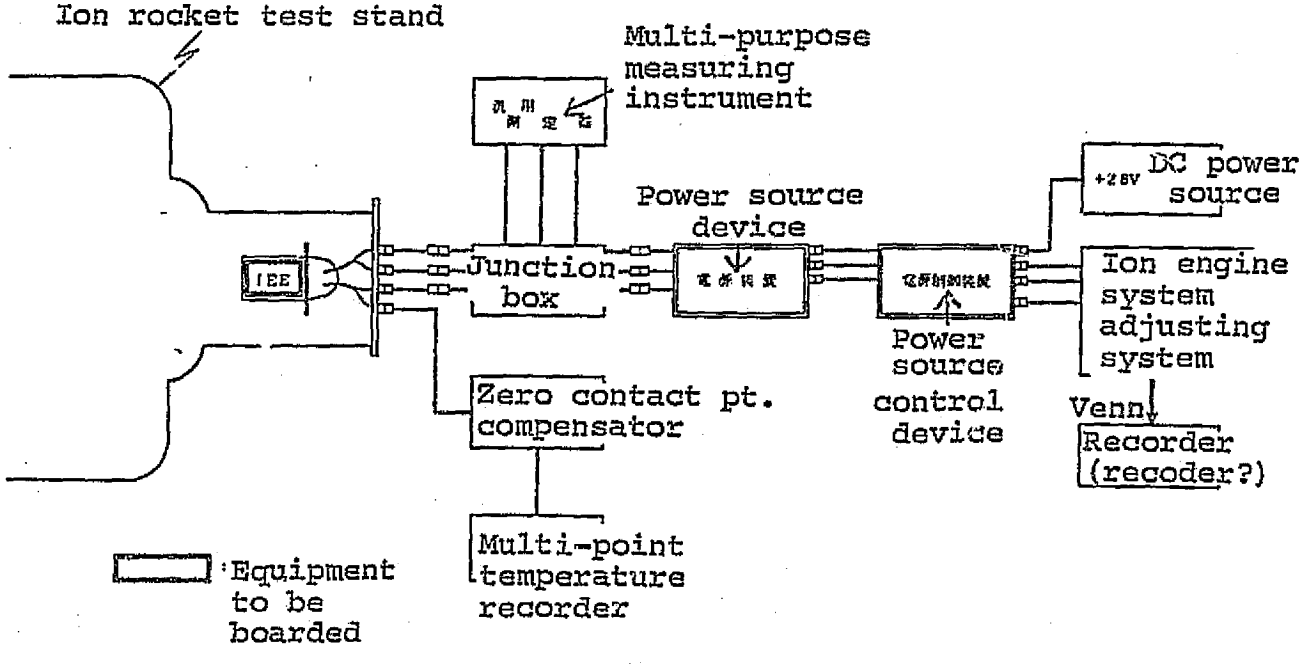

4.4.2 Measurement of Thrust

Although thrust was measured during IEE component test, it used different power sources. Therefore, thrust was measured again in IES using the configuration shown in Fig. 4.58, and compared against computed values. Measured and computed values are shown in Fig. 4.59. The figure shows that the measured values fall within 90% of computed values, similar to the results with IEE component (See Section 4.5.7(5)).

Fig. 4.58 Configuration of Thrust Measurement Test

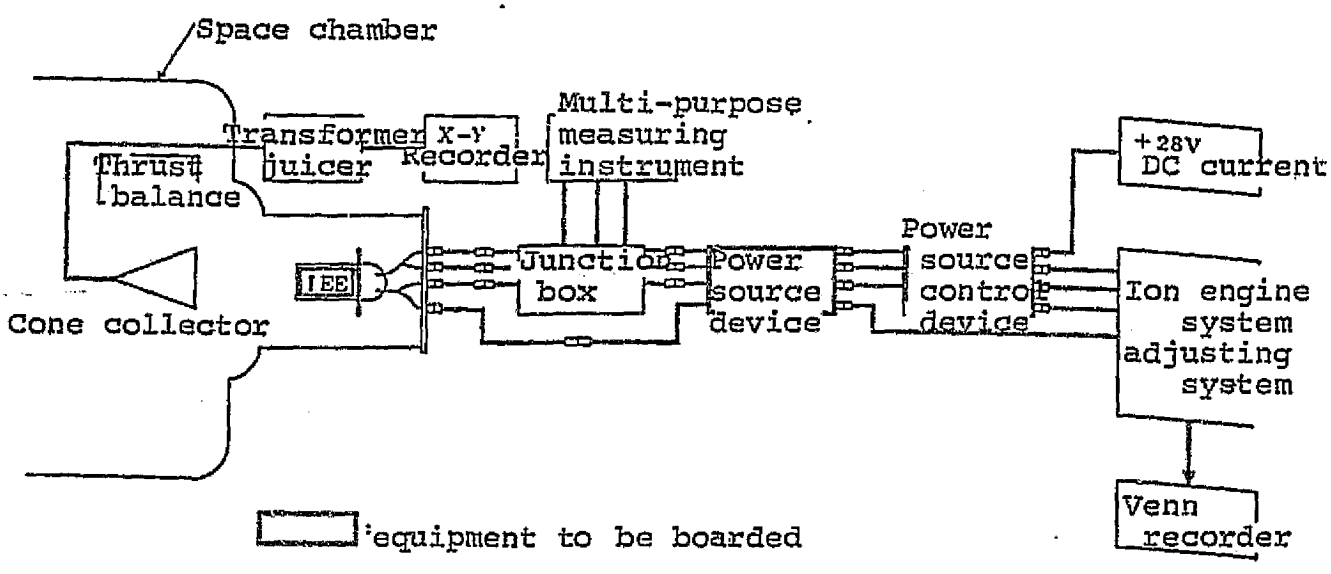

Fig. 4.59 Results of Thrust Measurement

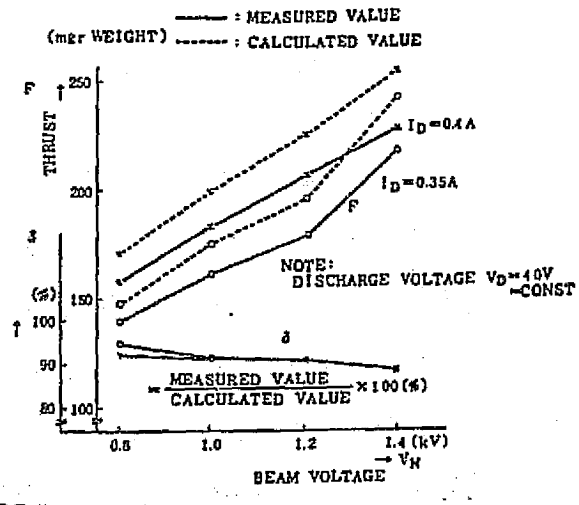

4.4.3 Measurement of Beam Diffusion Angle

Beam diffusion angles of mercury ion plume in IES were checked. Test configuration is as shown in Fig. 4.60. Measurements made with discharge voltage Vd and discharge current Id as parameters are shown in Fig. 4.61. Beam diffusion angle is the half angle of a cone covering the distance scanned by 95% of all ion current. Maximum diffusion angle was 27.3°.

Fig. 4.60 Configuration of Beam Diffusion Angle Measurement Test

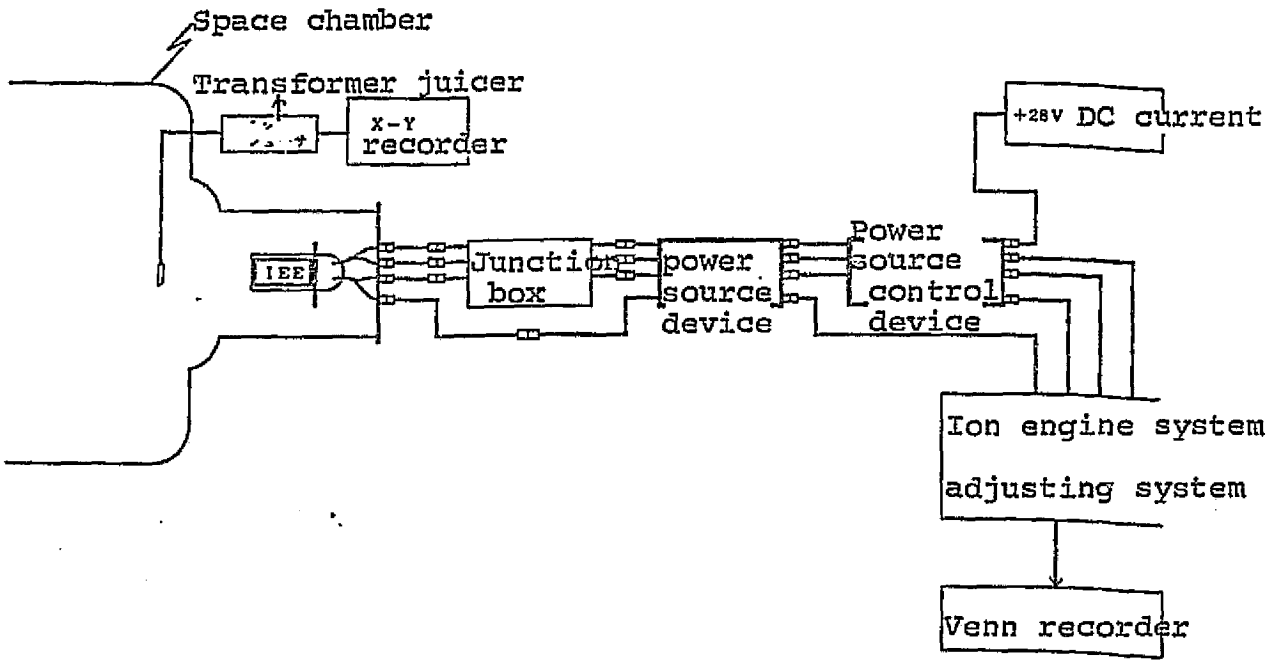

Fig. 4.61 Measurement of Beam Diffusion Angle

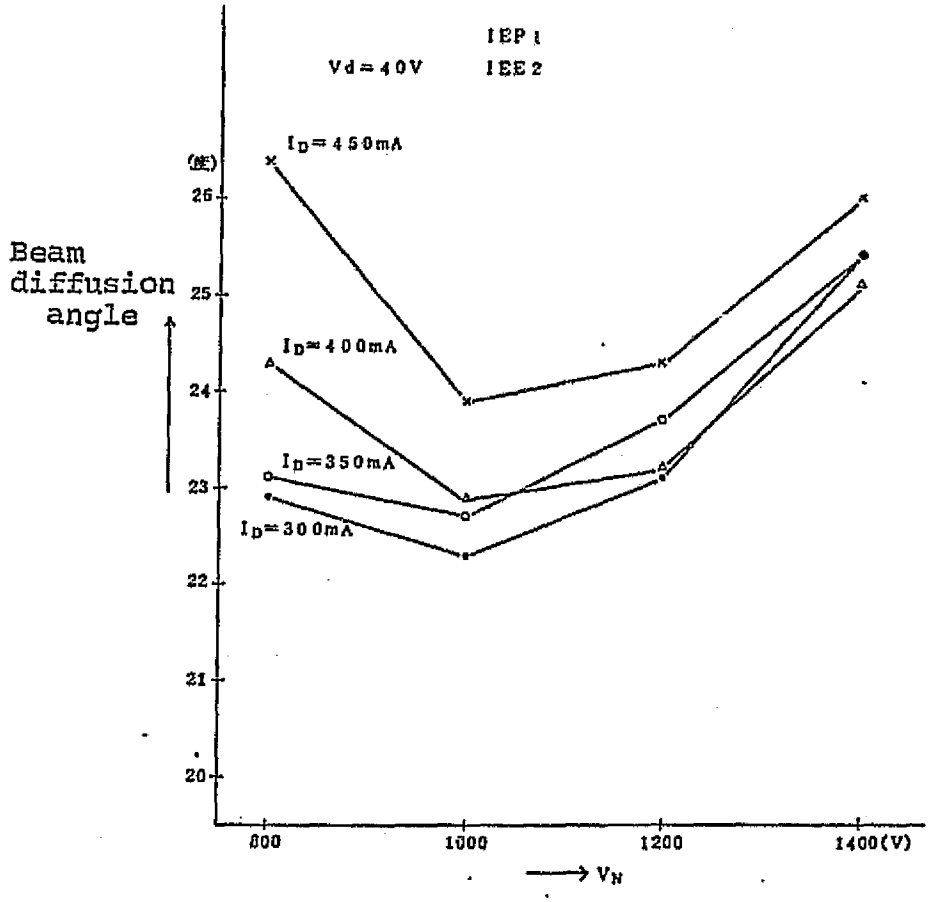

4.4.4 Heat Vacuum Test

This test is for checking IES functions under an environment similar to that of steady orbit. IES was installed in a heat controlled box and mounting area of each component was maintained at required temperature by a heat control device. Test configuration is shown in Fig. 4.62. Heat control box controls temperature with methyl alcohol as a refrigerant. In this test, neutralizer keeper voltage gradually rose in IEE(1), and eventually reached a state where there was not enough power from IEP to maintain neutralizer discharge(Fig. 4.63). This was thought to be due to deterioration of hollow cathode, caused by exposure of engine to air under high humidity. Thus, after PM, strict standards for air exposure time and humidity were set, and output of neutralizer keeper voltage was increased in case of emergency.

In order to continue the test, regular power source was connected in series to neutralizer keeper power source as a temporary measure to add power. Fig. 4.64 shows the results of the heat vacuum test. As clear from the figure, IEP controlled IEE normally.

Fig. 4.62 Configuration of Heat Vacuum Test

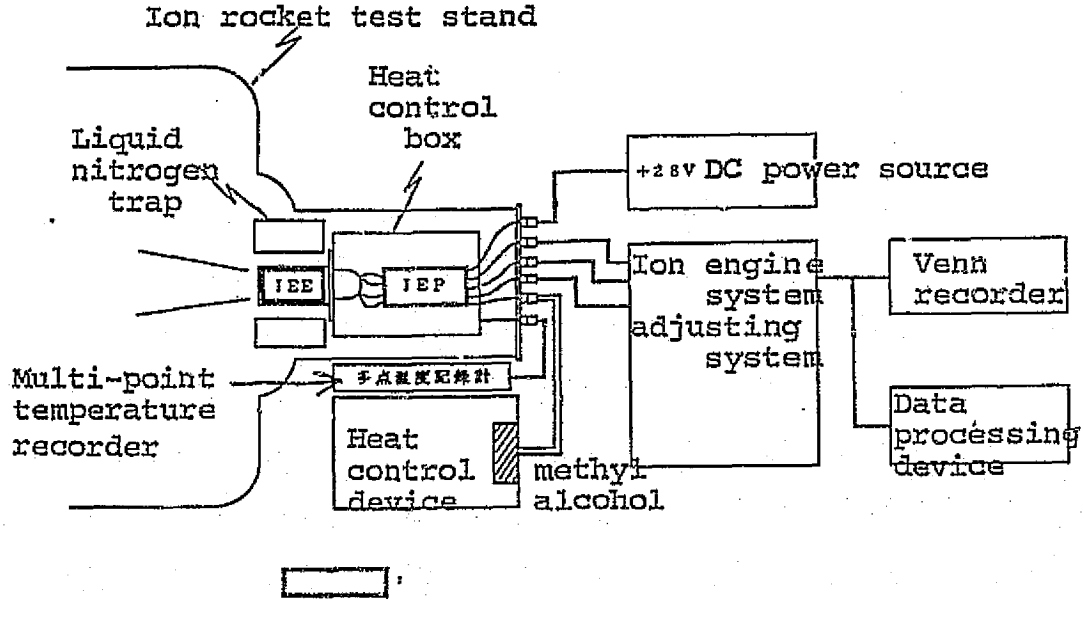

Fig. 4.63 Deterioration of Neutralizer

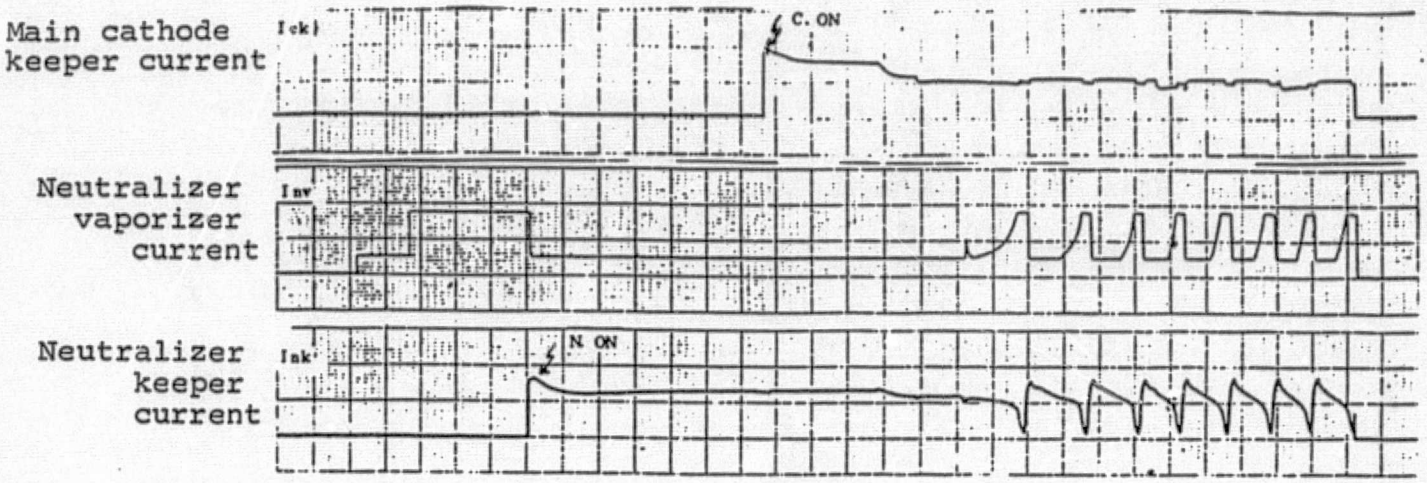

Fig. 4.64 Results of Heat Vacuum Test

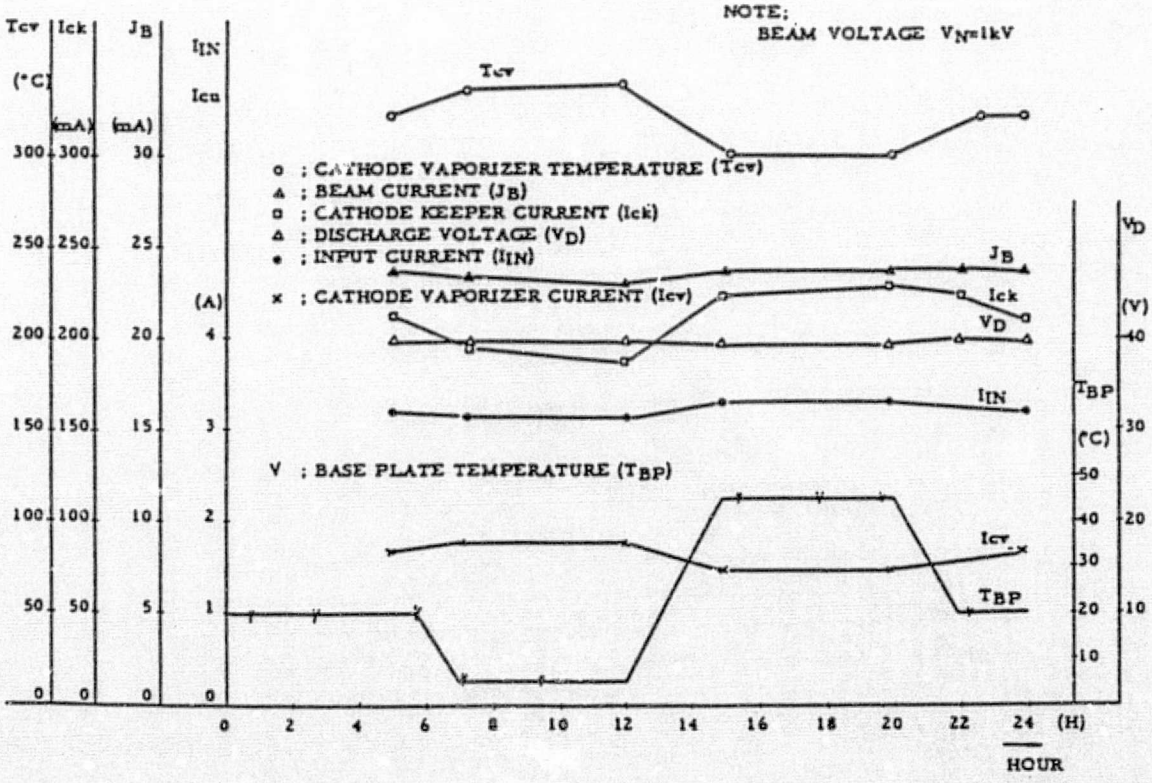

4.4.5 Electromagnetic Compatibility Test

This test was given under the configuration in accordance with MIL-STD-462, whoen in Fig. 4.65. Engine was placed in a glass cylinder of 600ø x 1000mm to allow for permeation of radiated electromagnetic wave. No problem was observed in neither transmission interference noise nor transmission sensitivity in power source lines. Measured results of electric field radiation are shown in Fig. 4.65. Off-standard values are seen sparingly in the narrow band of under 1MHz and the wide band of under 10MHz, but noise around VHF S-band in TTC system was below background level. As the off-standards were within the range that could be absorbed the the satellite system, changing the standards was decided.

IES functions were normal in the electric field radiation sensitivity test. Magnetic field radiation and magnetic field radiation sensitivity also satisfied the specification. Fig. 4.66 shows the ion engine during injection inside the glass vacuum container.

Fig. 4.66 Ion Engine during Injection(electromagnetic compatibility test)

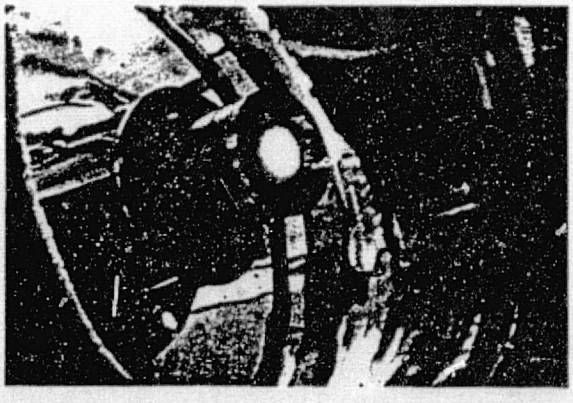

Fig. 4.65 Electromagnetic Compatibility Test

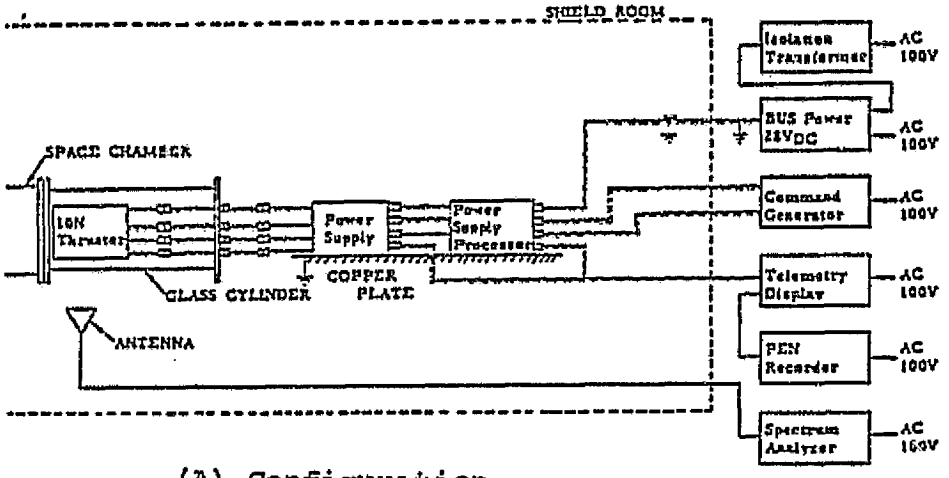

(A) Configuration

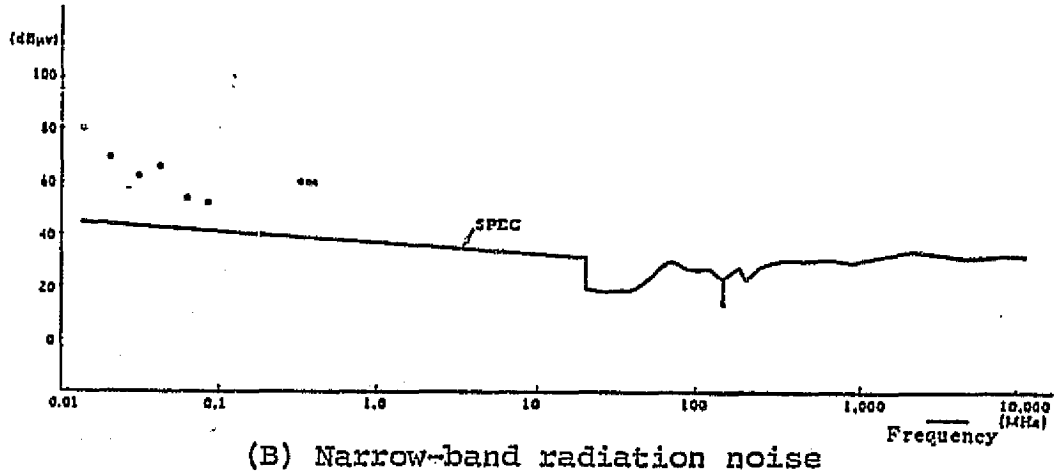

(B) Narrow-band radiation noise

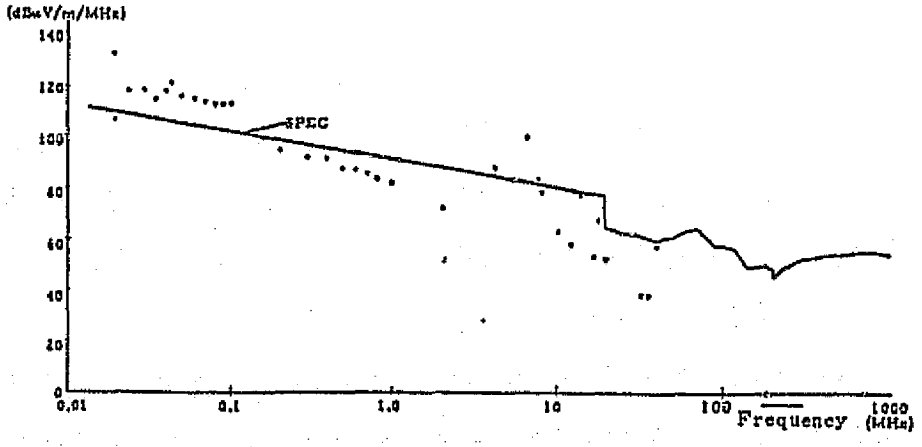

(C) Wide band radiation noise

4.5 Ground Support Equipments

Ground support equipments necessary for the ion engine system tests are listed. Those required for the engine unit are shown in Table 4.37, and those for power conditioner, in Table 4.38. Other equipments used are a heat control box and glass vacuum container (600ø x 1000mm), etc. for IES tests, and a mercury detector(0.005 - 0.1mg/m^3, 0.03 - 1mg/m^3) for safety management.

Ion engine injection was tested using facilities at the National Aerospace Laboratory and Electrotechnical Laboratory. Facilities used are listed in Table 4.39.

Table 4.37 Ground Support Equipments for Ion Engine Unit

Equipment	Specifications
Container for transporting and storage	·Size: large enough for one engine unit ·Withstand pressure: 2kg/cm^{2}abs ·Allowable leakage: under 1 x 10^{-5}atm cc/sec ·It should have an opening for connecting with a container exhaust/nitrogen gas purge device.
Container exhaust/ nitrogen gas purge device	·Container exhaust capacity: Connected to the container for transport and storage, it should be able to exhaust the container to the degree of vacuum of less than 1 x 10^{-3}Torr. ·Purge flow: Connected to the container, it should be capable of nietrogen gas purge at the rated 10ℓ/min.
Nitrogen gas purge device	·Purge flow: rated 120cc/min. ·Connected to the engine unit via a purge container, it should be capable of nitrogen gas purge.
Mercury/nitrogen gas charging/ discharging device	·It should be capable of charging mercury and nitrogen gas to engine unit. Mercury charging capability: 1kg. Minimum reading, 2g. Nitrogen gas charging pressure: Max. 3kg/cm^{2}abs ·It should be capble of discharging mercury from the engine unit. Amount of mercury discharged: Max. 1kg
Alignment device	·Mounted on the accelerator grid surface of the engine unit, it should provide a mirror for aligning the unit. Mirror surface: surface accuracy of less than ¼ wave length

C-3

Table 4.38 Ground Support Equipment for Power Conditioner

Item	#	Use	Function	Capabilities
1. Switch box	1	Adjustment and test of power source device (component test)	Manually operates power source device in combination with load element	ON/OFF signals for 10 systems ON: 10V±2V OFF: 0.5V±0.5V Level signals for 3 systems: Over 0.5V, or over 8V Reference signals (3 types): 0-5V
2. Sequence indicator	1	Adjustment and test of power source control device (component) and printer unit	Indicates with lamp the control functions of power source control device	Output Clock oscillation: 40Hz $10V_{o-p}$ Monitor signals: 5 items "0"0.5V±0.5V "1"10V±2V Indicators: ON/OFF signals - 10 Level signals - 8 Program counter Timer
3. Power source unit tester	6	Adjustment and test of power source units in power source device	Folloring are the types of this tester having and auxiliary power source, inverter block and load: *	Auxiliary power source: ±15V, +10V, +5V load: See Table 4.10 Inverter (nom. val.): DC1KV 30mA DC-1KV 1mA DC 40V 0.35A AC 5V 5A DC 15V 0.3A AC 35V 2A AC 3V 1A
4. Storage box	12	Storage and transport of power source device and power source control device		

* $Z_{T1,2}$, Z_{T3}, Z_{T4}, Z_{T5}, Z_{T6} and Z_{T10}

Table 4.39 Facilities

	Facility or equipment	*	**	Use	Outline
1.	Ion rocket test stand	ETL	IES	Function/performance, EMI, heat vacuum and long-mode tests of IES	·Exhaust 5500ℓ/S ·Degree of vacuum in test over 2×10^{-6}Torr ·LN_2 consumption 400ℓ/day
2.	Shield room	ETL	IES	Obtaining IES characteristics and data on EMI	·4.5m x 3.9m x 2.5m ·Attenuation: 0.5MHz 49dB, 20 • 55 •, 100 • 67 •, 500MHz 68dB, 1000 • 25 •, 2000 • 31 •, 4000 • 59 •
3.	EMI measurement device	ETL	IES	Obtaining EMI data	·Spectrum analyzer ·Current probe ·Bi-conical antenna ·Test antenna
4.	Data processing device	ETL	IES	Recording and indicating telemetry information from IES by teletype instructions	·Teletype ·Display ·Mini-computer
5.	Multi-point temperature measuring instrument	ETL	IES	Measuring temperature of each part of IES	·Total 20 channel
6.	IES automatic control device	NAL	IES	IEE component test	Simulates functions of power source control device, records and processes data.
7.	Ion engine test power source	NAL	IEE	IEE component test	Outputs power for 10 systems which simulate output characteristics of IP.
8.	Electric propulsion test facil.	NAL	IEE IES	Tesing functions and performances of IEE and IES	Building
9.	Electric propulsion vacuum tank	NAL	IEE IES	"	Degree of vacuum reached over 1×10^{-5}Torr Internal shroud wall temp. -185C Set temp. range of baseplate -40～60C
10.	Thrust measuring device	NAL	IEE	Measuring thrust of IEE	Detection range 0.1～3 Detection accuracy ≤±5%

(continued to next page)

11. Beam diffusion angle measuring device	NAL	IEE	Measuring beam diffusion angle of IEE	Detected ion current 0.1 - 3 Detection accuracy ∠ ±5%
12. EMI measuring device	NAL	IEE	EMI measurement of IEE component	•Spectrum analyzer •Current probe •Biconical antenna
13. Clean booth	NASDA	IEE IES	Maintaining work environment	3.5 x 2.1 x 2.2H(m), Class 100,000
14. Ion engine simulator	ETL	IEP	Adjustment and test of IEP	Dynamic load of 10 systems

* NASDA: Nat'l Space Development Agency
ETL: Electrotechnical Laboratory
NAL: Nat'l Aerospace Laboratory

** IEE: Ion Engine Unit
IES: Ion Engine System
IEP: Power Conditioner

Chapter 5

Production Tests

Chapter 5: Production Tests

5.1 Outline of Tests

Prototype Model(PM) was produced according to the detailed design finalized with the Development Test results. Qualifying Tests were given to this PM to verify the design and to study the propriety of production process. Due to some major problems discovered, the production process, test methods and procedures, IEE/IEP interface, etc. were re-examined, results of which were reflected in the Flight Model(FM) subsequently produced. Acceptance tests were then given to the FM. A problem with neutralizer during oscillation test, relating to production process, was solved by replacing it, and thus, the FM was found to meet flight requirements.

Tests were carried out consistently in the order of component test and evaluation of ion engine unit(IEE) and power conditioner (IEP), and then test and evaluation of the ion engine system(IES), a combination of IEE and IEP. Progress of test process was shown in Table 2.3. Each test was given for two units of each component ($\{$IEE(1), IEE(2)$\}$, $\{$IEP(1), IEP(2)$\}$, and $\{$IES(1), IES(2)$\}$), although test subjects were not necessarily the same. Subjects and the flow of Qualifying Tests are shown in Table 5.1 and those of Acceptance Tests are shown in Table 5.2. Configuration for each test subject is basically the same as in Development Tests.

Table 5.1 Flow of Qualifying Tests

(a) IEE

- Beginning-stage inspection
- Mass characteristic test without mercury
- Transportation (MELCO→NAL)
- Mercury filling
- Performance test (I)
- Heat vacuum test
- Mercury discharging/filling
- Transportation (NAL→MELCO)
- Mass characteristic test
- Oscillation test
- Remanence moment measurement
- Transportation (MELCO→NAL)
- Performance test (II)
  - Unit #1: Thrust measurement
  - Unit #2: Electromagnetic compatibility test
- Mercury discharging
- Transportation (NAL→MELCO)
- Final inspection

(b) IEP

- Inspection
- Mass characteristic test
- Electrical performance test
- Electromagnetic compatibility test
- Shock test
- Oscillation test
- Heat vacuum test
- Remanence moment test
- Final performance test

(c) IES

- Inspection
- Function/performance test
- Heat vacuum test*
- Long-mode test*
- Electromagnetic compatibility test*

*Unit #2 only.

Table 5.2 Flow of Acceptance Tests

(a) IEE

- Beginning-stage inspection
- Mass characteristic without mercury
- Transportation (MELCO→NAL)
- Mercury filling
- Performance test (I)
- Transportation (NAL→MELCO)
- Mass characteristic test
- Oscillation test
- Remanence moment measurement
- Transportation (MELCO→NAL)
- Performance test (II)
- Heat vacuum test
- Transportation (NAL→MELCO)
- Final inspection

(b) IEP

- Inspection
- Electrical performance test
- Mass characteristic test
- Oscillation test
- Heat vacuum test
- Final performance test

(c) IES

- Inspection
- Function/performance test
- Heat vacuum test
- Final inspection

5.2 Qualifying Tests

5.2.1 Engine Unit Qualifying Tests

(1) Structural design evaluation

Basic natural oscillation was almost the same as that of EM (Table 4.20), satisfying the requirements of over 100Hz.

Structural design was checked by sine wave oscillation and random oscillation tests. Five cases of problems occurred. Conditions and causes of the problems and countermeasures taken are shown in Table 5.3. All related to hollow cathode assembly, requiring improvements in the production process of FM. In PM, hollow cathode was replace and test was continued.

(2) Heat design evaluation

Propriety was verified by heat vacuum test. Table 5.4 shows the minimum temperature in non-motion and maximum temperature in motion.

(3) Performance design evaluation

As noted in the previous chapter, after EM, improvements were made in heat properties of main hollow cathode vaporizer and the diameter of neutralizer keeper hole was increased(from 1ø to 2ø).

Performance tests of engine unit were carried out using power sources for ground testing.

For performance characteristics in steady state, data was obtained by maintaining mercury flow in the main hollow cathode at $(0.9\pm0.2) \times 10^{-4}$g/s and $(0.1\pm0.05) \times 10^{-4}$g/s in the neutralizer hollow cathode. Interface with IEP was checked with power sources artificially equipped with IEP output characteristics(PS5 and PS8) and closed loop control(PS6 and PS9). Obtained data are shown in Table 5.5. Performance characteristics in steady state satisfied the requirements.

Examples of operating conditions are shown in Fig. 5.1. In (b), beam injection state was reached about 16 minutes after start.

Thrust was indirectly measured, 95% of which met the calculated ideal values.

For operation in a transient state, results showed improvements over EM. During interface check of IEE(1), however, discharge could not be maintained due to problems in controlling neutralizer hollow cathode keeper discharge, which caused unstable point of action in discharge. The causes were:

i) Keeper voltage was high at rated flow;

ii) Keeper voltage was high at a point where it was supposed to be at its minimum in relation to vaporizer flow; and

iii) Current/voltage characteristics of keeper discharge were close to those of power source output.

They were presumably due to ununiform characteristics of the neutralizer hollow cathode which was then replaced by another neutralizer hollow cathode having none of these factors. Selection standards for such hollow cathodes were established before the production of FM(See 5.3.1).

(4) Record of problems

Summary is given in Table A2.1 in Appendix.

Table 5.3 Oscillation Test Problem Situations/Causes/Countermeasures

	Situation	Cause	Countermeasure
Breaking of thermocouple in IEE(1) (main hollow cathode)	·Breaking near the area brazed to vaporizer. ·Clamp was not effective at a point about 5mm from the breaking point.	·Comparing with IEE(2), clamp was not effective - direct cause. ·If there is no clamp effect, stress applied to the breaking point is severe, with stress concentrated on brazed area.	Strengthen clamping in the designated area. For added safety, clamp end section on the tank support.
Breaking of cathode heater lead in IEE(2) (main hollow cathode)	·Twist observed at breaking point.	·Terminal was rotated during assembly, causing a twist and consequent deformation. Stress concentrated on this area.	Install spanner working face in the terminal to prevent rotation.
Breaking of insulator sheath heater in IEE(1)	·Breaking at the edge of brazed area.	·Stress concentrated on a slight crack in the brazed area.	Observe mechanical procedure strictly and enforce appearance test.
Breaking of vaporizer heater neutralizer hollow cathode)	·Breaking at the edge of brazed area.	·Stress was applied to the area near the breaking point during installation and removal, loosening the clamp and causing the stress to remain.	Provide instructions not to apply stress to this area during work. Make sure clamp is tight.
Slipping of cathode shield in IEE (1) (main hollow cathode)	·Spot-welded part of the heat shield came apart.	·Faulty spot-welding.	Check spot-welding conditions after welding, as well as before, as required. Inspect all of the welded items.

Table 5.4 Minimum and Maximum Temperatures

	Non-motion, low temp. heat balance test Base plate temp. -15^{0}_{-6}°C			In-motion, high-temp. heat balance test Base plate temp. $+55^{+6}_{0}$°C		
	QT results* IEH(1)/IEH(2)	EM	Computed value	QT results* IEH(1)/IEH(2)	EM	Computed value
Engine unit temp.	−22℃/−21℃	−19℃	−14℃	99℃/106℃	100℃	134℃
Tank temp.	−21℃/−18℃	−16℃	−13℃	76℃/ 77℃	68℃	76℃
Main hollow cathode temp.	−21℃/−19℃	−10℃	−13℃			
Neutralizer hollow cathode vaporizer temp.	−17℃/−14℃	−20℃	−15℃			

*IEE(1) 3:14, 4/23/80 data
IEE(2) 18:00, 5/6/80 data

**IEE(1) 11:50, 4/23/80 data
IEE(2) 7:00, 5/7/80 data

Table 5.5 Engine Unit Characteristics & Performance Data (PM)

Characteristics and Performance	Unit				
Voltage/current:					
Beam	KV/mA	0.99/26.9	0.99/27.1	−0.99/29.2	0.99/28.5
Accelerator grid	〃	−1.0/0.41	−10.0/0.37	−1.0/0.18	−1.0/0.33
Discharge	V/A	38.6/0.35	40.0/0.35	43.1/0.35	39.9/0.35
Main hollow cathode:	〃	—	—	—	—
Cathode heater	〃	17.1/0.3	17.6/0.24	15.5/0.30	16.8/0.26
Keeper	〃	2.99/1.78	2.92/1.78	2.66/1.59	2.9/1.74
Vaporizer heater	〃	—	—	—	—
Neutralizer hollow cathode:	〃	24.2/0.24	24.5/0.24	20.4/0.25	24.5/0.24
Cathode heater	〃	1.26/0.75	1.10/0.66	1.47/0.85	1.10/0.65
Keeper	〃	2.56/0.99	2.50/0.99	2.65/0.99	2.65/0.99
Vaporizer heater	℃	285.7	281.5	264.5	269.9
Insulator heater	〃	236.2	218.0	229.7	195.1
Temperature:	〃	75.2	74.8	71.7	59.3
Main hol. cath. vaporizer	〃	39.1	41.0	40.0	29.4
Neut. hol cath. vaporizer	〃	20.2	20.0	20.8	20.8
Engine unit	〃	−168	−178	−162	−168
Tank	$\times 10^{-5}$ ℃/sec	0.884	0.793	0.977	1.11
Base plate	〃	0.098	0.062	0.098	0.039
Shroud	gwt.	0.176	0.177	0.192	0.187
Mercury flow:	sec	1990	2225	1956	1630
Main hollow cathode	W	60.9	60.2	625	61.7
Neutralizer hollow cathode	%	63.0	71.0	62	53
Thrust	〃	43.7	44.4	46.3	45.8
Specific impulse	°	22.0°	—	—	—
Power consumption					
Propellent util. efficiency					
Power efficiency					
Beam diffusion angle					

Fig. 5.1(a) Engine Operating Conditions(PM IEE(1))

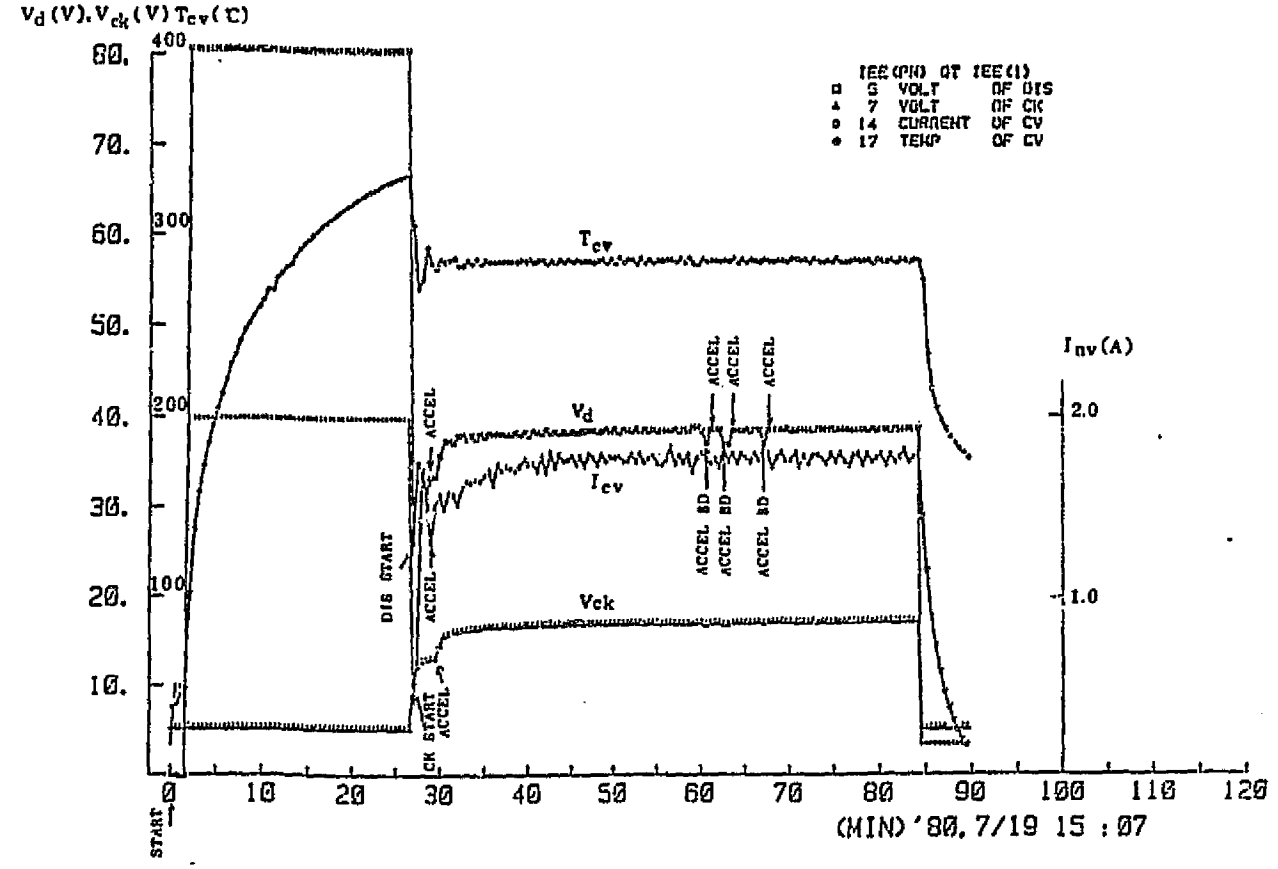

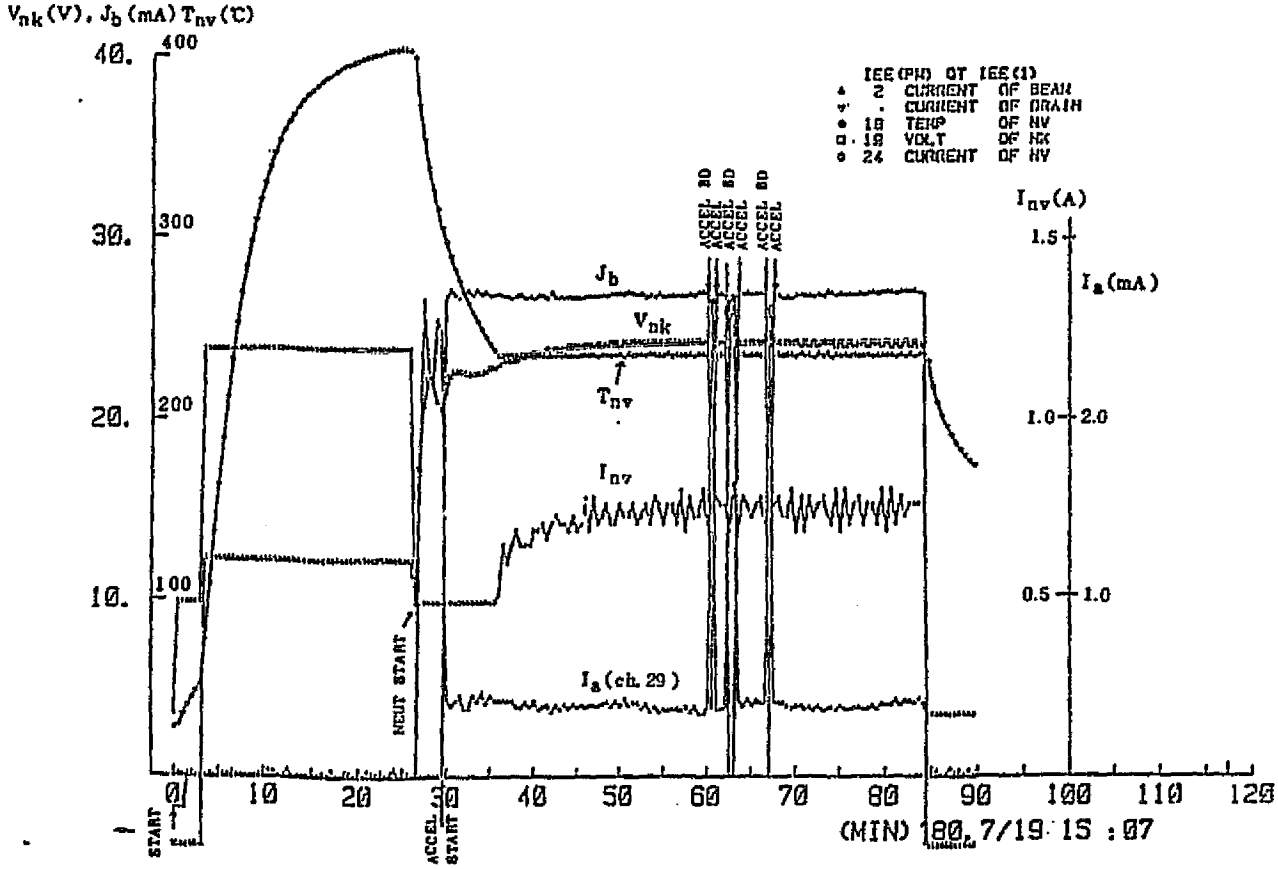

Fig. 5.1(b) Engine Operating Conditions(PM IEE(2))

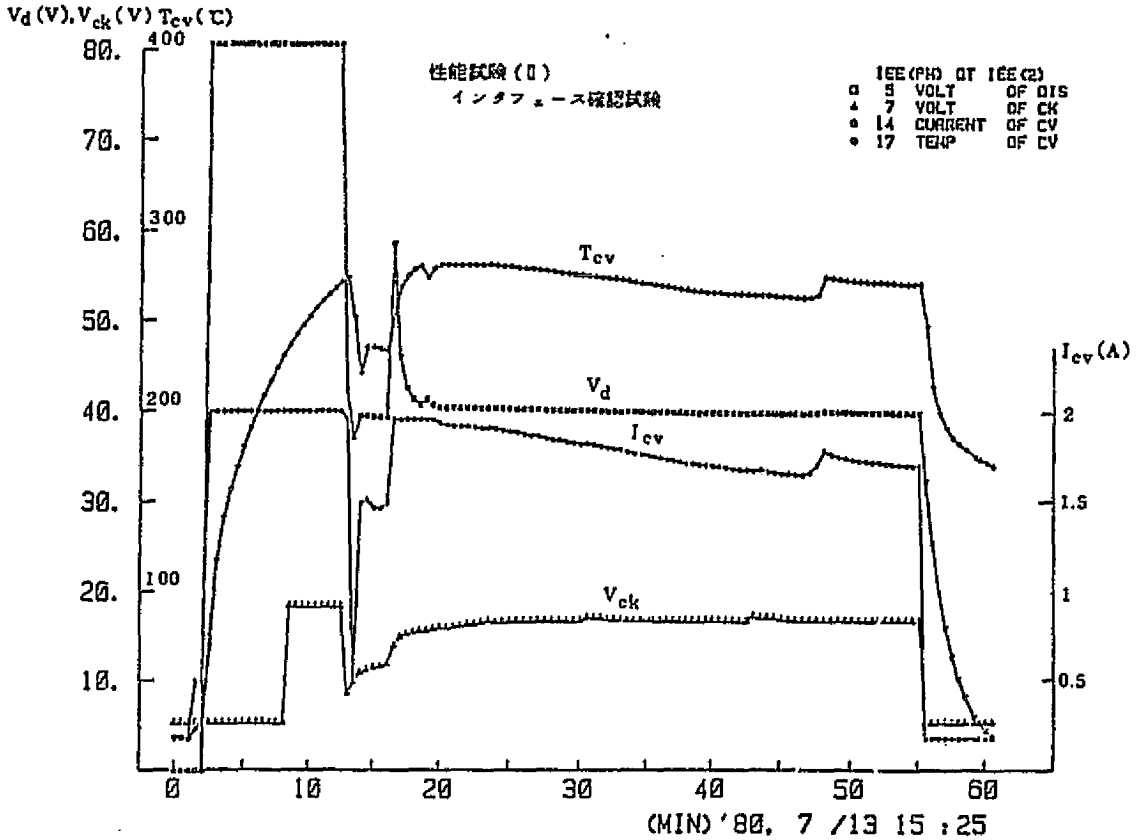

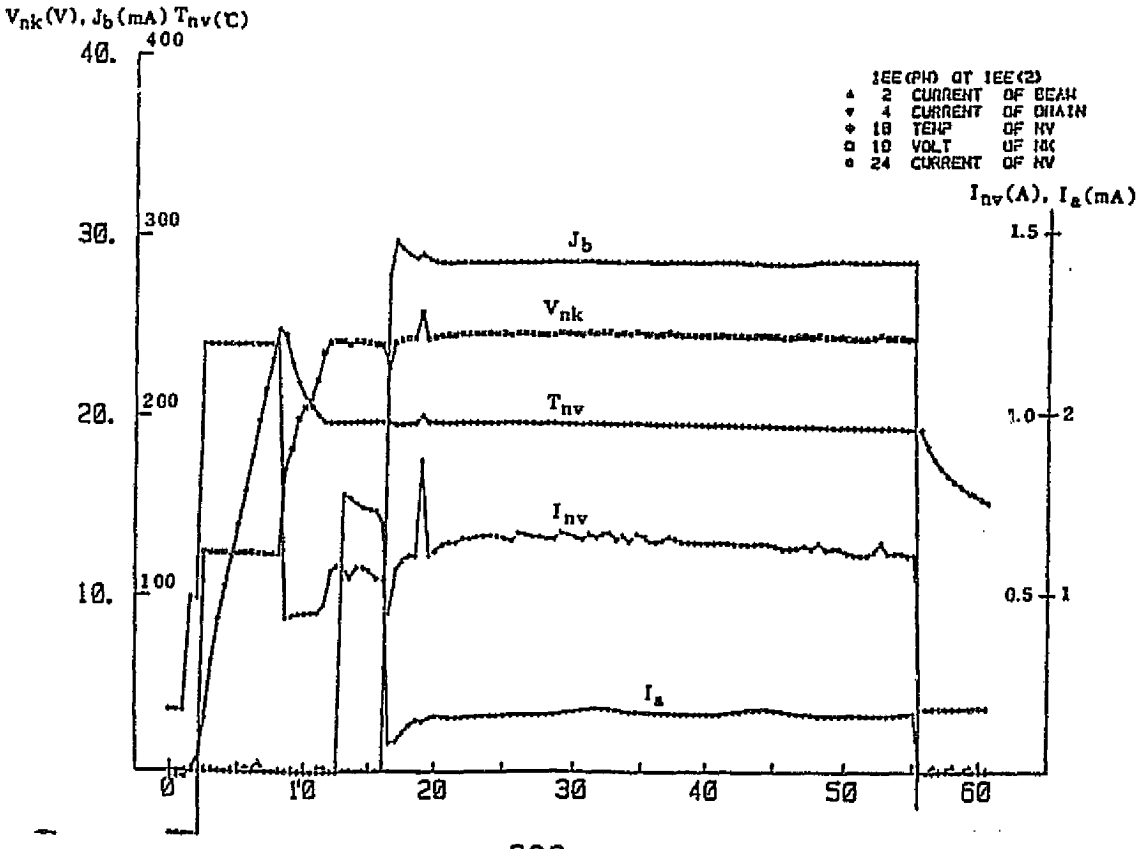

5.2.2 Power Conditioner Qualifying Tests

Qualifying Tests of power conditioner were completed without a single case of problem. Measured output of power sources (dummy load was used) in the heat vacuum test are shown in Table 5.6. As temperature fluctuation was large among unstable-type power sources, allowable range of output fluctuation was adjusted taking interface with engine unit into consideration. There was no other problems and it was thus concluded that the power conditioner could well meet the environment tests on the Qualifying Test level.

Table 5.7 shows the breakdown of weight.

Table 5.6 Thermal Vacuum Test Results

項目 \ I.P. / Base temp.		Unit No. 1			Unit No.2		
		−15℃	20℃	55℃	−15℃	20℃	55℃
PS1 output	(V)	996	994	992	998	1.000	1.000
PS2 "	(V)	−964	−966	−976	−970	−968	−978
PS3 "	(A)	0.348	0.352	0.351	0.346	0.351	0.349
PS5 "	(V)	13.62	15.11	16.55	12.86	14.57	15.93
PS6 "	(A)	1.94	1.94	1.94	1.94	1.93	1.94
PS8 "	(V)	20.92	23.68	26.59	21.53	24.90	27.33
PS9 "	(A)	0.459	0.470	0.760	0.458	0.470	0.920
PS10 "	(W)	2.22	2.42	2.81	2.28	2.53	2.85
IEP input	(W)	90.47	92.48	96.6	90.86	93.21	98.11

Table 5.7 Weight of Power Conditioner

Power source control device	3.58kg
Power source device #1	6.60kg
Power source device #2	6.65kg
Power conditioner	16.83kg

5.2.3 Ion Engine System Qualifying Tests

Test configuration was the same as that of Development Tests: IEP was placed outside the vacuum tank during function/performance tests(See Fig. 4.5.6) and placed inside during heat vacuum test and long-mode test, providing the same conditions as on-board(See Fig. 4.62).

(1) Function/performance tests

During the tests, a problem occurred in which output current of a discharge power source(PS3) latched at 5-6+ mA immediately after the start of main discharge. This was due to insufficient spare phase in excess current discharge circuit of PS3 which caused faulty action when discharge waveform was unstable, and it was solved by returning the constant in RC circuit to the same value as in EM.

Next problem was that the neutralizer hollow cathode of Unit No.1 could not be ignited by the neutralizer heater power of IEP. Details are given in Section 6.4. In conclusion, output of neutralizer heater power in FM was raised to the minimum of 5.25V, and at the same time, test procedures and measures to minimize deterioration of hollow cathode caused by grim during ground testing were employed. On the other hand, the neutralizer of Unit No. 1 has had a history of having slight problems with ignitability in the IEE eomponent test(Table A2.1, item 12). Thus, Qualifying Tests were performed on Unit No. 1 with which no such problem was expected. Neutralizer ignition time of Unit No. 2 wa about 20 minutes, with no problem observed in its functions and performances.

(2) Heat vacuum tests

Temperature profile was a heat cycle of -5C, 20C and +55C, based on the specification(Fig. 4.15). Fig. 5.2 shows the characteristic

changes in relation to temperature. During the heat cycle, five repetitive operations were performed at the base plate temperature of -15C and +55C. Results confirmed that IES functions and performances were satisfactory under the heat environment of QT level.

(3) Long-mode test

System was operated continuously for 50 hours at the base plate temperature of 20C. Results are shown in Fig. 5.3. Stable beam injection was evidenced over a long period of time.

(4) Electromagnetic compatibility test

Noise levels were similar to the measured results of EM(See Fig. 4.65), satisfying the specifications.

During this test, insulation failure of keeper electrode cause neutralizer(IEE(2)) to stop iginiting. It seemed to have been caused by accumulated backspattered metal from the vacuum chamber long-mode test, and a shield to protect the ceramic terminal of neutralizer keeper was added in FM.

(5) Record of problems

Summary is given in Table A2.2 in Appendix.

Fig. 5.2 Evaluation of Characteristic Change in Thermal Vacuum Test

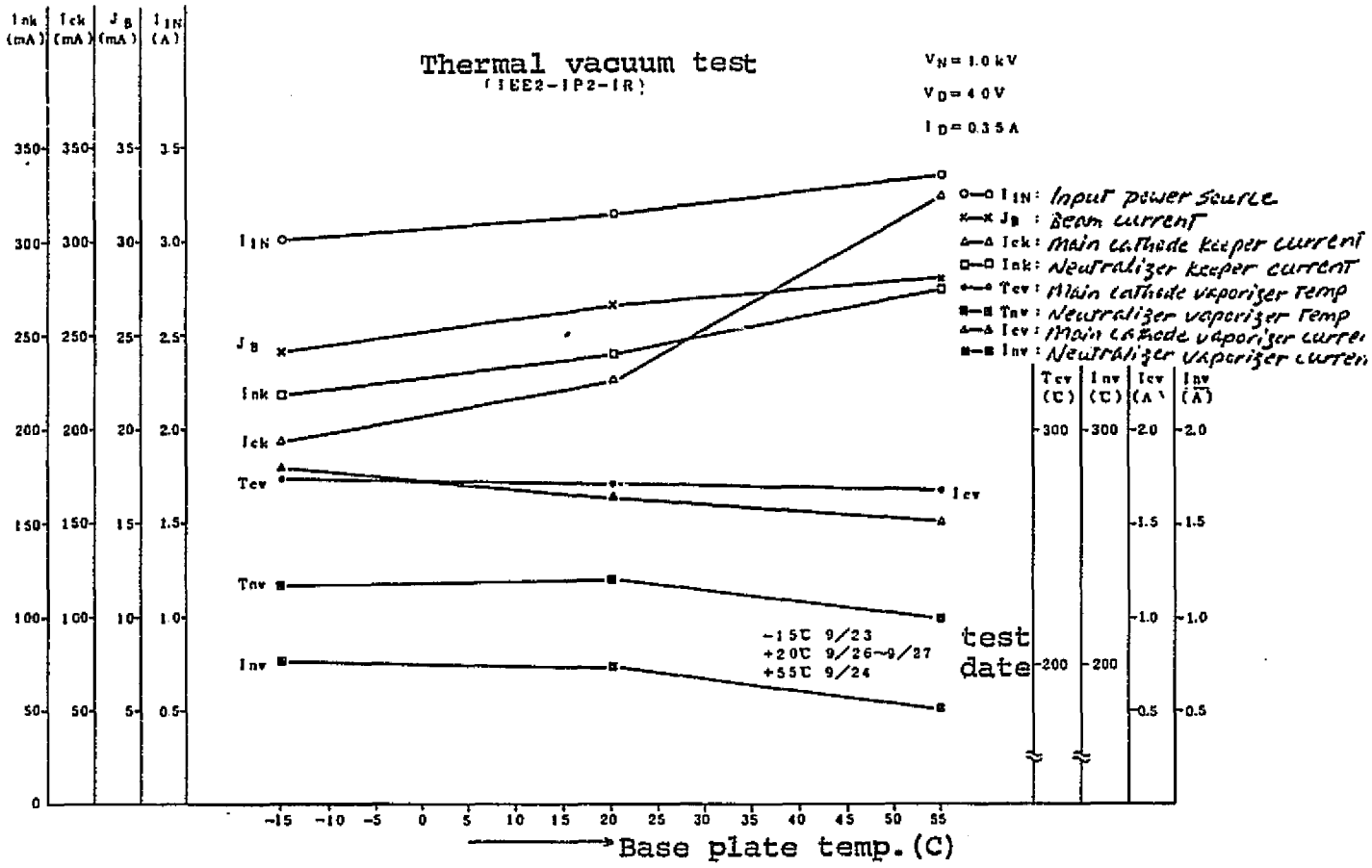

Fig. 5.3 Long-mode Test

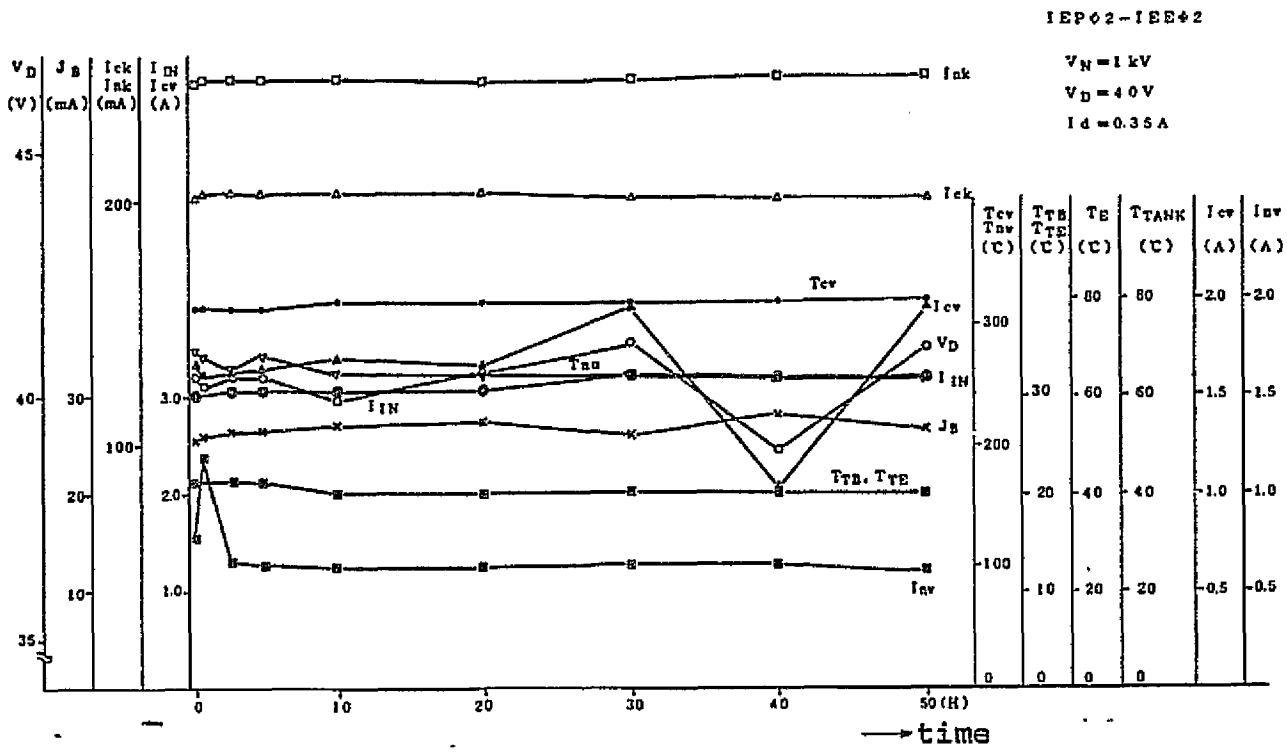

5.2.4 Summary

Qualifying Tests thus completed, there were some major problems which remained to be dealt with in FM. To summarize the measures to be taken,

i) Improve supporting method of lead wire, etc. in hollow cathode assembly and further, improve production process(including inspections) to ensure vibration resistivity;

ii) By establishing selection standards for neutralizer hollow cathode, obtain its control compatibility with power sources;

iii) Add shield, etc. to protect engine unit from grime during ground testing; and

iv) Review electrical interface conditions, including output fluctuation, of engine unit and power conditioner. Ignition of neutralizer must be assured.

As iv) was of particular importance, propriety of the measures was evaluated by testing the combination of PM-IEE No. 1 (neutralizer replaced) and EM-IEP(min. output of neutralizer heater power source modified to over 5.25V). Satisfactory results were obtained, and the production and tests of FM followed.

5.3 Acceptance Tests

Reflecting the results of Qualifying Tests, following was incorporated into FM: increased vibration resistivity of hollow cathode assembly and addition of spatter shield in IEE; and increased output of PS7 and PS8 in IEP. Also, a titanium spatter guard was placed inside vacuum chamber in the testing facilities in order to reduce back-spattering. Further, procedures for the first operation after exposure to air were revised(engine preheating step was added).

5.3.1 Engine Unit Acceptance Tests

Changes made in FM as a result of problems in PM are shown in Table 5.8. A difference made in appearance was that a tantalum spatter shield cylinder was installed on the neutralizer.

Tests were performed under the flow shown in Table 5.2(a). Neutralizer of Unit No. 2 short-circuited in the keeper electrode during oscillation test. It was found to have been caused by a faulty spot welding of keeper lead wire, and the neutralizer was exchanged. Regarding sizing, insulator heater lead wire was abnormally close (0.4mm) to the main support in the main hollow cathode of Unit No. 2. As the potential difference between them reaches a maximum of 1.4kV, its propriety was studied from the point of view of earthquake- and voltage-resistivities. As a result of oscillation analysis & test and voltage resistivity check, no change was made.

Both IEE(1) and IEE(2) satisfied performance requirements of the specifications without other problems. Following is the summary of data and evaluations obtained from the performance test.

(1) Power source input conditions

Performance test for the engine was given under the power source input conditions listed in Table 5.9 by using ground test circuits.

Power source conditions varied slightly depending on the test subject. As interface test was to take the output fluctuation based on IEP output change into account, following changes were made from PM:

i) DC constant voltage power source was used as a test power source corresponding to PS7, and input voltage conditions of neutralizer cathode heater were reviewed. (AC constant power source(5±0.1A) was used in PM.)

ii) Rated output of test power sources corresponding to PS5 and PS8 during interface test were changed. (In PM, PS5 was 15±0.5V(at 0.3A) and PS8 was 24±0.5V(at 0.25A).)

iii) Output of test power sources corresponding to PS5, PS6, PS7, PS8 and PS9 were ranked low, rated and high levels, and IEE operation was checked at low and high levels during heat vacuum test. (With PM, operation was checked only at rated level.)

(2) Discharge ignition characteristics

Discharge ignition characteristics can be evaluated by the starting time required for discharge. Ignition time was defined as the time required for each discharge to start after the end of idling. Fig. 5.4 shows the discharge ignition characteristics of IEE(1) and IEE(2). A new neutralizer was used in Unit No. 2 from the third test on, due to a short circuit in keeper electrode during oscillation test.

There were two main problems in the characteristics obtained:

i) Main hollow cathode keeper main discharge was not ignited after 30 minutes.

ii) IEE(1) and IEE(2) were unstable at the time of neutralizer keeper discharge ignition.

As for i), cathode heater input at nominal level is slightly critical

and ignition was checked at high level input. ii) is a phenomenon caused by the longer response time(approx. 100m^{sec}) of the output of power source used(PS8-equivalent),than PS8(10 ^{sec}) in IEP, to load fluctuation. It is not likely to occur with actual power sources on board and presents no problem in performance evaluation.

During low-temperature start tests (1), (2) and (3), neutralizer ignition was tested under the worst possible interface conditions: engine mount temperature of -5C and neutralizer heater voltage of 5.2V. Both No. 1 and No. 2 ignited in about 10 minutes. Thus, ignition problems with neutralizer observed in PM was considered solved.

(3) Performance in transient state

IEE's transition from the start to beam injection state was checked using IEP-equivalent operation sequence and control loop, and their compatibility was evaluated. Representative operating conditions are shown in Fig. 5.5. Test results show smooth transitions to beam injection state. Control property of neutralizer keeper discharge, a problem in IEE at QT level, was mostly solved in FM. Criteria for selecting this neutralizer hollow cathode were(see Fig. 5.9):

i) Minimum keeper voltage(Vnk(min.) at 0.25A) in the Vnk-Tnv characteristic of less than 23V;

ii) Discharge impedance in the Vnk-Jnk characteristic of less than 90Ω; and

iii) Keeper voltage at the constant current of 0.25A and the flow of 1 x 10^{-5}g/sec of less than 26V.

As in PM, increase in discharge voltage, a transient phenomenon, was observed in FM at the time of beam injection. The phenomenon accompanies shut-off of residual power(about 4W) from heating main cathode immediately before beam injection. Thus, factors such as

temperature of main cathode vaporizer at the start of main discharge affect discharge voltage. In this FM, fast ignition time for main discharge was obtained on the whole, which was not preferrable in terms of discharge voltage increase. The phenomenon, to an extent, cannot be avoided and if the transient increase is less than 500V, there is enough margin in the power source output(upper limit 60±2V) to prevent any problems.

(4) Performance in steady-state

Good results were obtained for both beam injection maintaining properties and performance parameters in steady state. The latter is shown in Table 5.10.

Points of action of main discharge and neutralizer keeper discharge in steady state, with both Vd-Icv closed loop and Vnk-Inv closed loop under control, are shown in Fig. 5.6 and Fig. 5.7. It is shown that control error occurred at high temperature in the closed loop of neutralizer keeper voltage in Unit No. 2. From this, it is supposed that the same would happen in the orbit in response to the changes in heat input. However, this control error was towards lowering keeper voltage, which was not in the reverse characteristics category observed during development tests. With no effects on maintaining discharge, the error was allowed.

(5) Test with varied parameters

Following is the list of parameters varied:

Beam voltage	0.8～1.4KV
Main cathode keeper current	0.25～0.40A
Discharge current	0.3～0.5A
Neutralizer keeper current	0.2～0.4A
Main cathode mercury flow IEE(1)	0.55～1.41×10^{-4}g/sec

Main cathode mercury flow IEE(2)
$0.64 \sim 1.51 \times 10^{-4}$ g/sec

Neutralizer mercury flow IEE(1), IEE(2)
$0.6 \sim 2.0 \times 10^{-4}$ g/sec

Fig. 5.8 shows the changes in parameters relative to changes in discharge current of IEE(1) and IEE(2). Fig. 5.9 shows current/voltage characteristics of neutralizer discharge.

(6) Physical properties

Tab. 5.11 shows measured weight of engine unit and remanence moment at the center of gravity.

Fig. 5.10 is a photograph showing the engine unit appearance. The shape is as specified(see Fig. 4.3).

(7) Record of problems

Summary is given in Table A2.4 in Appendix.

Table 5.8 Changes Made in FM Based on PM, and Results

	Problem in FM	Changes made in FM	Results
1.	Breaking of main hollow cathode vaporizer thermocouple in oscillation test (MR78-0115)	·Double bind + triple bind was used for the clamp. ·Ends of thermocouple were clamped on the tank support.	Good(no abnormality observed in oscillation test).
2.	Breaking of main hollow cathode heater lead wire in oscillation test(MP78-0117)	·Spanner working face was installed on the terminal. ·Tool for installing terminal was produced. ·Hole on the main support for mounting terminal was enlarged.	Good(no abnormality observed in oscillation test).
3.	Crack in the sealed end of main hollow cathode insulator heater	·Production steps were specified in the drawing. ·Angle tool was produced.	Good(no abnormality observed in appearance test at receipt of hollow cathode).
4.	Insulator heater voltage did not meet specification (MP78-0086)	·Real load was used in adjusting instrument system.	Same occurred partially in AT, but was covered by measuring voltage using instrument system for monitoring voltage at IEE connector end.
5.	Main discharge could not be maintained(MR78-0087)	·Stabilizing resistance was changed to 20Ω.	Good(No abnormality observed in performance test I & II and thermal vacuum test).
6.	Discoloring of metal part of D sub-connector(MR78-0096, MR78-0114)	·Connector was shielded with aluminum foil and capton(sp?) tape during ground test.	Good(no abnormality observed in final appearance test).
7.	3-minute wait for beam injection was skipped by mistake in test procedure (MR78-0171)	·Correct procedure was specified in the test manual.	Good(no abnormality observed in performance test I & II and thermal vacuum test).
8.	Short-circuit in cathode heater (MR78-0153, MR78-0168)	·Heat shield assembly was reinforced. ·Interim testing was reinforced.	Good(no abnormality observed in oscillation test).

(continued to next page)

9.	Neutralizer hollow cathode could not be controlled. (MR78-0155)	•Controllable cathodes were selected by adding specifications and tests.	Good(no abnormality observed in performance test I & II and thermal vacuum test).
10.	Repeated flashing of main discharge during beam injection(MR78-0156)	•Measuring time of mercury flow was doubled for improved accuracy. •Duration of vacuum exhaust when mercury was filled was increased.	Good(same as above).
11.	Breaking of neutralizer hollow cathode vaporizer heater wire during oscillation test	•Bending was added to thermocouple so that there was no space between the three when clamped.	Good(no abnormality observed in oscillation test).

	Item which required changes made in FM: Treatment in PM		Results
1.	Adjustment of interface with power source	•Test was performed taking output fluctuation based on power source output change into consideration.	Good(no abnormality observed in performance test I & II and thermal vacuum test).
2.	Neutralizer ignition characteristics	•In the first operation after exposure to air, IEE was started immediately after 105-minute idling. •In other operations, IEE was started immediately after 60-minute idling. •In the first operation after exposure to air, IEE was operated after 8-hour or longer vacuum exhaust period.	
3.	Pollution due to testing	•Neutralizer cathode heater power source input was maintained within the specified range. •Spatter shield was installed around neutralizer cathode. •In testing IEE(2), target of partially pure titanium was used. (No target was used in testing IEE(1).)	Good(no abnormality observed in neutralizer keeper insulator during final electrical performance test).

Table 5.9 Power Source Input Conditions

Test subject: OP-2: interface check
TV-2: low temp. motion start test(1)
TV-3: transient motion test(1)
TV-4: high temp. motion heat balance test
TV-5: low temp. motion start test(2)
TV-6: " (3)
TV-7: high temp. motion start
TV-8: transient motion test(2)

OP-1: rated operation test
OP-4: test with varied parameters

	Power source	Operation mode I	Operation mode II
PS1	Screen grid (beam)	DC constant voltage: 1±0.1kV(rated), changed to 0.8kV ~ 1.4kV in OP-4.	
PS2	Accelerating grid	DC constant voltage: -1±0.1kV(rated), changed to -0.8kV ~ -1.4kV in OP-4.	
PS3	Discharge	DC constant voltage: 0.35±0.02A(rated), changed to 0.3A ~ 0.5A in OP-4. (Output terminal is to maintain a series stabilizing resistance of 20Ω for IEE. (?))	
PS4	Main cathode heater	5KHz AC constant current: 5±0.1A(nominal level) 2.5±0.1A(idling level)	
PS5	Main cathode keeper	At no load: DC constant voltage of 300±10V Power source output at load: see fig.(a)	At no load: DC constant voltage of 300±10V At load: DC constant current of 0.3±0.02A(rated), changed to 0.25 ~ 0.4A in OP-4.
PS6	Main cathode vaporizer	Current output is determined by PS3 voltage feedback. For Vd-Jcv characteristic, see fig. (b). (5KHz, AC constant current)	Current output is determined by vaporizer temperature feedback. (2±0.05A until main discharge ignition) (5KHz, AC constant current)
PS7	Neutralizer cathode heater	DC constant voltage: 5.4±0.05V(N.L.(nominal level)) 1.6±0.05V(I.L.(idling level)) (N.L.)5.2±8.05V in TV-2, 5 and 6; and (N.L.)5.8$^{+0.05}_{-0}$V in TV-7.	
PS8	Neutralizer keeper	At no load: DC constant voltage of 300±10V Power source output at load: see fig. (c)	At no load: DC constant voltage of 300±10V At load: DC constant current of 0.25±0.02A(rated), changed to 0.2~0.4A in OP-4.

(continued to next page)

PS9	Neutralizer vaporizer	Current output determined by PS8 voltage feedback. For Vnk-Jnv characteristic, see fig. (d). (5KHz, AC constant current)	Current output determined by vaporizer temperature feedback. (1.2±0.02A until neutralizer keeper discharge ignition) (5KHz, AC constant current)
PS10	Main cathode insulator	5KHz AC constant current: 1±0.05A	

(a) Main cathode keeper power source (PS5)

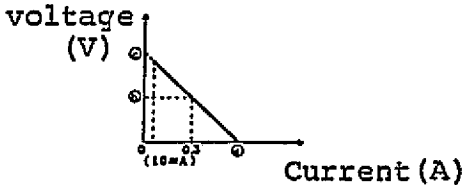

	①	②	③	
OP-2	0.62 ±0.02	16 ±0.5	31	
TV-2, 4,5,6	0.56 ±0.02	14 ±0.5	29	
TV-1, 7,8	0.64 ±0.02	17 ±0.5	32	

(b) Main cathode vaporizer power source (PS6)

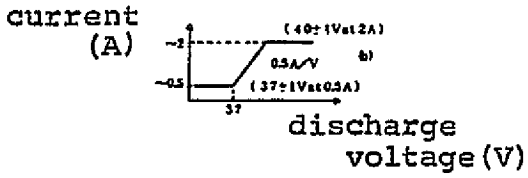

PS6 (M,L) until main discharge ignition:

OP-2: 2.0±0.05A
TV-2, ①, ④, ⑤, ⑥
: 1.96±0.05A
TV-7, ⑧: 2.35±0.05A

(c) Neutralizer keeper power source (PS8)

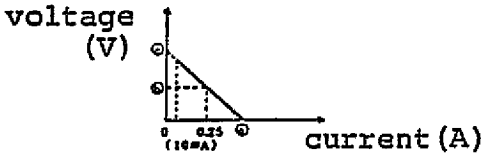

	①	②	③	
OP-2	0.62 ±0.02	27 ±0.5	51	
TV-2, 4,5,6	0.48 ±0.02	23.5 ±0.5	47.5	
TV-7,8	0.56 ±0.02	28 ±0.5	56	

(d) Neutralizer vaporizer power source (PS9)

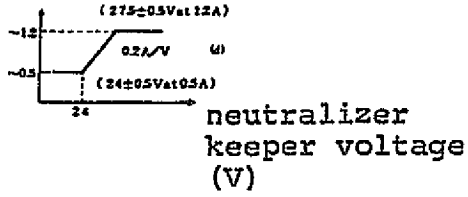

PS9 (M,L) until neutralizer keeper discharge ignition:

OP-2: 1.2±0.02A
TV-2, ①, ④, ⑤, ⑥
: 1.16±0.02A
TV-7, ⑧: 1.3±0.02A

Fig. 5.4(a) IEE FM(1) Discharge Ignition Characteristics

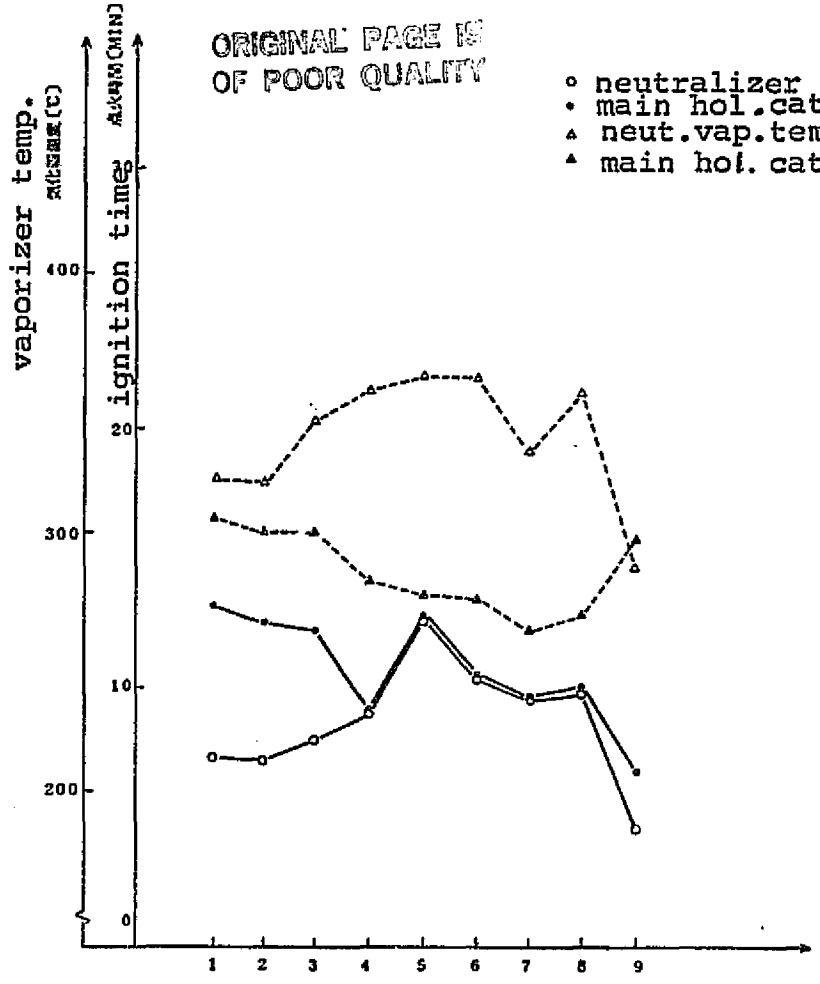

	Test subject	rated operation	interface check	rated operation	interface check	parameter change	low temperature motion start (1)	" (2)	" (3)	high temperature motion start
Idling time	IDLING時間(H)	105	60	105	60	1	60	60	60	60
	Vak (V)	54	54	54	54	52	52	52	52	58
	Jnv (A)	12	12	12	12	12	1.16	1.16	1.16	1.30
	Jcv (A)	20	20	20	20	20	1.96	1.96	196	215
Power at ignition	点火時パワー Pnk(W)	248	248	245	245	245	244	245	243	244
	Pnk(W)	270	270	271	270	254	254	254	253	307

Fig. 5.4(b) IEE FM(2) Discharge Ignition Characteristics

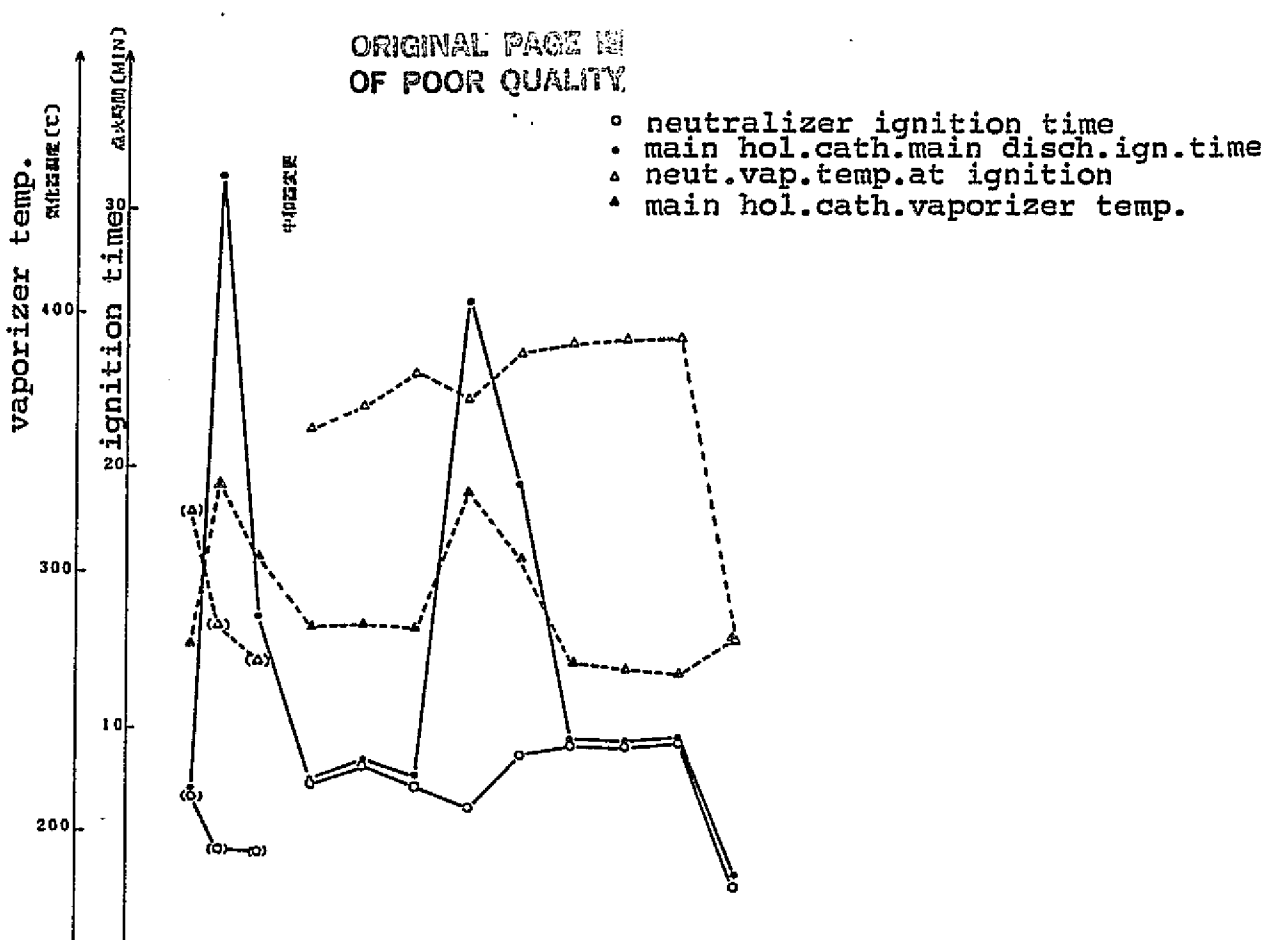

Test subject		rated operation	interface check	rated operation	interface check	rated operation	interface check	parameter change	low temperature motion start (1)	" (2)	" (3)	high temperature motion start
Idling time	IDLING RPM (H)	105/60	60	105	60	105	1	60	60	60	60	60
	Vah (V)	5.4/ 5.4	5.4	5.4	5.4	5.4	5.4	5.2	5.2	5.2	5.2	5.8
	Jnv (A)	1.2/ 1.2	1.2	1.2	1.2	1.2	1.2	1.2	1.16	1.16	1.16	1.30
	Jcv (A)	2.0/ 2.0	2.0	2.0	2.0	2.0	2.0	2.0	1.96	1.96	1.96	2.15
Ignition time	点火時間 Peh (W)	25.0/27.2	25.1	25.1	25.2	25.1	24.8	25.1	25.1	25.2	25.2	25.1
	Pnh (W)	27.3/27.3	27.3	25.9	25.8	25.9	25.9	24.4	24.3	24.3	24.2	29.1

Fig. 5.5(a) Operating Conditions(Interface Check, IEE #1)

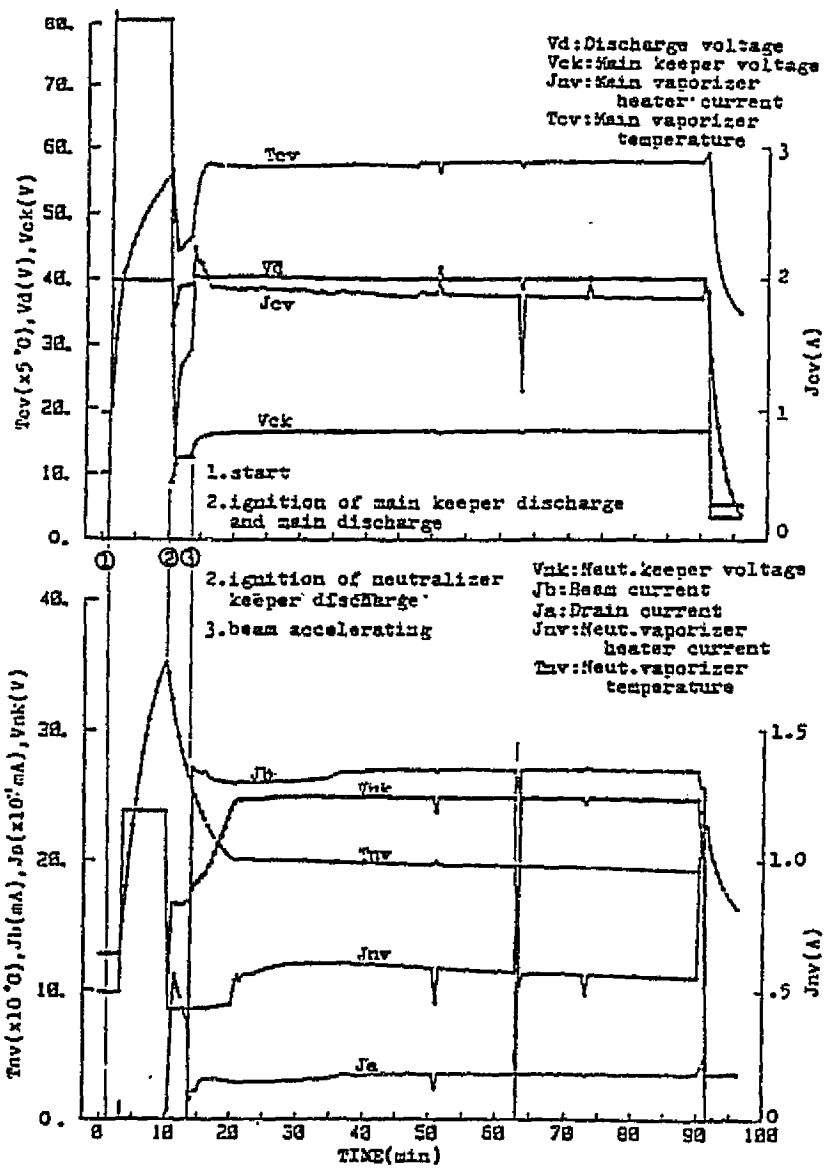

Fig. 5.5(b) Operating Conditions(Interface Check, IEE #2)

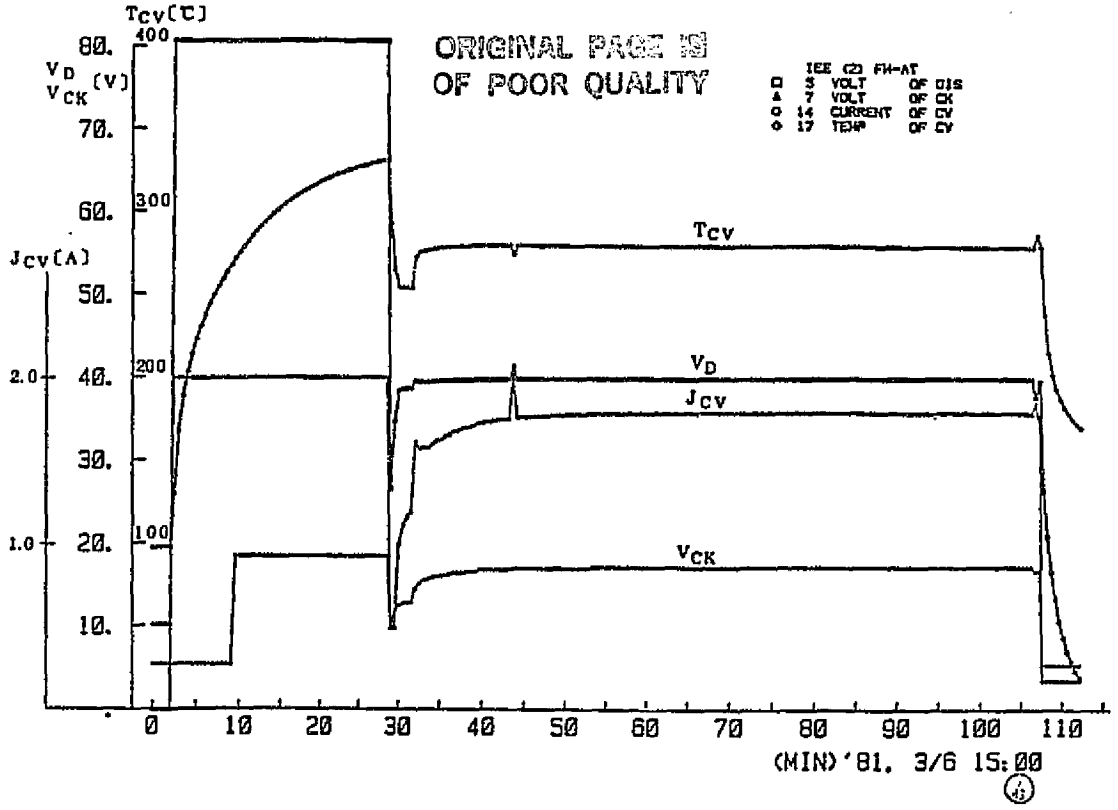

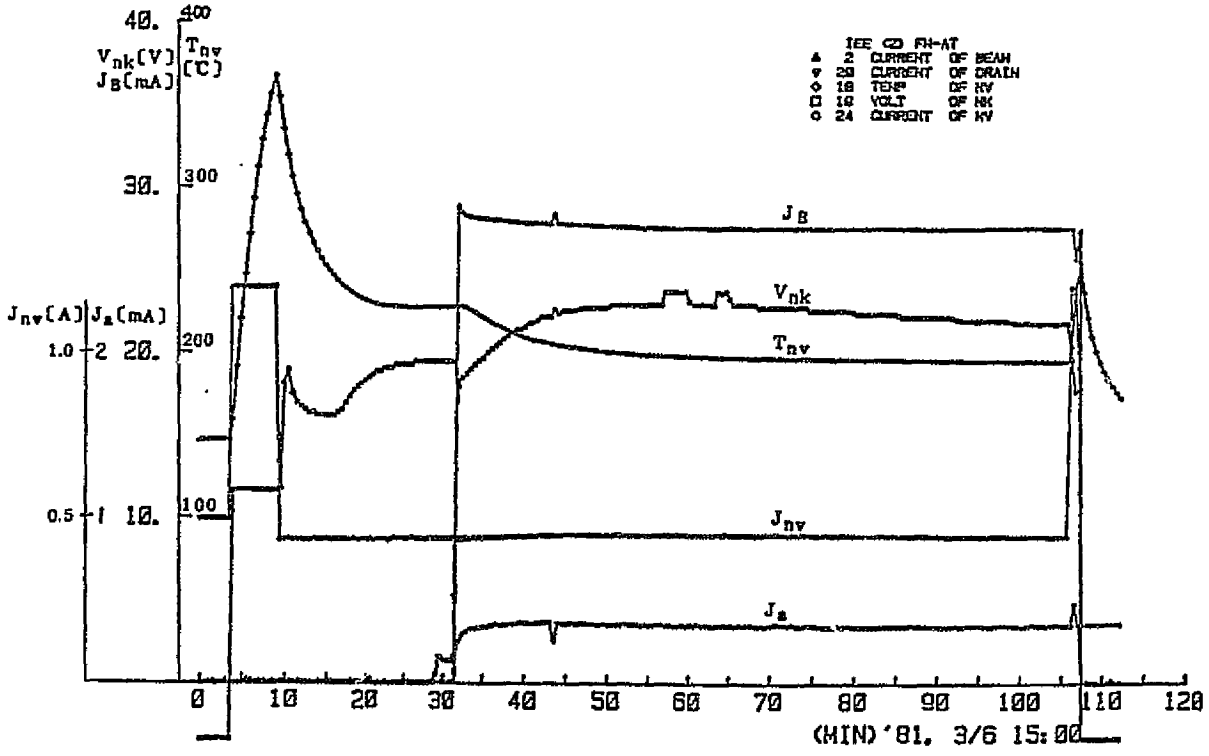

Table 5.10 Engine Unit Characteristics and Performance Values(FM)

	Parameter		Unit	Test subject: #1: rated operation test	interface check	low temperature motion start (3)	high temperature motion start	#2: rated operation test	interface check	low temperature motion start (3)	high temperature motion start
Electrical parameter and vaporizer temperature	Beam	Volt	KV	0.99	0.99	0.99	0.99	0.99	0.99	0.99	0.99
		Curr	mA	25.1	27.0	25.2	27.1	27.6	27.5	26.2	27.8
	Accel	Volt	KV	−1.00	−1.00	−1.00	−1.00	−1.00	−1.00	−1.00	−1.00
		Curr	mA	0.43	0.344	0.262	0.327	0.353	0.309	0.330	0.319
	Discharge	Volt	V	38.2	39.9	40.2	39.8	39.6	39.9	40.0	39.8
		Curr	A	0.35	0.35	0.35	0.35	0.35	0.35	0.35	0.35
	Cath Heater	Volt	V	/	/	/	/	/	/	/	/
		Curr	A	/	/	/	/	/	/	/	/
	Cath Keeper	Volt	V	16.7	16.6	17.0	16.2	17.2	1.71	17.9	17.0
		Curr	A	0.30	0.288	0.236	0.317	0.298	0.274	0.215	0.300
	Cath Vaporizer	Volt	V	3.04	3.00	3.03	2.84	2.86	2.89	3.00	2.83
		Curr	A	1.88	1.85	1.87	1.79	1.76	1.78	1.85	1.75
	Neut Heater	Volt	V	/	/	/	/	/	/	/	/
		Curr	A	/	/	/	/	/	/	/	/
	Neut Keeper	Volt	V	21.4	24.8	25.2	23.4	19.9	21.8	24.7	18.1
		Curr	A	0.244	0.276	0.236	0.331	0.245	0.310	0.241	0.387
	Neut Vaporizer	Volt	V	1.65	0.96	1.09	0.76	1.48	0.77	0.90	0.74
		Curr	A	0.96	0.55	0.64	0.45	0.85	0.44	0.52	0.43
	Isolator	Volt	V	27.3	27.1	27.2	27.4	28.1	27.6	27.7	27.5
		Curr	A	0.99	0.99	0.99	0.99	0.99	0.99	0.99	0.99
	Main Vap Temp		℃	29.5	29.0	28.2	28.6	28.1	27.9	27.5	27.6
	Neut Vap Temp		℃	25.3	19.4	20.1	18.2	24.5	19.5	20.2	18.6
	Engine Potential		V	−14.2	−10.7	−12.1	−9.34	−13.0	−7.7	−9.9	−6.6
	Target Potential		V	1.11	1.86	1.97	1.78	0.93	1.45	1.90	1.15
Performance parameter	Hg flowrate(Main)		$\times 10^{-1}$ g/min	8.99	7.76	6.26	7.36	9.06	8.64	7.82	8.04
	" (Neut)		$\times 10^{-2}$ g/min	1.01	0.19	0.23	0.13	1.04	0.29	0.35	0.23
	Thrust		g重	0.165	0.177	0.165	0.176	0.181	0.180	0.172	0.182
	Specific I		秒	1826	2277	2630	2407	1988	2080	2191	2260
	Prop Utilization Eff		%	58	72	64	77	63	66	70	72
	Total Power		W	589	615	583	621	606	612	588	619
	Power Eff		%	422	435	426	432	451	445	441	445
Date data acquired				'81.11.12 14:15'37"	'81.11.28 17:51'41"	'81.11.31 1 :32'.9"	'81.11.31 10:47'42"	'81.12.2 13:19'04"	'81.12.6 17:38'00"	'81.12.10 15:53'17"	'81.12.11 0:39'01"

Fig. 5.6 Points of Action of Main Discharge With Vd-Icv Closed Loop Under Control

Fig. 5.7 Points of Action of Neutralizer Keeper Discharge with Vnk-Inv Closed Loop Under Control

1. Interface check
2. "
3. Low temp. motion start test(1)
4. Transient action test(1)
5. High temp. motion heat balance
6. Low temp. motion start test(2)
7. " (3)
8. High temp. motion start test
9. Transient action test(2)

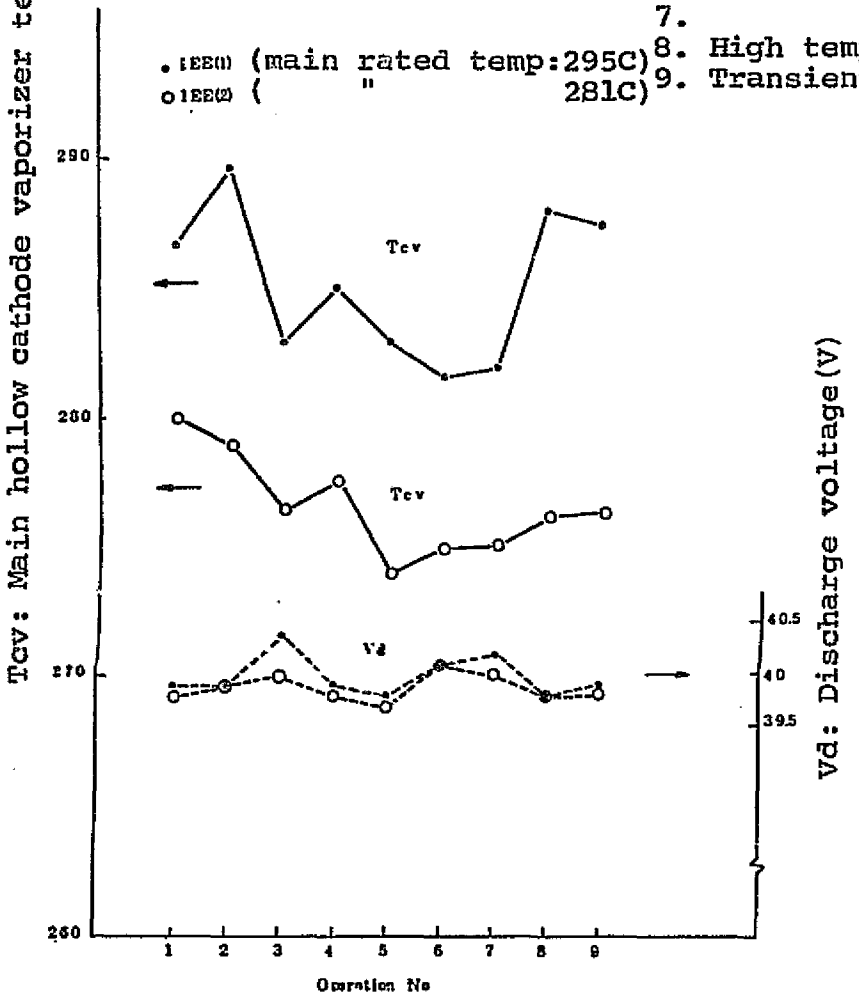

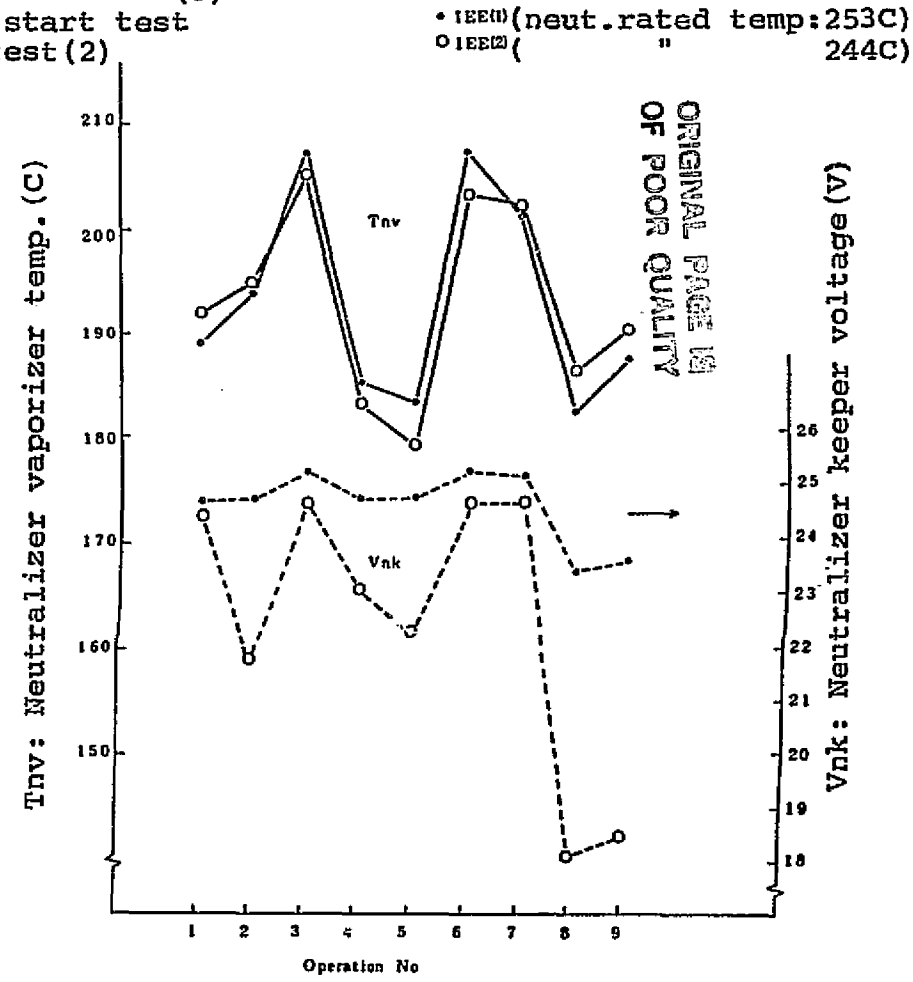

Fig. 5.8a Changes in IEE(1) Discharge Current

Fig. 5.8b Changes in IEE(2) Discharge Current

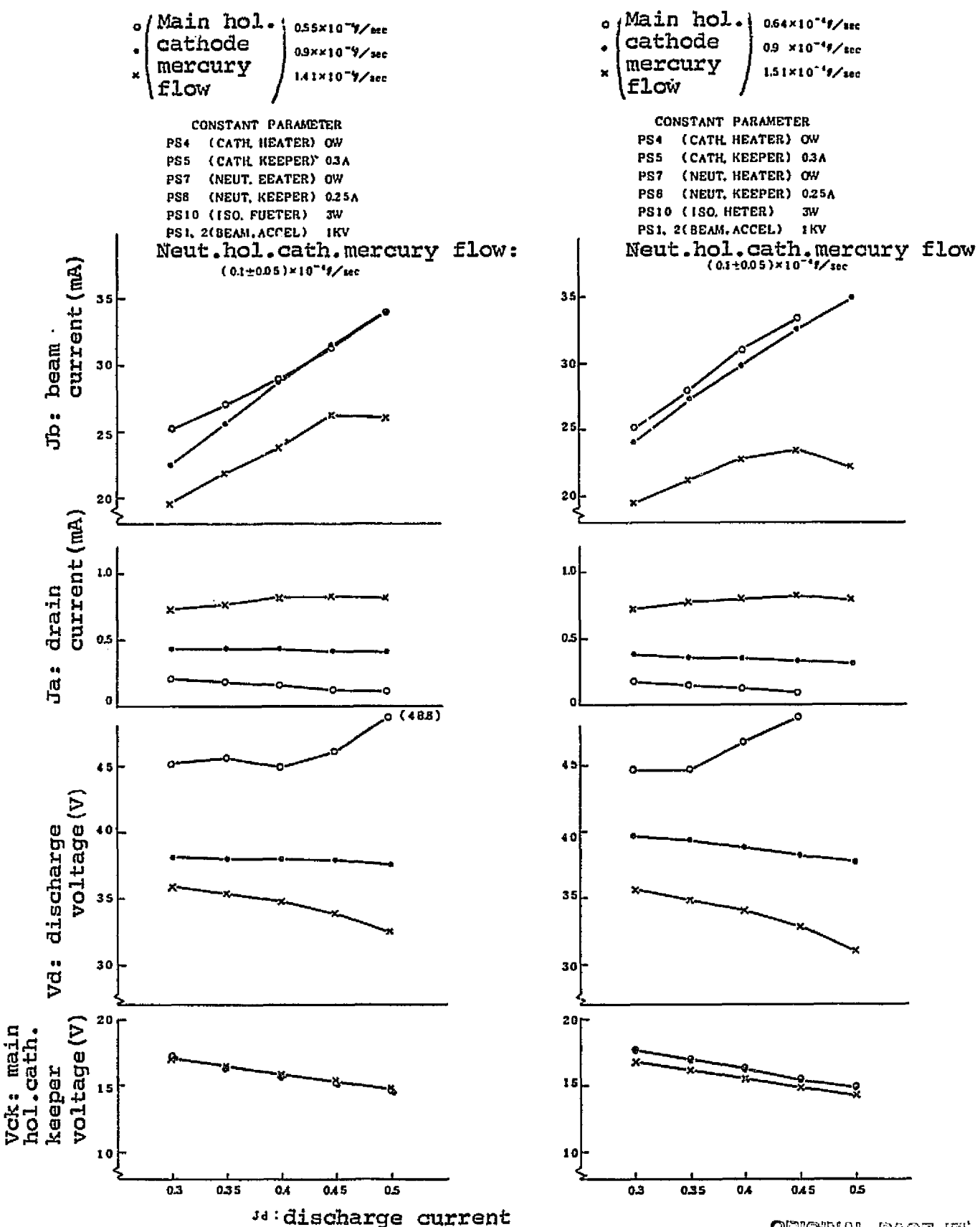

Fig. 5.9 Neutralizer Keeper Discharge Current/Voltage Characteristics

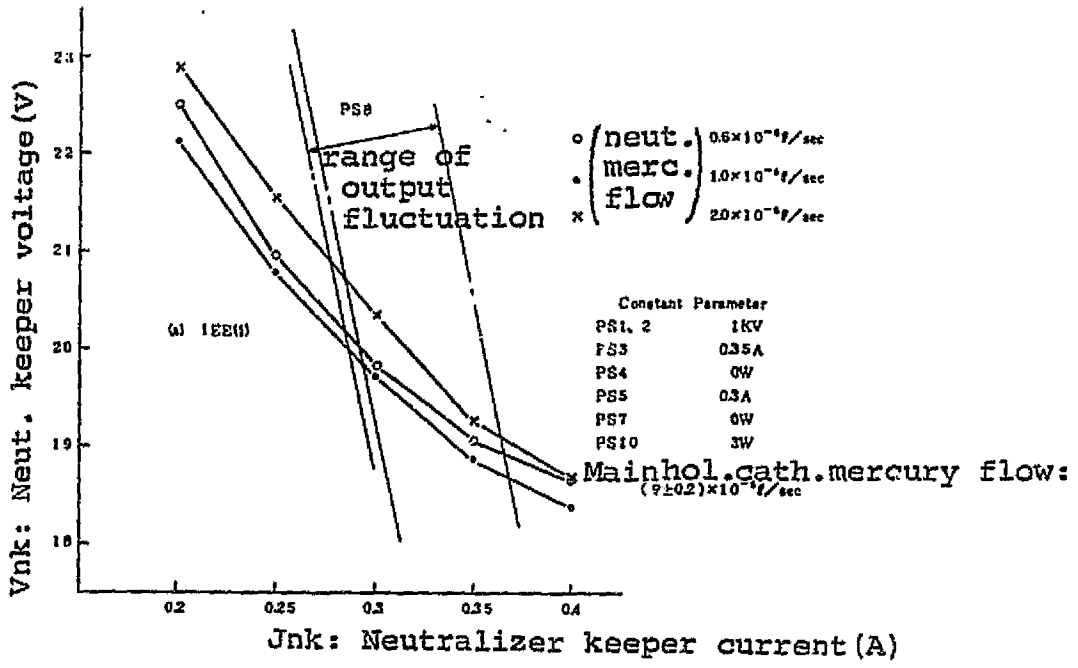

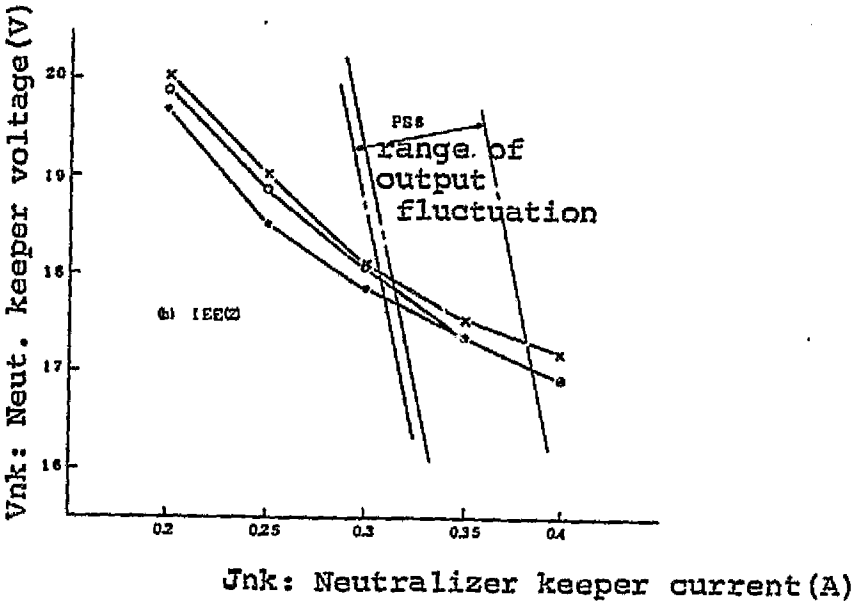

Table 5.11 Mass Characteristics and Remanence Moment of Engine Unit

	Unit No.1	Unit No.2	Specification
Weight (g)	2561.5	2580.0	≦3000以下
dry wt.	1963.0	1980.0	≦2400以下
mercury wt.	598.5	600.0	600±60
Center of gravity(mm)			
X	2.1	−0.6	
Y	8.3	8.0	
Z	14.5	16.2	
Remanence moment (μWb·m)	3.39	3.42	≦4.0以下

Fig. 5.10 Engine Unit(FM)

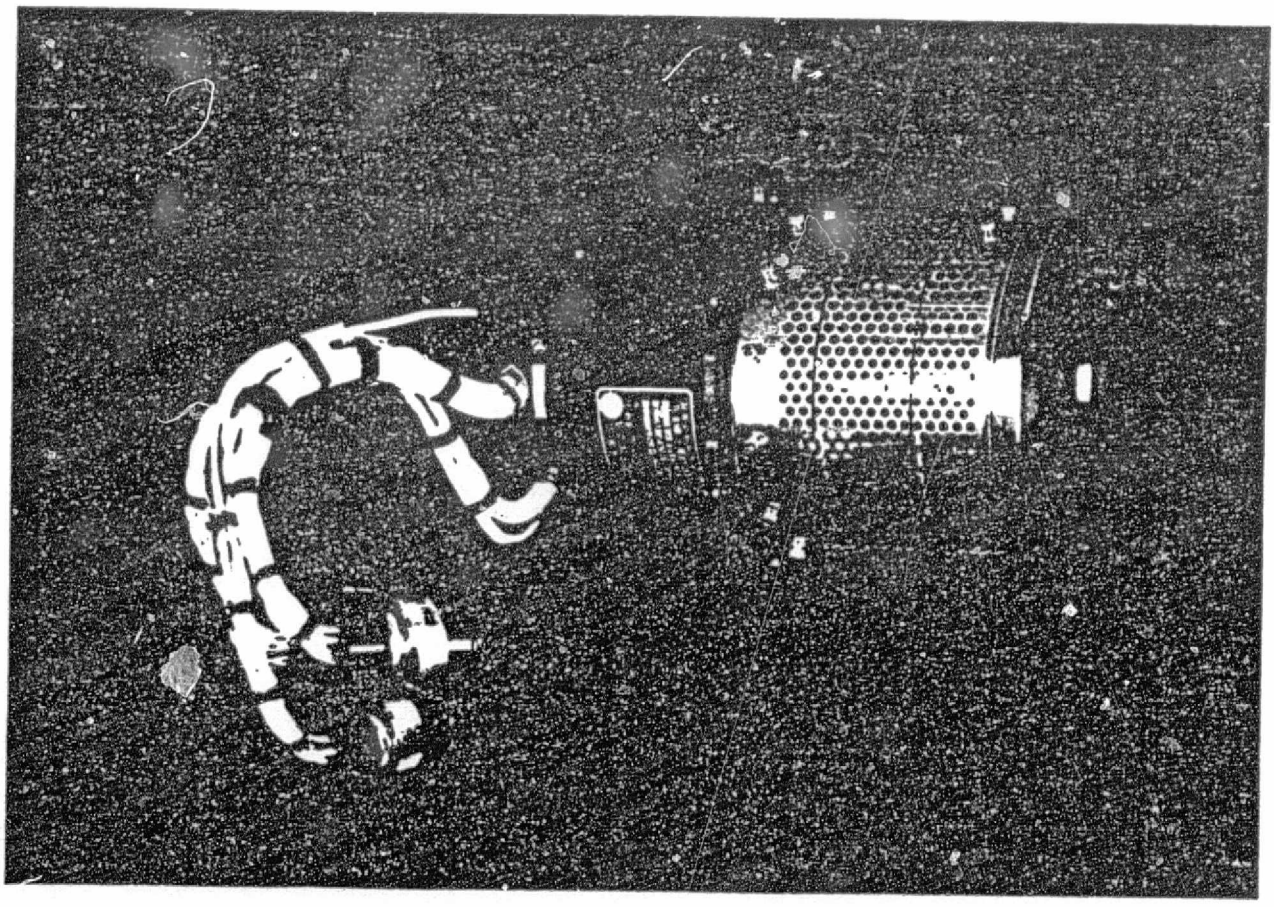

5.3.2 Power Conditioner Acceptance Tests

Problems at QT level in IES and the consequent review of conditions for power source interface with IEE were reflected in the FM of power conditioner: adjusted resistance of PS7 and PS8 were changed to increase output. With no problem observed, the FM was shown to satisfy the specifications. Following is the summary of electrical performance evaluation, weight, etc.

(1) Electrical performance

i) Power source output

For each output of power source, specification and production results are shown in Table 5.12. Output obtained satisfied IEE-interface conditions. Of the unstable power sources, output fluctuations of PS5, PS7 and PS8 are shown in Fig. 5.11 and Fig. 5.12. Measured values of output stability(regulation), ripple and transient response property, all of which completely satisfied the specifications, are shown in Table 5.13. With PS1, PS2, PS3 and PS6, particularly, there was sufficient regulation or ripple for possible future simplification of circuits.

ii) Set constant

Set values of control constant of each power source are shown in Table 5.14. Although smaller time constants are preferrable in dielectric breakdown protective logic, they fluctuate widely due to discharge characteristics of engine(especially discharge current waveform) which are difficult to control. Thus, larger values were set.

iii) Power consumption and efficiency

Power consumptions of power source control device and power source device are shown in Table 5.15(a). For power source device, converted values assuming the engine was under rated load(68W) are listed. Due to the test configuration, efficiency of each power source module in the power source device was not measured, but the overall conversion efficiency was about 75%.

(2) Weight

Shown in Table 5.15(b).

(3) Appearance

Shapes and sizes are as specified(see Fig. 4.4 and Fig. 4.7). Fig. 5.13 shows appearances of power source control device and power source device.

Fig. 5.11 Output Fluctuation of Keeper Power Source

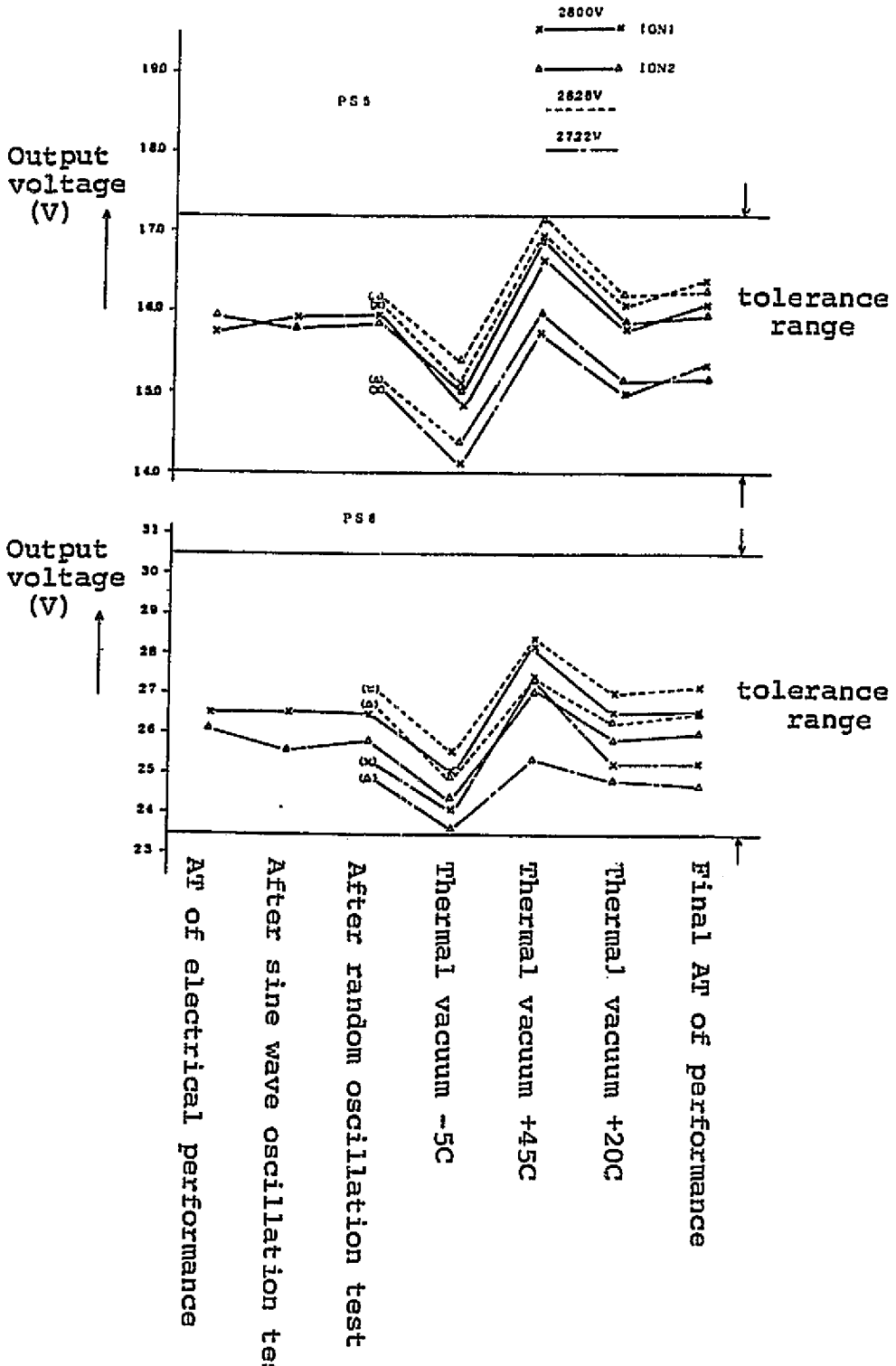

Fig. 5.12 Output Fluctuation of Neutralizer Heater Power Source

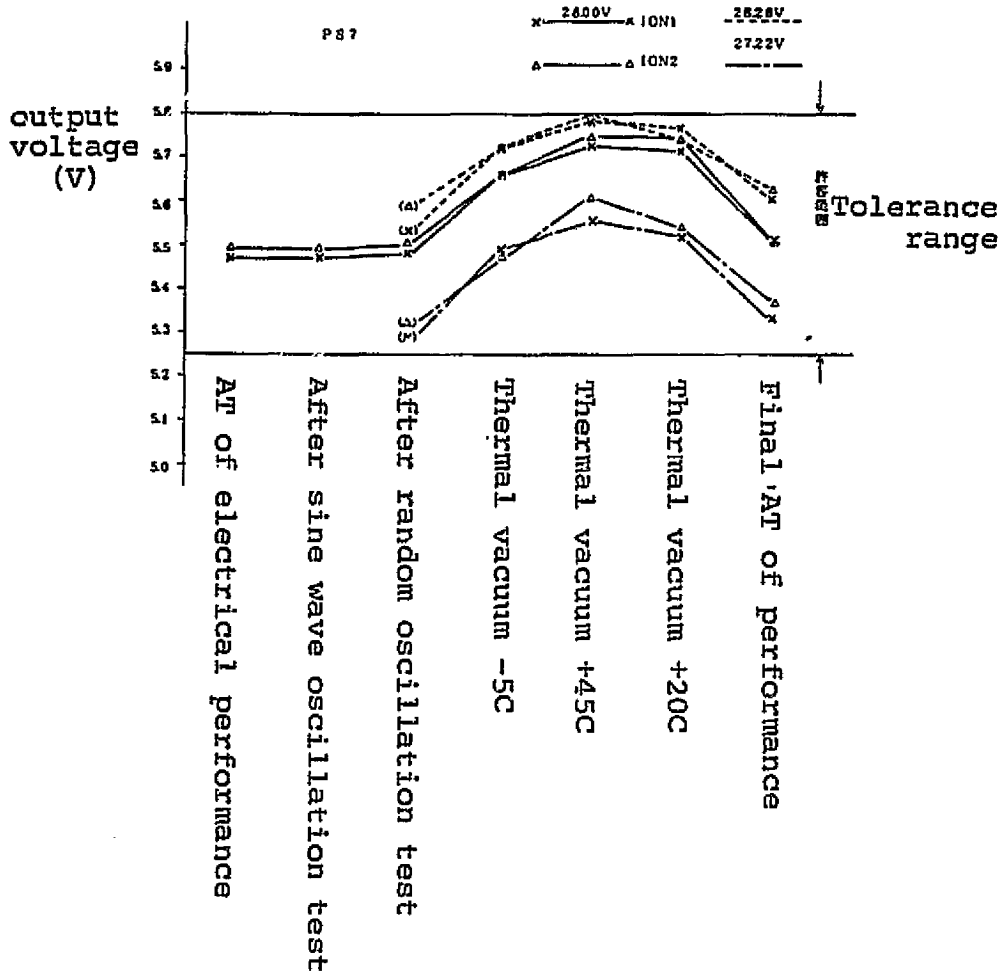

Table 5.13 Measured Values of Output Stability, Ripple And Transient Response

	Output stability (%)	Ripple (%)	Transient response
PS 1	0.6 / 0.6	0.7 / 0.6	20 / 20ms
PS 2	–	0.2 / 0.2	5 / 4 ms
PS 3	0.3 / 0.3	0.4 / 0.4	7 / 7 ms
PS 4	–	–	–
PS 5	–	22 / 24	23 / 26 μs
PS 6	1.0 / 0.5	–	–
PS 7	–	–	–
PS 8	–	21 / 23	1.2 / 1.3 μs
PS 9	3.2 / 24	–	–
PS10	–	–	–

Note) Unit No.1/No.2

Table 5.12 Output Fluctuation of Power Source Device

Power source		Level	Output condition *	Load condition	Results IEP #1		IEP #2	
PS 1	Beam	N.L	1000 ± 40V	30mA±2%	1000V*	1000V**	1000V*	1000V**
PS 2	Accelerator	N.L	1000^{+25}_{-65}V	1mA±2%	972~976V	975V	970~980V	980V
PS 3	Discharge	N.L	0.35 ± 0.01A	40V±2%	0.343~0.350A	0.350A	0.348~0.350A	0.350A
PS 4	Main cath.heater	I.L	1.6 ± 0.6V	$2.5A^{+0}_{-40}$%	1.46~2.19V	1.86V	1.28~1.97V	1.71V
		N.L	$5.0^{+0.55}_{-0.3}$V	5A±10%	4.92~5.50V	5.28V	4.98~5.46V	5.32V
		H.L	$6.0^{+0.3}_{-0.7}$ V	6A±10%	5.63~6.11V	5.95V	5.69~6.15V	5.98V
PS 5	Main cath.keeper	N.L	$15^{+22}_{-1.0}$ V	0.3A±5%	14.0~16.6V	15.7V	14.3~16.9V	15.9V
PS 6	Main cath. vaporizer	L.L	$0.5^{+0.04}_{-0.1}$A	0.8PV±10%	0.48~0.50A	0.50A	0.48~0.49A	0.49A
		H.L	$2.0^{+0.16}_{-0.04}$A	3.5V±5%	2.07~2.13A	2.10A	2.10~2.17A	2.13A
PS 7	Neutralizer heater	I.L	$1.6^{+0.3}_{-0.4}$ V	$2.5A^{+0}_{-30}$%	1.48~1.85V	1.71V	1.46~1.84V	1.65V
		N.L	$5.0^{+0.8}_{-0.25}$V	5.5A±10%	5.29~5.73V	5.71V	5.32~5.75V	5.74V
PS 8	Neutralizer keeper	N.L	$24^{+6.5}_{-0.3}$ V	0.25A±5%	24.1~28.2V	26.5V	25.5~27.0V	25.9V
PS 9	Neut. vaporizer	L.L	0.5 ± 0.05A	0.88V±10%	0.52~0.54A	0.53A	0.49~0.51A	0.50A
		H.L	$1.2^{+0.10}_{-0.04}$A	2.1V±10%	1.25~1.26A		1.24~1.25A	
PS10	Insulator heater	N.L	$3.0^{+0.5}_{-0.19}$V	1.0A±10%	3.10~3.34V	3.29V	3.08~3.36V	3.28V
		H.L	$5.0^{+0.09}_{-0.61}$V	1.6A±10%	4.71~5.06V	5.05V	4.66~5.02V	4.97V

* Range of output fluctuation at input voltage range of 27.22~28.00V and temperature range of 5~45C(base plate temp in vacuum).

** Input voltage 28.00V and base plate temperature 20C(in vacuum).

Fig. 5.13 Power Conditioner(FM)

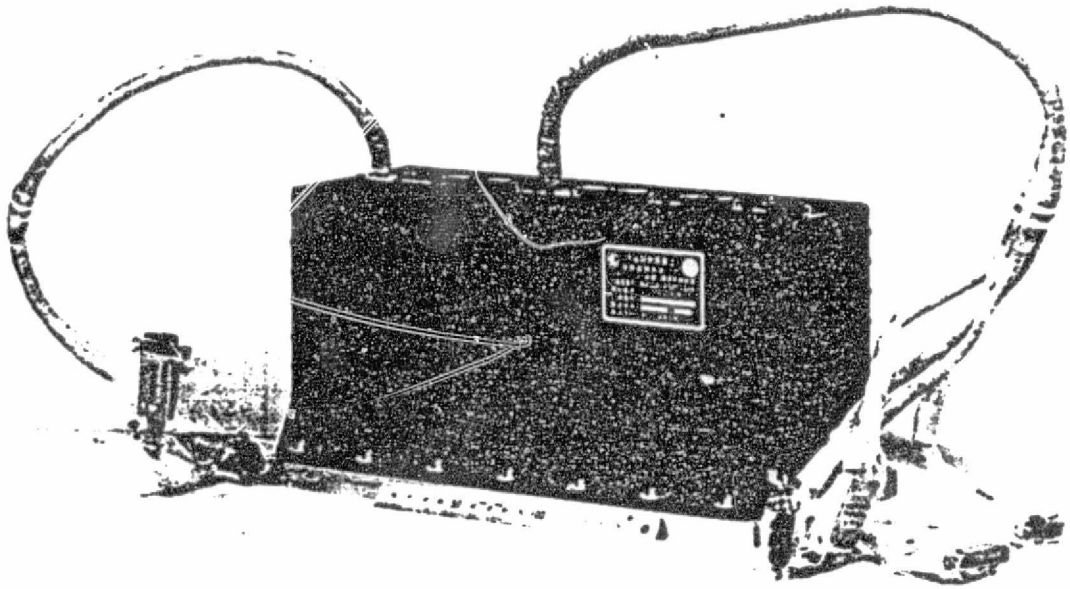

Power Source Control Device

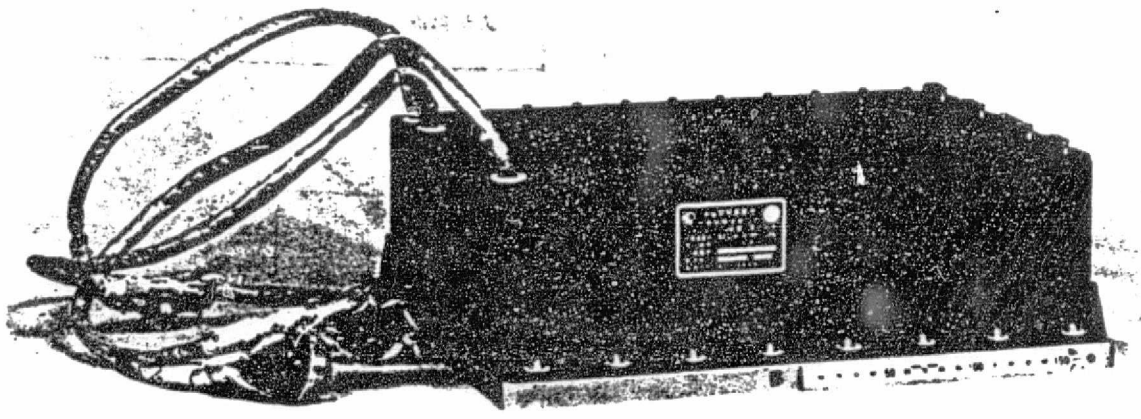

Power source device

5.3.3 Ion Engine System Acceptance Tests

Performances of ion engine system - the combination of engine unit and power conditioner - were already determined by the Sub-system Acceptance Tests. This time, objectives were set to check the compatibility of engine and power conditioner and to obtain basic data for experimenting in space. Results of function/performance tests (hollow cathode test and varied parameter test) and thermal vacuum test, performed to meet these objectives, are given in Table 5.15 and Table 5.17. Based on the data, the performances were evaluated as follows.

(1) Hollow cathode characteristics

Compared to AT, ignition characteristics of main hollow cathode were not satisfactory. Especially in No. 1, it did not ignite after 20 minutes, requiring high-level output from the heater power source (PS4). Pollution around the cathode from prior tests and repeated exposure to air seemed to be the cause. The hollow cathode was not replaced, however, as the deteriorated ignition property could be complemented by switching(by command) the output of PS4 to high level.

Ignition time of neutralizer hollow cathode was within 10 minutes, same as in the AT of engine unit.

As for decrease in keeper current - a sign of cathode deterioration - about 280mA was maintained overall, suggesting no problem. Also, it was determined to be compatible with keeper power sources (PS5 and PS9).

There was no problem with compatibility between the keeper voltage of neutralizer hollow cathode and flow control of power conditioner in Unit No. 1. With No. 2, control error, described in Sec. 5.3.1(4), occurred, but the flow, with the maximum steady state value of 7×10^{-5}g/s, was within the allowable range.

Above results indicate that the compatibility between the main and neutralizer hollow cathodes and power sources has been achieved.

(2) Beam injection characteristics

Beam injection characteristics were studied by testing with varied parameters. Data are summarized in Table 5.16. Fig. 5.14 shows the changes of main performance values in relation to set values of parameters(discharge current, discharge voltage and accelerated voltage). The figure shows that near the center of set values(Id=0.35A, Vd=40V and Vn=1.0kV) Unit No. 2 is superior in overall performance, to include thrust, specific impulse, power consumption, etc. In Unit No. 1, increase in thrust was large with respect to discharge voltage Vd, and reached the No. 2 level at Vd=44V. Fig. 5.15 shows the discharge power loss per ion beam, i.e. the cost of ion production. Comparison at the propellant utilization efficiency of about 70% showed that No. 1 was 550eV/ion against 500eV/ion of No. 2, indicating that the discharge power loss of No. 1 was 10% more. While No. 1 and No. 2 slightly differed in performances they both satisfied the required performance values.

Control property of discharge voltage during beam injection was satisfactory, with no fluctuation in beam current observed.

Compatibility with sequence control in power source control device was also satisfactory. Average starting time before reaching injection was 23 minutes for No. 1 and 19 minutes for No. 2. Discharge voltage transiently increased by about 5V when high voltage was thrown in, but in most cases returned to steady state in about 10 seconds. In starting under the worst conditions of 27.22V-bus voltage and base temperature of -5C, disappearance of main discharge, thought to be due to a delay in main vaporizer control, was observed. This was not

considered a problem, as it was a phenomenon particular to this case only and it recovered within several minutes by controlling the sequence.

Compatibility between the engine and power conditioner before and during beam injection was thus verified.

(3) Record of problems

Summary is given in Table A2.5 in Appendix.

Table 5.16(a) Beam Injection Operation Test Characteristics(Unit No.1)

Symbol	Name	Unit	Id parameter					Vd parameter			Vb parameter			
			0.30A	0.35A	0.40A	0.45A	0.50A	35V	40V	45V	0.8KV	1.0KV	1.2KV	1.4KV
			6/9 13:11	6/9 13:23	6/9 13:34	6/9 13:45	6/9 13:54	6/9 14:04	6/9 14:13	6/9 14:22	6/9 14:31	6/9 14:34	6/9 14:38	6/9 14:54
I_{IP}	入力 1	A	2.808	3.058	3.246	3.508	3.746	2.833	3.058	3.121	2.745	2.971	3.196	3.496
V_{IN}	入力 2	V	28.00	28.00	28.00	28.00	28.00	27.99	28.00	27.99	28.00	28.00	28.01	28.00
Vb	ビーム 3	KV	1.01	1.01	1.01	1.01	1.02	1.01	1.01	1.01	0.804	1.01	1.22	1.41
Ib	ビーム 4	mA	20.9	25.0	29.3	33.1	36.0	19.9	25.0	27.7	23.5	24.7	25.7	26.2
Ia	アクセラ 5	mA	0.353	0.323	0.323	0.313	0.294	0.589	0.323	0.235	0.323	0.333	0.333	0.323
Vd	放電 6	V	40.0	40.3	40.3	40.3	40.3	35.2	40.1	45.1	40.3	40.2	40.1	40.0
Id	放電 7	A	0.300	0.350	0.403	0.450	0.504	0.349	0.350	0.349	0.350	0.353	0.348	0.356
Ick	主陰極中 8	A	0.208	0.246	0.265	0.286	0.303	0.269	0.248	0.218	0.240	0.248	0.239	0.243
Icv	主陰極気 9	A	1.75	1.73	1.71	1.70	1.69	1.81	1.68	1.65	1.78	1.67	1.73	1.72
Tcv	主陰極気 10	℃	295	293	295	295	295	310	293	287	290	291	291	293
Ink	中和器中 11	A	0.285	0.287	0.285	0.285	0.285	0.287	0.286	0.287	0.287	0.286	0.287	0.281
Inv	中和器気 12	A	0.643	0.653	0.653	0.653	0.653	0.632	0.642	0.653	0.642	0.653	0.653	0.674
Tnv	中和器気 13	℃	228	231	231	235	235	231	233	229	231	235	235	233
Ths	ヒートシ 14	℃	24	24	24	24.5	24.5	24.5	24.5	24.5	24.5	24.5	24.5	25
T_{BP}	ベース板 15	℃	26	26	26	26	26	26	26	26	26	26	26	26
T_E	エンジン 16	℃	91	91	92	93	94	95	95	94	94	93	93	93
T_{TANK}	水槽タン 17	℃	60	60	60	60	60	61	61	61	61	61	61	61
V_{CH}	真空 18	Torr	8.9×10^{-7}	8.9×10^{-7}	9.5×10^{-7}	9.6×10^{-7}	9.8×10^{-7}	8.0×10^{-7}	8.0×10^{-7}	8.0×10^{-7}	7.0×10^{-7}	7.7×10^{-7}	8.3×10^{-7}	9.0×10^{-7}
Tsh	シュラウド 19	℃	-177	-177	-177	-177	-177	-177	-177	-177	-177	-177	-177	-177
T_{PB}	電力制御ベース 20	℃	21	21	21	21	21	21	21	21	21	21	21	21
T_{PE}	エンジンベース 21	℃	21	21	21	21	21	21	21	21	21	21	21	21
F	推力 22	gr重	0.136	0.165	0.194	0.218	0.239	0.131	0.165	0.183	0.138	0.163	0.187	0.205

Table 5.16(b) Beam Injection Operation Test Characteristics(Unit No.2)

略号	名称	単位	Idパラメータ					Vdパラメータ			Vbパラメータ			
			0.30A	0.35A	0.40A	0.45A	0.50A	35V	40V	45V	0.8KV	1.0KV	1.2KV	1.4KV
			6/19 12:22	6/19 12:34	6/19 12:44	6/19 12:55	6/19 13:00	6/19 13:15	6/19 13:26	6/19 13:36	6/19 13:46	6/19 13:55	6/19 14:03	6/19 14:12
I_{IP}	入力 1	A	2.91	3.18	3.42	3.62	3.77	3.01	3.20	3.22	2.90	3.20	3.52	3.82
V_{IN}	入力 2	V	27.99	28.00	28.01	28.00	28.00	28.00	28.00	28.00	28.00	27.99	28.00	28.01
Vb	ビーム 3	KV	1.00	1.00	1.00	1.00	1.00	1.00	1.00	1.00	0.800	1.00	1.20	1.41
Ib	ビーム 4	mA	23.4	27.5	31.8	34.0	36.1	23.6	28.2	28.2	26.8	28.1	29.5	30.6
Ia	アクセラ 5	mA	0.348	0.287	0.257	0.216	0.186	0.612	0.308	0.155	0.308	0.297	0.308	0.308
Vd	放電 6	V	40.1	40.2	40.1	40.1	40.0	35.1	40.0	45.0	40.0	40.1	40.1	40.2
Id	放電 7	A	0.305	0.351	0.402	0.450	0.501	0.352	0.352	0.352	0.352	0.351	0.352	0.352
Ick	主陰極中 8	A	0.233	0.279	0.313	0.345	0.367	0.318	0.288	0.291	0.287	0.285	0.285	0.282
Icv	主陰極気 9	A	1.75	1.71	1.69	1.65	1.63	1.80	1.65	1.55	1.68	1.66	1.70	1.68
Tcv	主陰極気 10	℃	285	281	281	280	280	300	282	274	281	282	281	283
Ink	中和器中 11	A	0.276	0.275	0.280	0.281	0.284	0.289	0.289	0.286	0.288	0.289	0.286	0.287
Inv	中和器気 12	A	0.521	0.500	0.500	0.490	0.490	0.490	0.490	0.490	0.490	0.490	0.490	0.490
Tnv	中和器気 13	℃	225	221	221	224	224	224	225	226	225	225	225	222
Ths	ヒートシ 14	℃	22	22.5	23	23.5	23.5	23.5	23.5	23.5	23.5	23.5	23.5	24.5
T_{BP}	ベース板 15	℃	25	25	25	25	25	25	25.5	25.5	25.5	25.5	25.5	25.5
T_E	エンジン 16	℃	72	74	76	77	79	80	79	79	79	79	78	78
T_{TANK}	水槽タン 17	℃	47	48	49	49.5	50.5	51	52	52	52	52	52	52
V_{CH}	真空 18	Torr	1.0×10^{-6}	1.0×10^{-6}	1.0×10^{-6}	1.0×10^{-6}	1.0×10^{-6}	7.8×10^{-7}	7.8×10^{-7}	7.0×10^{-7}	5.9×10^{-7}	6.7×10^{-7}	7.2×10^{-7}	7.6×10^{-7}
Tsh	シュラ	℃	-159	-159	-159	-159	-159	-159	-159	-159	-159	-159	-159	-159
T_{PB}	電力制ベー 2	℃	20	20	20	20	20	20	20	20	20	20	20	21
T_{PE}	エンジベー 2	℃	20	20	20	20	20	20	20	20	20	20	20	21
F	推 2	gr重	0.148	0.175	0.203	0.217	0.231	0.149	0.180	0.180	0.152	0.179	0.205	0.231

Table 5.17(a) Thermal Vacuum Test: Characteristics vs. Parameters in Rated Operation Test (No.1)

略号	名称	26V			26.22V	27.22V	28V
		+20℃	+45℃	−5℃	+45℃	−5℃	+20℃
		6/11 17:20	6/12 3:00	6/12 14:41	6/13 15:41	6/14 9:47	6/15 7:33
I_{IN}	入力1	3.06A	3.22A	3.03A	3.25A	3.05A	3.16A
V_{IN}	入力2	28.00V	28.00V	28.00V	28.23A	27.21V	28.00A
Vb	ビ3	1.01KV	1.01KV	1.01KV	1.01KV	1.01KV	1.01KV
Ib	ビ4	25.2mA	27.0mA	25.1mA	27.4mA	25.1mA	26.2mA
Ia	アク5	0.284mA	0.304mA	0.291mA	0.294mA	0.300mA	0.276mA
Vd	放6	40.3V	40.4V	40.0V	40.4V	40.3V	40.3A
Id	放7	0.346A	0.352A	0.351A	0.352A	0.353A	0.351A
Ick	主陰8	0.282A	0.321A	0.262A	0.347A	0.238A	0.313A
Icv	主陰9	1.75A	1.67A	1.79A	1.704A	1.86A	1.79A
Tcv	主陰10	289℃	293℃	289℃	292℃	290℃	290℃
Ink	中和11	0.282A	0.323A	0.258A	0.331A	0.237A	0.275A
Inv	中和12	0.684A	0.534A	0.818A	0.536A	0.858A	0.694A
Tnv	中和13	231℃	225℃	239℃	224℃	245℃	228℃
Tns	ヒ−14	23.5℃	47.5℃	0℃	47.5℃	−1.5℃	24.0℃
T_{BP}	ベ−15	26.0℃	48.0℃	4.0℃	48.5℃	2.5℃	24.0℃
T_E	エン16	85.0℃	100℃	29.0℃	96.0℃	89.0℃	79.0℃
T_{TANK}	水槽17	52.5℃	70.0℃	37.0℃	64.0℃	33.0℃	49.5℃
V_{CH}	真18	65×10⁻⁶Torr	15×10⁻⁶Torr	49×10⁻⁶Torr	15×10⁻⁶Torr	43×10⁻⁶Torr	43×10⁻⁶Torr
tn	中和23	6min	7min	6min	6min	9min	7min
tc	主陰24	20min(HL)	22min	21min(HL)	19min	22min(HL)	20min(HL)
T_{TS}	電力計ベ−20	21℃	45℃	−4℃	46℃	−5℃	20℃
T_{TE}	エンジベ−21	20℃	44℃	−4℃	46℃	−5℃	20℃
F	推22力	0.167gr重	0.176gr重	0.166gr重	0.181gr重	0.166gr重	0.173gr重

note) HL: PS4 high level

Table 5.17(b) Thermal Vacuum Test: Characteristics vs. Parameters in Rated Operation Test (No.2)

略号	名称	28V			28.22V	27.22V	28V
		+20℃	+45℃	−5℃	+45℃	−5℃	+20℃
		6/21 17:04	6/22 2:00	6/22 14:12	6/23 17:50	6/24 9:21	6/25 7:03
I_{IN}	入力1	3.20A	3.32A	3.17A	3.32A	3.12A	3.20A
V_{IN}	入力2	28.00V	28.01A	28.01V	28.22V	27.21V	28.00A
V_H	ビ3	1.00KV	1.00KV	1.00KV	1.00KV	1.00KV	1.00KV
J_B	ビ4	26.1mA	27.2mA	26.8mA	27.5mA	25.1mA	26.6mA
Ia	アク5	0.287mA	0.294mA	0.284mA	0.304mA	0.285mA	0.305mA
Vd	放6	40.1V	39.9V	40.4V	40.1V	40.5V	40.3V
Id	放7	0.351A	0.351A	0.351A	0.353A	0.353A	0.351A
Ick	主陰8	0.266A	0.298A	0.253A	0.310A	0.182A	0.272A
Icv	主陰9	1.75A	1.65A	1.78A	1.66A	1.86A	1.75A
Tcv	主陰10	280℃	282℃	279℃	282℃	287℃	280℃
Ink	中和11	0.276A	0.355A	0.274A	0.359A	0.240A	0.295A
Inv	中和12	0.498A	0.486A	0.567A	0.498A	0.587A	0.468A
Tnv	中和13	214℃	230℃	215℃	229℃	219℃	217℃
Tns	ヒ−14	22.0℃	47.0℃	−1.5℃	45.5℃	−1.5℃	22.5℃
T_{BP}	ベ−15	25.0℃	49.0℃	2.5℃	48.0℃	1.0℃	26.0℃
T_E	エン16	70.0℃	86.0℃	56.0℃	83.0℃	57.0℃	71.0℃
T_{TANK}	水槽17	44.5℃	63.0℃	28.0℃	59.5℃	28.0℃	46.0℃
V_{CH}	真18	50×10⁻⁶Torr	90×10⁻⁶Torr	43×10⁻⁶Torr	10×10⁻⁶Torr	33×10⁻⁶Torr	34×10⁻⁶Torr
tn	中和23	7min	7min	6min	6min	13min	8min
tc	主陰24	11min	15min	22min(HL)	9min	20min(HL)	21min
T_{TS}	電力計ベ−20	20℃	45℃	−5℃	45℃	−5℃	20℃
T_{TE}	エンジベ−21	20℃	45℃	−5℃	45℃	−5℃	20℃
F	推22力	0.172gr重	0.179gr重	0.176gr重	0.181gr重	0.165gr重	0.175gr重

Symbols for Tables 5.16 and 5.17

1. Input current
2. Input voltage
3. Beam voltage
4. Beam current
5. Accelerator current
6. Discharge voltage
7. Discharge current
8. Main cathode keeper current
9. Main cathode vaporizer current
10. Main cathode vaporizer temperature
11. Nuetralizer keeper current
12. Neutralizer vaporizer current
13. Neutralizer vaporizer temperature
14. Heat sink temperature
15. Base plate temperature
16. Engine unit temperature
17. Mercury tank temperature
18. Degree of vacuum
19. Shround temperature
20. Power conditioner base plate temperature
21. Engine unit base plate temperature
22. Thrust
23. Neutralizer ignition time
24. Main cathode ignition time

Fig. 5.14 Beam Injection Characteristics, (a) IES #1 and (b) IES #2

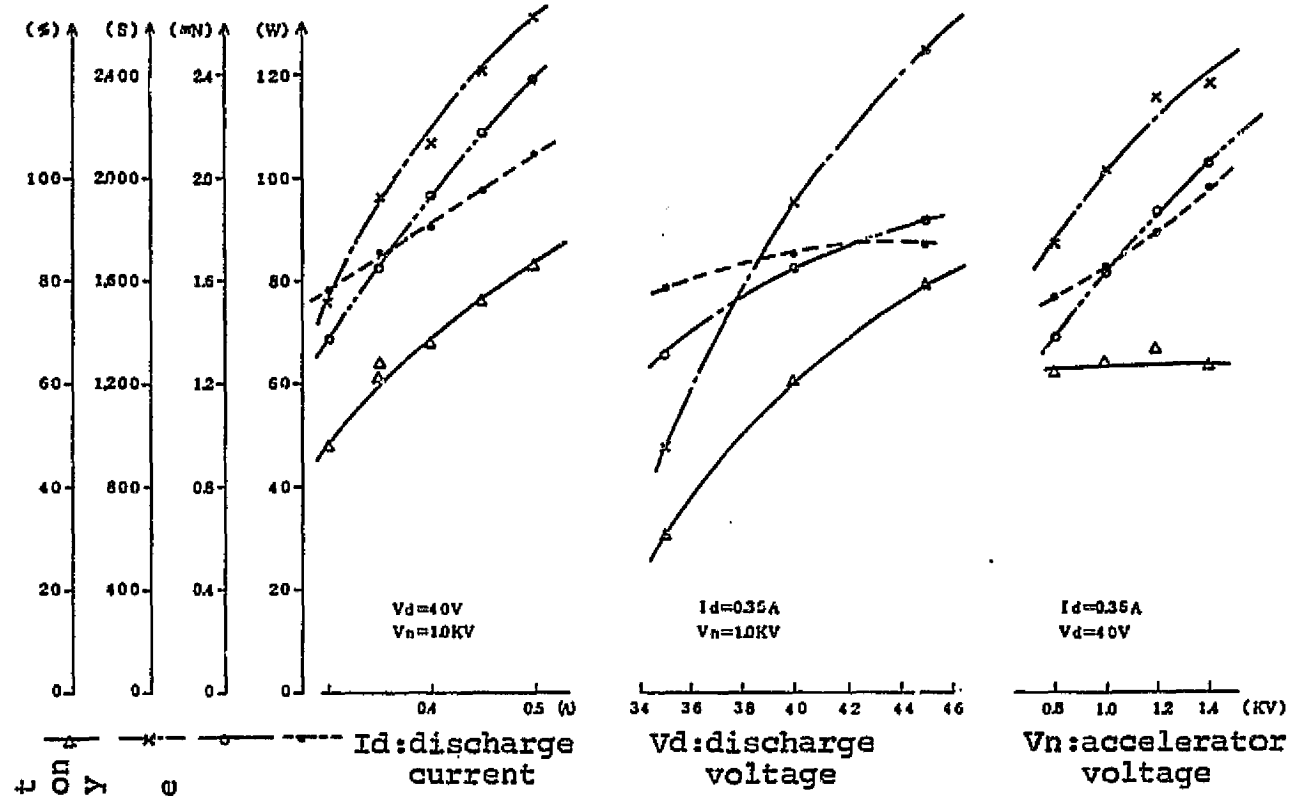

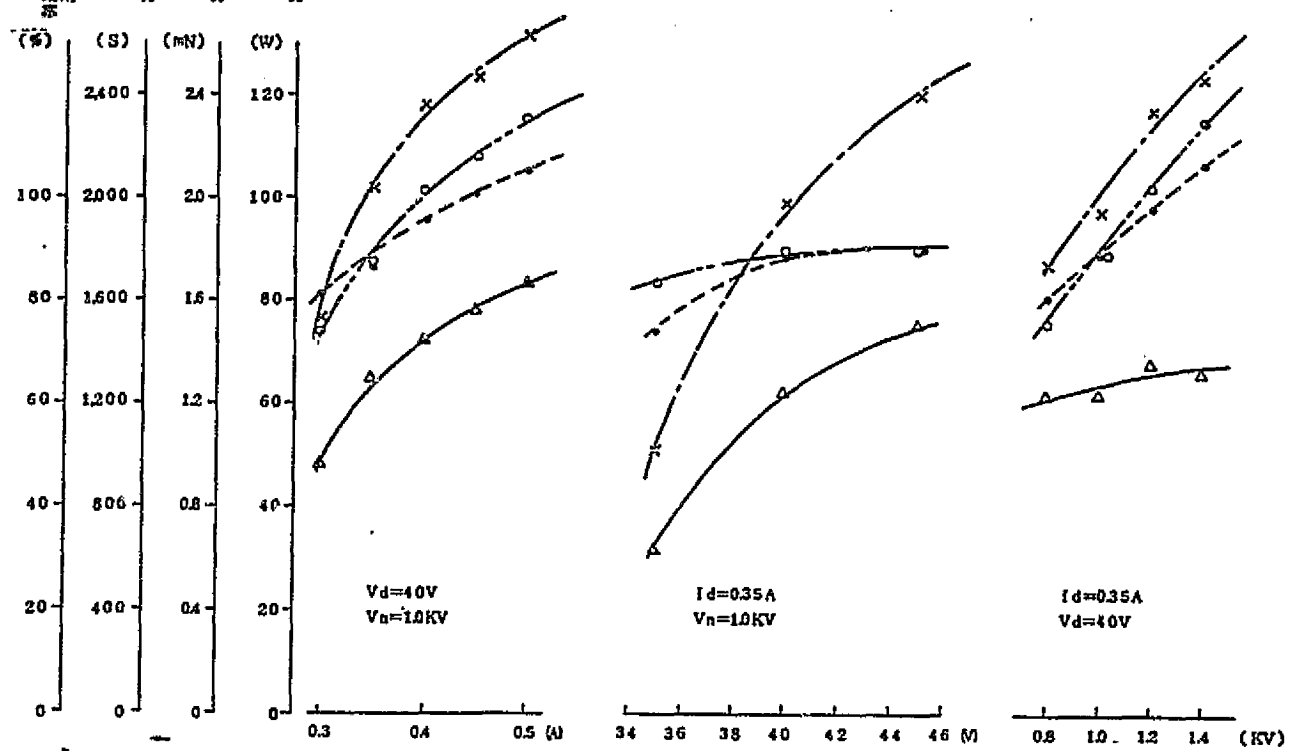

Fig. 5.15 Ion Production Cost

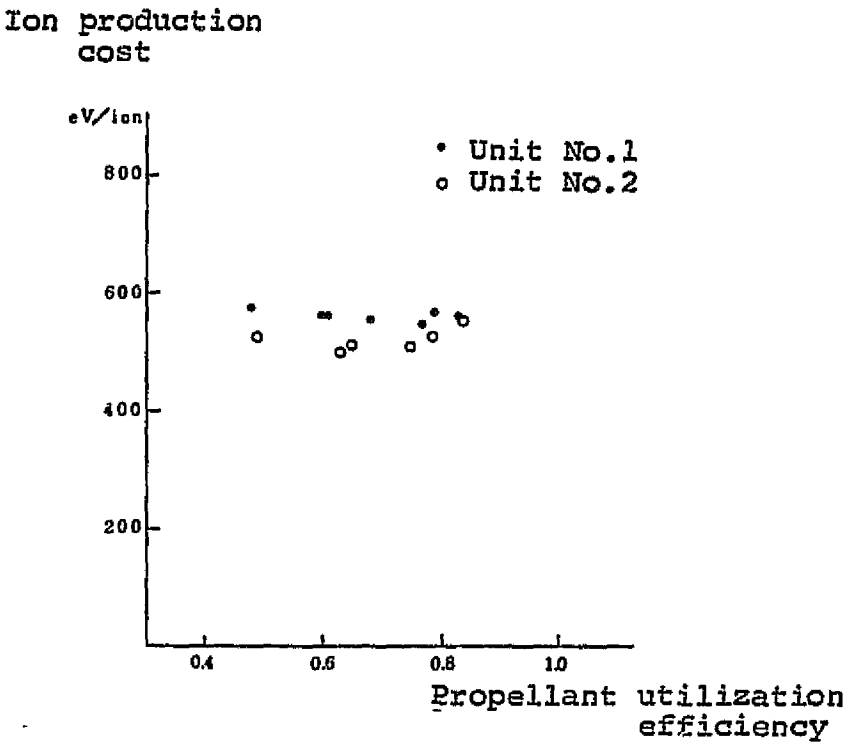

5.3.4 Summary

Based on the results of Acceptance Tests of IEE, IEP and IES, the FM of ion engine system was determined to be acceptable for flight, satisfying all requirements.

Summary of results with FM relative to the main requirements is given in Fig. 5.16.

Fig. 5.16 Ion Engine System(Flight Model)

Characteristic parameter:	Unit	Required value	Character-istic of #1	Character-istic of #2
Power consumption	W	≦100以下	85.6	87.6
Thrust	gr重 wf	0.18±0.03	0.167	0.172
Specific impulse	SEC	2000±200	2183	1938
Propellant flow	gr/sec	(1±0.25)×10⁻⁴	0.763×10⁻⁴	0.887×10⁻⁴
Propellant efficiency	%	70±10	68.7	61.3
Thruster power efficiency	%	44±5	42.3	44.0
Weight*	Kg	≦23.06 Kg以下	22.17 Kg	
Reliability	−	≧0.80 以上	0.96	

*Engine unit	1.96 + 1.98 Kg
Propellant	0.60 Kg × 2
IP	6.60 + 6.68 Kg
IR	3.59 Kg
Shield tape	0.16 Kg
TOTAL	22.17 Kg

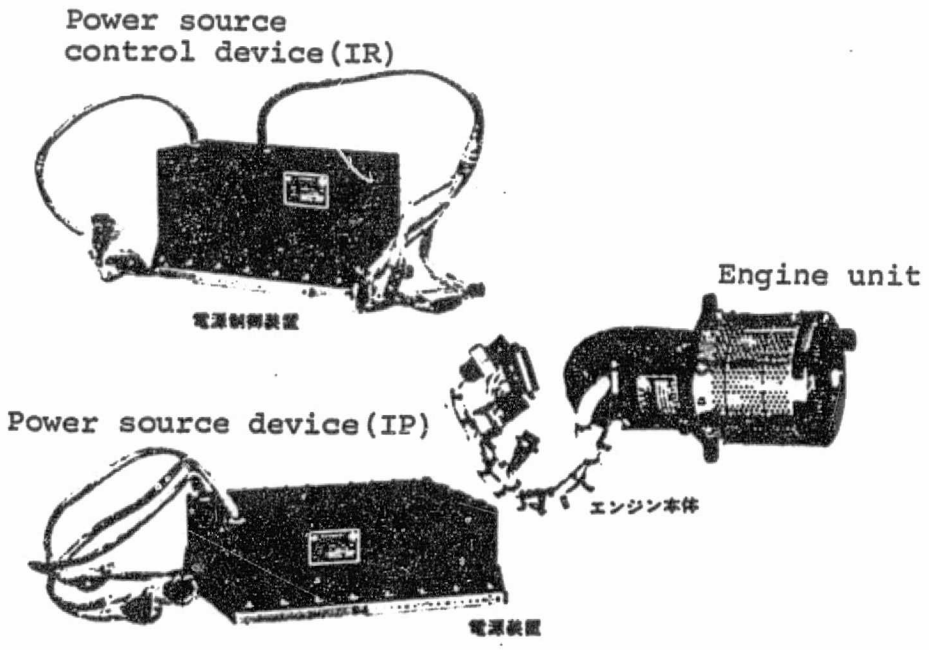

Chapter 6

Problems in Development and Countermeasures

Chapter 6: Main Problems in Development and Countermeasures

In this chapter, main problems which occurred during production and testing of EM, PM and FM and the countermeasures are discussed from the technical point of view.

6.1 Transient Characteristic of Discharge Voltage During Beam Injection

(1) Description of problem

In the EM of IEE Unit No. 1, beam injection caused discharge voltage to rise from about 40V to 55-70V(see Fig. 6.1), when the main discharge was maintained with the heater power source(PS10) output at its nominal level(constant output of 3V).

This phenomenon does not occur when the PS10 output is at a high level(constant 5V). Normal beam injection state at the nominal level of PS10 can be obtained if PS10 output is thrown in at a high level and then lowered in about an hour, but such an operation is not practical.

(2) Estimation of cause

The cause first assumed was that plasma density inside the discharge chamber was low, which may be due to an unbalanced supply of mercury and electron, or lack of mercury atom supply. As the normal flow control had been confirmed by the measured flow in component test, lack of mercury flow could be caused by an inefficient supply of mercury vapor from vaporizer. In any case, discharge voltage showed an almost normal value(about 40V) when the main discharge was maintained, which indicated that the cause was a subtle mismatching of discharge conditions which could be returned normal by adjusting the baffle position.

(3) Cause-finding steps

Steps shown in Fig. 6.2 were taken.

(4) Results of cause-finding steps

Results were as follows.

(a) Main hollow cathode in IEE(1) was replaced by a spare cathode: No major change and no major improvement resulted.

(b) With (a), discharge chamber was replaced by a spare chamber: No change resulted.

(c) Cathode removed from IEE(1) was tested independently: No abnormality found.

(d) A heat shield was installed in the insulator of the hollow cathode removed from IEE(1): 54V in transient and 38V in steady state resulted.

From the above results, it was supposed that the problem was due to a low insulator temperature which caused mercury to be condensed, resulting in an insufficient supply of mercury to the discharge chamber.

As the insulator is expected to have the lowest temperature in the main hollow cathode assembly, the temperature of its flange was measured. Following was observed.

i) At Vcv=3.5V and Viso=3V(nominal value for PS10):

·Temperature of insulator flange at main discharge ignition - 150C in IEE(1) and 175C in life test model.

·Minimum temperature of insulator flange - 140C in IEE(1) and 145 in life test model.

These temperatures are critical for mercury condensation.

ii) At Vcv=3.5V and Viso=5V(high level of PS10):

·Temperature of insulator flange at main discharge

ignition - 165C in IEE(1) and 205C in life test model.

- IEE(1) increased gradually then on, to steady state temperature of 192C.
- In the life test model, temperature lowered to a minimum of 175C and then reached a steady state of 178C.

(5) Areas of improvement

Based on the temperature and discharge transient characteristics described above, following improvements were planned in addition to the installation of heat shield in the insulator.

i) Match temperature increase characteristics of cathode and vaporizer by slowing the temperature rise in vaporizer.

ii) At the same time, increase the minimum temperature range in the main hollow cathode near the insulator.

For this purpose, the position of vaporizer heater was modified. Fig. 6.3 shows the main hollow cathode before and after the improvement. Heater was returned to almost the same position as in Pre-EM and BBM. Fig. 6.4 shows the insulator temperature change before and after the improvement. After improvement, the insulator flange temperature was 160C at the time of main discharge ignition and slowly rose to the steady state temperature of 180C.which was a 25C-increase from before and close to the temperature of case ii) in the preceding sub-section (PS10 high level). Transient changes of discharge voltage in the improved IEE(1) are shown in Fig. 6.5. In the improved IEE(1), response of discharge voltage was more sensitive to vaporizer temperature change.

(6) Comparison of characteristics before and after improvement

Characteristic changes due to the change in vaporizer heater

position are as follows.

	Before	After
i) Abnormal discharge ignition time	Yes	No
ii) Rise of vaporizer temperature	About 400C in 10 min.	About 270C in 10 min.
iii) Main discharge ignition time	About 10 min.	About 12 mir
iv) Steady-state temperature of insulator flange	About 155C	About 180C
v) Response of discharge voltage to to changes in vaporizer temp.	Dull	Sharp
vi) Discharge voltage change due to insulator power change	Sharp	None

(Constant vaporizer temperature F)

(7) Recurrence of the problem in PM and the measures taken

The problem seemed to have been solved when above-described steps were taken. However, the same phenomenon occurred again in a test by the manufacturer during production of PM.

Description of problem In a test during production of hollow cathode, PM07(internal code for main hollow cathode) did not start discharging 30 minutes after power was thrown in, or ignition was slow and accumulation of mercury on the insulator was observed after ignition.

Cause and measures As described earlier, accumulation of mercury on the insulator occurred in EM, and vaporizer heater was moved to the insulator side. As shown in Fig. 6.6(b), the heater was wound once on the vaporizer case and the rest was wound over vaporizer pipe. In PM, resistance of vaporizer heater was adjusted by shortening the heater wire, as that of EM was slightly larger than the standard. Because of this, the number of turns on the vaporizer pipe was reduced, causing the center of heat to move towards the vaporizer and thus increasing the heat resistance between the vaporizer and the insulator. In

comparing the two in a simple heat test it was found that the temperature increase of PM was 15-20C less than that of modified EM. Therefore, heater was wound sparingly around the vaporizer pipe in the second PM, as shown in Fig. 6.6(d), so that the end reached insulator flange. The result was satisfactory, and it was incorporated into FM.

Fig. 6.1 Abnormal Increase of Discharge Voltage

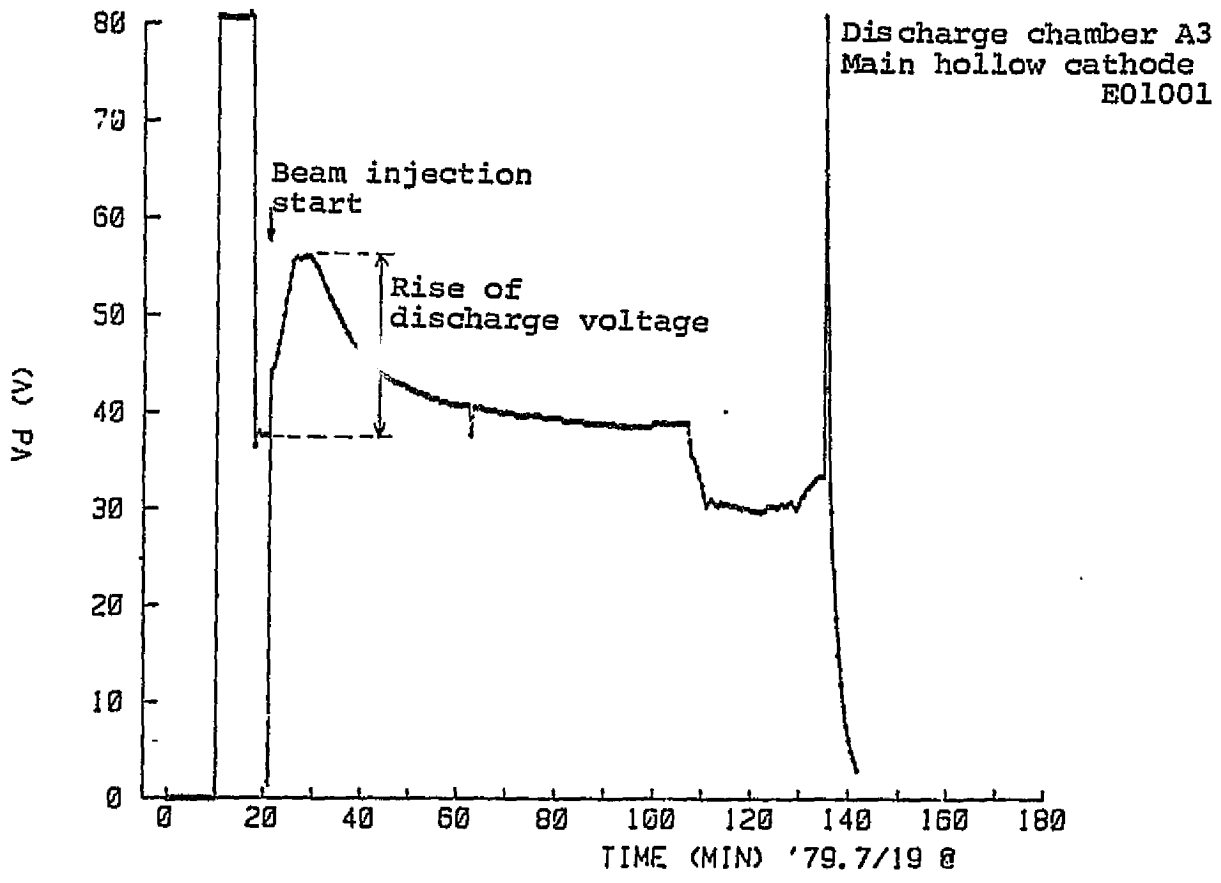

Fig. 6.2 Treatment of Problems

1. Study of countermeasures
2. Adjustment of baffle
3. Test
4. Cause-finging of problem product
5. CDR
6. Changes made in PM
7. Installation of heat shield on hollow cathode
8. Test
9. Cause-finding of problem product
10. CDR
11. Changes made in PM
12. Study of countermeasures?
13. Cause-finding test for problem product
14. Performance check with internal facilities
15. Performance check with replaced discharge chamber using internal facil.
16. Measurement of temperature
17. Cause-finding test with IEE life test model
18. Measurement of cathode flow with IEE life test model
19. Test for modified cathode with IEE life test model
20. (Adjustment of?) baffle position with IEE life test model
21. Modification of hollow cathode
22. Installation of modified product on
2 . IEE(1)
23. Performance test
24. Low-temperature test
25. Test with varied parameters
26. Report
27. Heat analysis based on measurement data
28. Heat analysis

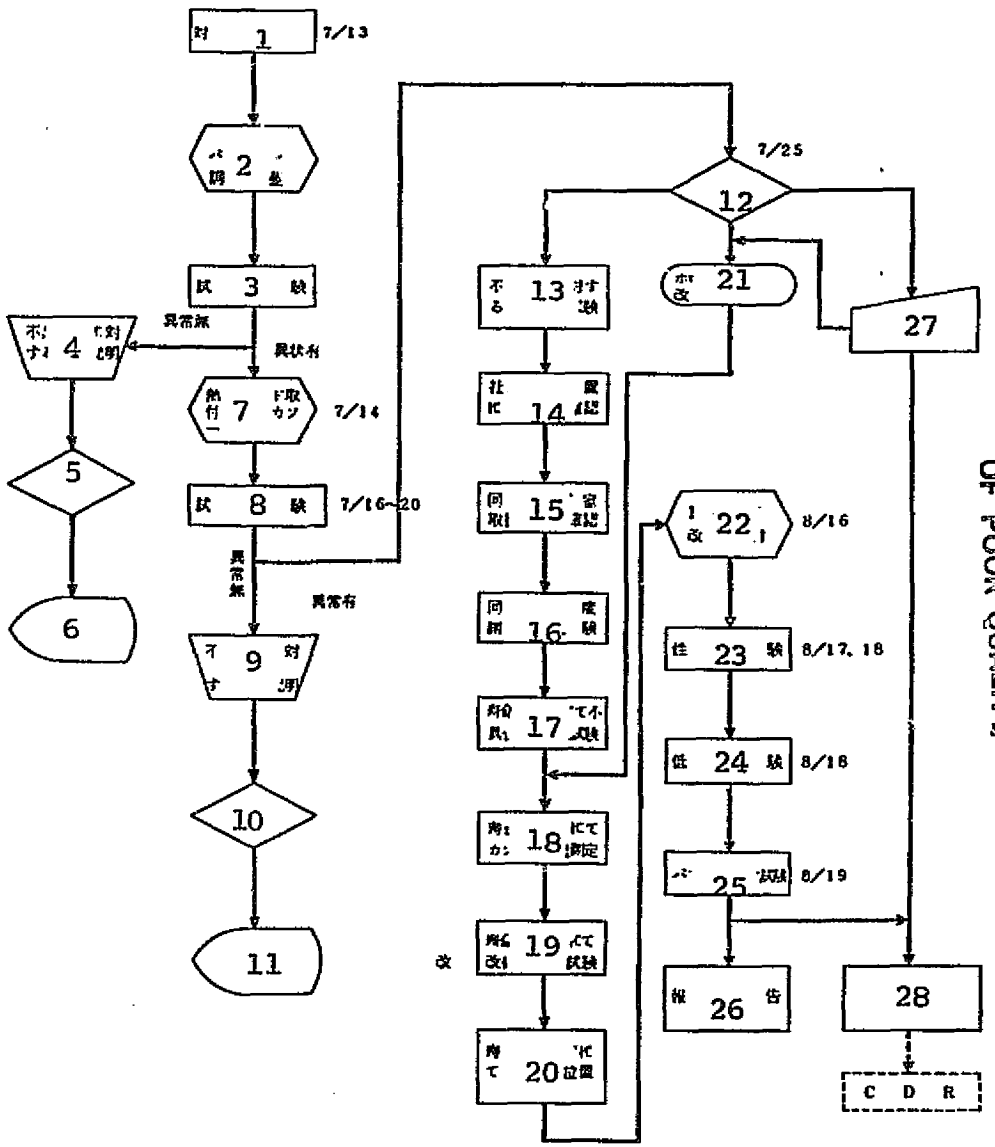

Fig. 6.3 Modification of Main Hollow Cathode

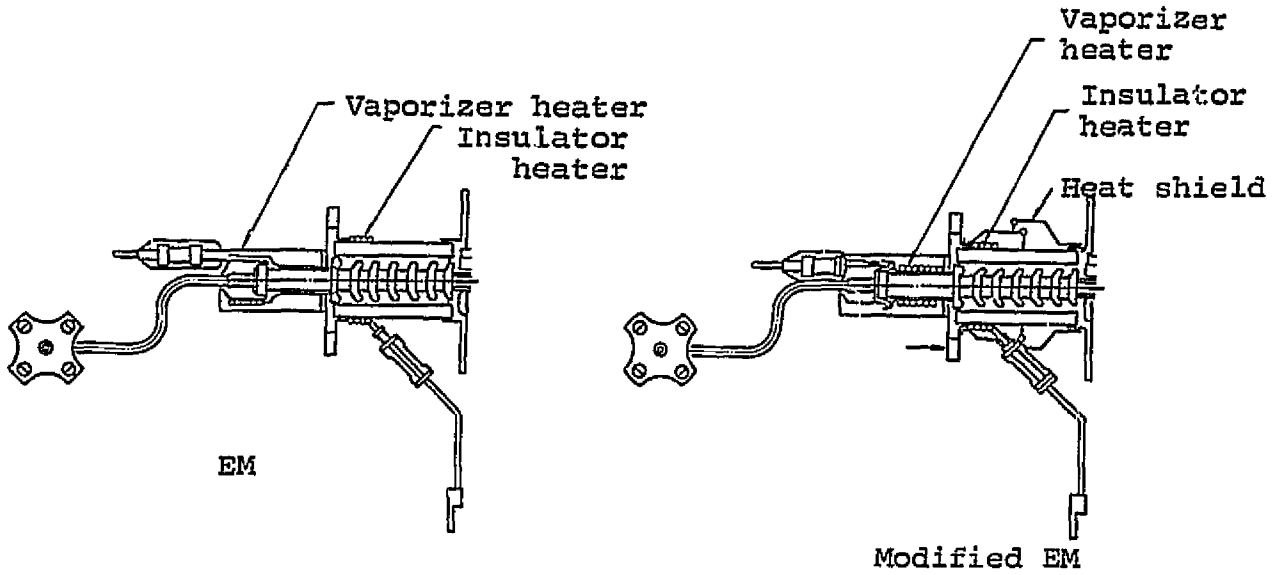

Fig. 6.4 Comparison of Temperature Near Insulator(before and after modification)

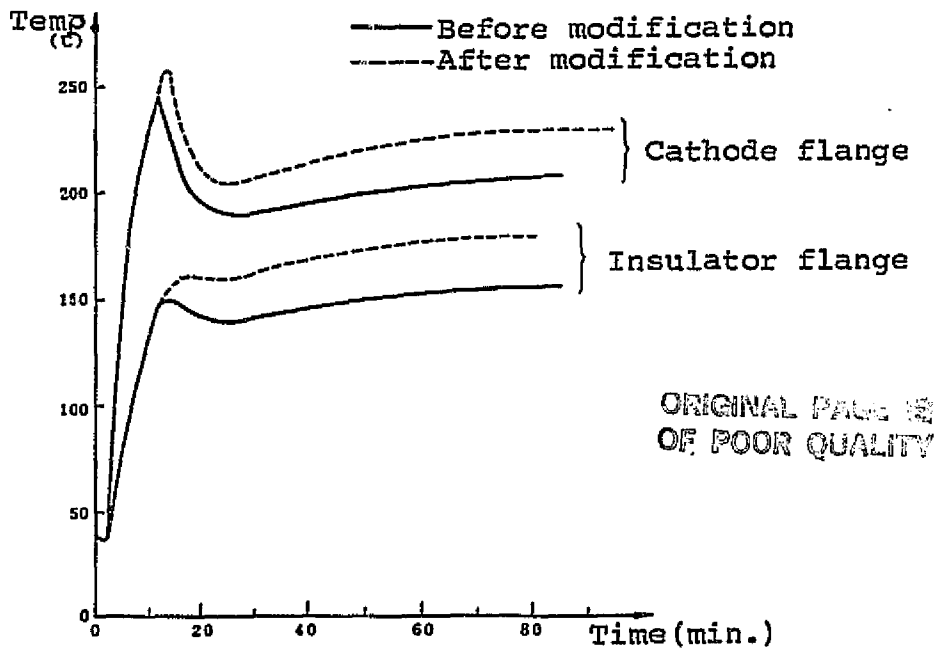

Fig. 6.5 Transient Change in Discharge Voltage of Modified IEE(1)

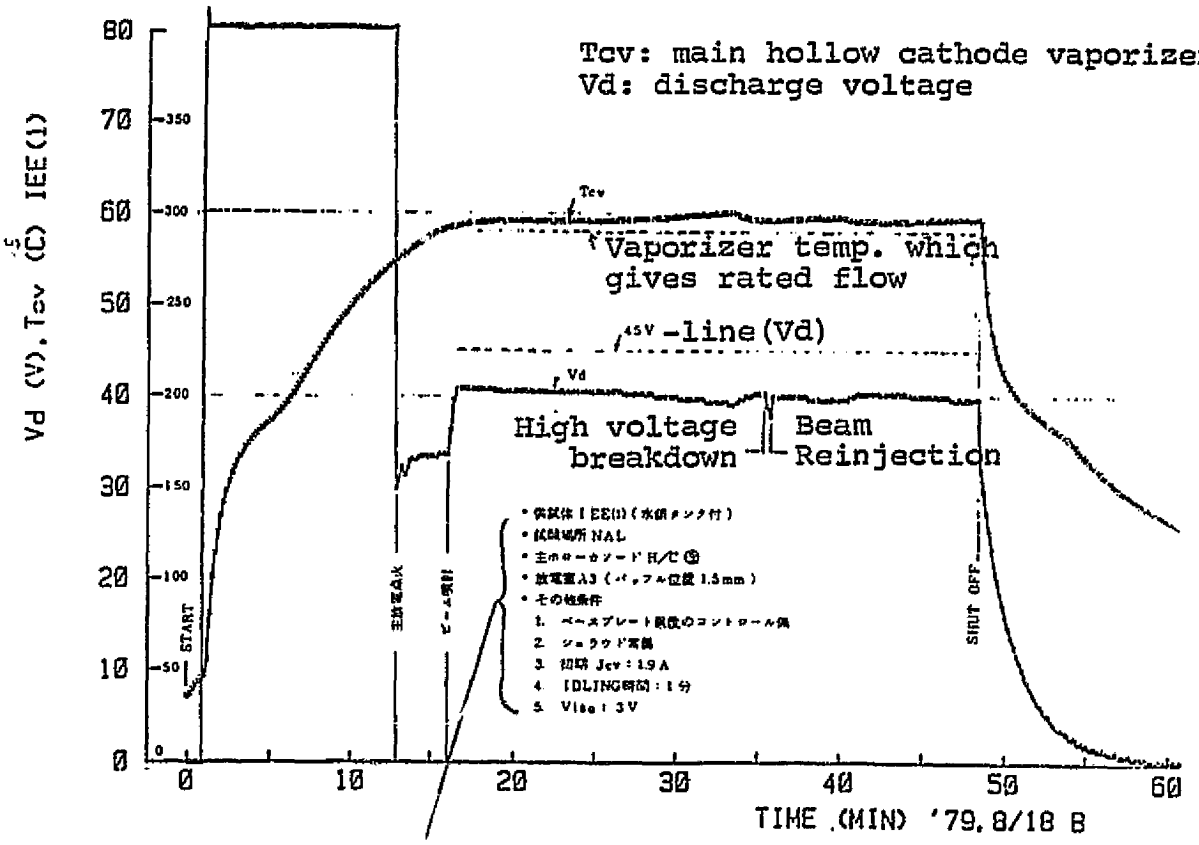

- Sample: IEE(1) (w/ mercury tank)
- Test location: NAL
- Main hollow cathode: H/C (modified)
- Discharge chamber: A3 (baffle position 1.5mm)
- Other conditions:
  1. No control on base plate temperature
  2. Constant shround temperature
  3. Early Jcv: 1.9A
  4. Idling time: 1 min.
  5. Viso: 3V

Fig. 6.6 Changes in Heater Position of Main Cathode Vaporizer

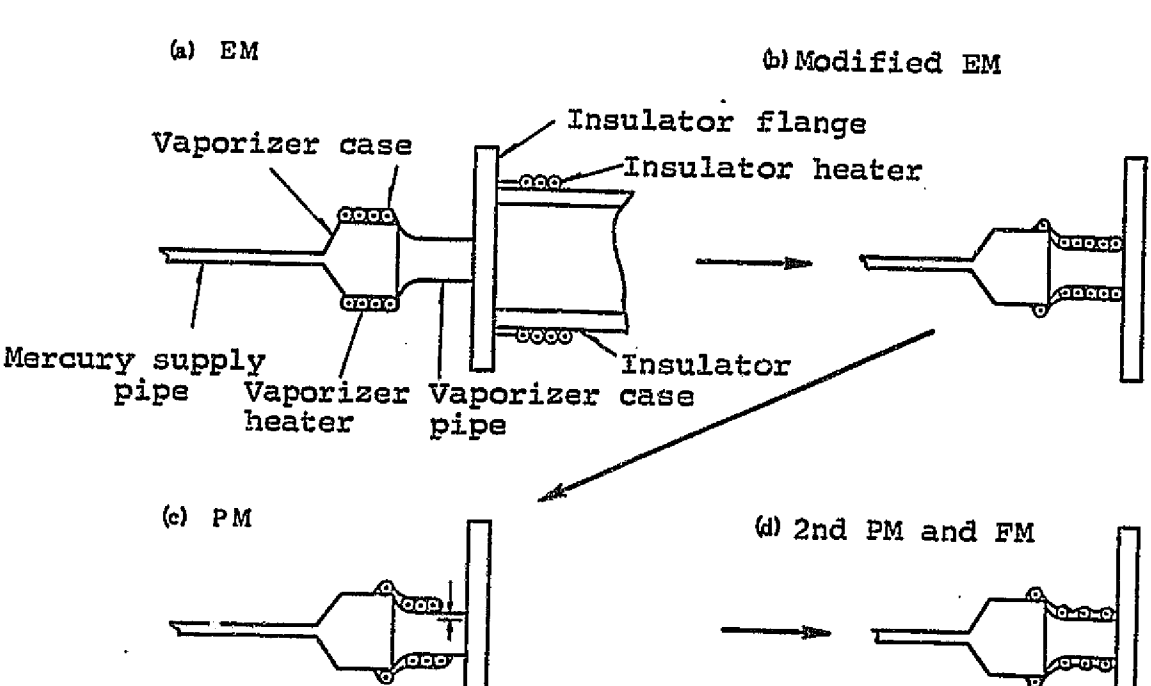

6.2 Flow Control of Neutralizer

Incompatibility of closed loop between neutralizer and vaporizer was found in the IES development test. The closed loop detects keeper voltage and sends feedback to vaporizer current, using the sequential characteristic: with increase in mercury supply due to increase in vaporizer current, plasma impedance between cathode and keeper decreases, reducing keeper voltage. Presumably, this sequential characteristic was not maintained and a reverse characteristic appeared instead, causing the closed loop function to fail and the vaporizer current to stay at its maximum. Therefore, the diameter of keeper hole was changed, in an attempt to convert the characteristic of neutralizer keeper into a sequential characteristic within the operation range. Fig. 6.7 gives test results showing the relationship between vaporizer temperature Tnv and keeper voltage Vnk with the keeper hole diameter as a parameter. It was found that smaller the diameter, closer the range of sequential characteristic is to the lower vaporizer temperature Tnv, i.e. smaller mercury flow. Relationship between vaporizer temperature Tnv and mercury flow is shown on the horizontal axis. Rated mercury flow(1×10^{-5}g/s) is obtained at Tnv$\sim$(=?)230C. Fig. 6.7 also shows that when the keeper hole diameter is 1ø, as soon as Tnv exceeds rated temperature it moves into the reverse characteristic range. With increased keeper hole diameter, the point of inflection of sequential characteristic and reverse characteristic moves towards larger Tnv, but keeper voltage Vnk increases. It was found that ignition time was slightly delayed at the same time. Taking the characteristic and keeper voltage into consideration, diameter of 2ø was chosen.

On the other hand, upper and lower limits of vaporizer power source current were narrowed so that a mercury flow which facilitates

normal neutralizer operation could be maintained even in case of control failure of the closed loop. Characteristics of control device for neutralizer keeper voltage(Vnk) and neutralizer keeper current(Inv) are shown in Fig. 6.8. Lower limit of Inv was changed from 0.4A to 0.5A and upper limit, from 1.4A to 1.2A. Upper limit affects the rise of neutralizer vaporizer temperature at the start of ion engine operation, i.e. ignition time. The relationship between neutralizer vaporizer current Inv and ignition time is shown in Fig. 6.9, for the keeper hole diameter of 1ø. After the change from 1.4A to 1.2A, about 2.5-minute delay was observed, but ignition time of 7 minutes was considered satisfactory.

Fig. 6.7 Vaporizer Temperature vs. Keeper Voltage, with Keeper Hole Diameter as Parameter

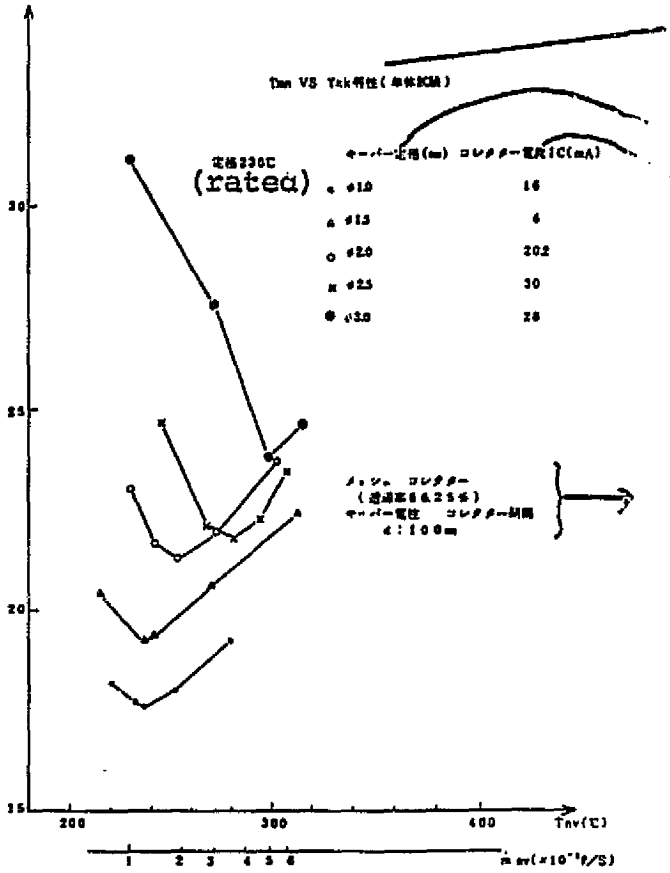

Tmn vs. Tnk characteristic (component test)

Keeper, rated(mm)
Collector current IC(mA)

Mesh collector(permeation rate, 66.25%)
Keeper pole and collector, d=100mm

Fig. 6.8 Control Property of Neutralizer Keeper Voltage/Vaporizer Current Closed Loop

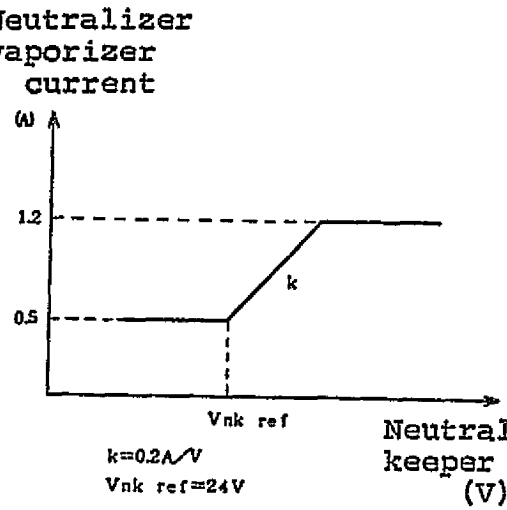

Fig. 6.9 Maximum Current of Neutralizer Vaporizer vs. Ignition Time

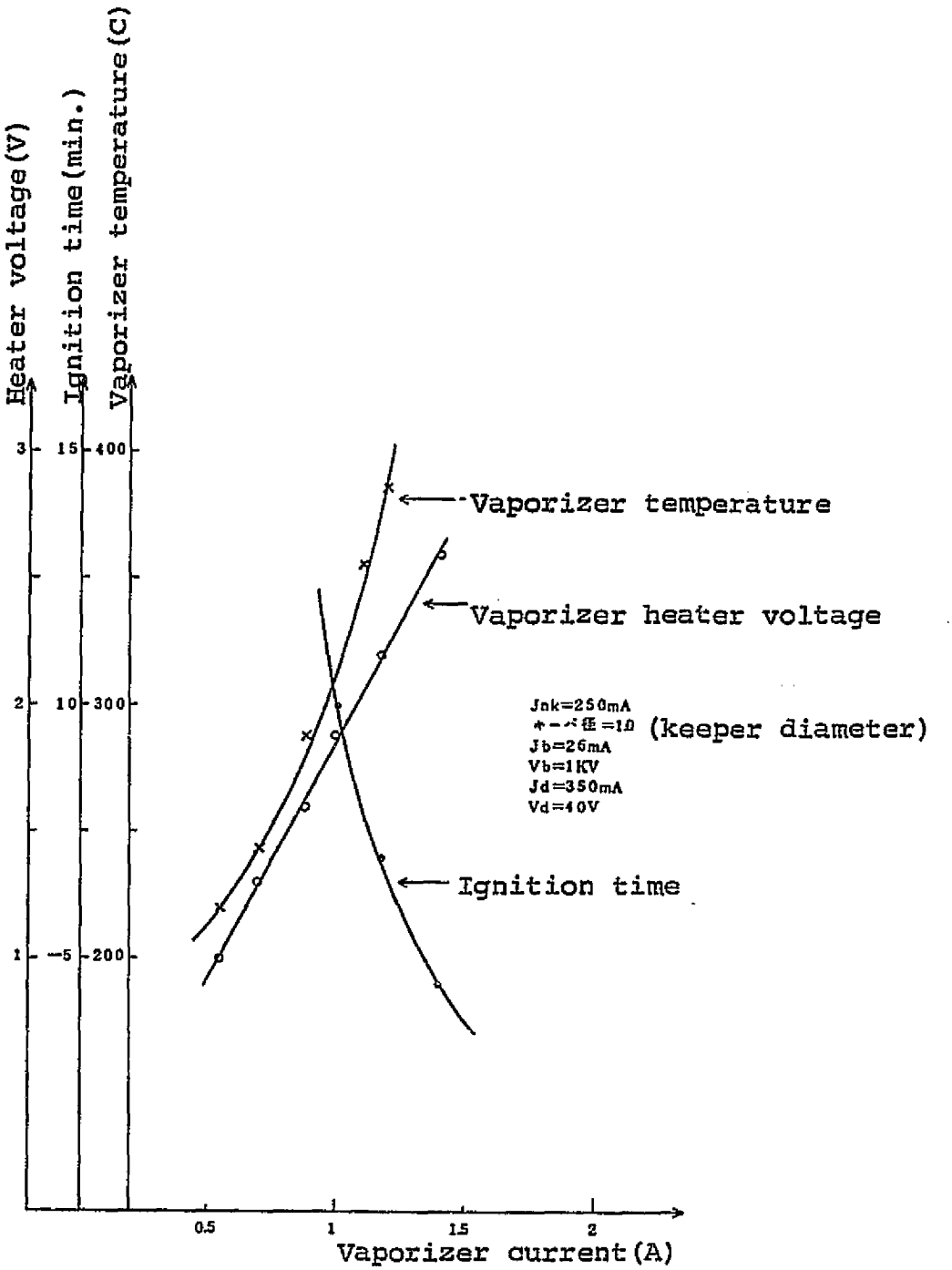

6.3 Mercury-pressure Resistivity of Vaporizer

(1) Description of problem

At the time of production(PM), inspection showed that the discharge voltage of main hollow cathode was high and unstable. It changed with time, but with a dull response to vaporizer temperature change, showing a similar pattern as in Development Test. As accumulation of mercury in the insulator was expected, its heater power was set to high level. This lowered discharge voltage, confirming mercury accumulation. At the end of operation, vaporizer heater power was shut off and insulator heater power was set to high level, in preparation for natural diminishing of discharge. However, discharge was still maintained after 3 hours. Temperature of main vaporizer was about 230C at this time, but the mercury flow registered on a mercury column was 3-4 times the normal amount. Mercury column continued to lower after the operation ended, suggesting a high possibility of liquid mercury leakage from the vaporizer.

(2) Developments around neutralizer

Due to an abnormal discharge voltage increase at the time of beam injection during Development Test, it was necessary to allocate part of vaporizer heater power to insulator side. Because of this, permeation coefficient of porous tungsten was increased in PM so that vaporizer could operate at a lower temperature: the temperature at which rated mercury flow could be obtained was 310C in EM, while in P01-001, for example, it was 264C. This was accomplished by decreasing the pressure in sintering.

(3) Cause and measure

In observing a cross section of a vaporizer which lacked in pressure resistivity for static pressure mercury, enlarged Ta crystals

were observed near the welded area. There was also a crack in the porous tungsten plug near the same area, which appeared to have been caused by heat stress(See Fig. 6.10). From these observations, lack of pressure resistivity seemed to have been caused by the crack and the permeation coefficient of porous tungsten which was slightly too large.

Therefore, as countermeasures, welding conditions were modified and the density of porous tunsten was increased from 70% to 71% in main hollow cathode and from 75% to 76% in neutralizer hollow cathode, a 1% increase for each.

Fig. 6.10 Crack in Vaporizer

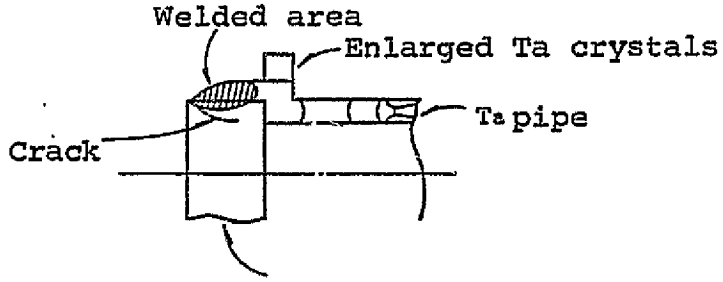

6.4 Ignitability of Neutralizer

(1) Description of problem

During neutralizer operation test of IEE(1) in the function test of QT, neutralizer was not ignited after power supply was on for 30 minutes. This was a preliminary test with power sources installed on the outside of vacuum tank, using a junction box and extension cable, and not an official configuration. Heater input power measured in the junction box was 23.3W.

(2) Steps taken and results

i) Under configuration shown in Fig. 6.11, power source PS7 was replaced by an external DC power source and a) maintained at 25W for 20 minutes and b) if not ignited, power was increased every 2 minutes until heater current reached 5A. Results: a) neutralizer did not ignite; and b) ignited at heater current of 5.0A and supplied power of 29.5W (junction box measuring terminal). Heater resistance at this time, calculated from voltage and current, was 1.180Ω.

ii) Neutralizer was operated with PS7 replaced by external DC power source of 25W(junction box measuring terminal) for 30 minutes. Result: Neutralizer did not ignite. Its heater current was 4.7A, voltage, 5.34V, and power, 25.1W at this time.

iii) DC resistance from the junction box measuring terminal to the engine unit was measured and compared with resistance of the engine unit at the connector end. 25W power was supplied to the connector end for 30 minutes by adjusting the external DC power source. DC resistance was 0.490Ω at the junction box measuring terminal and 0.459Ω at the

connector end. Results: Discharge was ignited 16 minutes after the power source was switched on. Measuring terminal voltage was 5.48V, connector voltage, 5.33V(calculated value), current, 4.80A and power at the connector end was 25.6W(calculated value) at this time.

iv) 25-25.3W power was supplied to the connector end of engine unit when the temperature of neutralizer vaporizer reached under 0C. Result: Discharge was not ignited. Connector voltage was 5.28V(calculated value), current 4.75A and power was 25.1W(calculated value).

Results called for re-examination of interface of ion engine unit and power source device. Power source output specified in Table 4.10 were nominal values that could be interpreted in different ways. This was not appropriate, especially with separate production of the engine unit and power conditioner, respectively by Mitsubishi Electric Co. and Tokyo Shibaura Electric Co. And, while the output from the power conditioner was AC(5kHz) constant voltage in the engine unit component test, it was actually tested with AC constant current and DC constant voltage due to the testing facilities at the National Aerospace Laboratory. Further, changing the diameter of neutralizer keeper hole from 1ø in EM to 2ø in PM seemed to have worsen the ignition property. Thus, it became necessary to provide a unified interpretation of power source output, and clarify and plan for any improvements necessary for flight model.

In actuality, it was decided to go ahead with the Qualifying Tests for IES(2), while countermeasures for IES(1) were being planned. Preparation for FM was particularly important.

(3) Power requirements of ion engine unit FM and power supply

range of power conditioner

The status as of the beginning of September, 1980, was as follows.

1) Neutralizer heater power

Engine unit

Power at the start of discharge(PM, IEE#1):

·With AC constant current power source

5.041A(constant current), 5.072V
Effective power(95% of observed power) 24.29W
Ignition time 26 min.

·With DC constant voltage power source

5.02V(constant voltage), 4.87A
Effective power 24.45W
Ignition time 18 min.

Required power: Min. 25W of effective power

Power conditioner

Estimated output range:

25W±5%(set deviation) $^{+3\%}_{-7\%}$(input voltage fluctuation)
$^{+15\%}_{-5\%}$(temperature fluctuation)

2) Neutralizer keeper voltage

Engine unit

In QT, operation checked at 0.25A and 24±0.5V

Required voltage: over 23.5V

Power conditioner

Estimated voltage range:

24V±5%(set deviation) $^{+3\%}_{-7\%}$(input voltage fluctuation)
$^{+5\%}_{-7\%}$(temperature fluctuation)

3) Main cathode keeper voltage

Engine unit

In QT, operation checked at 0.3A and 15±0.2V

Power conditioner

Estimated output range:

15V±5%(set deviation) $^{+3\%}_{-7\%}$(input voltage fluctuation)

$^{+5\%}_{-7\%}$(temperature fluctuation)

4) Insulator heater power

Engine unit

In QT, 1±0.1A, (blank)W

Power conditioner

Estimated output range:

3W±5%(set deviation) $^{+3\%}_{-7\%}$(input voltage fluctuation)

$^{+20\%}_{-10\%}$(temperature fluctuation)

Lower limit of 2.64W to be secured.

5) Main cathode vaporizer power source

Engine unit

Vaporizer heater resistance(max. value during operation): 1.89

No operational problem.

Power conditioner

Estimated output range: 2A$^{+7\%}_{-2\%}$(temperature fluctuation)

(4) Range of neutralizer heater power source output under the conditions of AT heat vacuum test

Causes of output fluctuation in unstabilized power source are i) temperature fluctuation of the environment(-5C~+45C in AT) and ii) input voltage fluctuation($28^{+0.22}_{-0.78}$V specified). These fluctuations added to the set deviations give the output fluctuation, estimated prior to the production of power source device FM. Fig. 6.12 shows the output power fluctuation range of neutralizer heater power source (PS7). Due to restrictions by converter transformer, the upper limit of voltage is 314W. Power source PS7 is for voltage output which is

based on neutralizer heater resistance of 1Ω. ① indicates a range of set deviation, taking temperature fluctuation range in AT and upper limit of converter transformer output into account with a steady input voltage of 28.0V. During operation, the center value of input voltage is 27.67V(taking voltage drop from PRU output of 28±1%V to IEP into consideration). According to heat analysis, estimated temperature fluctuation of base plate at this point is 9 - 29.7C and the output power range is an in ③. In order to obtain output of over 25W under the operating conditions, output power must be set between 25.77W and 28.87W, as in ④, and under the AT conditions output must be adjusted to 26.39W 28.55W, as in ②.

(5) Finalized interface conditions

Based on the requirements of IEE and IEP, power source input conditions were determined for AT. Input conditions at IEE connector end are shown in Table 6.1. Corresponding output fluctuation tolerance of IEP and its results were shown in Table 5.12.

Fig. 6.11 Configuration of Neutralizer Operation Test

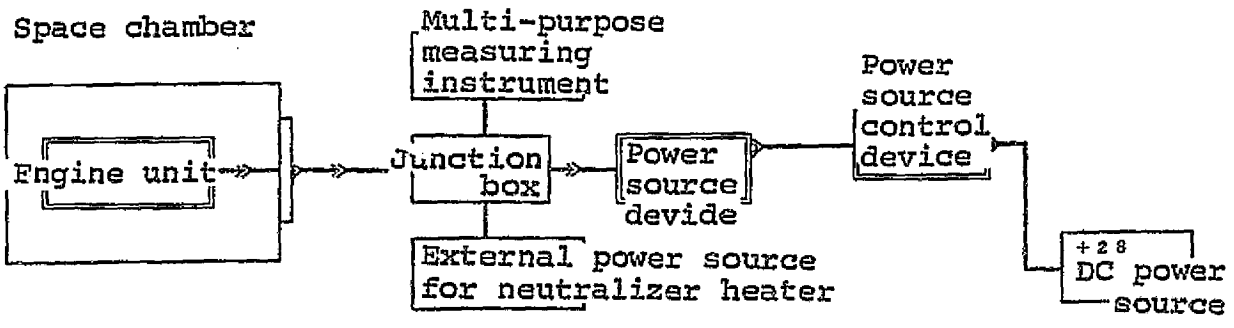

Fig. 6.12 Output Power of Neutralizer Heater Power Source (PS7)

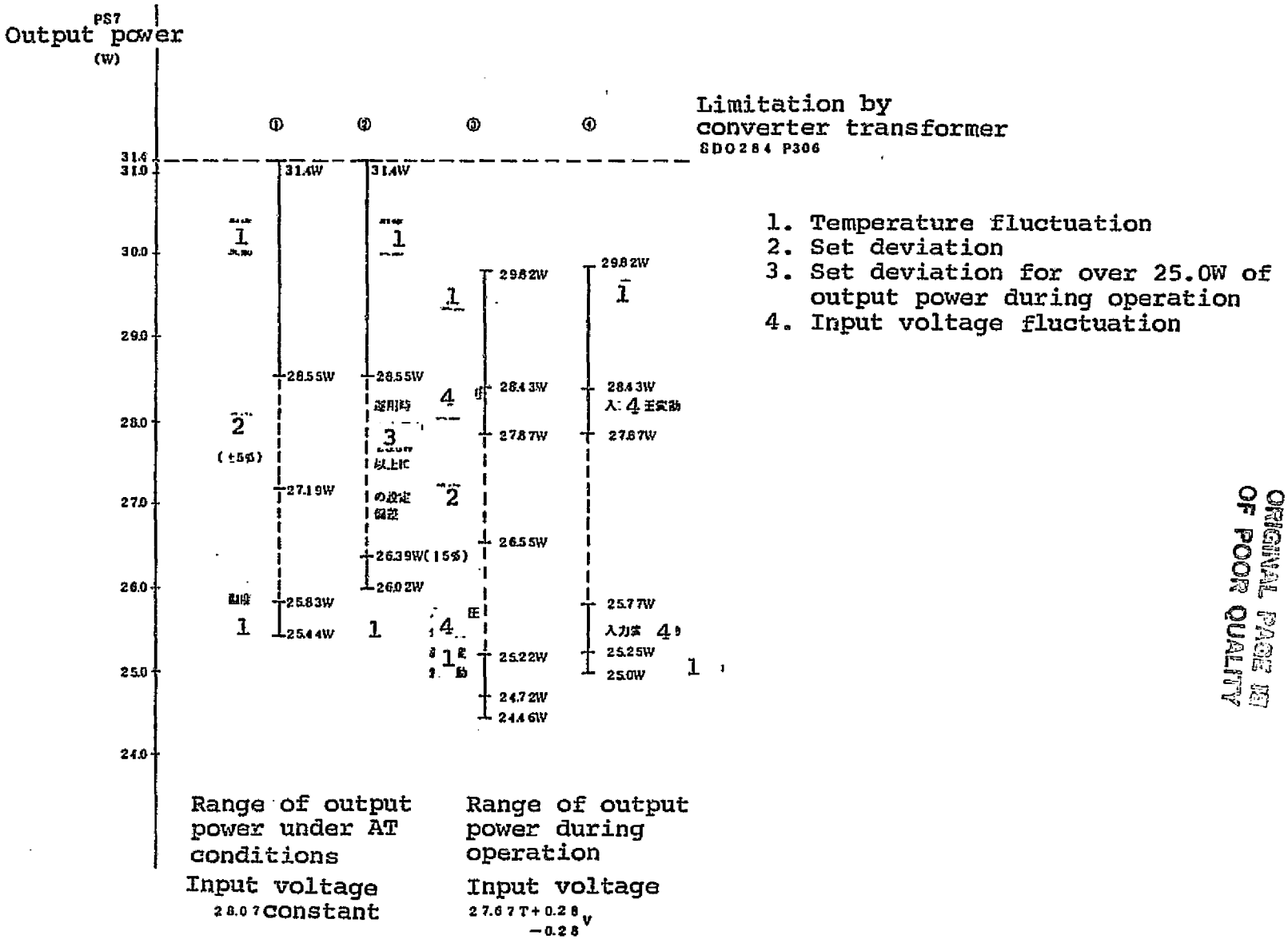

Table 6.1 Power Source Input Conditions at IEE Connector Terminal

Name of power source	symbol	level	Input conditions at IEE connector terminal(allowable range)		
Screen grid	PS 1	N.L	$1000V \pm 40V$	DC	30mA
Accelerator grid	PS 2	N.L	$-1000V^{+65}_{-25}V$	DC	1mA
Discharge	PS 3	N.L	$35A \pm 0.01A$	DC	40V
		I.L	$1.6V^{+0.3}_{-0.7}V$	AC	load 0.64Ω
Main cathode heater	PS 4	N.L	$5.0V^{+0.55}_{-0.3}V$	AC	load 1.0Ω
		H.L	$6.0V^{+0.3}_{-0.7}V$	AC	load 1.0Ω
Main cathode keeper	PS 5	N.L	$15.0V^{+2.2}_{-1.0}V$	DC	0.3A
Main cathode vaporizer	PS 6	L.L	$0.5A^{+0.04}_{-0.1}A$	AC	load 1.75Ω
		M.L	$2.0A^{+0.18}_{-0.04}A$	AC	load 1.75Ω
Neutralizer heater	PS 7	I.L	$1.6V^{+0.3}_{-0.4}V$	AC	load 0.64Ω
		N.L	$5.0V^{+0.8}_{-0.25}V$	AC	load 1.06Ω
Neutralizer keeper	PS 8	N.L	$24.0V^{+6.5}_{-0.5}V$	DC	0.25A
Neutralizer vaporizer	PS 9	L.L	$0.5V \pm 0.05V$	AC	load 1.75Ω
		M.L	$1.2A^{+0.1}_{-0.04}A$	AC	load 1.75Ω
Insulator heater	PS10	N.L	$3.0V^{+0.5}_{-0.19}V$	AC	load 3Ω
		H.L	$5.0V^{+0.09}_{-0.61}V$	AC	load 3Ω

Note: 1. Start level of PS5 and PS8 is $300V^{+100}_{0}V$(DC no load).

2. AC input level given is the input condition when power factor is 1 at pure resistance load.

3. If ignition of main hollow cathode keeper discharge and main discharge is difficult with PS4(NL), PS4(HL) is used.

6.5 Countermeasures for Deterioration of Hollow Cathode

In testing IES in the Development Tests, increase of neutralizer keeper voltage, thought to be caused by deterioration of neutralizer hollow cathode, was observed. In this IEE(1)(EM), total operation time was about 200 hours(including 100 hour IES testing) and the total air exposure time was about 1,500 hours(including 336 hour IES testing), and deterioration of neutralizer was already prominent half way through the IES test. On the other hand, in the life test of an EM-equivalent, total operation time was about 500 hours and the total air exposure time was about 3,100 hours(including about 2,900 hours under controlled humidity) and no deterioration was observed. Thus, deterioration of IEE(1)(EM) is assumed to be caused by the duration of air exposure and its environment(especially humidity) which were too harsh for the hollow cathode.

Fig. 6.13 shows the deterioration conditions after exposure (about 19 hours) to highly humid air(over 90%). Keeper voltage change before and after the exposure seems to be due to deterioration which did not sufficiently recover by activating cathode heater but returned to the pre-exposure performance level when the cathode was heated while maintaining keeper discharge. For IEP, deterioration of hollow cathode was deemed unavoidable to an extent, and thus, neutralizer keeper power source(PS8) capacity was raised from 0.25A and 24V to 0.25A and 31V.

With respect to the problem of non-ignition of neutralizer in the IES QT, electrical interface conditions of IEP and IEE were reexamined. In order to study IEE operation conditions and effects of repetitive operations, air exposure, etc. on ignition time, repetition test was performed using 2 neutralizers(FN01 and FN05)

which are equivalent of FM. The test is explained below.

6.5.1 FN01 Repetition Test

(1) Purposes

i) With cathode heater input of 5.2V_{DC}, check that ignition is smooth.

ii) Study effects of idling in the first operation after exposure to air.

iii) Evaluate ignition time under IEE operation mode of "Immediate start after idling."

iv) Study effects of heat shield.

v) Study effects of aging.

(2) History of neutralizer up to repetition test

Hollow cathode completion inspection:

Operation time 10 hours, repeated 4 times.

Exposure to air: 14 days

Oscillation test

Operation check after oscillation test:

Operation time 6 hours, repeated twice.

Exposure to air: 11 days

Characteristics study:

Operation time 20 hours, repeated 14 times.
Exposure to air during this time 3 times(total 20 days)

(3) Test conditions

Base plate temperature 20±3C

Shroud temperature -100C

Power sources: PS7 IL DC constant voltage of 1.6V
NL DC constant voltage of 5.0-5.2V
PS8 Drooping property equivalent of IEP
PS9 Closed loop to IEP-equivalent PS8

(4) Test results

Test conditions are shown in Table 6.2, performances under steady state, in Table 6.3, and the history of cathode heater input and ignition time, in Fig. 6.14.

In regard to ignition characteristics, Fig. 6.15 shows that

i) With input of 5.2 V_{DC}, ignition takes place regardless of idling after exposure to air;

ii) IEE operation mode of "Immediate start after idling" reduces ignition time by 2-4 minutes; and

iii) Effects of heat shield are not significant when there is sufficient heater power, but at a critical power level, the shield reduced ignition time by 4-5 minutes.

As for keeper discharge characteristics,

i) Changes in neutralizer vaporizer temperature seen in the data of steady state(about 60 minutes after beam injection) indicate that keeper discharge characteristics are slightly affected by exposure to air(See Fig. 6.16);

ii) The effect is one time only, and the characteristic recoveres with repeated operation; and

iii) There is no problem in control property.

With respect to aging, it is mostly completed before repetition test. Aging does not affect ignition time before or after heat shield is installed. (Fig. 6.15)

Fig. 6.13 Keeper Voltage Characteristic When Neutralizer Hollow Cathode Is Exposed To High Humidity

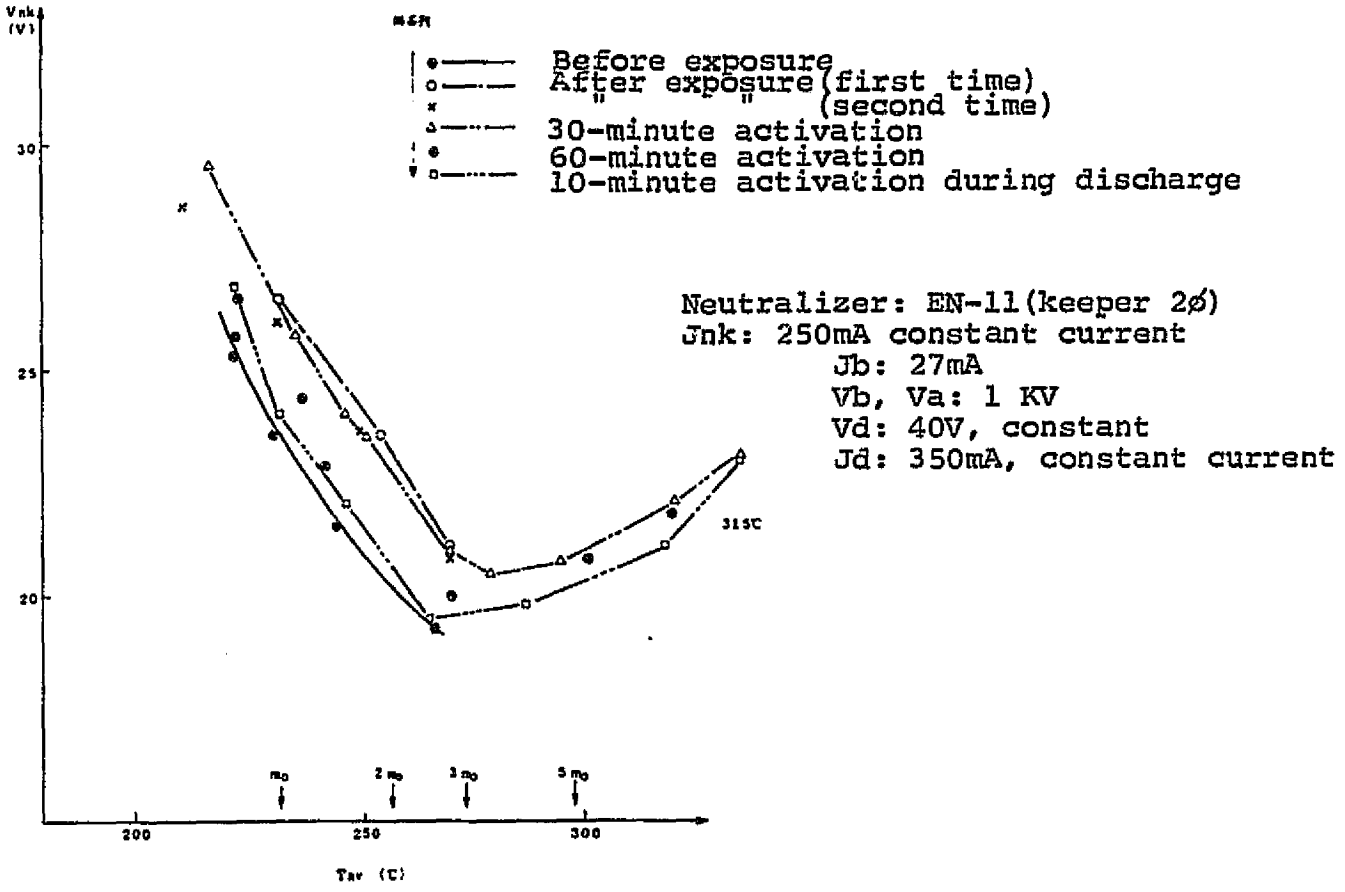

Neutralizer: EN-11(keeper 2ø)
Jnk: 250mA constant current
Jb: 27mA
Vb, Va: 1 KV
Vd: 40V, constant
Jd: 350mA, constant current

Table 6.2 IEE FM PILOT(1) Cycle Test Conditions

*Neutralizer keeper discharge ignition time
**minutes
A: Exposure to air
B: Vacuum evacuation
C: Beam injection
D: Rest period
E: Degree of vacuum
F: Continuous operation of vacuum tank
G: (with short stop(s))
H: Difficulties at ignition time but stabilized later.
*** Difficult first ignition but re-ignited immediately.

Run#	Idling time	Vab(N.L.)	Φ*	Test time IES START	ACCEL	SHUT	
	A 30 days. B (12/2 14:50~						
1	105 **	5.2 V_{DC}	9'21"	8:03	10:17	11:17	
	① C 1 Hour. D 1 Hour. E 2×10⁻⁴Torr (2/3						
2	1	5.2 V_{DC}	11'34"	12:25	12:48	13:48	
	① 1 Hour. D 1 Hour. 2×10⁻⁴ Torr						
3	1	5.2 V_{DC}	11'03"	14:55	15:11	16:11	
	① 1 Hour. D 1 Hour. 2×10⁻⁴ Torr						
4	1	5.1 V_{DC}	13'32"	17:20	17:38	18:40	
	① 1 Hour. 12/3 18:40 SHUT OFF E 2×10⁻⁴Torr/ F (E ~4×10⁻⁴Torr)						
5	1	5.1 V_{DC}	13'43"	8:50	9:15	10:15	
	① 1 Hour. D 1 Hour. 2×10⁻⁴ Torr						
6	1	5.0 V_{DC}	15'03"	11:25	11:48	12:48	
	① 1 Hour. D 1 Hour. 2×10⁻⁴ Torr						
7	1	5.0 V_{DC}	17'04"	13:55	14:17	15:17	
	① 1 Hour. D 1 Hour. 2×10⁻⁴ Torr						
8	60'	5.0 V_{DC}	13'02"	16:25	17:42	18:42	
	① 1 Hour. 12/4 18:42 SHUT OFF E 2×10⁻⁴Torr/ F (12/4 19:30~12/5 7:30)						
	A (12/5 8:40~14:40)6Hour. B (12/5 14:50~)/ F (E ~ 2×10⁻⁴Torr)						
9	1	5.2 V_{DC}	10'30"	8:51	9:06	10:22	
	① 1 Hour (G). D 1 Hour. 1.2×10⁻⁴Torr						
10	1	5.2 V_{DC}	10'31"	11:30	11:45	12:45	
	① 1 Hour. D 1 Hour. 1.2×10⁻⁴ Torr						
11	1	5.2 V_{DC}	10'19"	13:51	14:06	15:06	
	① 1 Hour. D 1 Hour. 1.2×10⁻⁴ Torr						
12	1	5.1 V_{DC}	12'13"	16:12	16:36	17:36	
	① 1 Hour. 12/8 17:36 SHUT OFF E 1.2×10⁻⁴Torr/ F (12/5 18:30~12/8 9:30)						
13	1	5.1 V_{DC}	12'06"	13:15	13:31	14:31	
	① 1 Hour. D 1 Hour. 1.3×10⁻⁴ Torr ***						
14	1	5.0 V_{DC}	19'08"	15:40	16:03	17:03	
	① 1 Hour. D 1 Hour. 1.4×10⁻⁴Torr						
15	60'	5.0 V_{DC}	17'18"	18:10	19:31	20:31	
	A (12/9 9:00~14:35)5.5Hours B (12/9 14:35~). H / F (E ~3.6×10⁻⁴Torr)						
16	105	5.2 V_{DC}	7'10"	8:30	10:27	11:27	* H
	① 1 Hour. D 1 Hour. 1.3×10⁻⁴						
17	1	5.2 V_{DC}	9'51"	12:50	13:04	14:05	* H
	① 1 Hour. D 1 Hour. 1.2×10⁻⁴						
18	1	5.2 V_{DC}	10'47"	15:10	15:24	16:24	
	① 1 Hour. D 1 Hour. 1.2×10⁻⁴						
19	1	5.1 V_{DC}	11'09"	17:30	17:45	18:45	
	① 1 Hour. 12/10 18:50SHUT OFF E 1.0×10⁻⁴Torr/ F (E ~3.0×10⁻⁴Torr)						
20	1	5.1 V_{DC}	12'16"	9:30	9:46	10:46	
	① 1 Hour. D 1 Hour. 1.4×10⁻⁴						
21	1	5.0 V_{DC}	12'16"	11:52	12:17	13:17	
	① 1 Hour. D 1 Hour. 1.0×10⁻⁴						
22	1	5.0 V_{DC}	12'31"	14:35	14:52	15:52	
	① 1 Hour. D 1 Hour. 1.1×10⁻⁴						
23	60'	5.0 V_{DC}	9'58"	17:10	18:23	19:23	
	① 1 Hour. 12/11 19:28 SHUT OFF E 1.0×10⁻⁴Torr/ F (12/11 20:30~)						
	Neutralizer keeper discharge ignition time: end of idling to ignition. Exposure to air: 70% for 5 min. and 42% for 15 min. Others in GN_2.						
24	105分	5.2 V_{DC}	7'28"	09:22	11:19	12:19	
25	1分	5.2 V_{DC}	10'34"	13:30	13:45	14:46	
26	1分	5.0 V_{DC}	17'03"	15:52	16:13	17:13	
27	1分	5.0 V_{DC}	16'37"	18:21	18:42'16"		

Table 6.3 Cycle Test Performance Characteristics

Run #	1	2	3	4	5	6	7	8	9	10	11	12	13	14	15	16	17	18	19	20	21	22	23	24	25	26	27
Jb[mA]	26.4	26.6	26.6	26.6	27.2	27.6	27.0	26.9	26.6	26.9	26.9	26.9	26.6	27.0	26.9	26.9	26.7	26.8	26.6	26.8	26.9	27.0	27.0	26.9	26.8	26.8	26.9
Ja[mA]	0.33	0.33	0.33	0.32	0.30	0.33	0.31	0.31	0.34	0.32	0.32	0.31	0.32	0.32	0.31	0.33	0.33	0.32	0.33	0.32	0.33	0.32	0.33	0.33	0.32	0.33	0.32
Va[V]	39.8	39.9	39.9	39.9	39.8	39.9	39.8	39.9	39.9	39.9	39.9	39.8	39.8	39.9	39.9	39.9	39.8	39.9	37.9	39.9	39.8	40.0	39.8	39.9	39.8	39.8	39.9
Vck[V]	17.9	17.8	17.9	17.7	17.1	17.2	17.3	17.3	18.1	17.5	17.5	17.3	17.6	17.3	17.2	17.8	17.8	17.6	17.6	17.6	17.3	17.3	17.3	17.5	17.6	17.4	17.3
Jck[A]	0.23	0.24	0.24	0.24	0.25	0.25	0.25	0.25	0.23	0.24	0.24	0.25	0.24	0.25	0.25	0.24	0.24	0.24	0.24	0.24	0.25	0.25	0.25	0.24	0.24	0.25	0.25
Vcv[V]	281	293	281	291	289	292	289	289	292	290	283	285	289	288	280	288	283	290	291	290	284	291	287	292	291	287	290
Jcv[A]	1.72	1.75	1.73	1.74	1.74	1.76	1.74	1.74	1.81	1.75	1.74	1.73	1.75	1.75	1.74	1.74	1.75	1.76	1.77	1.76	1.72	1.77	1.75	1.75	1.74	1.73	1.75
Vnk[V]	27.5	27.3	26.3	26.1	26.0	26.0	26.0	26.0	26.3	25.8	25.8	25.9	25.8	25.8	25.7	25.4	25.4	25.5	25.5	25.5	25.4	25.4	25.4	25.6	25.8	25.0	24.9
Jnk[A]	0.21	0.21	0.22	0.23	0.23	0.23	0.23	0.23	0.22	0.23	0.23	0.23	0.23	0.23	0.23	0.23	0.23	0.23	0.23	0.23	0.23	0.23	0.23	0.23	0.23	0.28	0.28
Vnv[V]	202	202	172	166	164	162	162	162	173	156	156	158	156	156	152	146	149	152	150	148	146	147	145	151	156	129	128
Jnv[A]	1.15	1.15	0.99	0.95	0.94	0.93	0.92	0.93	0.98	0.89	0.89	0.90	0.89	0.89	0.87	0.81	0.83	0.84	0.83	0.83	0.82	0.82	0.82	0.85	0.8	0.73	0.73
Vis[V]	244	258	245	258	257	258	257	257	245	257	244	256	256	258	244	258	243	257	257	257	252	257	256	259	259	259	259
Jis[A]	0.99	0.99	0.99	0.99	0.99	0.99	0.99	0.99	0.98	0.99	0.99	0.99	0.98	0.99	0.99	0.99	0.99	0.99	0.99	0.99	0.99	0.99	0.99	0.99	0.98	0.99	0.99
Tcv[℃]	274	273	274	273	273	273	272	271	275	274	274	273	274	273	272	276	275	273	273	274	273	274	273	275	275	274	274
Tnr[℃]	318	318	281	272	271	268	267	266	280	259	260	260	258	258	254	247	251	252	252	252	249	249	245	253	253	230	229
in(Main) [×10⁻³ g/sec]	7.8	7.7	7.9	7.8	7.6	7.6	7.5	7.4	8.1	7.9	7.9	7.8	7.8	7.7	7.5	8.2	8.1	7.8	7.8	7.9	7.6	7.8	7.8	8.1	8.1	8.0	7.9
in(№ 1) [×10⁻³ g/sec]	5.0	4.9	2.0	1.7	1.6	1.5	1.5	1.4	2.0	1.2	1.2	1.2	1.2	1.2	1.1	0.9	1.0	1.0	1.0	1.0	1.0	0.9	0.9	1.0	1.0	0.6	0.6
Isp[sec]	2200	2248	2208	2250	2326	2318	2346	2389	2151	2214	2238	2266	2235	2291	2343	2140	2156	2254	2258	2216	2304	2265	2279	1931	1931	2205	2220
THRUST[gWt]	0.17	0.18	0.18	0.18	0.18	0.18	0.18	0.18	0.18	0.18	0.18	0.18	0.18	0.18	0.18	0.18	0.18	0.18	0.18	0.18	0.18	0.18	0.18	0.18	0.18	0.18	0.18
η [%]	70	71	70	72	74	74	75	76	68	70	71	72	71	73	75	68	69	72	72	70	73	72	72	61	61	70	71
IDLING時間[min]	105	1	1	1	1	1	1	60	1	1	1	1	1	1	60	105	1	1	1	1	1	1	60	105	1	1	1
Total Power[W]	60.4	61.1	60.3	60.5	60.9	60.9	60.7	60.7	60.7	60.5	60.2	60.5	60.4	60.6	60.1	60.3	59.9	60.3	60.4	60.4	60.2	60.7	60.5	59.9	59.9	61.2	61.4
Test date	'80123				'80124			'80126				'80128				'801210				'801211				'801213			
Time data acquired	12/33 11:15'	12/ 3 13:43'	12/ 3 16:07'	12/ 3 18:38'	12/ 4 10:10'	12/ 4 12:43'	12/ 4 15:13'	12/ 4 18:37'	12/ 6 9:35'	12/ 6 12:43'	12/ 6 15:03'	12/ 6 17:29'	12/ 8 14:31'	12/88 16:59'	12/ 8 20:33'	12/10 11:25'	12/10 14:00'	12/10 16:19'	12/10 18:40'	12/11 10:41'	12/11 13:12'	12/11 15:47'	12/11 19:18'	12/13 12:19'	12/13 14:44'	12/13 17:10'	12/13 19:42'

Note:
Output of other power sources:
Vb, Va=1KV
Ja=0.35A
Vch, Jch, Vnh, Jnh = 0

- Data obtained 60 min. after beam injection.

Symbols -- Continued to next day while:

- O continuous evacuation
- ● exposure to air
- △ stopping evacuation

- Output of PSnk for runs #2,6 & 27 (others in broken line):

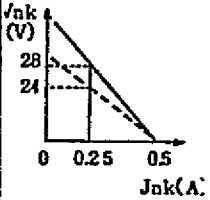

Fig. 6.14 Neutralizer Keeper Discharge Ignition Time vs. Cathode Heater Input

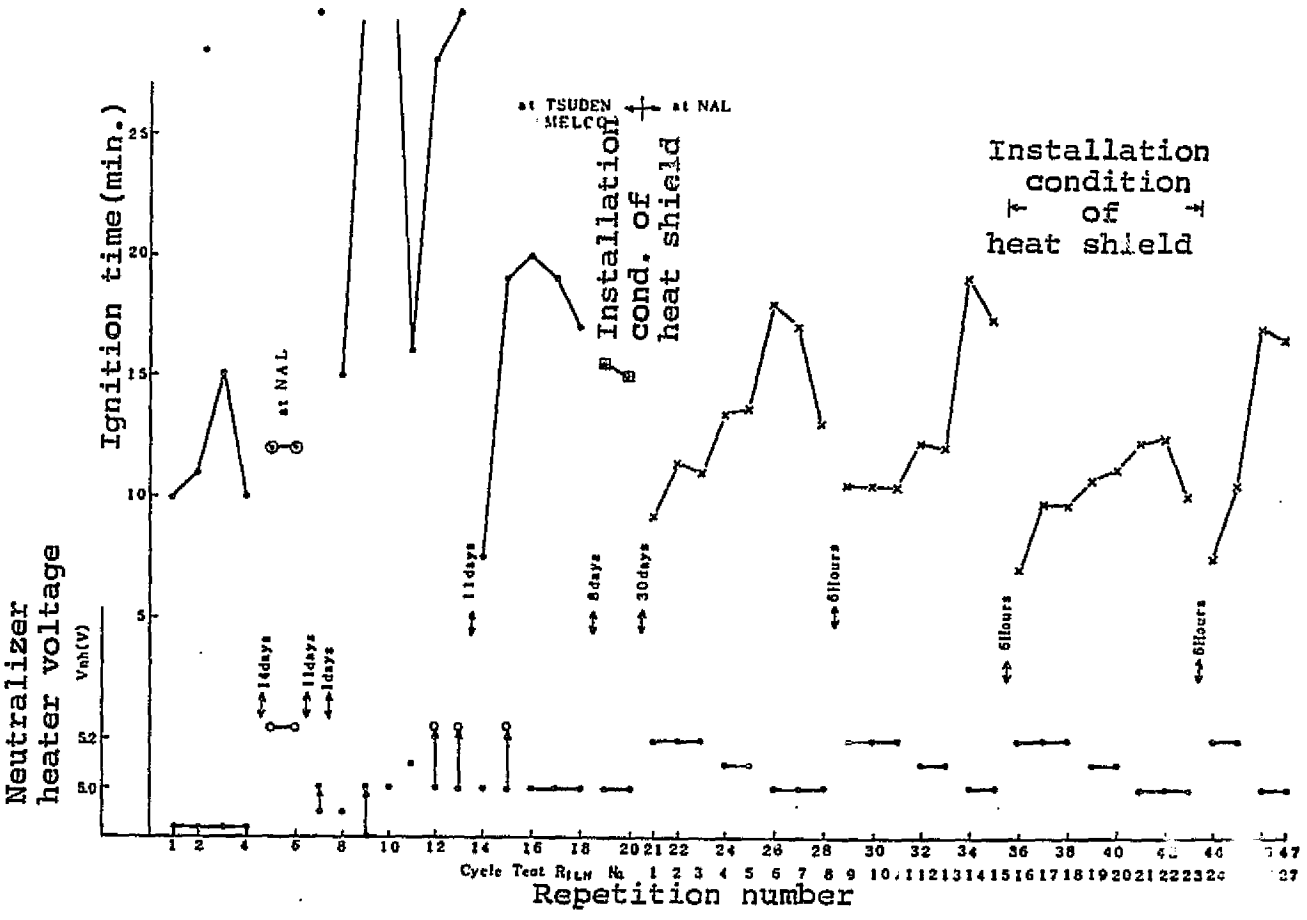

Fig. 6.15 FM PILOT(1) Neutralizer Ignition Time

Cycle 1: IDC after exposure to air = 105 min.
Cycle 2: " " " 1 min.
Cycle 3: " " " 105 min.
(w/ heat shield)
Cycle 4: IDL " " " 105 min.

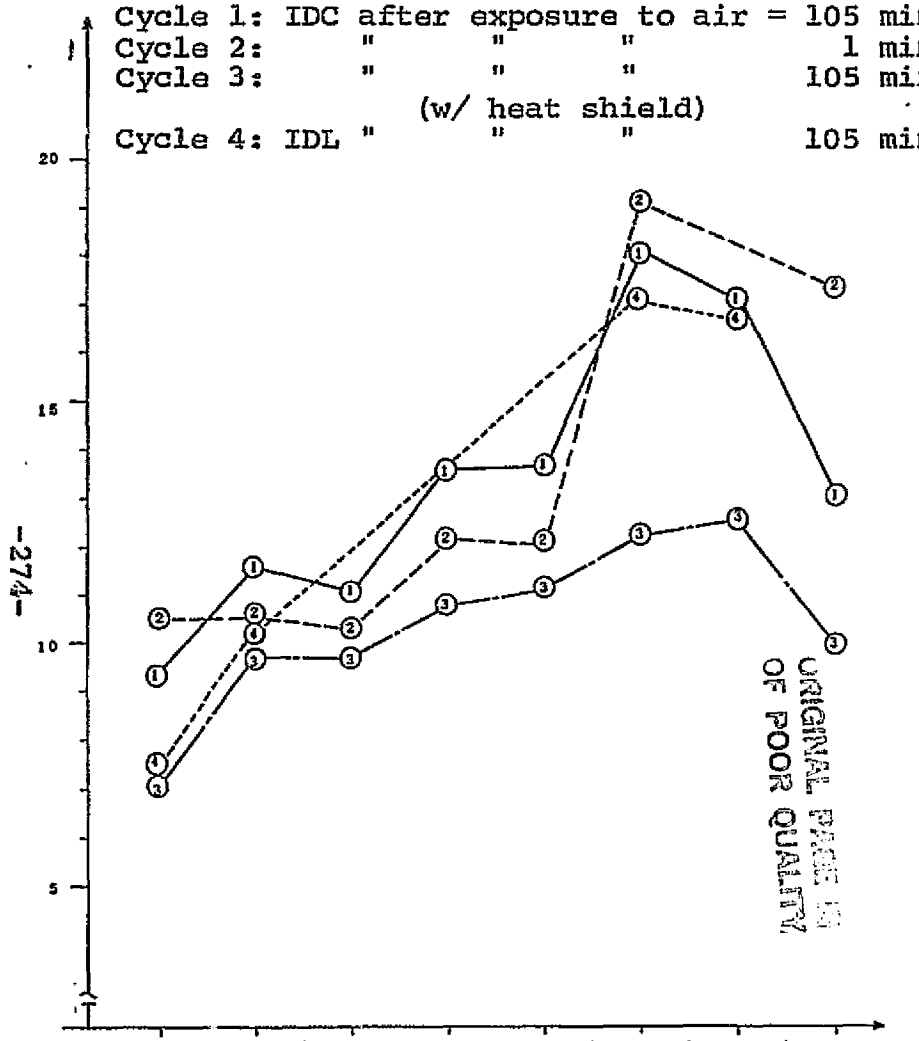

No. of tests	1 9 16 24	2 10 17 25	3 11 18 –	4 12 19 –	5 13 20 –	6 14 21 26	7 – 22 27	8 15 23 –
IDL	(1分) 105分	1分	1分	1分	1分	1分	1分	60分
Vnh	5.2V	5.2V	5.2V	5.1V	5.1V	5.0V	5.0V	5.0V

Fig. 6.16 FM PILOT(1) Neutralizer Ignition Temperature/Steady State Temperature

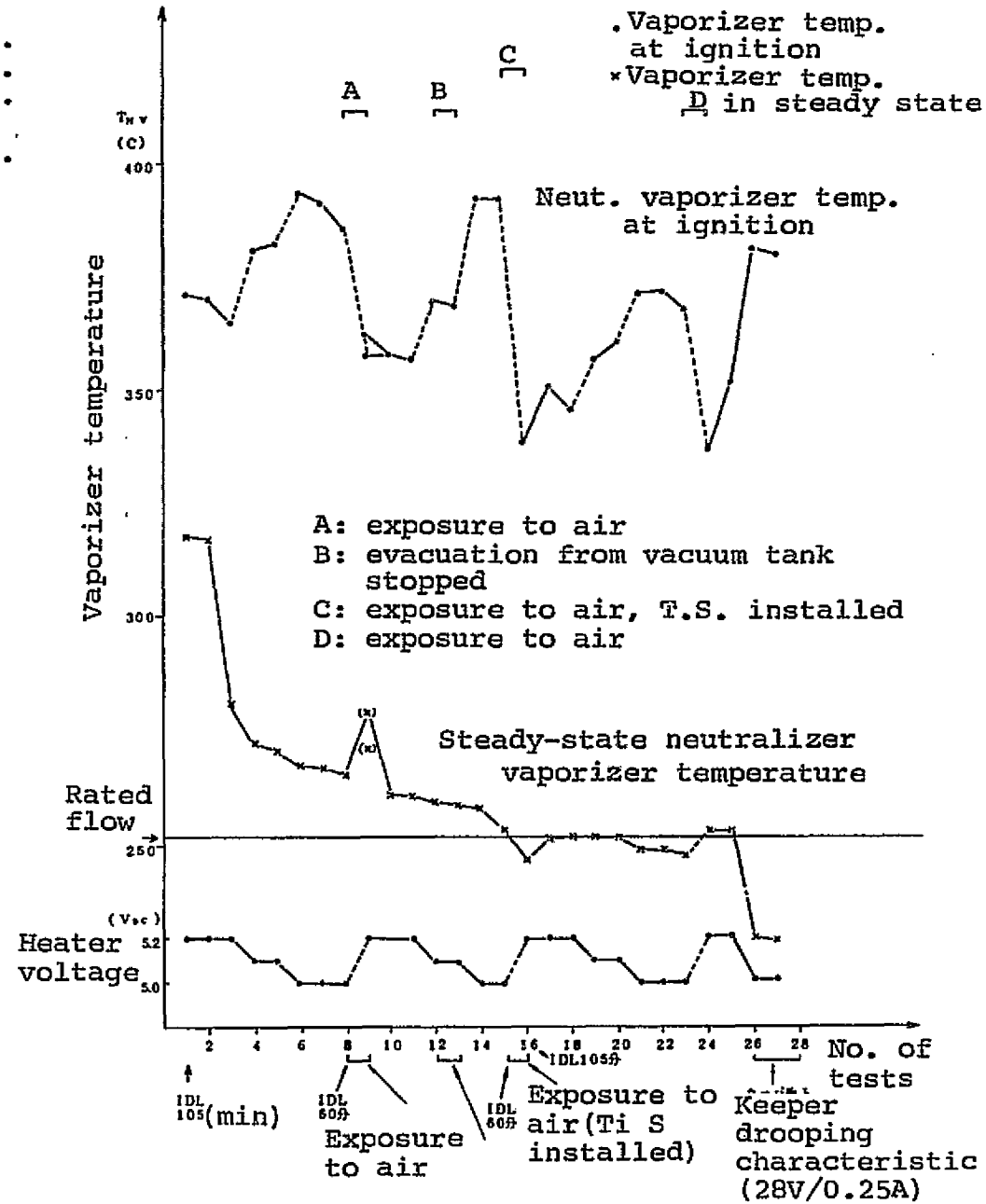

6.5.2 FN05 Repetition Test

(1) Purpose

Study operation conditions under which stable ignition characteristics of neutralizer keeper discharge are obtained.

(2) Test results

History of cathode heater input and ignition is shown in Fig. 6.17. Based on the results,

i) For a certain time after completion, ignition characteristics of hollow cathode are likely to be affected to an extent by exposure to air;

ii) During this time, ignition conditions can be returned to normal with 2-5 operations after exposure(cathode heater input($5.2V_{DC}$) required); and

iii) After this period ignition characteristics are stabilized, with no ill effects from the exposure.

From the above results, following was to be reflected in the FM, Acceptance Tests and Space Tests:

i) Input to neutralizer cathode heater will be a minimum of 5.25V; and

ii) After exposing to air, the first operation will be started immediately after 90-120 minutes idling.

Fig. 6.17 FN05 Ignition Time(Life Test)

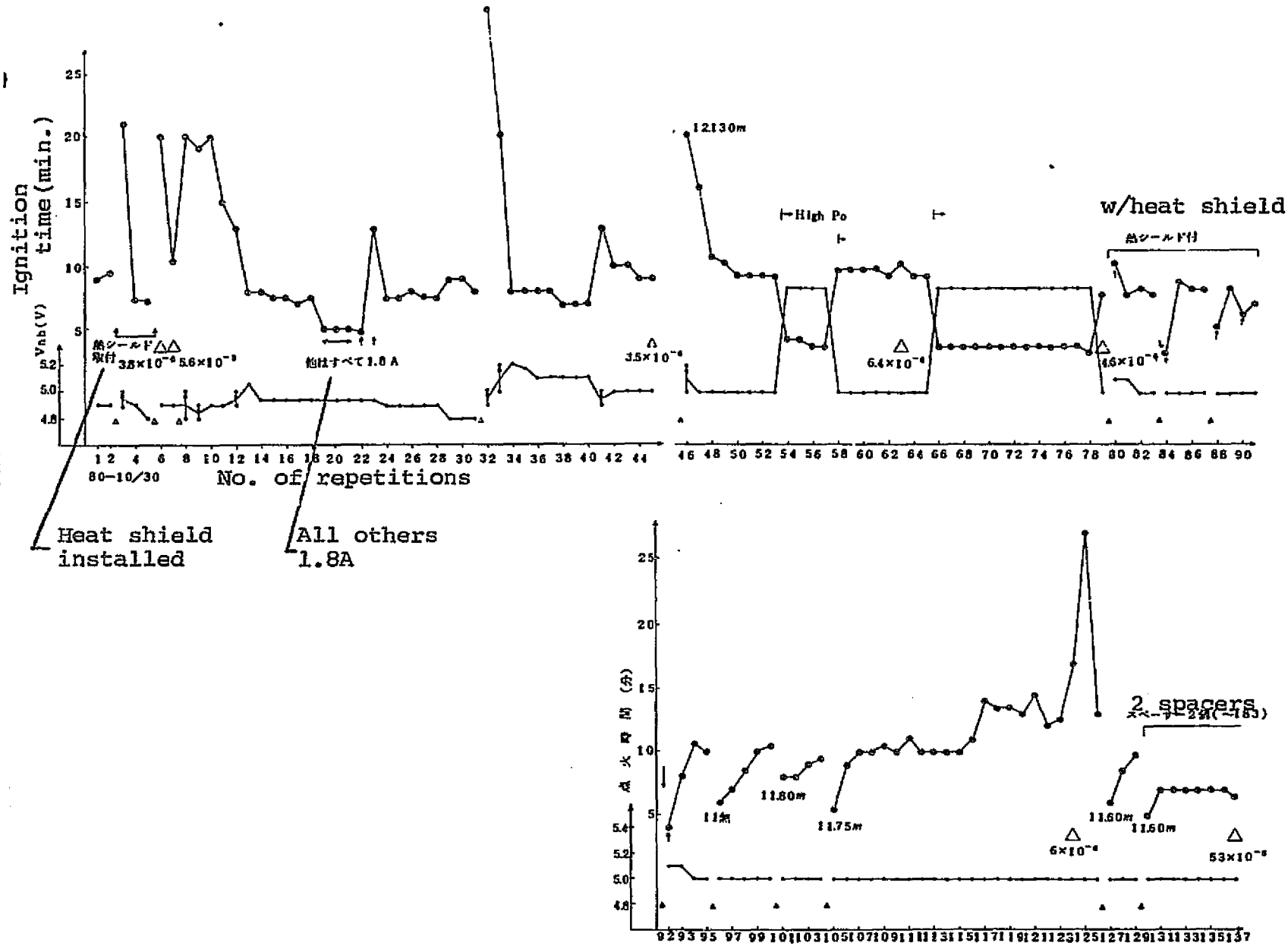

6.6 Contamination from Back-spattering

(1) Description of problem

Neutralizer keeper did not ignite in the electromagnetic compatibility test of IES(2) in QT.

(2) Steps taken

·Operation attempted again(twice) - No ignition resulted.

·Keeper electrode insulation resistance measured from the outside of the tank.

Main cathode keeper Rck=123.9kΩ
Neutralizer cathode keeper Rnk=5.98kΩ
15-minute activation
Rck ~20MΩ
Rnk ~ 3KΩ

·Neutralizer heated (junction box used)

Inh=2 A, 30 min Rnk= 18KΩ → 14.2KΩ
Inh=3 A, 30 " Rnk=18.3KΩ→11.8KΩ
Inh=4 A, 30 " Rnk=11.8KΩ→12 KΩ

·Operation attempted under the original configuration - No ignition resulted. Heated again to see if mercury adhesion was the cause.

Results indicated that there was no possibility of mercury adhesion. Visual inspection of IEE#2 and measurement of resistance of engine unit as a single component were carried out next.

(3) Results of visual inspection

The entire surface of neutralizer keeper lead support was contaminated.

Measured resistance:

Connector	18.63KΩ
①	1.2MΩ
②	14.99KΩ
③	4.44KΩ

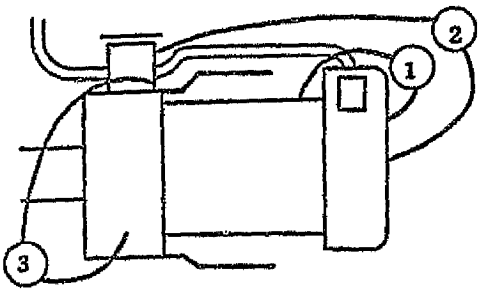

With these results, Mitsubishi Electric was asked to inspect and treat IEE#2.

(4) Inspection and treatment

Recovery of insulation was attempted by self-heating of neutralizer keeper. Neutralizer was placed in a chamber and voltage of 4V and 200V were respectively applied to cathode heater and keeper. Keeper voltage was increased to 1.8kV and the final leakage current was 2mA. Insulation resistance recovered to 50M and no disorder was observed during ignition check.

(5) Causes and measures

Decrease in keeper insulation resistance was caused by metal material adhering to the ceramic keeper lead support during long-duration test. Judging from the conditions of contamination, the material seems to have been backspattered from vacuum tank by ion engine injection beam. Especially with the position of ion engine inside the chamber, it is possible that injected ion beam hits the gate valve flange near the engine.

Based on the above, following countermeasures were planned for FM.

i) For operating environment, degree of vacuum of under 2×10^{-6}Torr during non-operation and under 5×10^{-6} Torr during operation.

ii) Duration of evacuation after exposure to air of over 8 hours.

iii) Installation of a spatter guard of Ti plate. Ti has the smallest mercury spattering rate among metals and also has a good absorbency of spattered material. Shape of the spatter guard is shown in Fig. 6.19.

iv) As above measures do not entirely prevent contamination,

a shield will be installed on a neutralizer, which serves not only as a spatter shield but a heat shield as well. Shape of this guard is shown in Fig. 6.20.

Fig. 6.19 Spatter Guard

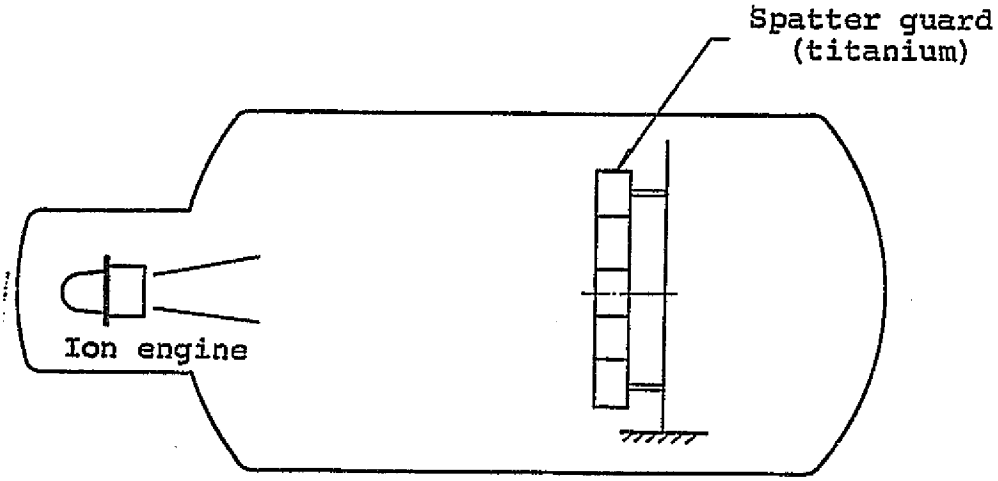

Fig. 6.20 Shape of Neutralizer Shield(See Fig. 4.3 for mounting conditions)

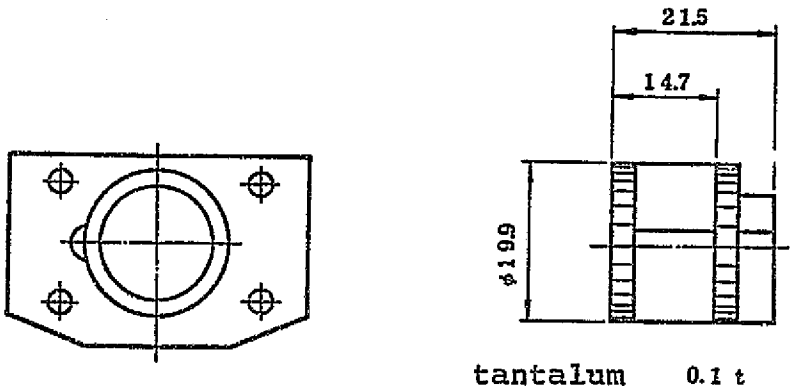

6.7 Reduction of Power Consumption of Power Sources

Main problem in the development test of IEP component and in the production of its PM was with electric power. For PS1 and PS2, which use the largest power and high voltage, converter transformers made by Tamura Manufacturing Co. were to be used.

However, with Tamura's model 301, efficiency of circuits in PS1 and PS2 was found to be considerably lower(73-74%) compared to the calculated value(83%). When replaced by a converter transformer made by Toshiba(TNQ2772) used in BBM and PreEM, value equal to the calculated value was obtained. In order to meet the schedule, this Toshiba model was used in IEP of EM until an improved Tamura model was ready. Model 301-4, reaching the efficiency of 77%, was planned to be used from PM on, when it was determined that no more improvements could be expected. This model had 2.8W more power than the Toshiba model, and, with 93.8W in power source device and 98.0W in IEP, was designed to meet the specification of less than 95W and less than 100W, respectively. However, there was a calculation mistake of power consumption in the CDR input package, and it was found that power consumption of IEP exceeded 100W(105.8W) when the engine unit operated at the specified maximum of 68.6W. As the maximum of power source PS9 was lowered from 1.4A to 1.2A(See Section 6.2) in IEE, specified maximum operation power of IEE was changed from 68.6W to 68.0W, and at the same time efforts were made to save power in IEP. In spite of this, it became increasingly difficult to continue the use of this Tamura model in PS1 and PS2 in view of power loss. It was because NASDA-approved Tamura model used a special insulation method in order to accommodate high corona voltage(AC 2.3kV). It was therefore decided that the same insulation method as Toshiba model would be employed and the corona

resisting voltage would be lowered to AC 1.3kV(equivalent of DC 1.4kV x 3), based on which trial products were made and evaluated. Finally, 1086W-loss was obtained with trial product #3, which was selected for use in PM and subsequent models. It was also found that about 1W could be saved by eliminating choke coil for EMC countermeasure. In order to do so, specified value of allowable transmission interference noise of power source line was changed from 10mAp-p to 30mAp-p at 100KHz - 10MHz. Power consumption cut was attempted also by switching to a low-loss operatinal amplifier, reviewing the standard voltage circuit for possible sharing, etc. In this way, input power of IEP satisfied the specified value of 100W or less(93W in PM and 95W in FM).

6.8 Measures For High Voltage Unit of Power Source

IEP generates a maximum voltage of 1.4kV and minimum of -1.4kV. Measures for prevention of high voltage accident in space environment are summarized below. An accident in the high voltage unit of BS had just been reported, with which comparison was made.

Configuration of high voltage unit was designed with the following guidelines.

i) High voltage circuit will be potted with epoxy resin(STYCAST 1090 SI) to improve pressure resistivity and to scale down.

ii) Base plate components will be potted with epoxy resin or given conformal coating of polyurethane resin(SOLITHANE 113) to improve pressure resistivity.

iii) Flying lead wire will be used for connection between high voltage circuits, except for interface between devices, and ends are either potted or given conformal coating.

iv) In order to prevent deterioration with time, wire-wound part where AC voltage operates will be designed in such a way that it does not generate partial discharge(corona-free).

Parts used in high voltage unit in IEP are listed in Table 6.4. Design and analysis of each part are discussed below.

(1) Converter transformer

Converter was produced according to NASDA-QTS-39013(Common Specifications(plan)for Reliability-guaranteed Low-frequency Coil, Power Source Transformer and Low-frequency Transformer for Space Development), and its voltage, withstand voltage and corona voltage are shown in Table 6.5. High voltage breakdown/deterioration mode to be considered and analysis results are given below.

i) Insulation breakdown due to deterioration caused by

partial discharge

Each converter transformer does not generate partial discharge at operating potential level.

ii) Insulation breakdown due to heat/mechanical deterioration

Each part of converter transformer has been tested for heat shock, partial discharge and withstand voltage and passed evaluation test, and thus considered safe for this mode.

iii) Insulation breakdown due to heat deterioration of materials

Withstand heat range of main materials used in each converter transformer are as shown in Table 6.6. Heat deterioration due to operation temperature can be ignored.

(2) Printed substrate

Spacing of high voltage patterns inside the printed substrate was designed with the values set under "conductor gap when protective film is used" in Table 1, NASDA-QTS-1023/101. For example, design standard for voltage of 1.4kVo-p is over 4.27mm, but the design value for minimum conductor gap, under the table, is 8mm.

(3) High voltage connectors

Connectors made by AMP Co. for IEP are of the standards shown in Table 6.4. Joints with high voltage wires potted, they were used in combination with high voltage connectors, made also by AMP Co., and given 3-month continuous tests by applying twice the voltage to be used under a thermal vacuum(55C, 10^{-8}Torr) to check that there were no discharge and deterioration.

(4) High voltage cables

MIL-W-81044 polyalkene wires were used.

(5) Materials for potting and conformal coating

Potting resin below was selected for material stability, specific gravity, resin setting conditions, insulation properties, etc.

Material...Heat-setting epoxy resin

Manufacturer...Emerson & Cumming, Japan, Inc.

Product name...Stycast 1090SI

Its properties are shown in Table 6.7. Glass setting temperature was about 80C.

Coating material was selected for material stability, resin setting conditions, electrical properties, temperature characteristics, etc.

Material...Heat-setting polyurethane resin

Manufacturer...Thickol Chemical Corp.

Product name...Solitane 113

Its properties are shown in Table 6.8.

These materials have been approved by NASA for potting and coating.

In order to evaluate reliability of potting and coating of printed board, heat shock test was given. Stycast 1090SI was potted on IEP high voltage unit(without electronic parts mounted on the board, one sample) and given the tests shown in Fig. 6.21. Results were good, as shown in Table 6.9. Similar tests were performed for the coating material, with distribution capacity and tanδ tests added to the early-stage and final-stage performance tests. Results were also satisfactory. Further, heat shock test(washer test) was performed to evaluate crack resistivity of potting material(Stycast 1090SI). As shown in Fig. 6.22, 5 samples with washers potted were tested. No cracking or chipping was observed on the resin surfaces.

Table 6.4 Parts Used In High Voltage Unit

Circuit symbol	Name	Parts no.	Rated	Design standards	Design value
A3CR1 ~A3CR4	Diode	R9208P1 (F30)	V_R = 3 KV I_O = 100mA	V_R < 1.5KV I_O < 50mA	V_R = 1.4KV I_O = 30mA
A3CR5 ~A3CR8	Diode	R9208P1 (F30)	V_R = 3 KV I_O = 100mA	V_R < 1.5KV I_O < 50mA	V_R = 1.4KV I_O = 1mA
A3C1 A3C2	Paper condenser	43-B3004S-003 (CMR1A302502K)	0.05 μF 3 KV	1.5KV以下	1.4KVmax
A3R2 A3R8	Wire wound resistor	MSFC85M03560 SHV70F1505	15MΩ 1W 3.5 KV	0.5W以下 4.375KV	0.13W 1.4KVmax
IPA(B)J5 IPA(B)J6	Round high voltage connector	41-B0234S-002 (862004-1)	15KV	3.75KV	2.8KVmax
A1T1	Converter transformer	SD0284P301	–	–	–
A1T2	Converter transformer	SD0284P302	–	–	–
A1T3	Converter transformer	SD0284P303	–	–	–
A1T5	Converter transformer	SD0284P304	–	–	–
–	Wiring material	44/0611A	25KVrms	1.77KVo-p	1.4KVo-p
–	Printed board	MPC30183B	–	–	–

Table 6.5 Voltage Used, Withstand Voltage and Corona Voltage Specifications For High Voltage Converter Transformer

Parts no.	Location used	Voltage used	Withstand voltage (reduced pressure, ↓ 減気圧8mmHg)	Corona voltage
SD0284 P301	IEP PS1, 2	1400Vo-p	1750V r.m.s	>1300V r.m.s以上
SD0284 P302	IEP PS3	+1400V Float 40Vo-p	1250V r.m.s	>1400VD.C以上
SD0284 P303	IEP PS4	+1400V Float 6Vo-p	1250V r.m.s	>1400VD.C以上
SD0284 P304	IEP PS5	+1400V Float 300Vo-p	1250V r.m.s	>1400VD.C以上
SD0284 P332	Visi-con(?) high voltage power source	500Vo-p	625V r.m.s	>1400VD.C以上

Table 6.6 Main Insulation Materials for Conver Transformer and Their Withstand Heat

Parts	Material	Product name	Withstand heat
Electrical wire	PEW	Esmet Wire	130C
Insulation tape	Poly imid film	Capton	180C
Impregnant	Epoxy resin	Stycast 1090SI	107C

Table 6.7 Characteristics of Potting Material

Subject	Unit	Value
Electrical characteristics:		
Dielectric breakdown strength	V/mil	375
Permittivity(1MHz)		29
Dielectric power factor(1MHz)		0.001
Volume resistivity	Ω-cm	10^{14}
Physical characteristics:		
Compressive strength	Kg/cm²	703
Elasticity	Kg/cm²	1.4×10^{4}
Bending strength	Kg/cm²	281
Shrinkage rate when hardened	cm/cm	0.003
Hardness		78D
Thermal characteristics:		
Thermal conductivity	cal/cm. sec. ℃	4.1×10^{-4}
Coefficient of thermal expansion	cm/cm℃	54×10^{-6}
Temperature used	℃	−73~+107
Total weight loss(TWL)	%	0.74
Vaporized condensed material(VCM)	%	0.09

Table 6.8 Characteristics of Coating Material

Subject	Unit	Value
Electrical characteristics:		
Dielectric breakdown strength	V/mil	378
Permittivity(1KHz)		4.2
Dielectric power factor(1KHz)		0.162
Volume resistivity	Ω-cm	25×10^{14}
Physical characteristics:		
Tensile strength	Kg/cm²	28
Extension rate	%	100
Tear strength	Kg/cm	25
Hardness(27C)		60A
TWL	%	0.31
VCM	%	0.04

Fig. 6.21 Heat Shock Test of Potting Material(sample: printed substrate equivalent of high voltage unit)

Test sequence

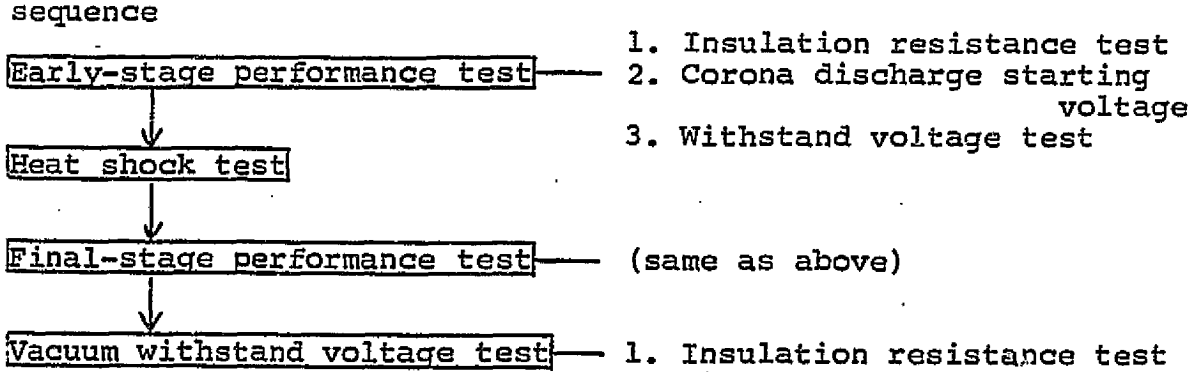

Heat shock test conditions:

Temperature profile -

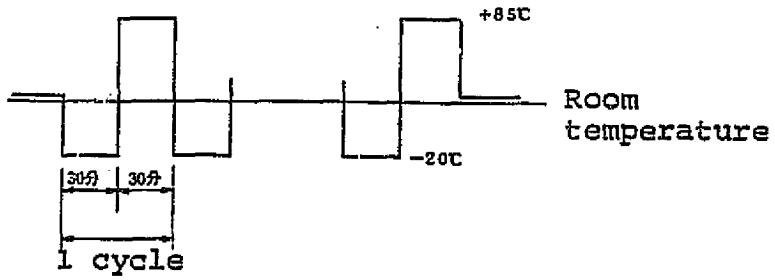

Number of test cycles - 120

Table 6.9 Results of Heat Shock Test

	Performance test: early stage	Performance test: final stage	Vacuum test
1. Insulation resistance test	DC500V	DC500V	DC500V
1) +1400V line	>100×10⁴Mn.	>100×10⁴Mn	>100×10⁴Mn
2) −1400V	〃	〃	〃
2. Corona discharge starting voltage	AC25KV	AC25KV	
1) +1400V line	No corona	No corona	—
2) −1400V 〃	No corona	No corona	
3. Withstand voltage test	DC28KV1	DC28KV1	DC28KV1
1) +1400V line	Normal	Normal	Normal
2) −1400V 〃	〃	〃	〃
4. Visual inspection of appearance	Normal	Normal	Normal

Fig. 6.22 Heat Shock Test of Potting Material(sample: washer)

Sample: Washer potted in dimensions shown at right.
5 samples.

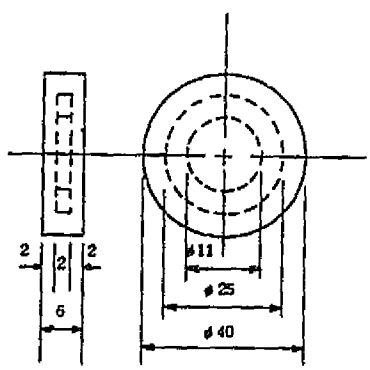

Heat shock test conditions:

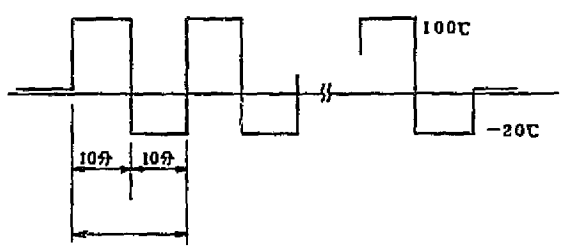

Room temperature

1 cycle 5 cycles repeated continuously.

Chapter 7

Satellite System Test and Compatibility

Presented in this chapter are the results of system-level tests with the ion engine system installed on a satellite and the evaluation of their compatibility. Section 7.3 contains evaluation based on the system analysis.

7.1 Outline of Tests

Development tests for ETS-III at system level involved, for the purpose of solidifying design, EM combination tests, structural model tests(static and dynamic load structural model tests), heat model test, etc. Of special concern to IES were electromagnetic compatibility test in the combination tests and heat model tests. They are discussed in detail in Section 7.3. Actual EM of the engine was used in IES electromagnetic compatibility test, while in other tests dummies of electrical load, mass and heat were used instead.

In the production tests, Qualifying Tests were given to PM and Acceptance Tests were given to FM. Qualifying Tests were aimed at establishing design and production schedule, and were executed for the subject matters and under the flow shown in Fig. 7.1. As an unexpected trouble occurred in the Acceptance Tests which required a testing schedule change, the flow is partially irregular. Acceptance Tests were given for the subject matters and under the flow shown in Fig. 7.2 for the purposes of checking functions and performances and verifying propriety of production schedule. Acceptance Tests followed the basic launch(?) sequence, with acoustic test eliminated.

Although power conditioner was installed on the satellite for the production tests, it was decided that, as a rule, the actual engine would not be used in the system test for the following reasons: Deterioration of engine performance due to air-exposure is expected;

In the event of mercury leakage, safety of people and satellite would be a problem; It can operate only in vacuum, etc. Engine substitutes are indicated in ◯ in the figure. In the Acceptance Tests, actual FM of the engine was used only in alignment test and the rest used dummies or actual PM. Thus, environment resistivity could be checked only for the power conditioner in the system tests. In the electrical performance tests before and after environment test, electrical load dummy was used to check telemetry/command function, power source device output, and logical control function of power source control device against telemetry output.

Qualifying Tests were completed in 9 months and Acceptance Tests, in 7½ months. For overall system tests, refer to the "Report on ETS-III Development Results."[1)]

Fig. 7.1 Qualifying Test Execution Schedule for ETS-III PM System

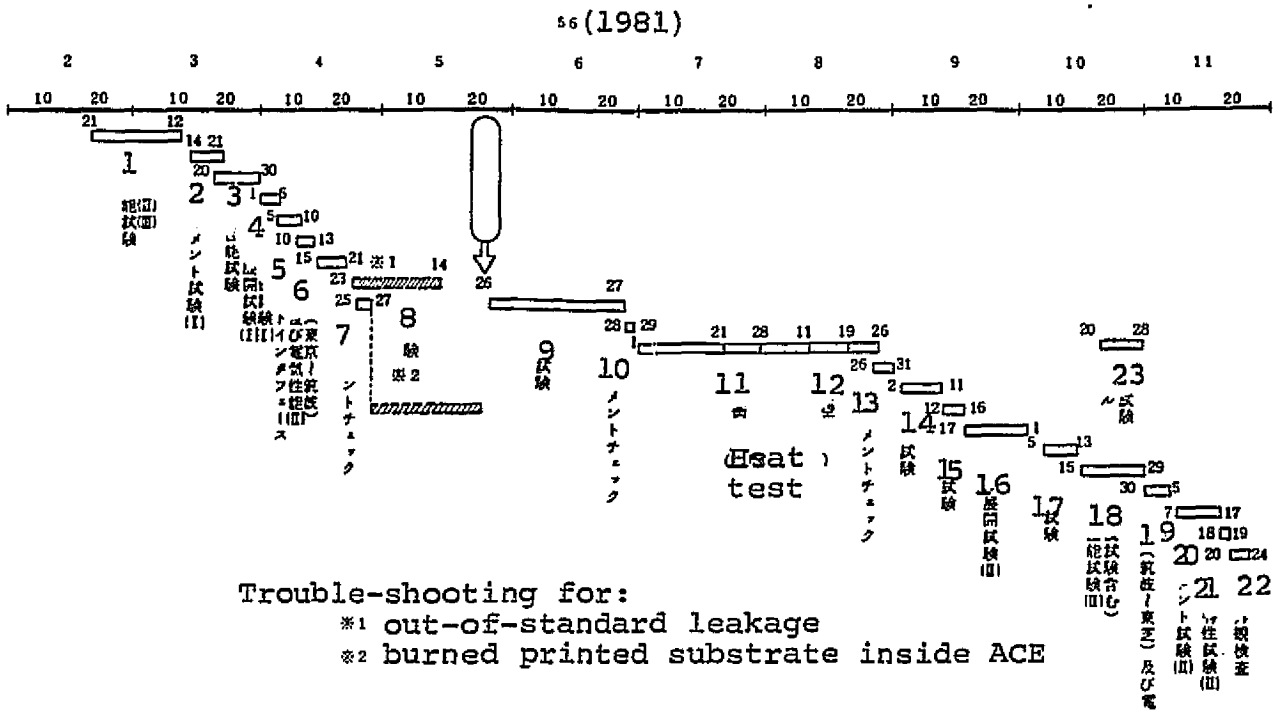

Trouble-shooting for:
※1 out-of-standard leakage
※2 burned printed substrate inside ACE

1. Electrical performance test(I),(II) and (III)
2. Alignment test(I)
3. RF performance test
4. Paddle turning test(I)
   Mass characteristic test(I)
5. Rocket interface
6. Transporting(Tokyo to Tsukuba) and electrical performance(II)
7. Alignment check
8. Leakage test
9. Oscillation test
10. Alignment check
11. Heat balance
12. Thermal vacuum
13. Alignment check
14. Acoustic test
15. Shock test
16. Paddle turning test(II)
17. Magnetic test
18. Electrical performance test(II)(includes leakage test)
19. Transporting(Tsukuba to Tokyo) and electrical performance(II)
20. Alignment test
21. Mass characteristic test
22. Final appearance inspection
23. Paddle irradiation test

Fig. 7.2 Acceptance Test Execution Schedule for ETS-III FM System

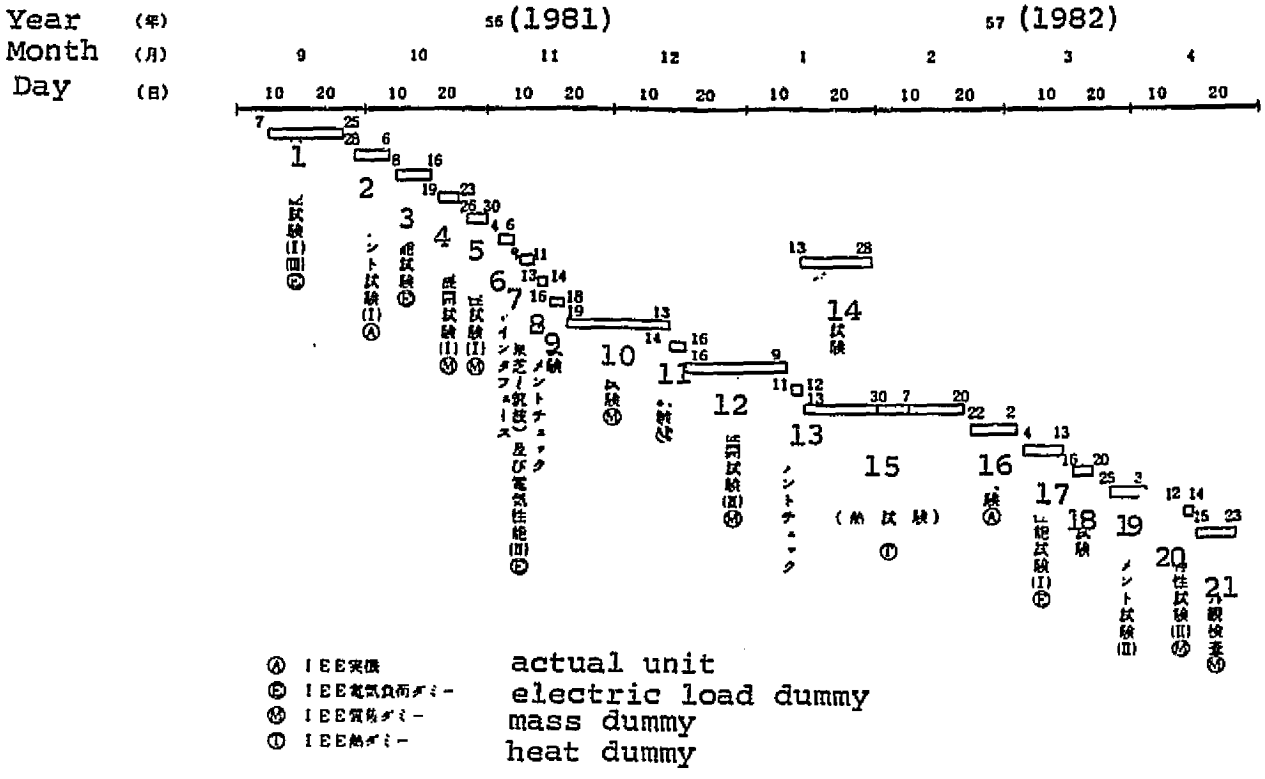

1. Electrical performance test(I) and (III) Ⓔ
2. Alignment test(I) Ⓐ
3. RF performance test Ⓔ
4. Paddle turning test(I) Ⓜ
5. Mass characteristic test(I) Ⓜ
6. Rocket interface
7. Transporting(Tokyo to Tsukuba) and electrical performance(II) Ⓔ
8. Alignment check
9. Leakage test
10. Oscillation test Ⓜ
11. Shock test Ⓜ
12. Paddle turning test(II) Ⓜ
13. Alignment check
14. Paddle irradiation test
15. (Heat test) Thermal vacuum Ⓣ
16. Magnetic test Ⓐ
17. Electrical performance test(I) Ⓔ
18. Leakage test
19. Alignment test(II)
20. Mass characteristic test(II) Ⓜ
21. Final appearance inspection Ⓜ

7.2 Test Results

Development tests relating to IES were those of electromagnetic compatibility and heat model. There was no problem with the former, while results of heat model test called for a review of some aspects of heat design of the satellite, which was reflected in detail design.

In the production test, a trouble occurred during QT of RF performance test in which telemetry output of IES main cathode keeper current shut off. The cause was determined to be that the diode (NASDA TX1S-2204),used for rectifying telemetry signal power source, opened and failed due to insufficient derating of transient current when power was supplied. Transient current in similar type circuits was studied using EM, etc., and 13 diodes with insufficient derating (50%) were replaced by JAN TXV IN645-1. Same was done for FM. As this required digging up potted diodes and repotting the replacements, oscillation and heat cycle tests were performed and any presence of cracks was checked by X-ray.

There were no other IES-related problems in the system production tests, and thus, it was determined that functions and performances of power source device and power source control device satisfied requirements. Table 7.1 is a summary of IES-related Qualifying and Acceptance Tests. As stated previously, performance of the engine unit was not tested on the system level.

Table 7.1 IES-related Results of Satellite System Tests

	QT	AT
EPT(I) first time	I_{in} #1 Bus On 0.300A, Beam On 3.34A #2 Bus On 0.300A, Beam On 3.31A	I_{in} #1 Bus On 0.321A, Beam On 3.37A #2 Bus On 0.321A, Beam On 3.42A
Alignment(I)	#1 $\theta_y = 0.096°$ $\theta_z = 0.151°$ #2 $\theta_y = -0.027°$ $\theta_z = 0.050°$ 再現性 0.07°	#1 $\theta_y = -0.238°$ $\theta_z = -0.008°$ #2 $\theta_y = 0.022°$ $\theta_z = 0.059°$ 再現性 0.03°
Mass characteristic IEE position (−439, ±100, 916) Center of gravity	At launch / After paddle expansion / Final stage operation 重心 x 0.05 / −0.7~0.7 / −0.6~0.8 y 0.03 / −0.4 / −0.3 z 731.4 / 673.1~674.4 / 665.5~666.9 unit **	At launch / After paddle expansion / Final stage operation 0.01 / −1.0~0.9 / −1.0~1.1 0.01 / 0.4 / 0.5 730.7 / 672.5~674.5 / 664.9~667
Shock	X-component Peak G M(III) SRS 17, 13G *M(III): Mission Panel II	M(III) - not measured
Paddle expansion (II)	X-component peak G EPS / M(III)* -Y expansion: 66, 75 / 120, 93 +Y expansion: 770, 660 / 160, 90	M(III) - not measured
Heat balance	Low temp. case** min. / High temp. case*** max. IP base 0.7℃ / 21.2℃ IR base −0.4 / 14.8 IEE base 2.0 / 26.2 ** solar On/Off, α=90°, IR_s 380W/m², spin, IES Off ***solar On, α=21.5°, IR_s 380W/m², spin, IES On P_{th} = 35W, P_{in} = 581W	
EPT(I) Final	I_{in} #1 Bus On 0.300A, Beam On 3.36A #2 - not tested.	I_{in} #1 Bus On 0.321A, Beam On 3.40A #2 Bus On 0.321A, Beam On 3.42A

7.3 System Compatibility

7.3.1 Electromagnetic Compatibility

Ion engine basically generates electromagnetic waves in order to accelerate discharged and charged particles. Power source device is composed of many switching regulators which generate higher harmonic noise. Based on the flight data from the U.S. it was thought that with grounding system, shield, etc. in the sub-system, noise would not be a problem. However, data on radiation noise obtained by operating PreEM engine with ground testing power source in the engine unit PDR showed that noise level was not within tolerance. Therefore, in EM, electromagnetic interference was measured in the engine and in the power conditioner separately, and also in the combination of the two as a sub-system. Further, it was decided that electromagnetic compatibility would be tested at the system level.

EM of IES was later produced. Measurements made of the engine unit with the ground testing power sources were over the tolerance level, while measurements in a single power conditioner unit and in the sub-system were within the tolerance(See Section 4.4.5).

In order to study electromagnetic compatibility with TTC system on the system level, the engine(EM) was placed in an FRP vacuum chamber called EMI simulator, as shown in Fig. 7.3 and operated under the similar configuration to that in actual boarding. FRP was chosen for its superior electromagnetic wave permeability and little danger of breaking, as it is stronger than glass. TTC system was boarded on the +X-plane of the satellite, power conditioner was boarded on the inside of -X-plane and ion engine, on the outside, with -X-plane separating the vacuum and atmosphere. Satellite(S/C) and vacuum chamber were placed inside wave darkroom, and simulated S/C power

source and evacuation system(helium compressor for cryo pump, rotary pump, etc.) were placed outside. Outline of the vacuum chamber is shown in Fig. 7.4. The chamber was developed specifically for this test. It is unique in that its main structural material is FRP, and with the degree of vacuum of 4 x 10^{-4}Pa, degasing is no longer a problem.[2)]

When the engine was beam-injected, AGC level of VHF command receiver on the satellite side increased by 8dBm, to -95dBm. This was 1dBm less than the worst case reception level of -94.2dBm (ground transmitter output of 40W, altitude of 1,200km and elevation of 5°), but judging from the sub-system test results shown in Section 4.4.5, it was thought to be a problem of test configuration(effects of multipassing into the wave darkroom of vacuum device, equipments, etc., or effects of grounding system) No fluctuation of AGC level was observed with S-band.

From these results it was concluded that there was no operational problem even in the worst case if S-band was used in command transmitter or if the output was 400W in VHF.

No significant increase in AGC level of VHF by IES operation has been confirmed by the flight data of ETS-III so far obtained.

Fig. 7.3 EMC Test Configuration

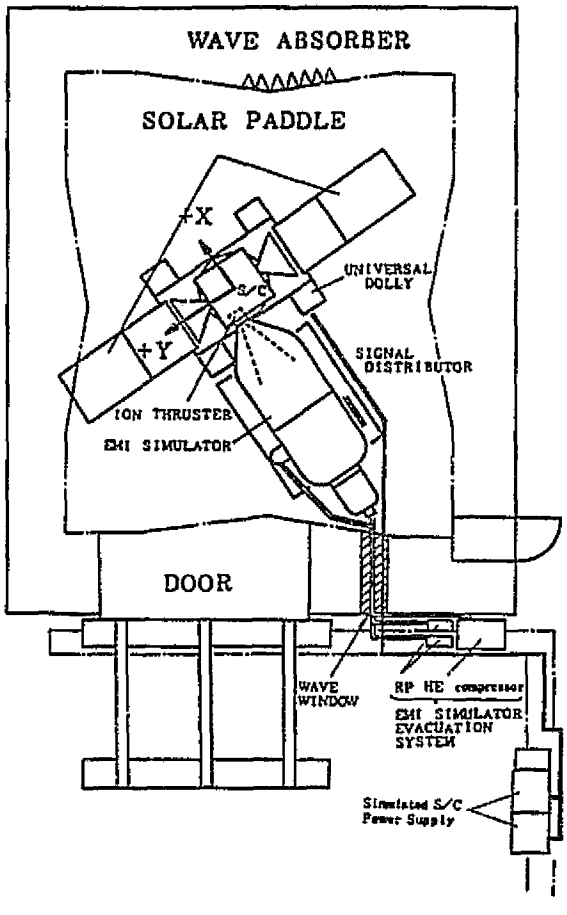

Fig. 7.4 Composition of EMI Simulator

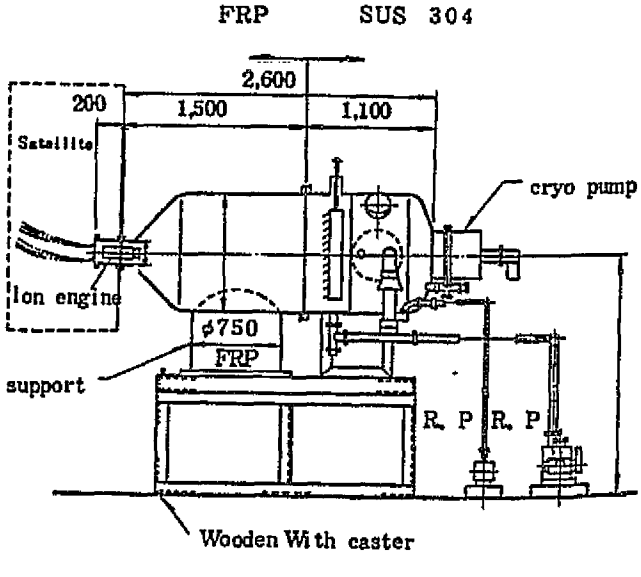

7.3.2 Heat Control System

(1) Development test

Engine and power conditioner are boarded on a louver heat control surface called Mission Panel II(See Fig. 4.10).

To check the propriety of heat design, heat model utilizing a structure of a static load structural model was made, and heat balance test was performed. Heat dummy, described later, was used in place of engine.

As a result of its evaluation and analysis, changes in mathematical model of the satellite and in ACS-related power consumption became necessary.

Based on the results of heat analysis it was estimated that with the present design the temperature increase inside satellite over a long period of IES operation was large, with some components(batteries, tape recorder, etc.) exceeding AT temperature. Therefore, it was decided that radiation surfaces of TTC and EPS panels would be enlarged and that the heater on the Mission Panel II would be removed. Also, with the knowledge that the ion engine was the largest heat generating equipment on the ETS-III, its mathematical heat model and heat dummy were reviewed for accuracy.

As a mathematical heat model of the engine unit, 3-node model shown in Fig. 7.5 had been submitted by Mitsubishi Electric Co. Because of the accuracy improvements required by the heat analysis, it was changed to a 10-node model shown in Fig. 7.6. Steady-state temperature distribution during beam injection with a constant satellite base plate temperature of 55C, determined by the 10-node model, is shown in Table 7.2. Overall, the results are higher than the actual engine, with the heat flow into satellite being about 20% more than

the actual. Thus, mathematical heat model and engine unit are not in complete agreement, which, along with operational analysis, requires further work.

Heat dummy of the engine used in development test was produced by Toshiba based on a 3-node model. Because this in itself was a rough model and because of lack of information on the surface optical properties of the engine, etc., the dummy's heat flow into satellite was considerably more than the actual engine's.

On one hand, heat-simulated ion engine had been studied jointly by NAL and NASDA in 1979. It was a structure similar to the actual engine, with plasma load replaced by a sheath heater. Heater resistance was matched with plasma impedance. As mercury's effects on heat capacity and heat transmission could not be ignored, the tank was filled but the supply was cut off by a blind board, inserted between vaporizer and mercury tank flange. Heat vacuum test of this heat-simulated ion engine confirmed that it had heat characteristics similar to the actual engine.[3)]

The results were incorporated into the Toshiba model and a modified version was used in the heat test of the system. Main modifications were: surface optical properties were made closer to those of the actual engine; and in stead of substituting keeper discharge by a cathode heater, another heater for keeper power source was installed. The latter improvement was based on the interface requirements of power conditioner. Diagram of this heat dummy model is shown in Fig. 7.7. In order to study its heat characteristics, thermal vacuum test was performed under the configuration shown in Fig. 7.8 in a space chamber at Toshiba's Komukai Plant.[4)] A relay, acting as hollow cathode and main discharge ignition, served to connect

heater load to the corresponding power source. Power conditioner (IR and IP) and heat dummy were mounted on separate power control boxes which were cooled by the chamber shrouding liquid nitrogen and temperature-controlled by the heater. Fig. 7.9 shows the measured temperature distribution in steady-state(long mode) when the base plate temperature was 55C. Table 7.3 shows heater power. Temperature distribution of main and neutralizer hollow cathodes differ considerably from the actual(for example, in the main hollow cathode, vaporizer is about 300C and cathode is about 500C, while in the heat dummy they are 192C and 230C, respectively). Presumably, this is due to the structural change required by addition of the heater, which allowed easier heat transmission. Also, mercury tank temperature was 106C, against the actual temperature of 70-80C. While internal conditions thus lack in accuracy, temperatures of the area bordering satellite and the shell which radiates heat to the outside, etc. are closer to those of the actual engine, and it was considered sufficient for the testing purposes. Gain/loss of heat control box 1, calculated from the test results of this dummy is as shown in Table 7.4. Heat transferred from the dummy to box was 30-40% of the heat generated by the engine.[4] This is very close to the value calculated from the actual engine data(39%) in the 1979 ETL/NASDA joint research.[5]

This heat dummy was used in the heat test of the Qualifying and Acceptance Tests of the system.

(2) Qualifying Tests

In the Qualifying Tests, heat balance test for checking heat design and thermal vacuum test for checking resistivity under the environment were performed.

Heat balance was tested for two angles of incidence of the sun ($\angle\beta$),

shown in Fig. 7.10. Satellite was mounted on a test fixture of 2-axis gimbals and rotated around Y-axis according to the orbit cycle. Solar simulator light was radiated from directly above, facing the page. Effects of earth's infrared radiation and (aru-be-do ?) are simulated by IR lamp, mounted on a cage. When $\angle\beta$ is 0°, average orbit heat input is at its minimum, and when β =63.5°, which is equivalent of the total duration of sunshine, it is at its maximum. β =68.5° and IES long mode operation provide the maximum heat input conditions. Heat balance was tested for each case. Temperature measurement points on the Mission Panel II are shown in Fig. 7.11.

Average temperatures of engine mounting area(2047B), power source device mounting area(2043) and power source control device mounting area(2040) are shown in Table 7.5. Inside the parenthesis are the minimum temperature at minimum heat input and the maximum temperature at maximum input. The table shows that heat is controlled well around IES and that the temperature at the start is relatively low. Temperature at the measuring point 2043 is defined as the temperature of Mission Panel II. Fig. 7.12 shows the results obtained by testing and measuring thermocouple at β=68.5° during non-operation and long operation. Fig. 7.13 gives temperature data on power source device, Mission Panel II, EPS panel, etc., obtained by a flight sensor when β =68.5° and IES is in long operation mode.

Although temperatures in the heat balance test do not directly reflect the temperatures in the orbit because of a slightly different environment, they are estimated to be close.

Difference between estimated and actual temperatures in heat balance test exceeded 5C in the Mission Panel II, eath-oriented panel and RCS panel. After correcting the set values of components'

calorific values, fixture temperature, interface temperature, etc. based on the actual values, remeasurement showed that the difference was less than 5C in all panels. Propriety of heat design was then checked and mathematical heat model was inspected.

In the thermal vacuum test, heat stress was applied to each panel by irradiation from infrared lamp with the temperature profile shown in Table 7.6. Heat control loop was removed in order to reach the QT level. Table 7.7 shows estimated maximum and minimum temperatures of IES in orbit and those measured in the test. Functions and performances of IES during the test were normal, and heat environment resistivity was thus confirmed.

(3) Acceptance Tests

On the premise that heat design has been verified, equivalency of heat design to PM was checked by a benchmark test in the Acceptance Tests, and no heat balance test was given. Difference of panel temperatures between PM and FM under the same heat environment in the benchmark test was under 1.5C, which established the equivalency.

Thermal vacuum test was given with the same temperature profile as in QT with louver attached, assuming that it would exceed the estimated in-the-orbit maximum and minimum temperature levels. Because louver control was working well, external heat input by IR lamp was not enough for setting high temperature, requiring special means to increase internal heat generation. Table 7.7 shows temperature conditions imposed around IES. During this time, IES' functions and performances were normal, and its resistivity for heat environment was verified.

Fig. 7.5 3-node Model

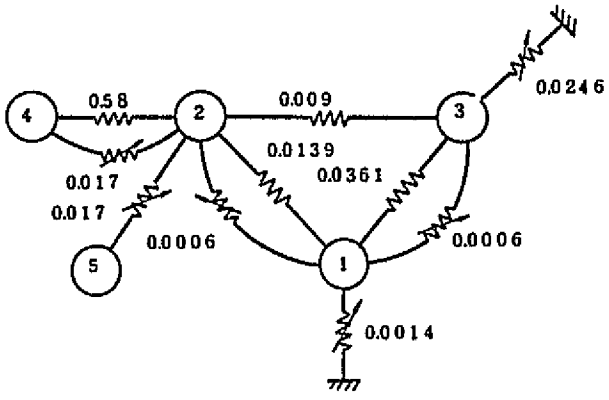

1. Discharge chamber, main hollow cathode, neutralizer hollow cathode and cone support
2. Housing and tank
3. Shell
4. Mission Panel II
5. Radiation sink

Unit: conductance - W/K; coefficient of radiation heat exchange - m^2

Fig. 7.6 10-node Model

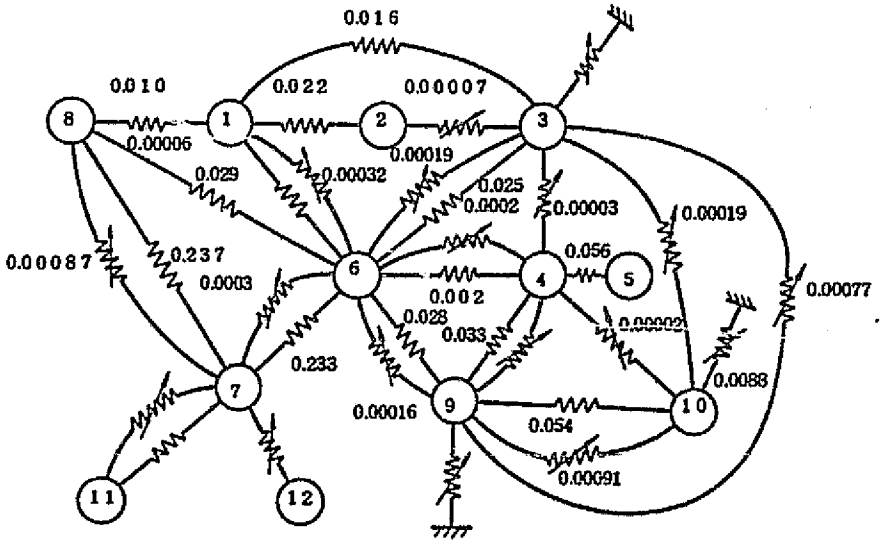

1. Main vaporizer and insulator
2. Main cathode
3. Discharge chamber
4. Neutralizer vaporizer
5. Neutralizer cathode
6. Cone support
7. Housing
8. Tank
9. Outer tube of shell
10. Outer rim of shell
11. Mission Panel II
12. Radiation sink

Unit: conductance - W/K; coefficient of radiation heat exchange - m^2

Interface with outside of system:
- ϑ=0.4 and ε=0.2 of node 3, 9 and 10; ϵ=0.8 of node 7
- Radiation/absorption area - 0.0016m^2 in node 3, 0.0436m^2 in node 7; 0.0339m^2 in node 9 and 0.0085m^2 in node 10.

Table 7.2 Sample Analysis of 10-node Model

Node	Heat input(W)	Analysis value(℃)	Measured value(℃)
1	10.03	392	290
2	4.4	543	
3	14.97	364	
4	1.67	359	230
5	5.95	465	
6	0	149	99~106
7	0	73	
8	0	86	76
9	6.57	170	
10	0.75	157	
11	0	55	

Analysis conditions:
1. External heat input - 6.57W in node 9 and 0.75W in node 10.
2. Conductance between node 7 and node 11(satellite base plate) is 0.84W/K.
3. Node 11 is designated as a border node and is fixed at 55C.

Note) Measured values were taken during IEE QT and the heat input were slightly different from the analysis conditions.

Fig. 7.7 Diagram of Heat Dummy

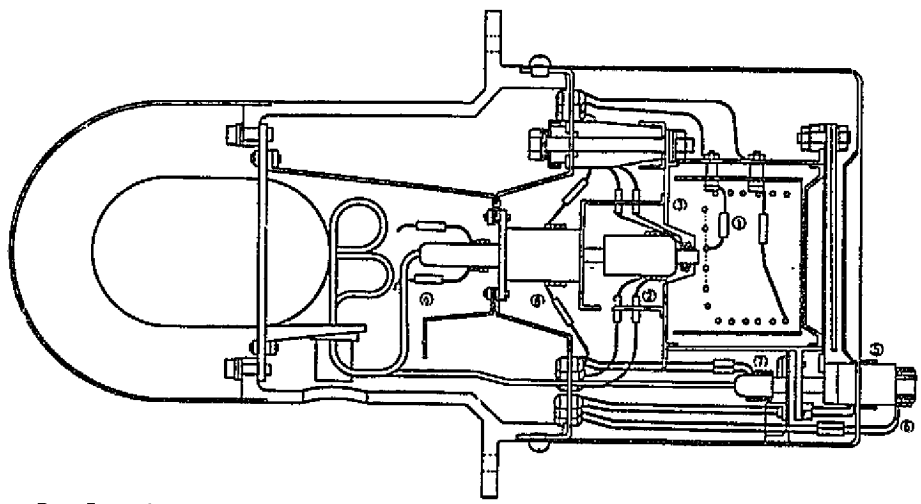

1. Anode heater
2. Main cathode heater
3. Main cathode keeper heater
4. Main vaporizer heater
5. Neutralizer heater
6. Neutralizer keeper heater
7. Neutralizer vaporizer heater
8. Insulator heater

Fig. 7.8 Test Configuration

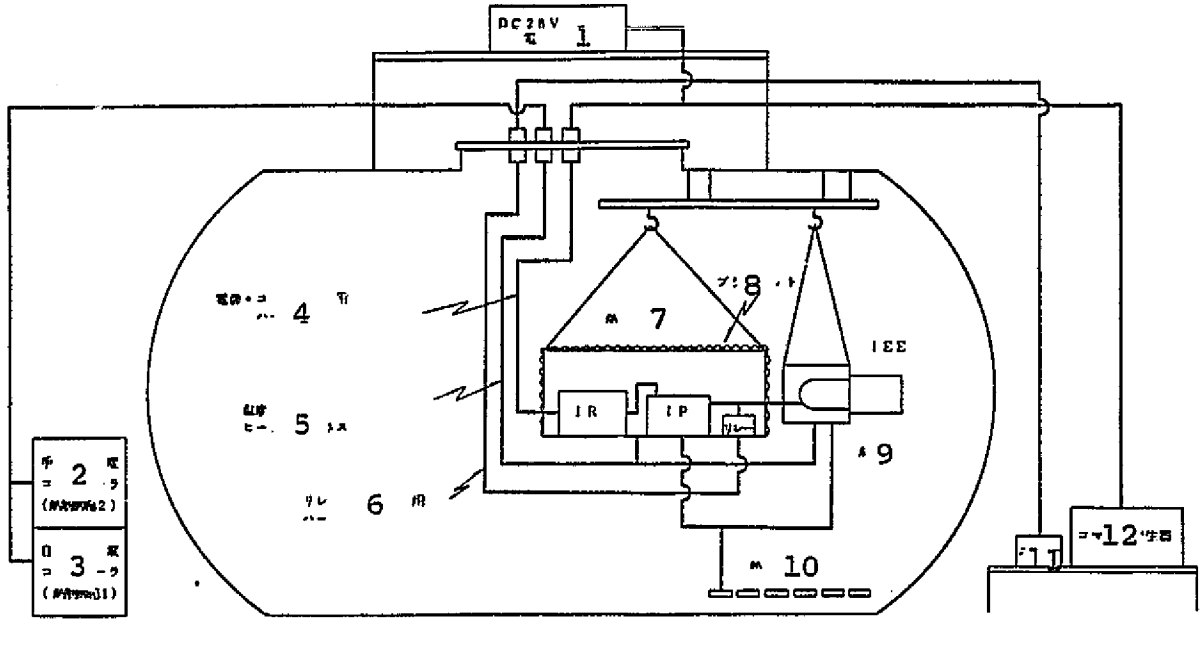

1. Power source
2. Manual temperature controller (heat control box 2)
3. Automatic temp. controller (heat control box 1)
4. Harness for power source and command signals
5. Heater harness for temp. control
6. Harness for relay switch
7. Heat control box 2
8. Blanket
9. Heat control box 1
10. Thermocouple
11. Switch
12. Command generator

Fig. 7.9 Heat Dummy Temperature Distribution in Long Duration Mode (at base plate temperature of 55C)

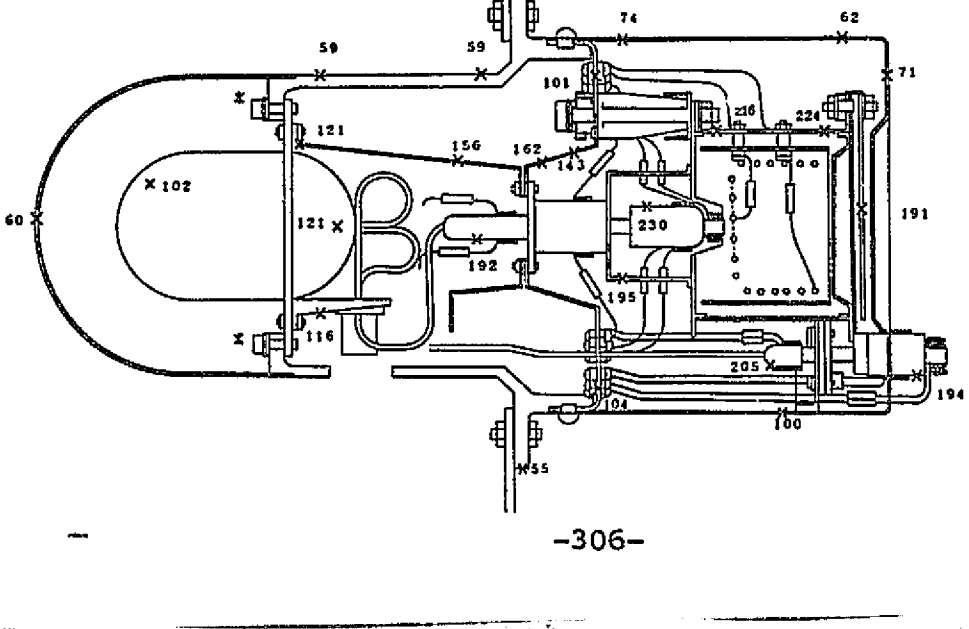

*These bolts were loose during test.

Table 7.3 Supplied Power in Heat Dummy

HEAT DISSIPATION (WATT) / DUMMY HEATER		SHORT MODE		LONG MODE	
		SPEC. VALUE	MEASURED VALUE	SPEC. VALUE	MEASURED VALUE
Z 3	ANODE HEATER	0	0	14.0	14.97
Z 4	MAIN HOLLOW CATHODE HEATER	25.0	21.3	0	0
Z 5	MAIN HOLLOW CATHODE KEEPER HEATER	0	0	4.5	4.4
Z 6	MAIN HOLLOW CATHODE VAPORIZER HEATER	7.0	6.93	0.43~7.0	7.08
Z 7	NEUTRALIZER HEATER	4.0	2.67	0	0
Z 8	NEUTRALIZER KEEPER HEATER	6.0	5.85	6.0	5.95
Z 9	NEUTRALIZER VAPORIZER HEATER	0.43~2.5	1.47	0.43~2.5	1.67
Z10	ISOLATOR HEATER	3.0	2.95	3.0	2.95
TOTAL		45.43~47.5	41.17	28.36~37.00	37.02

Note) Short mode is a test which gives the equivalent of average calorific value of a cycle in repetition test.

Table 7.4 Heat Gain and Loss

BASE PLATE TEMP. (℃) / OPERATION MODE / HEAT QUANTITY(WATT)	−15℃		20℃		55℃	
	SHORT MODE	LONG MODE	SHORT MODE	LONG MODE	SHORT MODE	LONG MODE
HEAT QUANTITY RADIATED FROM BOX(I)	39.9	41.3	68.4	72.8	127.0	128.2
HEATER POWER TO CONTROL TEMP. OF BOX(I)	19.7	25.9	53.5	63.3	108.4	115.5
HEAT QUANTITY TRANSFERED FROM THERMAL DUMMY TO BOX(I)	20.2	15.4	14.9	9.5	18.6	12.7
HEAT DISSIPATION IN THERMAL DUMMY	41.2	37.5	41.3	37.6	41.2	37.0

Fig. 7.10 Heat Balance Test Configuration

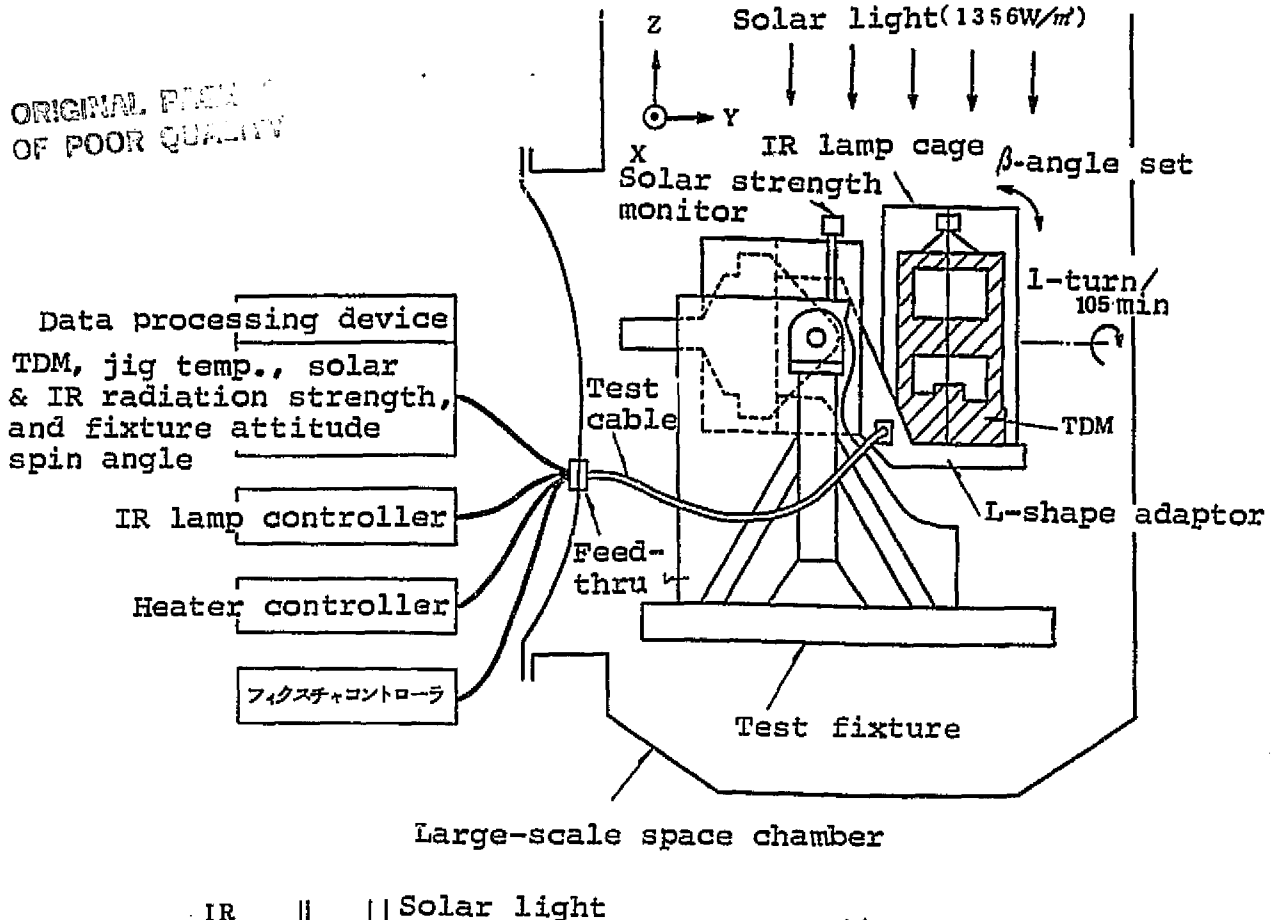

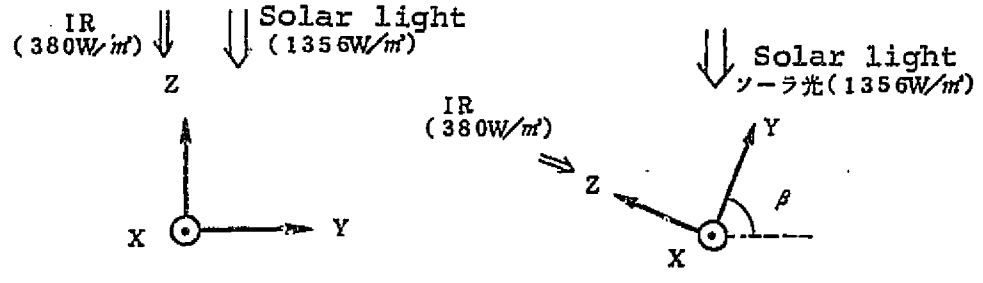

Case 1; $\beta = 0°$

Case 2; $\beta = 68.5°$

Fig. 7.11 Temperature Measuring Points on Mission Panel II

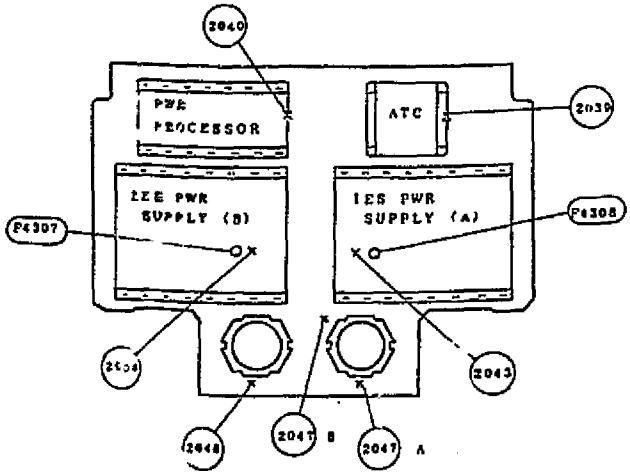

x: thermocouple for measurement
o: flight sensor

Fig. 7.12 IES Temperature During Heat Balance Test

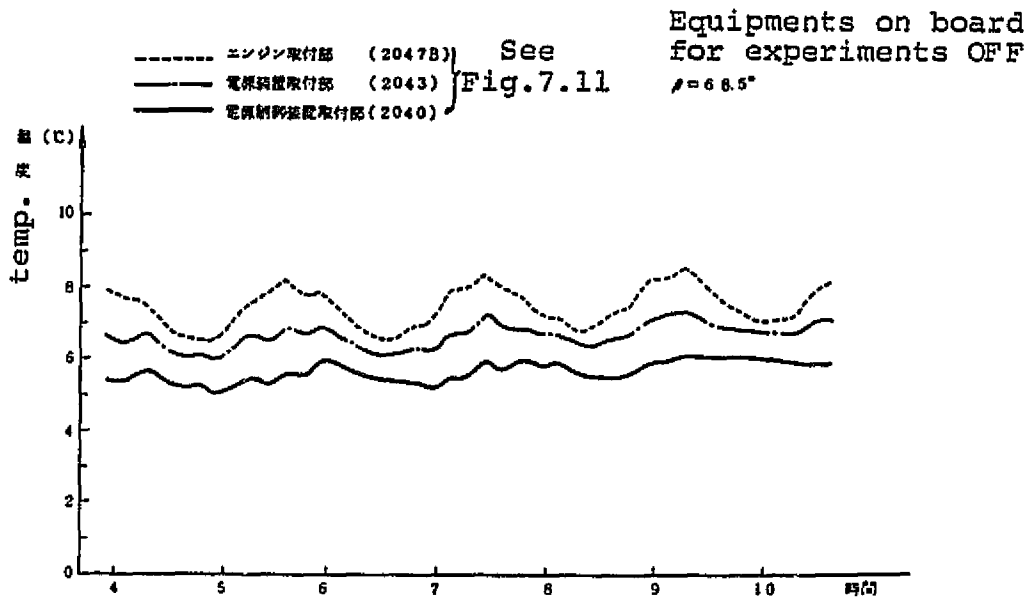

(a) IES non-operation

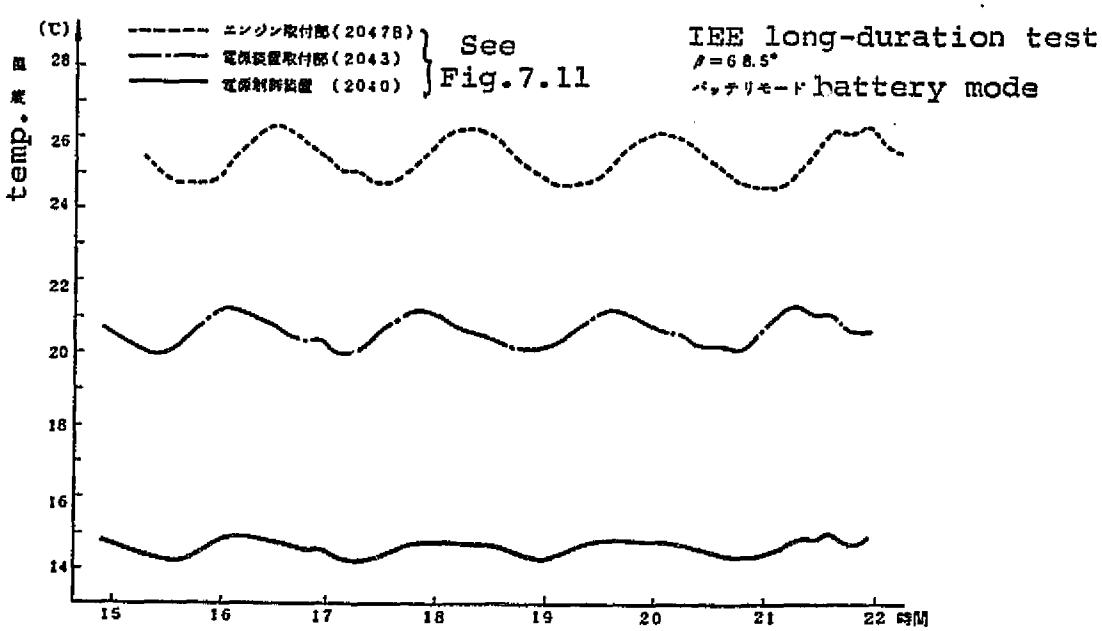

(b) IES long-duration test

Table 7.5 Measured Temperatures of Mounted Area on IES (unit:℃)

Component	Sensor no.	Equipments on board for experiments OFF		IES long duration
		$\beta = 0°$	$\beta = 68.5°$	$\beta = 68.5°$
Ion engine	2047B	5.5 (mini 2.0)	8.0	25.5 (max 26.2)
Power source device	2043	0.6	7.0	20.7 (max 21.2)
	F4308	1.5	6.9	20.7
Power source control device	2040	1.0 (mini −0.4)	6.0	14.5 (max 14.8)

Fig. 7.13 Heat Balance Test

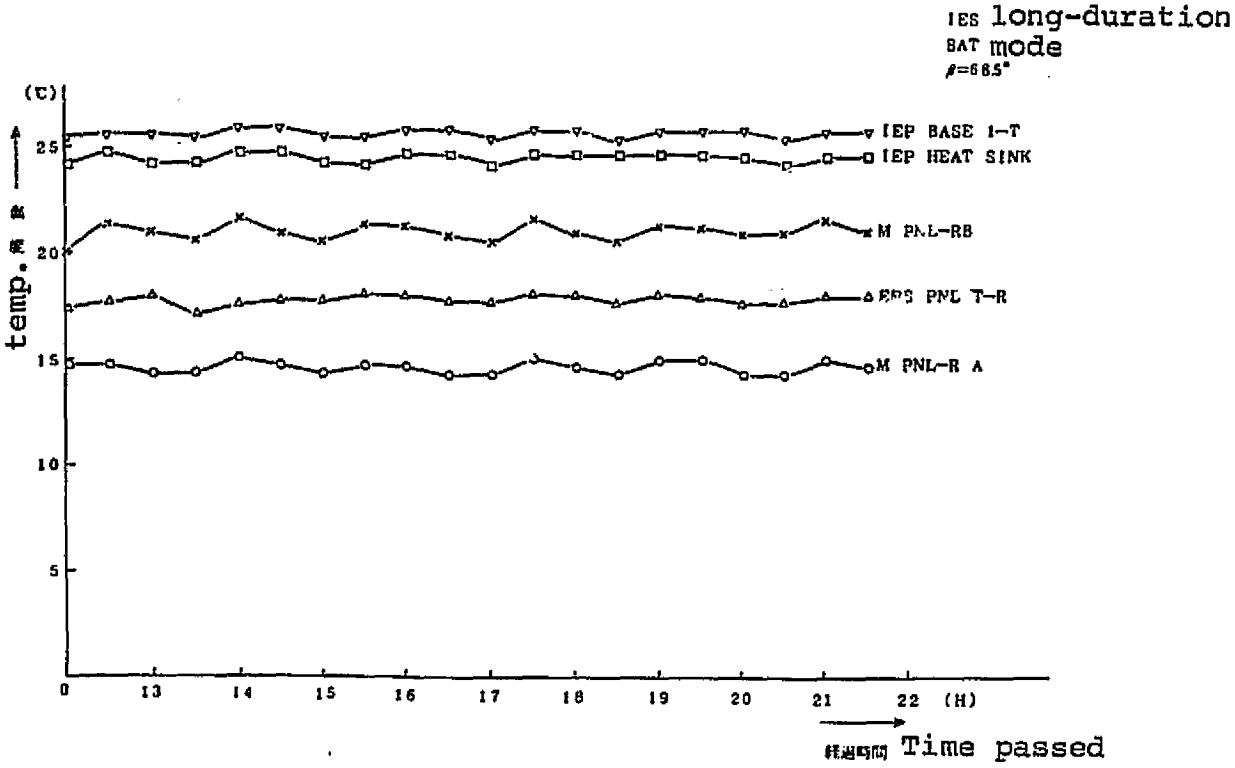

Table 7.6 Thermal Vacuum Test

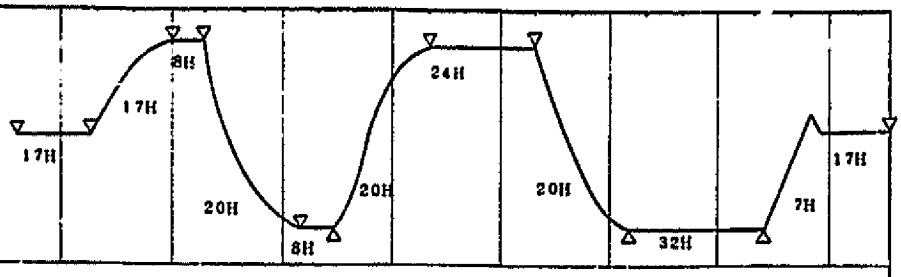

		Thermal vacuum test											
			A (1)		B (1)		C (2)		D (2)				
Name of test			1	2	3 低 4	5	6 高	7 高	8 低	9 高	10	11 圧
elec. performance test (III) subject			12	13	14 15	16	17	18	19	*20	21	22
Test conditions	solar light		OFF									
	spin angle		0°									
	attitude angle		90°									
	infrared lamp	+ Z	ON									
		+ X	OFF	ON	OFF	ON	ON		OFF	ON	ON	OFF
		− X	OFF	ON	OFF	ON			OFF	ON		OFF

A: high temperature 1
B: low temperature 1
C: high temperature 2
D: low temperature 2
1: evacuate
2: move to high temperature 1
3: expose to high temperature
4: move to low temperature
5: expose to low temperature
6: move to high temperature
7: expose to high temperature
8: move to low temperature
9: expose to low temperature
10: return to normal temperature
11: return to atmosphere

12: LAUNCH mode B
13: SUPPLEMENT mode
14: NORMAL A-1
15: " B-1
16: " A-1
17: " B-2
18: " A-2
19: " B-1
20: " A-2
21: " B-2
22: LAUNCH mode B

Table 7.7 Temperature Measurements in Thermal Vacuum Test

Sensor point \ 試験	QT		AT		Estimated in orbit	
	max	min	max	min	max	min
2047B	42.8	3.7	—	—	45.9	6.4
2043	45.7	−0.3	37.7	1.6	33.4	2.6
F4308	—	—	35.4	−0.3		
2040	47.6	−1.6	28.8	−0.1		

7.3.3 Oscillation and Shock

(1) Oscillation test

Qualifying Test was given under severe oscillation conditions of 1.5 times the flight level G for 2 hours. Responding acceleration rates of Mission Panel are given in Table 7.8. They are considerably lower than the component test level, which indicates that the IES has been designed and produced to meet the vibration level of launching, with sufficient margin.

IES was tested with flight level vibration during Acceptance Test. No faulty workmanship in the satellite, including IES, was observed.

(2) Satellite separation shock

High shock level was observed on the separation surface of the satellite when the three stage rocket was separated, but it was much lower on the equipment-boarded surface: peak G level of shock response spectrum(SRS) on Mission Panel II was about 17G(X-axis)(Fig. 7.14), considerably lower than the component test level(See Fig. 4).

(3) Impact of paddle expansion

Impact from power cartridge operation for paddle expansion is larger than that of satellite separation. An example of SRS of Mission Panel II is shown in Fig. 7.15. Peak G level is 90-160G, much lower than the component test level(Fig. 4) of 1,190G.

Table 7.8 Results of Oscillation Test(System QT)

	Z-axis			X-axis			Y-axis		
	Required value*	Measured val.		Required value*	Measured val.		Required value*	Measured val.	
		>100Hz	<100Hz		>100Hz	<100Hz		>100Hz	<100Hz
Sine wave (正弦波)	5~200Hz: 12.0 G_0-p 200~2000Hz: 5.0 G_0-p	8 G	2 G	5~200Hz: 15.0 G_0-p 200~2,000Hz: 5.0 G_0-p	7 G	1 G	5~200Hz: 15.0 G_0-p 200~2,000Hz: 5.0 G_0-p	7 G	1 G
Random (ランダム)	20~2,000Hz: 15.64 Grms	3 Grms		20~2,000Hz: 15.64 Grms	2 Grms		20~2,000Hz: 15.64 Grms	2 Grms	

*Required value at component level(QT)

Fig. 7.14 SRS of Mission Panel II During Satellite Separation Shock Test

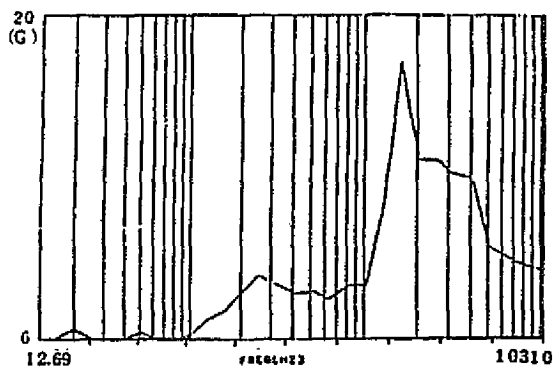

Fig. 7.15 SRS of Mission Panel II During Paddle Expansion Test

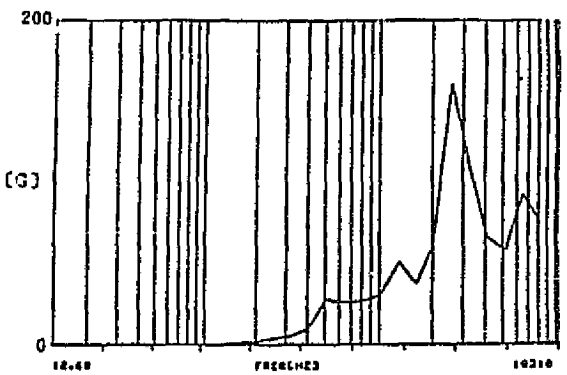

7.3.4 Alignment

As the final installation of ion engine is doen at the launch complex, the alignment test was for fluctuations caused by removal and for the initial setting. Auto-collimation was used for measurement, with an alignment mirror mounted on a grid. Results were, as shown in Table 7.1, within 0.24°, with good reproducibility. RSS due to misalignment in FM(including hysteresis, heat distortion, etc.) was 0.25°.

7.3.5 Remanence Moment

Remanence moment of ETS-III is required to be less than $1ATm^2$ for each axis. An engine unit uses 3 permanent magnets of alnico-5, magnetized to about 10,000 Gauss, and, by inverting the polarity of one of the two units, generation of remanence moment is prevented. Remanence moment of a single engine unit is shown in Table 5.11. Flux direction of the engine is in the X-axis.

Fig. 7.16 shows measured results of magnetic field of X-component in the system test. Two symmetrical leaf patterns indicate the existence of the two engines. Difference of remanence moment between the two is small enough($0.03\mu Wb \cdot m \approx 0.02ATm^2$) that there was no problem as a system.

Fig. 7.16 An Example of Magnetic Field Distribution(X-component;QT)

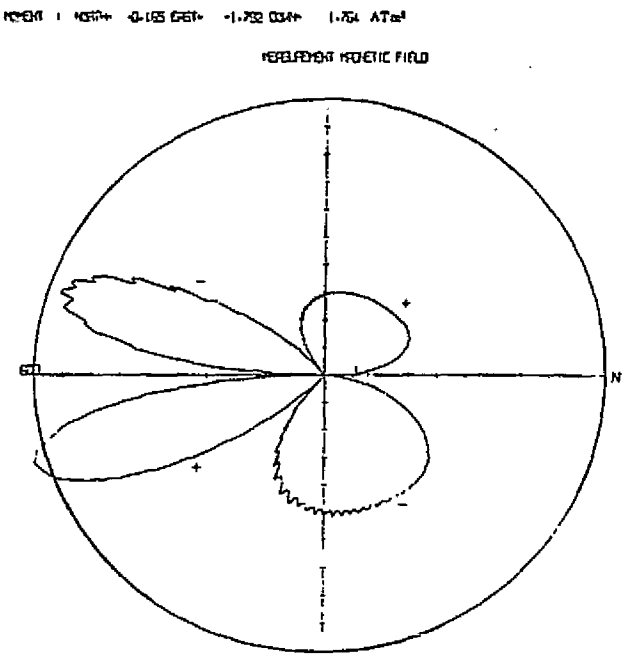

7.3.6 Power Source System

(1) Input current

IES is connected to bus power source via fuses(5A x 2) and a relay. Transient current of IES, as shown in Fig. 7.17, is about 4.8A and 10-30ms at the maximum at the start of beam injection. Prearcing time-current characteristic of the fuse is 14A for continuous 30ms, which gives large enough margin.

(2) Power analysis

The worst case of power distribution during IES operation was assumed to be at the orbit altitude of 800km and IRU or battery(1 out of 3) breakdown. Results of power analysis with the assumed IES power profile of 26.5 minutes starting time and 100W and 13-minute beam injection are shown in Table 7.9. In repetition test(IES SHORT) DOD of batteries is tolerated up to 25% and thus it is operable for each cycle on all orbits in the worst case. On the other hand, DOD is tolerated up to 50% in long-duration test, in which case accumulated test hours(over 10 hours of continuous operation) over the duration of a mission(1 year) are estimated to be as shown in Table 7.10. Accumulated hours are 30-50 in the worst case. Presumably, close to the targeted 100 hours can be accomplished if there is no breakdown (normal case).

Fig. 7.17 IES Transient Input Current

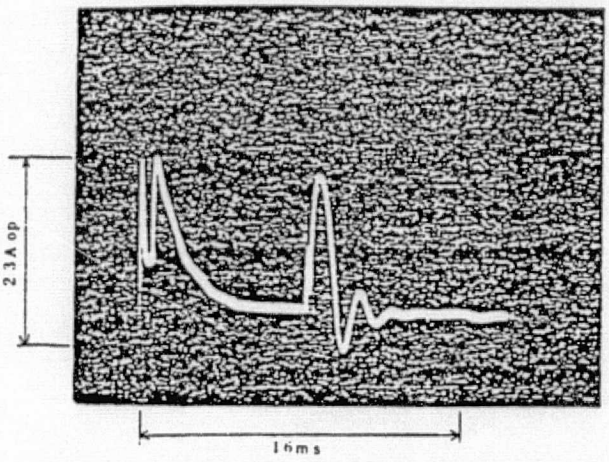

(a) IES on(0.5A/div, 2ms/div)

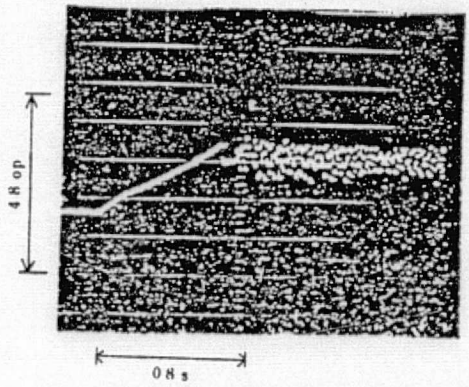

(b) Start of beam injection
(1A/div, 0.2s/div)

Table 7.9 IES Repetition Test

MISSION NAME	IES SHORT		IES SHORT	
ALTITUDE (km)	800.00		800.00	
NUMBER OF IRU	1		2	
NUMBER OF BATTERY	2		3	
SUN ANGLE (DEG)	POWER MARGIN(W)	MAX DOD(%)	POWER MARGIN(W)	MAX DOD(%)
90.0	2.3	23.97	7.0	16.81
80.0	7.3	23.80	12.3	16.69
70.0	10.0	23.24	15.2	16.30
60.0	13.7	22.18	19.2	15.56
50.0	16.7	20.35	20.5	14.27
40.0	22.6	17.00	21.3	11.92
30.0	29.2	9.62	23.2	6.93
21.5	8.4	13.56	2.3	9.97

Table 7.10 Possible Hours For IES Long-duration Test

Orbit altitude

Breakdown mode

故障モード \ 軌道高度	800km	875km
NORMAL	93.9h	124.0h
IRU	49.5	71.2
BATTERY	28.2	44.3

7.3.7 Attitude Control System

Engine has torque arms with respect to the pitch shaft and yaw shaft. Attitude control system is that of 3-axis zero momentum. Torque around yaw shaft, with a short arm length of 10cm, is not of a major concern, as there are many external disturbances such as earth's magnetism and gravity inclination and angular motion is not accumulated during a cycle. Torque arm length around the pitch shaft is analytically estimated to be 24.4 ± 0.1 cm in the early stage and 25.5 ± 0.1 cm in the final stage, based on the test results of mass flow characteristics. ± range depends on the paddle turning position and the difference between BOL and EOL comes from the decrease in the amount of RCS propellant. Amount of accumulated angular motion by a 10-minute injection of the engine is 0.264Nms in BOL at the thrust of 1.8mN. Thus, it takes 70 minutes for the accumulated angular motion of reaction wheel to reach from zero to the maximum of 1.856Nms and 42 minutes to the normal unloading level(60%). It is also estimated that more than 210 pitch unloadings are generated during 150-hour injection. Amount of RCS propellant required for this is about 0.4kg. As alloted amount for IES unloading is 0.97kg, there is enough margin during operation.

7.3.8 Contamination

Main waste materials from ion engine are i) mercury ion beam, ii) neutral mercury particles and iii) spattered grid materials.

i) is the injected ion, and as thrust, it has a speed of about 30km/s and its direction is within a 27°-half angle cone, as noted in Section 4.4.3. These particles, making up about 70% of mercury flow, exceeds earth escape velocity and do not return. Thus, they are of no concern to the ETS-III.

ii) makes up about 30% of mercury consumption and is exhausted from the grid in the discharge chamber with maxwell distribution of average speed 0.22km/sec by heat movement(about 300C) having cosine direction distribution. It is safely assumed that mercury molecules do not collide with each other, and thus there is no possibility of their moving to the inside of the grid(satellite side).

iii) is a result of slow moving mercury ion, produced by charge exchange of i) and ii), spattering against accelerating grid, having been pulled by its potential(-1,000V). Angle of incidence of charge exchanging ions is about 90, and the direction and amount of such spattered grid material(stainless steel) are known to be as shown in Fig. 7.18. Thus, the spattered material is not likely to move to the inside of the grid. In the case of ETS-III, however, as there is a louver radiation surface near the grid surface(See Fig. A1, 2 in the Appendix) contamination was monitored by injection experiments in the NAL/NASDA joint research. In conclusion, at half angle of over 80° from the axis of thrust, neither the sunlight absorption rate nor the infrared radiation rate of a sample(molten silica second surface mirror) was affected(See Fig. 7.19) and analysis of adhered materials (by electron spectrum, fluorescent X-ray and atomic light absorption)

also showed that they were of insignificant amounts to yield any effects.[6] The slight increase of α at θ>80C was found to have been contributed mostly by Fe, Al, etc. spattered from the vacuum chamber wall, a phenomenon peculiar to ground testing.

From the above analysis and experiments, it is assumed that contamination of satellite by ion engine would be very little during a mission of ETS-III.

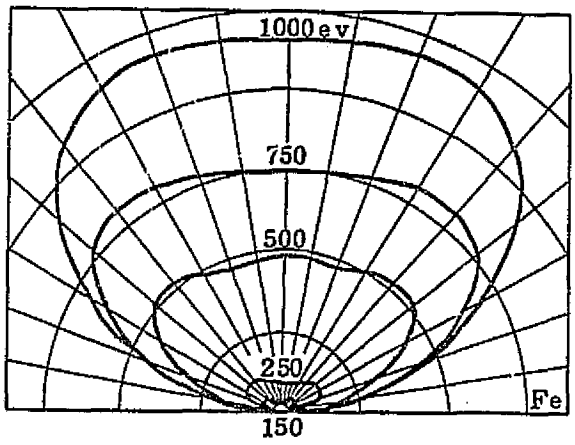

Fig. 7.18 Direction and Amount of Iron Material Spattered by Vertically Entered Mercury Ion

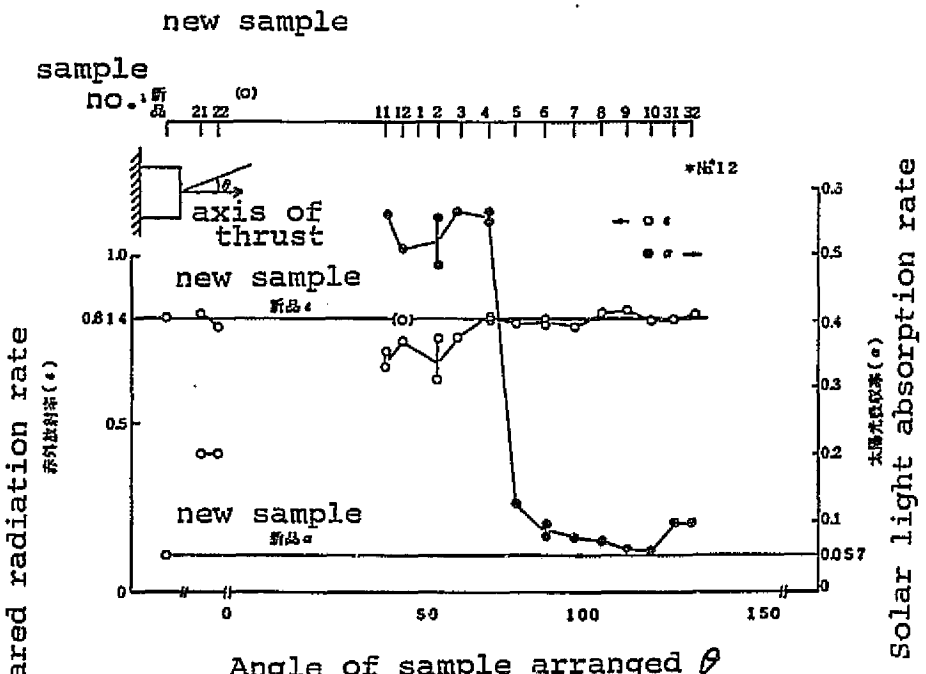

Fig. 7.19 α and ε of Second Surface Mirror in Relation to Sample Arrangement

Reference

1) NASDA: Report on the Development of ETS-III, to be published October, 1983.

2) H. Azuma, T. Sasaki, et al: EMI Test Chamber for Ion Engine Mounted on Satellite, AIAA81-0725.

3) NAL/NASDA: Report on the Joint Research - Study(I) of Testing and Evaluation of Ion Engine System(thermal dummy and heat vacuum test), March, 1981.

4) K. Nitta, K. Machida, Y. Nakamura, Y. Kuriyama, et al.: The Development of Ion Engine Thruster Thermal Dummy, ISTS, 1982.

5) ETL/NASDA: Report on the Joint Research - Study(II) of Testing and Evaluation of Ion Engine System(control functions of power control device), March, 1981.

6) NAL/NASDA: Report on the Joint Research - Study of Ground Simulation of Ion Engine(Study of optical characteristic changes of satellite surface by ion engine operation), March, 1982.

Chapter 8

Launch Complex Maintenance

8.1 Outline

IES-related maintenance work flow at the launch complex is shown in Fig. 8.1. Power conditioner, installed on the satellite, received maintenance work as a part of the satellite. Engine unit received the performance test at the NAL testing facility before being sent to the launch complex and was inspected upon arrival. Wire harness shield was mounted at the complex, after which the engine unit was installed on the satellite. Performance check was performed because the engine unit had been stored in a container for almost one year since the sub-system AT. In order to shorten the air-exposure time the engine was installed near the final stage, immediately before hydrazine filling. Thermal blanket was placed around the engine after installation.

Engine unit's air-exposure time was kept to a minimum by as much as dry nitrogen gas purge as the configuration allowed. Gas purge was continued throughout MST until Y-4(?), when the fairing was installed. As a result, the air-exposure time at the launch complex, which was a major concern, was kept to 140 hours, well within the targeted "500 hours or less." Connections to power conditioner were checked by an indirect method of monitoring temperature telemetry of the engine to see if it agrees with room temperature with the power conditioner ON, instead of sending power to the engine.

For the hollow cathode assembly of the engine, which is of similar structure as electron tube and thus delicate and prone to deterioration in air, main and neutralizer hollow cathode replacements had been prepared in case of emergency. Fortunately, there was no need for exchange. The replacement cathodes had been tested for the same performance requirements as FM in the assembly stage.

After preparation was completed, ETS-III was launched by the N rocket No. 9(F) from Tanegashima Space Center Osaki launch complex at 14:00:00 Japan time, September 3, 1983, and became our first medium atlitude, 3-axis attitude controlled satellite, "Kiku No. 4."

The series of preparation carried out at the launch complex this time can basically be followed in the future, but the following should be noted: Piping of the nitrogen gas purge device not only lowers the efficiency of satellite/rocket-related work, but presents danger to the engine and thus, nitrogen sealing method should be considered instead; shielding of wire harness, done at the complex, should be done before AT, and; refilling mercury and checking injection before transporting have advantages and disadvantages which should be weighed on a case by case basis.

Fig. 8.1 IES-related Work Flow(actual) in Preparation at Launch Complex

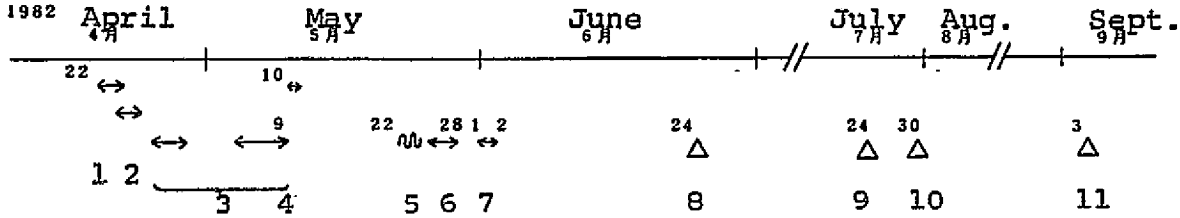

1 ~ 7: Engine unit preparation

1. Appearance, charge/insulation and resistance value tests
2. Draining and filling of mercury
3. Performance test
4. Weight inspection
5. Transporting
6. Unpacking/inspection(appearance, charge/insulation, resistance and weight)
7. Wire harness shield installation and weight inspection
8. Electrical performance test of power conditioner(system level)
9. Installation of engine on satellite
10. Inspection of IEE/IEP connections(system level)
11. Launch

8.2 Performance Test

The test was performed before transporting the engine unit to the launch complex, for the purpose of draining and filling propellant and inspecting performances including beam injection. Appearance, charge/insulation, resistance and weight were checked, mercury was drained and refilled, and performance test was given. Then, appearance, weight, charge/insulation and resistance were checked again, after which the engine was sealed in a container with nitrogen gas.

For performance test, rated operation test, interface check and low-temperature starting test were chosen in order to verify the performance-maintaining conditions. Test methods were the same as those of engine unit AT(see Table 5.(blank)). Low-temperature starting conditions were the equivalent of the worst case of power supply interface, i.e. base plate temperature of -5C and neutralizer heater voltage of 5.2V.

8.2.1 Test Results

Summary of performance test is as follows.

i) Fluctuation in ignition characteristic of main hollow cathode in Unit #1 was observed(ignition at 5.34V/5.30A for cathode heater, against 4.94V/5.0A in IEE AT).

ii) Fluctuation in ignition characteristics of neutralizer hollow cathode in Unit #2 was observed(ignition at 5.29V/4.82A for neutralizer heater, against 5.20V/4.69A in IEE AT).

iii) Transient and steady state characteristics other than the above were the same as those shown in IEE AT.

8.2.2 Evaluation

(1) Ignition characteristics of hollow cathode

As noted in the previous sub-section, fluctuation was observed in the ignition characteristic of hollow cathodes. In neutralizer, especially, ignition could no longer be guaranteed in the worst case of interface conditions. Based on the past development results (including IEE life test) and data from output voltage measurements of FM power supply, following conclusions were obtained.

i) Fluctuation in ignition characteristic seems to have been caused by contamination of keeper electrode or cathode from ground testing, and it is not expected to worsen as this is the last of the tests.

Contamination of keeper electrode changes the distribution of electric field in the surrounding area and that of cathode lowers thermion radiation rate, thus affecting ignition.

Contamination occurs when materials, absorbed during air exposure, or air, mixed into pipes during mercury filling, oxidize cathode or the inside of keeper under high temperature in operation, or when spattered materials from vacuum tank adhere. Which factor contributed this time could not be determined. So far, many cases of wide fluctuation of ignition characteristic at the beginning of operation after exposure to air which recovered with repeated operations under high vacuum environment have been observed, and it is expected to be the case this time also.

Among the factors of contamination, air-exposure will be

carried out at the launch complex from now on. It was determined that by sufficiently degasing under high vacuum environment after launching and carrying out step-by-step degasing process(preheating and activation) during operation, its effects could be kept to a minimum. Fluctuation of ignitability in the main hollow cathode of Unit #1 had already occurred in the IES AT, and the output voltage data of main cathode heater power source of the power source device #1 indicate that the range of fluctuation has not changed since that time.

ii) Minimum output voltage of this cathode heater power source was slightly above the minimum ignition voltage of the hollow cathode measured this time(margin of 0.29V in Unit #1 main hollow cathode and 0.10V in Unit #2 neutralizer hollow cathode), and combined with power source device, there should be no problem with ignition.

From the above observations it was determined that even with the fluctuation, these two hollow cathodes were useable for flight.

Fig. 8.2 show the histogram of ignition characteristic of the flight model through IEE and IESS Acceptance Test the performance test given this time. Clearly, under the same conditions(worst case indicated by "L"), ignition characteristic deteriorated with each ground test. This means the characteristic deteriorates with each repetition of injection test and air-exposure, at least for the first several times after exposure. In this test, ignition of neutralizer hollow cathode in Unit #2 reached a critical level where no more ground test could be performed. Therefore, for future development,

i) re-examine ground testing policies

·less tests for flight models(for example, IEE and IES can

be tested in succession)
•possibility of refilling of propellant; and

ii) study what can be done on the power source side for passing type of deterioration of the characteristic.

For the deterioration of neutralizer hollow cathode ignition characteristic in Unit #2, it was decided that cathode orifice would be cleaned at the launch pad, as it seemed effective in the first ignition in the space experiment. This involves rubbing the surface layer of orifice lightly with a pin gauge, removing oxidized film, etc. to expose the active surface. While a permanent recovery of ignition characteristic cannot be expected, it is known to be effective for the first ignition.

(2) Performance in steady state

Final performance data on the engine units are given in Table 8.1. These values are within the fluctuation range of previous tests(see Table 5.10), which inditates that the same steady-state characteritic was maintained after 10 months of storage.

Fig. 8.2 Hollow Cathode Ignition Time

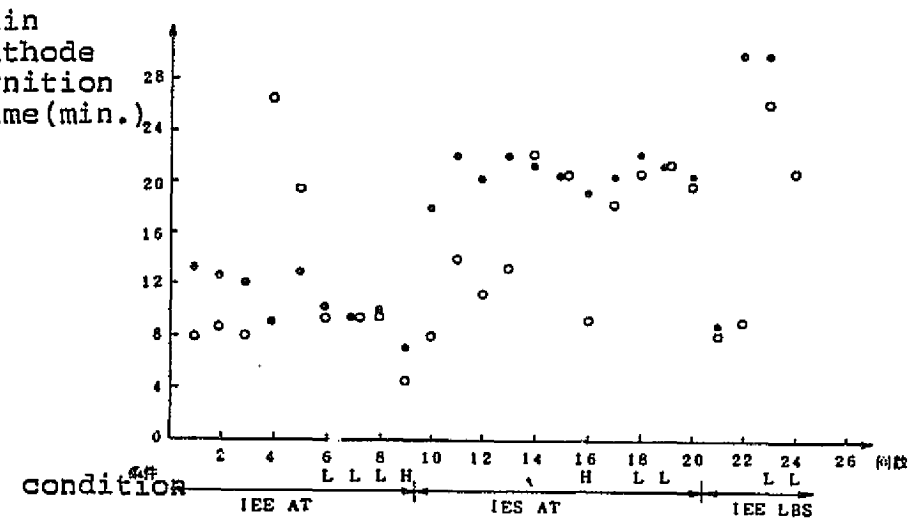

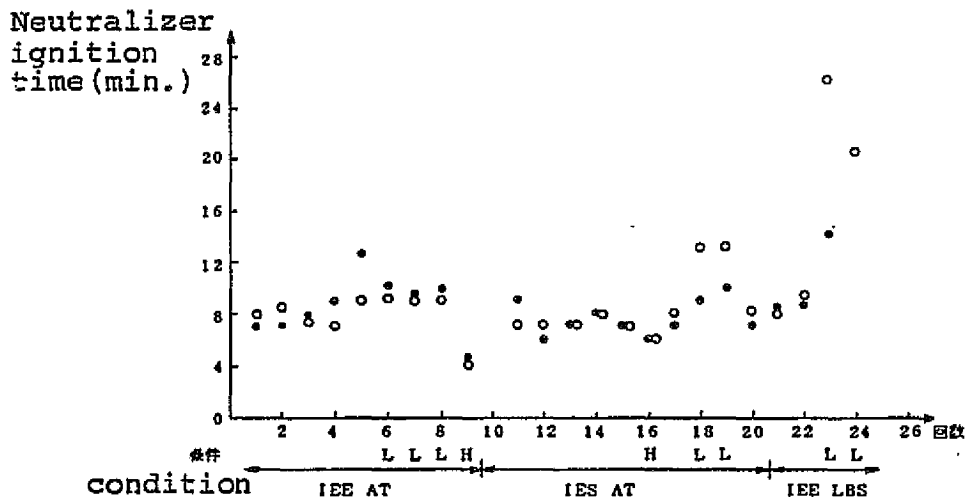

• : Unit #1
∘ : Unit #1
L : Low temperature case(equivalent of base plate temperature of -5C and bus voltage of 27.22V)
H : High temperature case(equivalent of base temperature of 45C and bus voltage of 28.0V)

Table 8.1 Performance Parameter in Steady State

	Parameter		Unit	IEE FM(1) 定試 1 (OP-1)	IEE FM(1) イフ確 2 (OP-2)	IEE FM(1) 低開 3 (OP-3)	IEE FM(2) 定試 4 (OP-1)	IEE FM(2) イフ確 5 (OP-2)	IEE FM(2) 低開 6 (OP-3)
Test subject 試験項目									
Electrical parameter and vaporizer temperature	Beam	Volt.	KV	0.99	0.99	0.99	0.99	0.99	0.99
		Curr.	mA	24.0	24.8	24.2	27.1	27.5	25.40
	Accel.	Volt.	KV	−1.00	−1.00	−1.00	−1.00	−1.00	−1.00
		Curr.	mA	0.40	0.35	0.33	0.33	0.31	0.34
	Discharge	Volt.	.V	37.6	39.3	39.7	38.7	39.3	39.5
		Curr.	A	0.345	0.345	0.345	0.345	0.345	0.344
	Cath. Heater	Volt.	V	/	/	/	/	/	/
		Curr.	A	/	/	/	/	/	/
	Cath. Keeper	Volt.	V	17.24	17.57	18.02	15.37	15.82	17.58
		Curr.	A	0.304	0.268	0.219	0.300	0.302	0.226
	Cath. Vaporizer	Volt.	V	3.21	3.04	3.16	2.95	2.96	3.08
		Curr.	A	1.86	1.82	1.89	1.79	1.79	1.85
	Neut. Heater	Volt.	V	/	/	/	/	/	/
		Curr.	A	/	/	/	/	/	/
	Neut. Keeper	Volt.	V	25.8	24.5	25.5	19.4	23.0	23.8
		Curr.	A	0.244	0.275	0.224	0.246	0.287	0.244
	Neut. Vaporizer	Volt.	V	1.38	1.15	1.52	1.31	0.78	0.93
		Curr.	A	0.84	0.66	0.85	0.77	0.45	0.53
	Isolator	Volt.	V	2.74	2.74	2.74	2.83	2.84	2.85
		Curr.	A	1.00	1.00	1.00	0.91	1.00	1.00
	Main Vap. Temp.		℃	295	291	289	280	278	281
	Neut. Vap. Temp.		℃	253	224	254	244	204	208
	Engine potential		V	−18.7	−14.9	−18.1	−12.1	−9.35	−10.2
	Target potential		V	1.73	1.91	1.88	1.81	2.01	2.2
Performance parameter	Hg Flow rate (Main)		$\times 10^{-3}$ g/sec	9.0	8.1	7.7	8.9	8.5	9.0
	〃 (Neut)		$\times 10^{-3}$ g/sec	1.0	0.44	1.0	1.0	0.36	0.40
	Thrust		g重 wt.	0.158	0.163	0.159	0.178	0.181	0.167
	Specific Impulse		sec	1743	2005	2053	1988	2123	1845
	Propel. Utilization Eff.		%	55	64	65	63	67	59
	Total Power		W	58.5	58.9	57.7	58.8	61.0	57.9
	Power Eff.		%	40.6	41.7	41.5	45.6	44.6	43.4
Date data acquired				'82 5.5 13:22	'82.5.5 19:02	'82.5.6 15:30	'82.4.26 19:41	'82.4.27 17:19	"82.4.29 7:20

1. Rated operation test
2. Interface check
3. Low temperature operation start test
4. Rated operation test
5. Interface check
6. Low temperature operation start test

8.3 Installation of Engine on Satellite

After the performance test, engine unit was sent to the 3-stage satellite assembly facility of Tanegashima Space Center. The container was placed in an airtight bag with a dryer sealed in, which was then placed in a cushioned wooden box. Transportation route was the same as that of satellite, and appearance, weight, resistance and insulation were tested afterwards to check that transporting did not cause any problem. Also, at this time, neutralizer cathode orifice of Unit #2 was cleaned.

Then, EMI shield tape(copper foil) was wound on the engine unit wire harness and soldered onto shield cable. At the same time, scratches on the teflon film of high voltage cable were covered with mylar tape.(maximum depth of scratch was 0.25mm, to the film thickness of 0.85mm.) Fig. 8.3 shows the completed shield tape treatment. The surface layer has been reinforced by mylar tape,and partially by silicone rubber tape.

Then, the engine was installed on the satellite. The procedure consisted of appearance inspection, thermal grease coating, engine installation, blanket installation(I), insulation check, connector installation, charge check, blanket installation(II), and a final appearance inspection. Insulation resistance between the engine base plate and satellite frame was over 6MΩ(above the full digital voltmeter scale) and charge resistance between the engine shell and satellite frame after the connectors were placed was less than 0.6Ω.

Clamp torque was 36kg-cm at the engine and 4.5kg-cm at the connector, which were within the standards. Thermal blanket covered the engine shell 16mm from the flange at the maximum, also within the standard. Final appearance was also normal. Thus, it was confirmed

that the conditions of the installed engine had no problem in electrical and mechanical configuration.

In placing a thermal blanket around the engine, several steps were taken for FM: Capton insulation film was placed over the inside of the blanket, so that its conducting surface could not affect the engine insulation; standards were set so that the blanket would not cover too much of the shell to cause heat problems; and glued area of blanket around the engine was increased so that lifting could not occur to cause heat or insulation problems.

Fig. 8.4 shows the conditions of the engine installed on the satellite.

Fig. 8.3 Wire Harness Shield

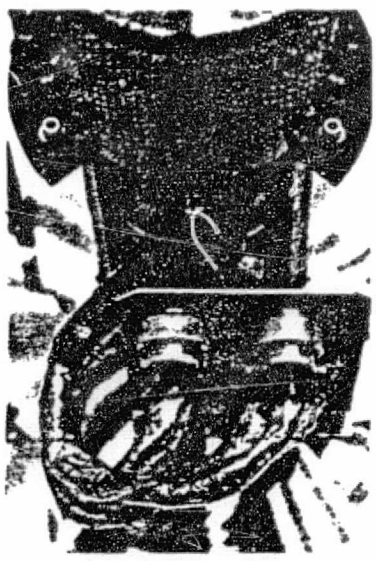

Fig. 8.4 Engines Mounted on Satellite (Unit #1 on left)

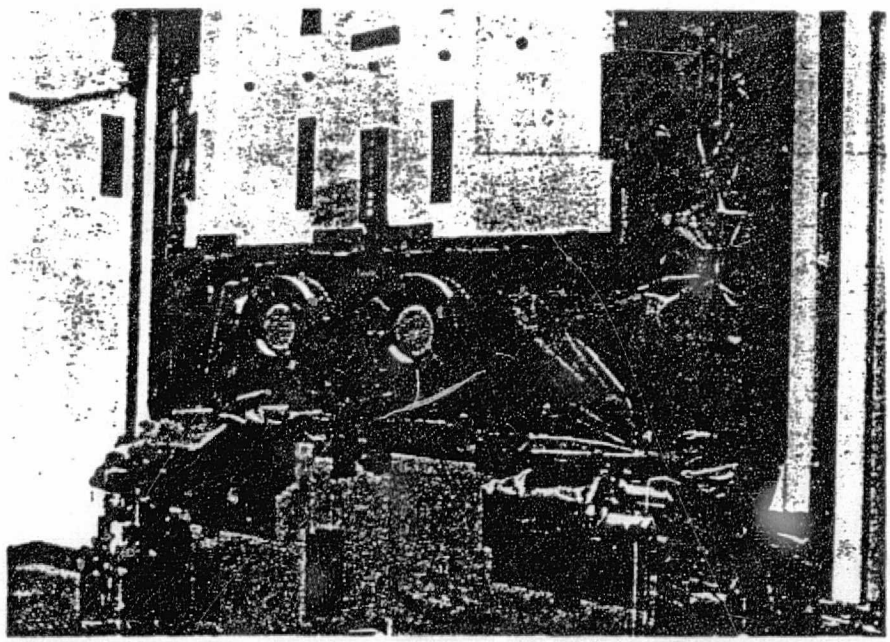

8.4 Histogram of Equipments and Final Conditions

The final conditions of the ion engine before launching are described in this section.

Table 8.2 shows the items on the engine unit with limited life. Air-exposure time and operation time for Unit #1 were 80 hours and 220 hours, respectively, and 99.5 hours and 219.6 hours for #2, each leaving about 4/5 of life before launching. Sufficient effective life was left for other items as well. Although power conditioner is not included in this group, the accumulated operation time at delivery (before transporting to launch complex) was 75.6 hours for the power control device, 167.4 hours for power source device #1 and 92.2 hours for power source device #2.

Table 8.3 shows the weight of the engine unit of the final configuration(after shielding) and the amount of propellant filled. Values of resistance in the engine unit are shown in Table 8.4.

For about 30 hours before launching, humidity exceeded 60%(max. 75%) due to a typhoon. Nitrogen gas purge was on, however, and it is assumed to have had no effects on the engine.

Thus, it was determined that the ion engine system was in ready conditions for launching.

Fig. 8.5 shows the appearance of satellite and engine immediately before the fairing installation.

Table 8.2 IEE Limitations

Subject	Effective life	IEE(1)	IEE(2)
Operation time	500 hr.	79.95 hr.	99.51 hr.
Air-exposure time	1,000 hr.	220 hr.	219.6 hr.
* On/off # cycles	500 times	23回	32回
Connector pull in/out			
P5	250回	18回	24回
P6	250回	18回	24回
P7	250回	18回	23回
P8	250回	16回	21回
Valve open/close			
G	50回	2回	3回
L	50回	3回	5回

Table 8.3 Weight of Engine in the Final Condition

	Engine wt.	Propellant wt.
Unit #1	2621g	602g
Unit #2	2634g	596g

Fig. 8.5 Final Appearance of the Satellite

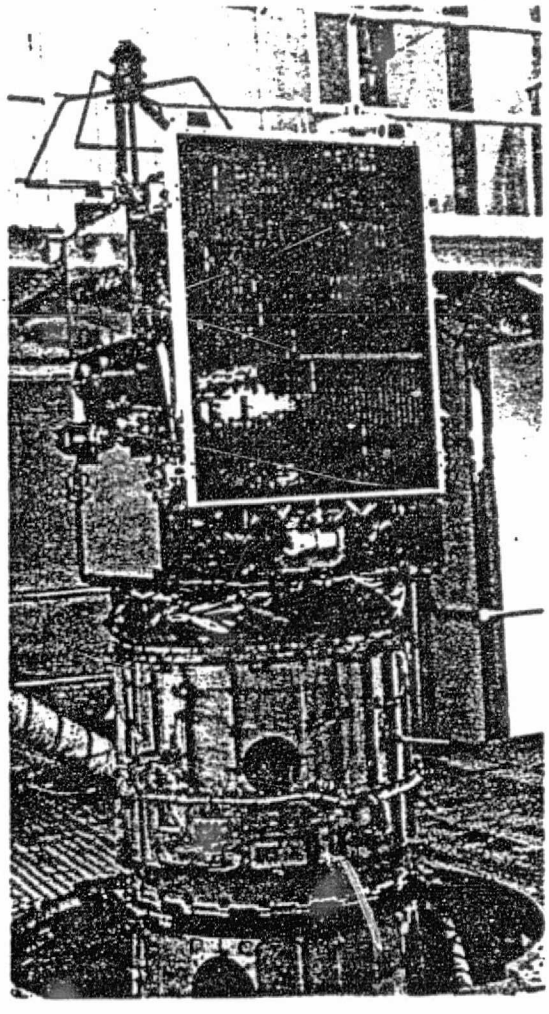

Table 8.4 Resistance of Engine Unit

	Unit #1		Unit #2	
	IEE AT	最終点検 (Final inspection)	IEE AT	最終点検 (Final inspection)
Main cathode heater	0.44Ω	0.44Ω	0.44Ω	0.44Ω
Main vaporizer heater	1.68Ω	1.69Ω	1.67Ω	1.66Ω
Insulator heater	2.75Ω	2.75Ω	2.85Ω	2.86Ω
Neut. cathode heater	0.45Ω	0.45Ω	0.44Ω	0.44Ω
Neut. Vap. heater	1.68Ω	1.68Ω	1.71Ω	1.72Ω
Main cathode keeper	>20MΩ	>20MΩ	>20MΩ	>20MΩ
Neutralizer keeper	〃	〃	〃	〃
Screen grid	〃	〃	〃	〃
Accelerator grid	〃	〃	〃	〃
Anode	〃	〃	〃	〃

IEE AT: March 1981
Final inspection: May 1982

Chapter 9

Conclusion

Development of ion engine system, despite some problems encountered along the way, has resulted in the system that is suitable for flight on board ETS-III. Currently in operation in the orbit, both Unit #1 and #2 are showing fine performance and the operation experiments are progressing smoothly. This is the second successful space experiment with ion engine following SERT-II of the United States, and the first involving a small ion engine.

Technical knowledge accumulated through the development has been significant, to the level quite competitive to that of European and American countries. Some of the major accomplishments are as follows.

(1) Necessary technology was acquired for the development of mercury electron bombardment type ion engine.

i) Production technique for hollow cathodes was improved, resulting in stable quality products.
This was achieved by clarifying selection standards in each step of assembly and stricter management of production process.

ii) Much knowledge was gained on the deterioration mechanism of hollow cathodes during ground testing.
With the knowledge, procedure and means to prevent contamination during ground testing were improved.

iii) Heat design around vaporizer and insulator proved important for motive characteristic, and necessary techniques were learned.

iv) For other components, technology developed since basic design was established.

(2) Necessary technology was acquired for the development of power conditioner which runs the engine.

i) Through production of power source devices of multi-module structures, techniques for circuit system, heat design, layout, weight reduction, electromagnetic compatibility, efficiency improvement, systematization, etc. were acquired.

ii) For high voltage power sources, techniques for insulator circuit, transformer, potting, etc. were acquired.

iii) Techniques for stabilizing power source for plasma load were learned. Also, techniques for control or protective circuit for transient fluctuation of plasma load were acquired.

(3) Techniques for interface of engine and power conditionwer were acquired.

i) Ability to achieve system compatibility such as electromagnetic compatibility was proved.

ii) Techniques for incorporating ion engine into satellite, testing techniques, etc. were acquired.

On the other hand, following are some assignments for the future.

i) Further improve design and production techniques for hollow cathodes, with respect to higher reliability and stable product quality. Also, quantitatively analyze deterioration mechanism in the ground testing and take sufficient countermeasures.

ii) By improving heat design of the engine, improve transient characteristics during operation and control the influence of external heat environment.

iii) Stabilize power supply in those power sources for which electrical interfacing with engine is critical. On the other

hand, simplify circuits where there is too much margin in power source functions and performances.

iv) Establish management standards for interface of engine unit and power conditioner in the detailed design stage at the latest. If manufacturers are different, standardize the system, including sub-system integrater, to avoid faulty interface.

v) Unify engine dummies in system tests.

vi) Study an air-tight structure of systems including hollow cathode in order to reduce the influence of air-exposure.

Technological position attained so far in this development can be summed up as "a stage where, in the development of mN-class mercury electron bombardment type ion engine system, requirements for practical use, except for that of longer life, can be met."

1990's is expected to be the beginning of a new era where stationary satellites of larger size and longer life will be in demand worldwide. With a stationary satellite weighing several tons, required designed life will be about 10 years and higher orbit maintaining accuracy will be required. In such a system, weight advantage brought by the application of ion engine system over chemical propulsion reaches over 10%, and its superiority will be apparent.

From this viewpoint, and based on the development results of ETS-III ion engine system, plans are being made for the development of 10mN-class ion engine system which can be used in orbit-maintenance of 1 - 2 ton, large size stationary satellites of the next generation. Also, with the view towards developing the independent space technology and thrust system technology in our country, it is hoped that the development of ETS-III ion engine system will be continued into the future.

Acknowledgements

The development of ETS-III ion engine system owes its success to many people. Our appreciation to those at NAL and ETL for their efforts in development, Messrs. Tahata and Ohara of NASDA Satellite Design First Group for their guidance, and those at Mitsubishi Electric Co. and Tokyo Shibaura Electric Co.(Toshiba) for their efforts in producing the hardware. The results presented here would not have been possible without the support of these people.

Appendix

A1 Outline of Engineering Test Satellite III

A1.1 Purpose of development

Engineering Test Satellite (III) is a medium altitude, 3-axis attitude controlled satellite, developed to establish common technologies for artificial satellites requiring large power of the future, and has the following four missions.

(1) Verification of 3-axis attitude control function.

(2) Verification of solar battery paddle expansion function.

(3) Verification of active heat control function.

(4) Experiments with equipments on board:

1. Vi-si-con (vision-controlled? computerized?) camera
2. Ion engine system
3. Active heat control system
4. magnetic attitude control system.

The satellite will be launched into an orbit of 45 inclination at an altitude of 1,000km by an N-1 rocket from the Tanegashima Space Center in the summer of 1982 for a one-year mission.

A1.2 Composition and shape of satellite

Composition of the satellite is shown in Table A1.1. It is grouped into basic equipments and equipments for experiments on board, with the former comprising 6 sub-systems and the latter, 4 sub-systems.

Dimensions and shapes of the satellite are shown in Fig. A1.1. Positions of each sub-system and component are shown in Fig. A1.2. System block diagrams are given in Fig. A1.3(basic equipments) and in Fig. A1.4(equipments for experiment). Fig. A1.5 is a conceptual diagram of the satellite in orbit.

A1.3 Performance of each sub-system

Main performances of basic equipments are shown in Table A1.2 and those of equipments for experimentts are shown in Table A1.3.

Table A1.1 Structure of Satellite

See next two pages

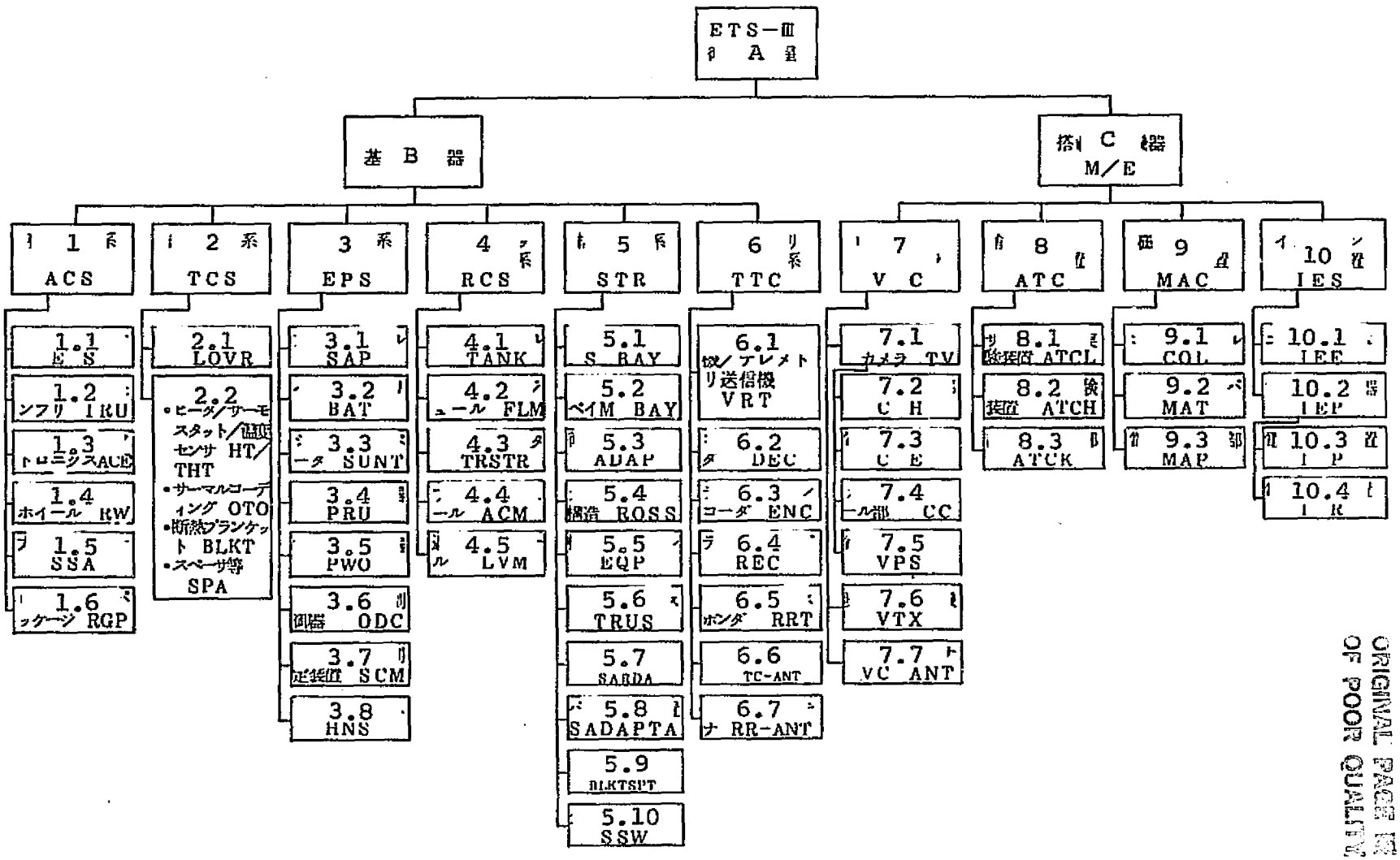

(Explanation for Table A1.1)

A. Satellite
B. Basic equipments
C. Equipments for experiments on board

1. Attitude control system
   - 1.1 Earth sensor
   - 1.2 Rate measurement assembly
   - 1.3 Attitude control electronics
   - 1.4 Reaction wheel
   - 1.5 Solar sensor
   - 1.6 Rate gyro package
2. Heat control system
   - 2.1 Thermal louver
   - 2.2 Parts: Heater/thermostat/temperature sensor HT/THT
     Thermal coating OTO
     Insulating blanket
     Spacer, etc.
3. Power source system
   - 3.1 Solar battery panel
   - 3.2 Battery
   - 3.3 Shunt dissipator
   - 3.4 Power control unit
   - 3.5 Power distributor
   - 3.6 Ordnance control unit
   - 3.7 Solar cell characteristic measurement unit
   - 3.8 Harness
4. Gas ject system
   - 4.1 Tank module
   - 4.2 Filter module
   - 4.3 Thruster cluster
   - 4.4 Access module
   - 4.5 Breaker valve module
5. Structural system
   - 5.1 Service bay
   - 5.2 Mission bay
   - 5.3 Satellite adaptor
   - 5.4 Gas jet system structure
   - 5.5 Equipment panel
   - 5.6 Supporting transformer
   - 5.7 Solar cell paddle maintaining/expansion structure
   - 5.8 Paddle drive unit
   - 5.9 Blanket support
   - 5.10 Separation switch
6. Telemetry command system
   - 6.1 Command receiver/telemetry transmitter
   - 6.2 Command decoder
   - 6.3 Telemetry encoder
   - 6.4 Taperecorder
   - 6.5 R & RR transponder
   - 6.6 Antenna for telemetry commands
   - 6.7 Antenna for R & RR

7. Camera equipment
   - 7.1 Television camera
   - 7.2 Camera head
   - 7.3 Electronic circuits
   - 7.4 Camera control unit
   - 7.5 Power source unit
   - 7.6 Picture transmitter
   - 7.7 Antenna

8. Active heat control system
   - 8.1 Device for thermal louver experiment
   - 8.2 Device for heat pipe experiment
   - 8.3 Instrument unit

9. Magnetic attitude control system
   - 9.1 Coil
   - 9.2 Timer driver
   - 9.3 Power source unit

10. Ion engine system
   - 10.1 Engine unit
   - 10.2 Power conditioner
   - 10.3 Power source device
   - 10.4 Power control device

Table A1.2 Main Performances of Main ETS-III Equipments

Subject	Performance			
Approximate size	Box-shaped main body: 0.85m x 0.85m x 2.1m Solar cell paddle part: 0.88m x 6m (paddle cant angle - 20°)			
Weight	At the beginning in orbit: 385^{+0}_{-5}kg			
Accuracy of attitude control (orbit altitude: 1,000km)		Roll	Pitch	Yaw
	During steady state control (regulation)	0.5° (0.01°/S)	0.5° (0.01°/S)	0.7° (0.01°/S)
	During thruster backup	1.0°	1.0°	1.0°
Accuracy of paddle control	Angle of incidence of the sun: ±5°			
Reaction wheel	Angular momentum: 1,856Nms, three			
Thruster	Thrust: 1N, twelve			
Propellant	Hydrazine (effective propellant 18kg)			
Propellant tank	0.31m sphere-shape, two			
Solar cell element	Silicon N/P-type, 2cm x 2cm, 7,140			
Solar cell paddle power generation	(perpendicular incidence) At beginning: over 300W After 1 year: over 260W			
Battery	Ni-Cd, capacity 8AH, 16 in series, 3 systems			
Bus power voltage	+28VDC ±1%			
Ordnance conditioner	Ignition current: 3.5-7A, 16 systems Duration of current supply: over 20mS, time difference within 10mS			
VHF telem.transmis.	136.112MHz, 1W, PCM-PM, beacon 0.1W			
•Data format	Measure frame matrix: 128 words x 8 Word length: 8 bit Bit rate: 1024 BPS (real time); 26,624 BPS (stored) PCM coding: bi-phase level			
•Input gate capacity	Analog 256, bi-level 176, serial 16			
VHF command recept.	148.27MHz, PCM-FSK-AM-PM			
•Command capacity	Discrete 255, magnitude 63, stored 16			
•Timer command	17 min. (at satellite separation and command) and 10 sec. (at satellite separation only)			
S-band reception	2116.6MHz {Range finding channel: PN-PSK-PM {Command channel: PCM-FSK-AM-PM Range finding channel frequency: 2.4MHz			
S-band transmission	1705MHz, 1.4W {Range finding channel: PN-PSK-AM-PM {Telemetry channel: PCM-FM-PM Telemetry sub-carrier frequency: 87.5KHz			

(continued to next page)

(Table A1.2 continued)

Thermal louver	Operation temperature: -15C ~ +55C Bi-metal/substrate temperature difference: ∠ 3C Effective radiation rate: blade closed ∠ 0.11 blade open ≻ 0.35
Thermostat set temperature	For mission panel heater control: 16C(standard) For TTC panel heater control: 8.8C(standard) For battery and RCS panel heater control: 11.6C(standard)
Insulating blanket	Effective radiation rate: 0.015 +0.005 -0.01
Reliability/ duration of mission	Over 0.6/1 year

Table A1.3 Main Performances of Equipments for Experiments Boarded on ETS-III

Subject	Performance
Vi-si-con(?) camera	
Effective pickup range	280km x 210km(altitude 1,000km)
Visual field angle of TV camera	15.9° horizontal direction, 120° vertical
Surface picture element distance	437m(altitude 1,000km)
	Effective no. of scanning lines: 480TV
	Horizontal picture element: 680
Pickup wave length band	Channel 1: 0.48 - 0.60μm
	Channel 2: 0.60 - 0.70μm
	Channel 3: 0.70 - 0.88μm
TV camera	CdSe visicon(vision-controlled?) 3-tube type
Intermittent exposure type	Exposure time: 8, 11, 16, 22, 32 x 10^{-3}sec.
	Exposure cycle: 5.25 sec.
Low-speed scan	Frame scanning time: 1 sec.
Output signal type	3-channel sequential system
Picture signal band width	180KHz
Picture transmitter	1705MHz, 0.8W, FM modulation
Power consumption	During pre-heating: $\angle$ 10.3W
	During operation: $\angle$ 70W
Active type heat control unit	
Heat pipe	Variable conductance type
	Heat transmission capacity: >15W
	Operation temperature(heated part): 5 - 35C
Thermal louver	Bi-metal type
	Heat transmission capacity: >15W
	Operation temperature(substrate surface): 0-40C
Instrument unit	Heat pipe: 10(pre-heat) 5, 10, 15W
Simulated heater heating level	Thermal louver: 5, 10, 15W
	Temperature data: 60 items
Multiplex telemetry	Heater voltage: 3 items
	Temperature data correcting voltage: 1 item
Power consumption	During heat pipe operation: $\angle$30W
	During thermal louver operation: $\angle$25W
Magnetic attitude control unit	
Coil	
Magnetic moment characteristic	0.171 ± 0.026 ATm^2/mA
	linear, 0.15 ATm^2 and less
Remanence moment	$\angle$ 0.05 ATm^2
Timer/driver unit	
Max. coil control current	±37.2mA
Control current steps	0 ± 31 steps
Memory capacity	265 words/8 bit

(continued to next page)

(Table A1.3 continued)

Generated magnetic moment	$0 \sim \pm 6.36$ ATm^2
Power consumption	$\angle$ 12W

Ion engine system

Engine unit	Electron bombardment type mercury ion engine			
Thrust	0.2 gr wt.			
Specific impulse	2,200 sec.			
Propellant flow	1 x 10^{-4}gr/sec			
Propellant utilization factor	70%			
Propellant loaded	600 gr.			
Power source control device	Sequence program control method			
Power source device			nominal voltage	nominal current
10-system power sources	PS1	beam	1KV	30mA
	PS2	accelerator electrode	-1KV	1mA
	PS3	discharge	40 V	0.35A
	PS4	cathode heater	5 V	5 A
	PS5	cathode keeper	15 V	0.3 A
	PS6	cathode vaporizer	3.5V	2 A
	PS7	neutralizer heater	5 V	5 A
	PS8	neutralizer keeper	24 V	0.25A
	PS9	neutralizer vaporizer	2.1V	1.2 A
	PS10	insulator heater	3 V	1 A
Power consumption	$\angle$ 100W			

Fig. A1.1(1/2) Size and Shape of ETS-III

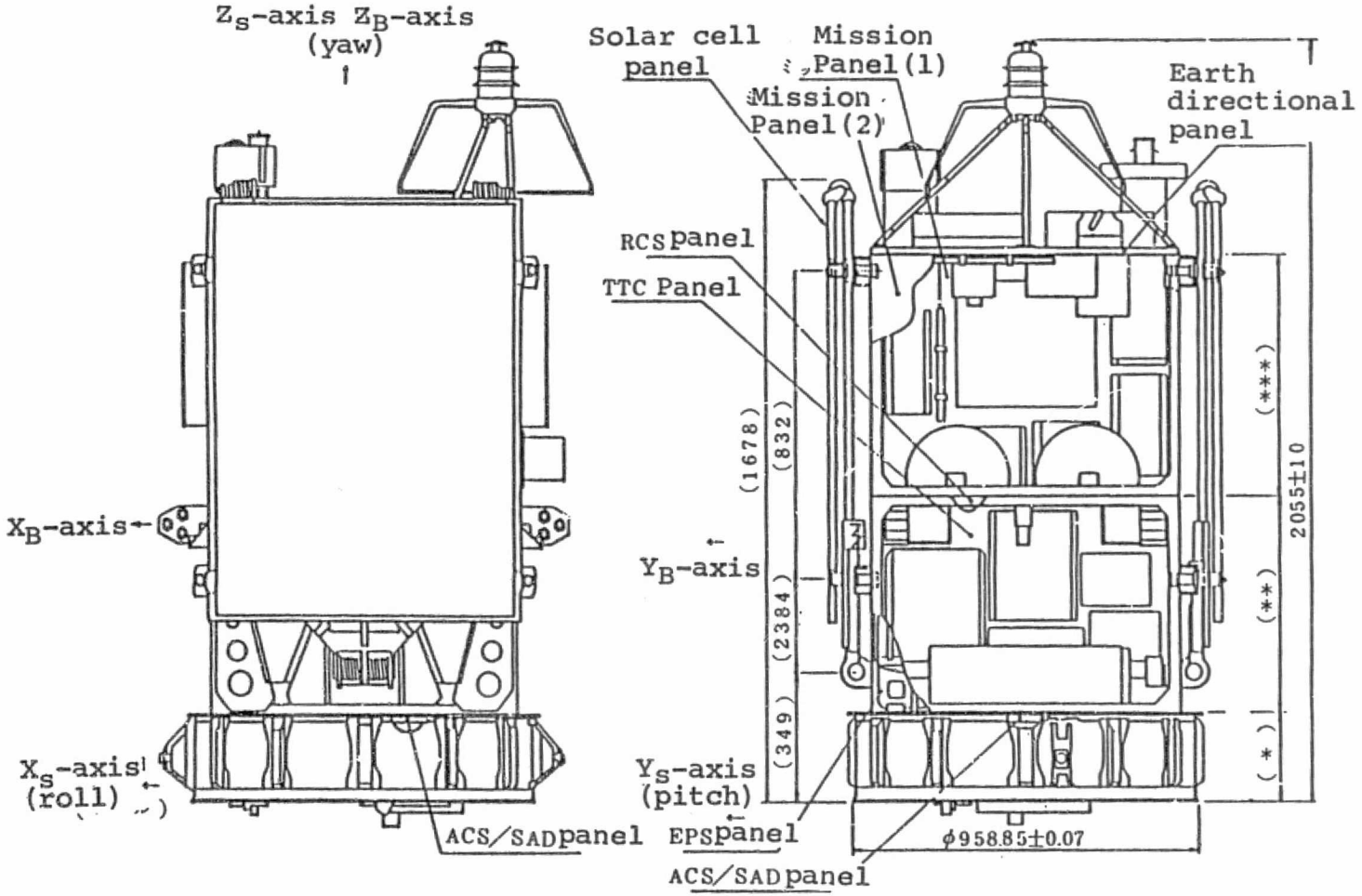

Notes:
1. Co-ordinates X_S, Y_S and Z_S are formed on the satellite separation surface, with the center of the surface as the origin. X_B, Y_B and Z_B have the center of gravity of the satellite as the origin, and are parallel to X_S, Y_S and Z_S.
2. Insulating bracket and bracket support are not shown.
3. Unit: mm
   (*) satellite adaptor
   (**) service bay
   (***) mission bay

Fig. A1.1(2/2) Size and Shape of ETS-III (Configuration in Orbit)

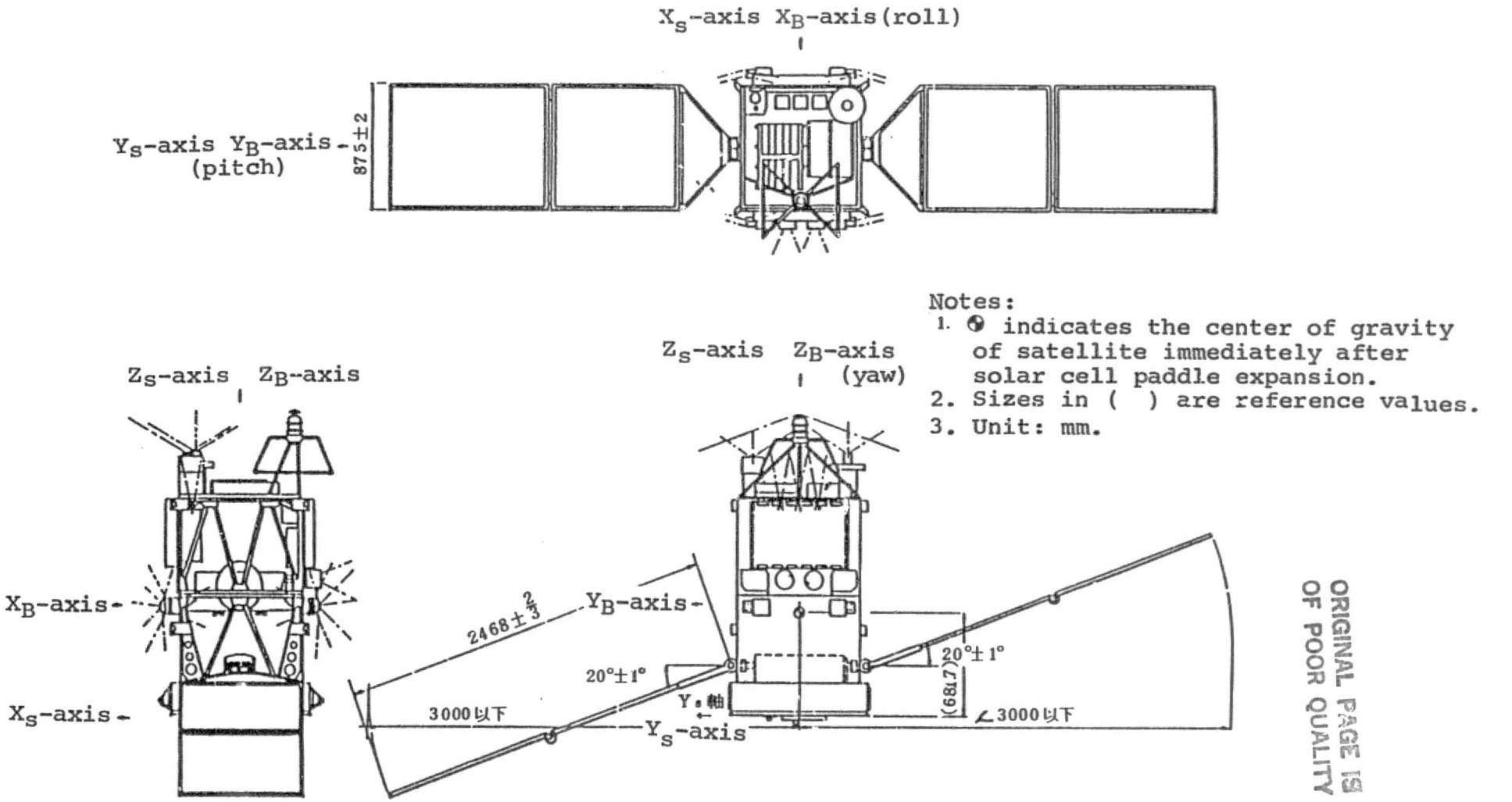

Notes:
1. ⊕ indicates the center of gravity of satellite immediately after solar cell paddle expansion.
2. Sizes in ( ) are reference values.
3. Unit: mm.

Fig. A1.2 Layout of Sub-systems

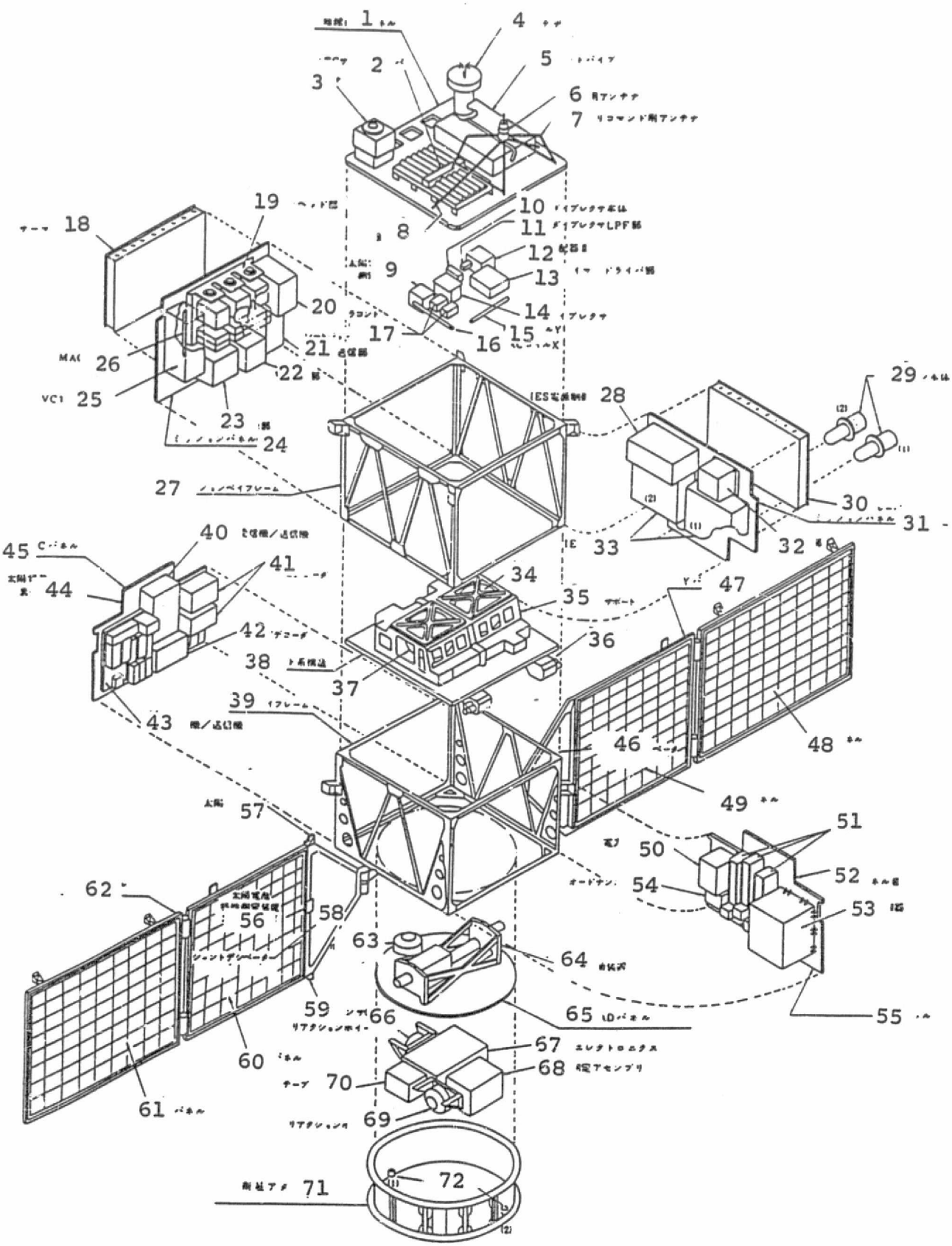

(Explanation for Fig. A1.2)

1. Earth directional panel
2. ATC thermal louver
3. Earth sensor
4. VC antenna
5. ATC heat pipe
6. Antenna for R & RR
7. Antenna for telemetry command
8. Support truss
9. Solar cell characteristic measuring device
10. S-band diplexer
11. S-band diplexer LPF unit
12. Power distributer II
13. MAC timer driver unit
14. VHF diplexer
15. MAC coil Y
16. MAC coil X
17. Rate gyro package
18. Thermal louver
19. VC camera head
20. VC camera control unit
21. VC picture transmission unit
22. VC power source unit
23. MAC power source unit
24. Mission Panel(I)
25. VC electronic circuit unit
26. MAC coil Z
27. Mission bay fram
28. IES power source control unit
29. IES engine unit
30. Thermal louver
31. Mission panel(II)
32. ATC instrument unit
33. IES power source unit
34. Tank(1)
35. Blanket support
36. Thrust cluster
37. Tank(2)
38. Gas jet system structure
39. Service bay frame
40. S-band receiver/transmitter
41. Telemetry encoder
42. Command decoder
43. VHF receiver/transmitter
44. Solar cell element panel II
45. TTC panel
46. Shunt dissipator
47. Y paddle
48. Outer panel
49. Inner panel
50. Power distributor I
51. Battery
52. Solar cell element panel III
53. Power conditioner
54. Ordnance conditioner
55. EPS panel
56. Solar cell characteristic measuring device element panel I
57. Solar sensor(2)
58. Shunt dissipator
59. Solar sensor(1)
60. Inner panel
61. Outer panel
62. +Y paddle
63. Reaction wheel(Y)
64. Paddle drive device
65. ACS SAD panel
66. Reaction wheel(R)
67. Attitude control electronics
68. Rate measurement assembly
69. Reaction wheel(P)
70. Tape recorder
71. Satellite adaptor
72. Separation switch

Fig. A1.3 System Function Block Diagram (Basic Equipments)

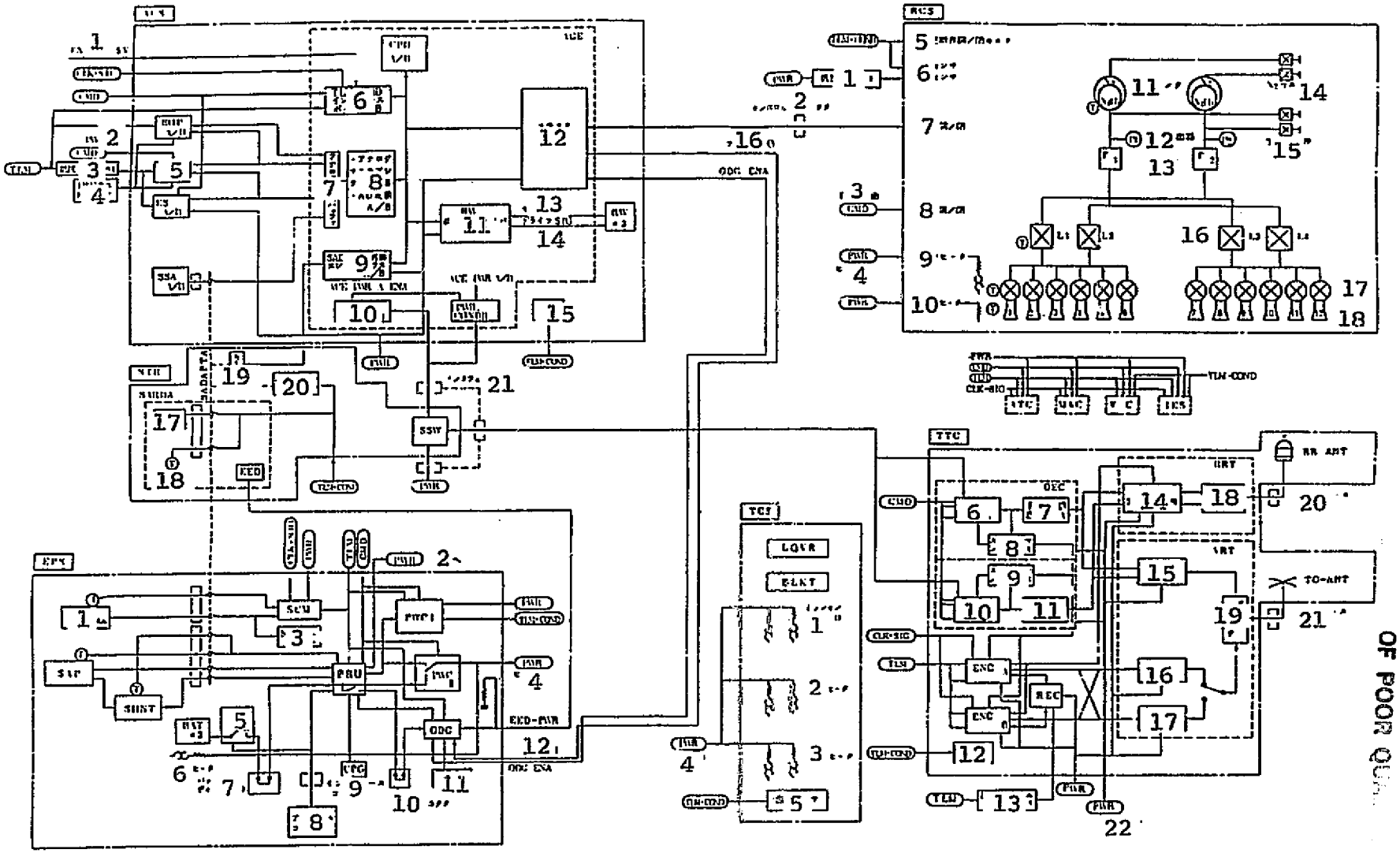

(Explanation for Fig. A1.3)

ACS
1. +5V from ENC
2. via PWC
3. Resistance module I
4. IRU test connector
5. IRU gyro 3
6. TLM/CMD interface port A/B
7. Analog signal buffer
8. Analog multiplexer A/B · AD transformer A/B
9. SAD paddle control electronics
10. Start timer
11. RW port/driver x 3
12. Thruster port
13. Sensor SIG
14. Drive SIG
15. Temperature sensor
16. Fire SIG
17. Potentiometer
18. Damper
19. Motor
20. Position indicater
21. Interface connector

EPS
1. SCM monitor panel
2. To TTC
3. SCM monitor panel
4. Heater bus
5. Relay module
6. Battery heater
7. Battery disconnect
8. Empirical connector
9. Interface connector
10. Ordnance turn-on connector
11. EED test connector
12. Fire SIG

RCS
1. Resistance unit
2. Interface connector
3. via PWC
4. Heater bus
5. Propellant shut-off valve Open/Close monitor
6. Temperature sensor · pressure sensor
7. Propellant valve Open/Close
8. Shut-off valve Open/Close
9. Propellant valve heater
10. Catalyzer tank heater
11. Propellant tank
12. Pressure detector
13. Filter
14. N_2 gas exhaust valve
15. Propellant drain valve
16. Shut-off valve
17. Propellant valve
18. Thruster

TTC
1. Mission Panel I heater
2. TTC panel heater
3. RCS panel heater
4. Heater bus
5. Temperature sensor
6. Processor A
7. FSK demodulator A
8. Stored command memory A
9. " " " B
10. Processor B
11. FSK demodulator B
12. Temperature pressure sensor
13. Resistance module 1
14. S-band transmitter/receiver
15. CMD receiving unit
16. TLM transmitting unit A
17. TLM transmitting unit B
18. Diplexer
19. Diplexer
20. Interface connector
21. " "
22. From PRU

T : Temperature sensor

(PWR) : S/C bus power source

(CMD) : Command signal

(TLM) : Telemetry signal

(CLK, SIG) : Clock, enable, MAFS, MIFS

(TLM, COND) : Telemetry conditioning

Connectors and modules outside the broken lines (——·——) belong to EPS.

Fig. A1.4 System Function Block Diagram(Equipments for Experiments on Board)

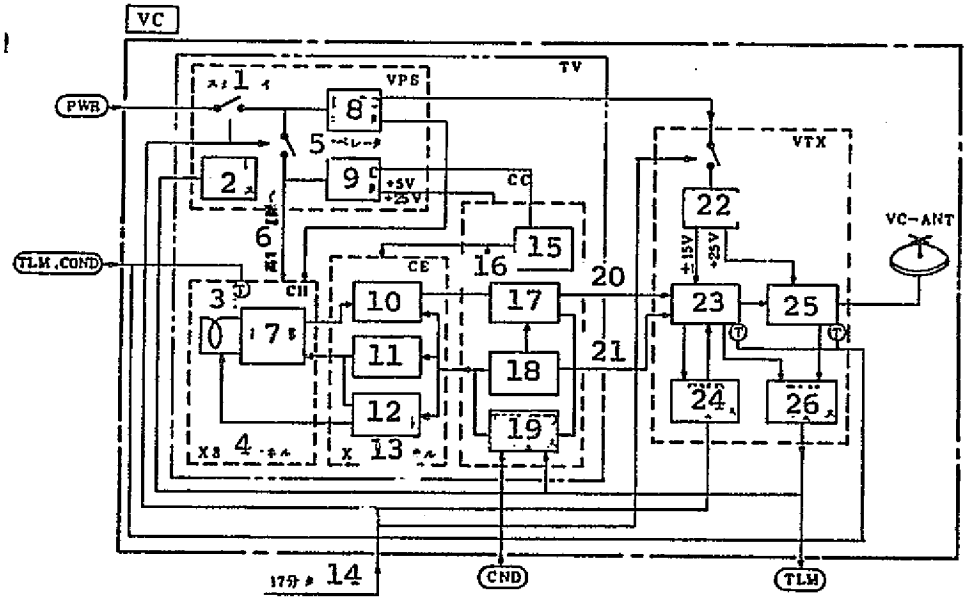

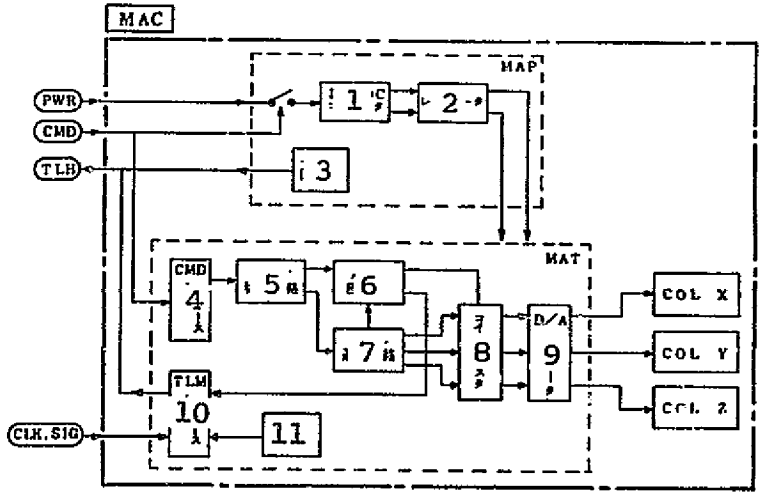

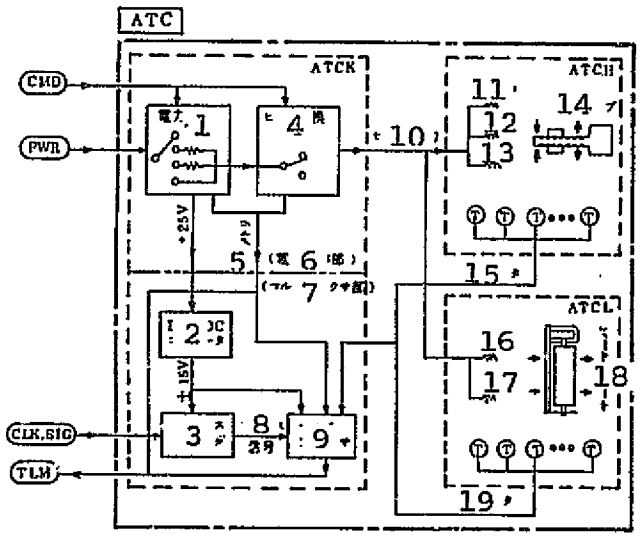

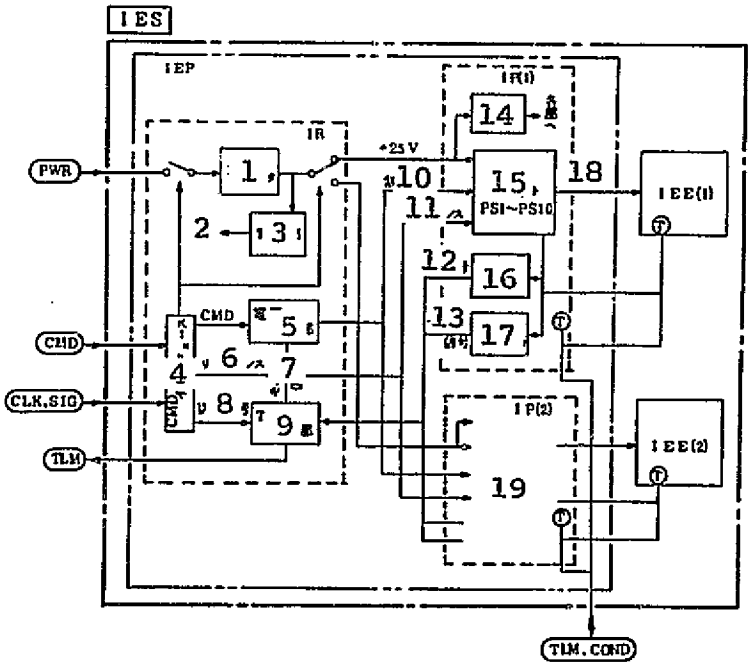

(Explanation for Fig. A1.4)

VC
1. Stand-by
2. TLM interface
3. Optical unit
4. X3 channel
5. TV operator
6. To high voltage power source
7. Picture unit
8. DC/DC converter
9. DC/DC converter
10. Process amplifier
11. Deflection circuit
12. Drive control circuit
13. X3 channel
14. 17-min. timer CMD
15. Regulator
16. To each unit
17. Multiplexer
18. Pulse generating circuit
19. TLM CMD interface
20. Picture signal
21. Periodic signal
22. Regulator
23. Modulating unit
24. CMD interface
25. Amplifying unit
26. TLM interface

ATC
1. Power switch
2. DC/DC converter
3. Address decoder
4. Heater switch
5. Telemetry
6. (Power control unit)
7. (Multiplexer unit)
8. Address signal
9. Multiplexer
10. Heater power
11. Pre-heater
12. Heater A
13. Heater B
14. Heat pipe
15. Temperature data
16. Heater A
17. Heater B
18. Thermal louver
19. Temperature data

MAC
1. DC/DC converter
2. Regulator
3. Monitor circuit
4. CMD interface
5. Mode switching circuit
6. Memory circuit
7. Coil selecting circuit
8. Coil register
9. D/A converter
10. TLM interface
11. Monitor circuit

IES
1. Input filter
2. To each unit
3. Power source unit
4. CMD interface
5. Power source control unit
6. Reference
7. Monitor signal
8. Switching signal
9. TLM switching unit
10. Control signal
11. Reference
12. Monitor signal
13. TLM signal
14. Drive power source
15. Power source unit(PS1-PS10)
16. Monitor circuit
17. TLM circuit
18. 10 system power
19. (same as above)

(T) : Temperature sensor

(PWR) : S/C bus power source

(CMD) : Command signal

(TLM) : Telemetry signal

(CLK, SIG) : Clock, enable, MAFS, MIFS

(TLM, COND) : Telemetry conditioning

Fig. A1.5 ETS-III

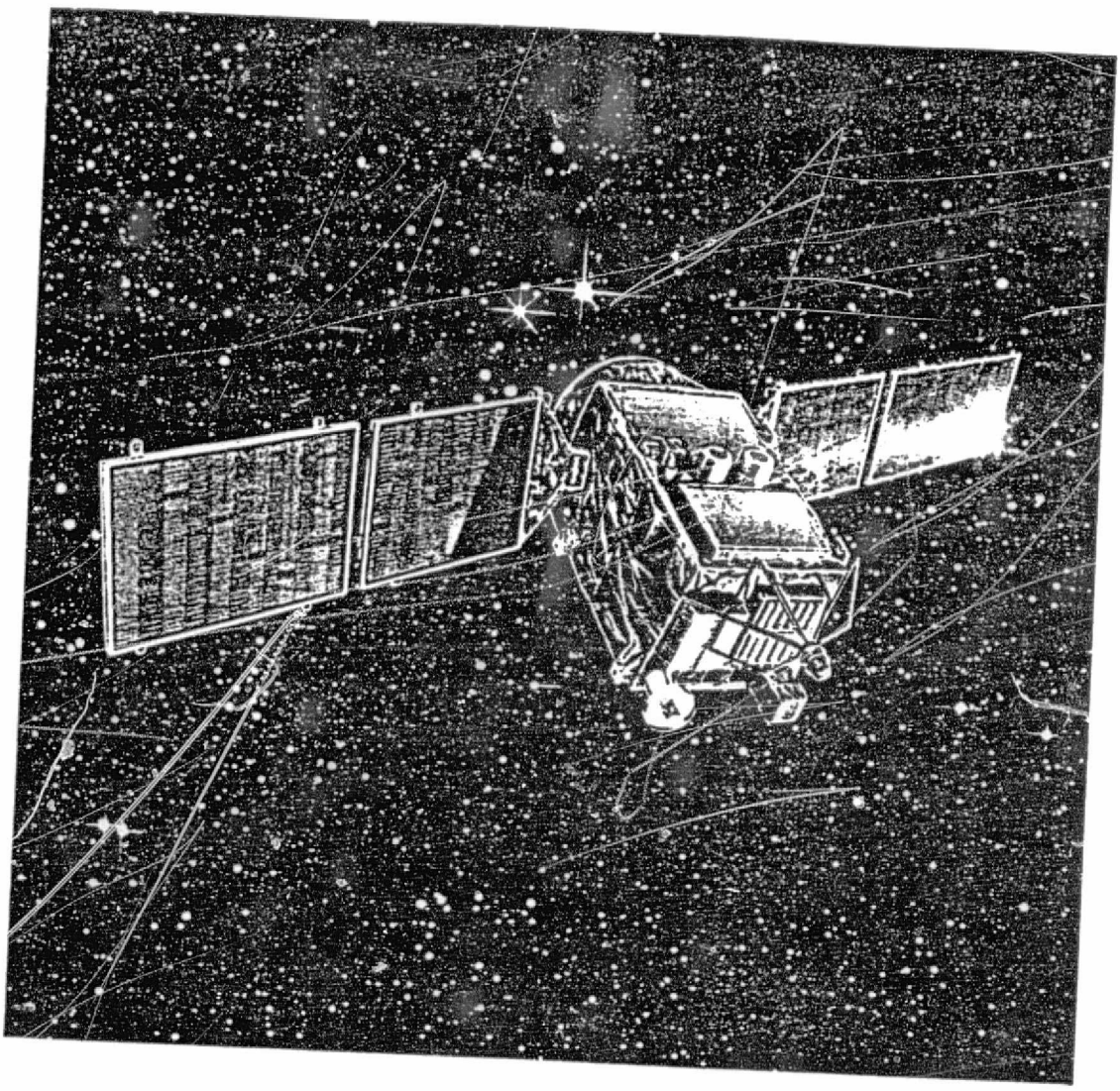

A2 Record of problems

A summary of problems recorded during post-PM developments is given. Table A2.1 and A2.2 list the problems occurred in QT of the engine unit component test and in the sub-system test of ion engine system. Table A2.3 lists the problems occurred in the sub-system evaluation (PM engine #1 and modified EM of power conditioner). Table A2.4 and Table A2.5 list the problems occurred in the AT of engine unit component test and in the sub-system test of ion engine system. With power conditioner, component test showed no problem in neither QT nor AT.

Table A2.6 and Table A2.7 are the lists of problems in the Qualifying Test and in the Acceptance Test of the system. Not listed here is the problem described in Section 8.2.1, of ignitability fluctuation of hollow cathode during engine unit performance check before delivery to the launch complex.

Table A2.1 Record of Problems(IEE QT)

IEE #1

1. Insulator heater voltage did not meet the standard range during rated operation test of performance test(I). (Measured: 2.593～2.600V. Standard: 3± 0.3V)

   Cause and treatment: Dummy load smaller than the actual. No problem in performance evaluation, and test continued.

2. Main hollow cathode discharge could not be maintained after ignition during interface check of performance test(I).

   Cause and treatment: Influence of capacitance on the testing power source side. Stabilizing resistance changed to 20Ω.

3. Neutralizer cathode was not ignited 30 minutes after start during parameter test of performance test(I).

   Cause and treatment: Insufficient activation of neutralizer hollow cathode. Retested after activation.

4. Main discharge alone broke down during thermal vacuum test.

   Cause and treatment: Main hollow cathode keeper discharge manually stopped and thrown into forced recovery mode.

5. Base plate temperature was outside the range of testing standard in the performance test(I) and in thermal vacuum test.

   Cause and treatment: Off-the-standard temperature range and its duration too insignificant to affect performance check, and testing continued.

6. Performance characteristic data could not be obtained due to a faulty mi-ni-con(? micro computer?) during thermal vacuum test.

   Cause and treatment: Data on real time characteristics obtainable under this condition. Testing continued.

7. Discoloring of metal part of D subconnector discovered in the appearance inspection after thermal vacuum test.

   Cause and treatment: Caused by chamber test. No affect on the connector performance. Testing continued.

8. Breaking of main hollow cathode vaporizer thermocouple was found during charging/insulation test after oscillation test(random wave, X-axis).

   Cause and treatment: Thermocouple replaced. For prevention of recurrence, ends of thermocouple secured on tank support.

9. Appearance defects were found in the vaporizer heater lead wire of main hollow cathode, i.e. Ni-plating disappeared and turned to copper color.

   Cause and treatment: Due to exposure to temperature of about 970C for the brazing treatment of 8 above. Vaporizer heater replaced.

10. Neutralizer hollow cathode could not be controlled during interface check of performance test(II).

    Cause and treatment: Neutralizer hollow cathode replaced, due to a possibility of its affecting interface with power source.

11. Short-circuit occurred in cathode heater of main hollow cathode during rated operation test of performance test(II).

    Cause and treatment: Faulty spot welding of hollow cathode unit. Repairing difficult, and the main hollow cathode replaced.

12. Forced ignition was required due to slow ignition of neutralizer hollow cathode keeper discharge during rated operation test of performance test(II).

    Cause and treatment: This treatment was for checking ignition. No effects on performance. No action taken and rated operation retested.

13. Beam injection was started without a 3-minute waiting time, as manual operation was started immediately after NEU START during interface check of performance test(II).

    Cause and treatment: Secere conditions for a test. No effect on evaluation. No action taken.

14. Defects discovered in the final appearance inspection.

    Cause and treatment: Due to handling in tests. No effects on functions and performances, and no action taken.

IEE #2

1. Dent was found on the shell in appearance inspection.

   Cause and treatment: Mishandling during assembly. Dent minor, and no action taken.

2. Beam could not be injected during thermal vacuum test.

   Cause and treatment: Misconnection(between beam power source and accelerating grid power source). Little effects on the unit. Connected properly and retested.

3. Discoloring of metal part of D subconnector found in appearance inspection during thermal vacuum test.

   Cause and treatment: Caused by chamber tests. No effects on connector performance and no action taken.

4. Oscillation patterns did not meet the standards during oscillation test(random wave, Z-axis).

   Cause and treatment: No effects on strength. No action taken.

5. Resistance of main hollow cathode heater increased during charging/ insulation test after oscillation test(random wave, Z-axis).

   Cause and treatment: Breaking of cathode heater lead wire at the terminal. Repaired and reconnected by spot welding.

6. Cracking was discovered in the sealed end of main hollow cathode insulator heater. (Found while treating 5 above.)

   Cause and treatment: Mishandling during hollow cathode test. Insulator heater replaced.

7. Appearance defects were found in the vaporizer heater lead wire of main hollow cathode, i.e. Ni-plating disappeared and turned to copper color.

   Cause and treatment: Due to exposure to temperature of about 970C for the brazing treatment of 6 above. Vaporizer heater replaced.

8. Relative humidity exceeded the standard during preparation for performance test(II). (69-71%, about 30 minutes.)

   Cause and treatment: Duration short and no effects on performance and reliability. No action taken.

9. Main hollow cathode keeper discharge was not ignited after 30 minutes during rated operation test of performance test(II).

   Cause and treatment: Faulty ignition due to the first time operation after exposure to air. Main hollow cathode replaced because of a short circuit of cathode heater found at the same time.

10. Beam injection could not be tested due to repeated disappearance of main discharge during rated operation test after main hollow cathode was replaced.

    Cause and treatment: Mismeasurement of flow and temperature. No effects on performance and no action taken.

11. Breaking of neutralizer hollow cathode vaporizer heater was discovered during oscillation test(random wave, Y-axis) under MR treatment.

Cause and treatment: Oscillation under increased stress from many installation/removal of MR treatment. Repairing difficult and neutralizer hollow cathode replaced.

12. Data on neutralizer keeper voltage, mercury flow, etc. did not meet the standards during rated operation test of performance test(II).

    Cause and treatment: No effects on performance, and no action taken for neutralizer keeper voltage. Mercury flow remeasured and the standards met.

13. Defects discovered in the final appearance inspection.

    Cause and treatment: Due to handling in tests. No effects on functions and performances, and no action taken.

Table A2.2 Record of Problems(IES QT)

IES #1

1. During hollow cathode operation test of functionality test of ion engine system(combination of IEE#1, IR and IP#1), keeper discharge stopped twice after main discharge was ignited. Keeper discharge ignited three times but main discharge current did not flow normally.

   Cause: Due to a transient phenomenon during main discharge of the engine unit, excess current protection circuit for main discharge unit in the power source device latched.

   Action taken: Constant of the excess current protection circuit changed. Unit UPC30180B-C1(0.01μ) eliminated and R8 changed from 1MΩ to 100kΩ.

2. During beam injection operation test of function/performance check of ion engine system(combination of IEE#1, IR and IP#L) beam could not be injected.

   Cause: Same as above.

   Action taken: Same as above.

3. During neutralizer operation test of function/performance check of ion engine system(combination of IEE#1, IR and IP#L), 23.3W power from PS7 of the power source device(IP) was supplied to the engine (IEE) for 30 minutes, but the neutralizer in the engine did not ignite.

   Cause: Insert loss of extension cable connecting the main unit and power source via junction box in the test configuration, and, assumably, higher-than-estimated load impedance(IEE) with respect to power source.

   Action taken: External power source used for neutralizer heater power source(PS7) and testing continued. If the same same occurred in the combination of IEE#2, test to be performed withe external power source. TASK REVIEW given after the combination test to determine whether to move onto next TASK.

4. During rated operation test of thermal vacuum test of ion engine system(combination of IEE#1, IR and IP#1), neutralizer keeper discharge did not turn ON.

   Cause: Assumed lack of compatibility between power source device(#1) and engine unit(#1) with respect to neutralizer heater.

   Action taken: Function/performance on the component level reviewed(review of IEE#1 requested to MELCO). Testing halted for ion engine system #1 and test performed for #2.

IES #2

1. (Electromagnetic compatibility test) During QT for electromagnetic compatibility of ion engine system(combination of IEE#2, IR and IP#2), neutralizer keeper discharge did not turn ON.

   Cause: Contamination on neutralizer keeper and lead support by backspattering from the lower engine body.

   Action taken: Engine unit#2 sent back to Mitsubishi Electric for inspection and treatment.

2. (Electromagnetic compatibility test) During appearance inspection after QT for electromagnetic compatibility test of the system (IEE#2, IR and IP#2), discoloring(dark brown) was found on beam injection surface and on sides of engine body. especially where the neutralizer was mounted.

   Cause: Oil splashed and adhered to IEE#2 during EMC test and discolored under heat, etc.

   Action taken: As ion engine unit was placed in vacuum of 10^{-6}Torr for two days after completion of test, no possibility of adhered material further affecting the engine. No effects on performance and no action taken.

Table A2.3 Record of Problems(IES Evaluation Test)

1. In the combination of IEE#1, IR(EM) and IP(EM), power was OFF for two minutes during idling.

   Cause: Based on that IES bus power power source and vacuum meter both turned off, a temporary outage in their power source system(AC100V) suspected.

   Action taken: Following done and testing continued. 1) IES OFF CMD executed; 2) power source of 28V bus power checked; 3) IES ON CMD executed; 4) Input current checked; 5) MAG CMD executed; 6) IDL CMD executed, and 7) Input current checked. (As IES was in IDLING, AC 100V OFF did not affect IES functions.)

2. In the combination of IEE#1, IR(EM) and IP(EM), four minutes after START CMD was sent, abnormality was observed in the telemetry data on pen recorder.

   Cause: Burning of rush current damping resistance R1 in IR (EM), assumably due to some faulty movement of latching relay which short-circuits R1.

   Action taken: Resistance R1 replaced in IR. Testing continued after IR component(single unit) check.

3. In the combination of IEE#1, IR(EM) and IP(EM), neutralizer vaporizer temperature Tnv was lower than estimated. Estimated: Tnr $\simeq$ 227C. Measured: Tnv=159C.

   Cause: Tnv telemetry drifted with a drift in offset voltage of operational amplifier IC 23(LM108AF) in the printed unit of IP(EM#1).

   Action taken: IC23(LM108AF) replaced and corrected Tnv curve taken.

4. In the combination of IEE#1, IR(EM) and IP(EM), injection was not reached when beam voltage of V_N=1kV was applied to the engine unit.

   Cause: Beam voltage thrown in before main discharge was sufficiently stabilized, which caused accelerator current(Ia) to flow in excess, activating protection circuit in power source device which shut off beam voltage.

   Action taken: Main discharge maintained for 1 hour after ignition for stabilization. Then, discharge current changed from 0.35A to 0.3A immediately before throwing in beam voltage. (Change to be made in testing procedure manual.)

5. In the parameter test of neutralizer keeper voltage Vnk of the combination of IEE#1, IR(EM) and IP(EM), ion injection was not reached when beam voltage of V_N=1kV was applied to engine unit.

Cause: Presumably, accelerator current flowed in excess when beam voltage was thrown in, causing insulation breakdown.

Action taken: Time constant of IP(EM) inhibit circuit changed from 0.8 sec to 1.4 sec, same as PM. Amount of mercury flow, MAG CMD V_D=38V changed to 36V. Discharge current MG CMD I_d= 0.35A changed to 0.30A.

6. During thermal vacuum test of the combination of IEE#1, IR(EM) and IP(EM), beam injection was not reached when beam voltage of V_N=1kV was applied.

Cause: Presumably, high voltage was thrown in twice without setting V_N(operation mistake), leaving large amounts of vaporized mercury in the engine unit and thus causing plasma density to increase.

Action taken: Discharge current(I_d) set to 0.3A and high voltage thrown in; after stabilizing, discharge current(I_D) set to 0.35A to obtain data.

7. In the combination of IEE#1, IR(EM) and IP(EM), discoloration (light brown color) of beam injection surface on the engine unit was found during appearance inspection after completion of tests.

Cause: Presumably, spattering from vacuum tank during ground testing. (This problem peculiar to ground testing.)

Action taken: Discoloring occurred when IEE was in operation, and not likely to progress during storage and exposure to air. No action taken.

Table A2.4 Record of Problems (IEE AT)

IEE #1

1. Defects in appearance and mislabelling found in appearance inspection of early stage mechanical function test.

   Cause and treatment: Defects minor and no action taken. Mislabelling of parts numbers and manufacturing dates to be corrected by the completion of AT.

2. Main vaporizer heater current did not meet the standards during rated operation of performance test(I).

   Cause and treatment: This data obtained immediately after ignition and is due to noise generated by ignition. No effects on performance and no action taken.

3. During rated operation of performance test(I), 1) propellant utilization efficiency, 2) beam current and 3) insulator heater voltage did not meet the standards.

   Cause and treatment: Does not occur if mercury flow is slightly reduced. Also, tolerable overall performance with respect to interfacing achieved. No action taken.

4. During interface check of performance test(I), unstable conditions were observed at the beginning of ignition of neutralizer hollow cathode keeper discharge.

   Cause and treatment: Phenomenon does not occur when combined with IEP. Ignition can be achieved by normal recovery sequence. No action taken.

5. In the interface check of performance test(I), beam current during steady state injection did not meet the standards.

   Cause and treatment: Caused by turbulence of discharge current waveform. No effects on total performance or interface. No action taken.

6. At the start of rated operation test of performance test(II), degree of vacuum did not lower below targeted value.

   Cause and treatment: Due to chamber capacity. No effects on IEE operation. No action taken.

7. In the parameter test of performance test(II), base plate temperature did not meet the standard.

   Cause and treatment: Control mistake. No effects on evaluation of performance data. No action taken.

8. In the appearance inspection of the final mechanical funtion test, scratches, etc. were found.

   Cause and treatment: No effects on functions. No action taken.

IEE #2

1. Defects in appearance and mislabelling found in appearance inspection of early stage mechanical funtion test.

   Cause and treatment: Defects minor and no action taken. Mislabelling of parts numbers and manufacturing dates to be corrected by the completion of AT.

2. During rated operation of performance test(I), insulator heater voltage and main vaporizer heater current did not meet the standard during transient state before injection.

   Cause and treatment: Insulator heater voltage meets the standard when measured at monitor terminal, and main vaporizer heater current a short-lived phenomenon. No effects on performance. No action taken.

3. During rated operation of performance test(I), beam injection could not be achieved.

   Cause and treatment: IEE was normal during charge check before performance test. Connections changed to equivalent line at the output terminal board of power source and testing continued.

4. During rated operation of performance test(I), main hollow cathode keeper discharge and main discharge did not ignite after 30 minutes.

   Cause and treatment: Input of PS4 changed from 5.0A to 5.2A (constant current) and keeper discharge ignition resulted within 5 minutes. Testing continued.

5. During interface check of performance test(I), unstable conditions were observed at the beginning of ignition of neutralizer hollow cathode keeper discharge.

   Cause and treatment: Phenomenon does not occur when combined with IEP. Ignition can be achieved by normal recovery sequence. No action taken.

6. During rated operation of performance test(II0, short circuit occurred in the neutralizer keeper immediately after operation was started.

   Cause and treatment: Caused by short-circuit inside neutralizer hollow cathode. Neutralizer hollow cathode replaced and AT given again.

7. Main hollow cathode insulator heater lead wire was found closer to the main support(found as a result of 6 above).

   Cause and treatment: Already close when produced. No plastic deformation and no visually observable abnormality. No action taken.

8. There were two spots on the housing insert where screws for mounting the shell were hard to go through (found as a result of 6 above).

   Cause and treatment: Tapped to let through.

9. In the acceptance test of hollow cathode, melted area of spot welding was found larger on the cathode heater side(replaced item in 6).

   Cause and treatment: Unevenness in workmanship. No effects on strength. No action taken.

10. During rated operation of performance test(I), main hollow cathode vaporizer heater power source and neutralizer hollow cathode keeper discharge voltage did not meet the standards.

    Cause and treatment: Main vaporizer current a short-lived phenomenon and no effects on performance. With keeper discharge, no effects on maintaining interface stability and neutralizing function verified. No action taken.

11. In the interface check of performance test(I), main hollow cathode vaporizer heater current did not meet the standard.

    Cause and treatment: Short phenomenon(about 10 sec.) immediately after neutralizer ignition and no effects on performance. (Same as 10 above.) No action taken.

12. Im the random oscillation test(X-axis), the pattern exceeded the standard.

    Cause and treatment: Due to control capability of oscillator. No resonance point near 1,300Hz. Under QT level. No negative effects, and no action taken.

13. During rated operation of performance test(II), neutralizer hollow cathode keeper discharge voltage did not meet the standard.

    Cause and treatment: Due to characteristics of neutralizer hollow cathode. (Same as 10.) No problem in maintaining interface stability and neutralizing function confirmed. No action taken.

14. In the thermal vacuum test, main hollow cathode vaporizer heater power source loop could not be controlled properly and beam injection could not be performed.

Cause and treatment: Caused by faulty action of closed loop control circuit in the power source. Beam injection achieved by maintaining main vaporizer current at about 2A, indicating no effects on performance.

15. In the low-temperature starting test(2) of thermal vacuum test, discharge voltage immediately after the start of beam injection exceeded 60V.

    Cause and treatment: Due to low temperature of main hollow cathode vaporizer at the time of beam injection. Performances same as PM and no effects on interface. No action taken.

16. In high temperature starting test of thermal vacuum test, unstable conditions were observed at the beginning of ignition of neutralizer hollow cathode keeper discharge.

    Cause and treatment: Phenomenon does not occur when combined with IEP. Ignition can be achieved by normal recovery sequence. No action taken.

17. In the final appearance inspection, scratches, stains, adhesion of foreign material, etc. were found.

    Cause and treatment: Minor. No effects on performance. No action taken.

Table A2.5 Record of Problems(IES AT)

1. Ion engine unit #2 was unpacked by mistake instead of #1.

   Cause: Carelessness of workers who failed to check product no.

   Action taken: Engine unit #2 returned to freight container. Air-exposure time recorded. Unit #1 unpacked and tests given.

2. Instead of 300ℓ/min rotary pump, 1,500ℓ/min rotary pump for main vacuum tank was mistakenly switched off.

   Cause: Operation mistake due to unclear TD instruction.

   Action taken: When the diffusion pump for main vacuum tank is mistakenly shut off during operation, protective circuit acts to close clapper valve of the pump and electromagnetic valve between the diffusion pump and rotary pump. Thus, contamination by diffusion of oil does not occur.

3. Degree of vacuum reached only 5×10^{-1}Torr instead of the specified 5×10^{-2}Torr.

   Cause: Presumably, a leakage from a very small scratch found on the flange of heat control box.

   Action taken: Metal gasket, inserted into the flange, was replaced by a fluorine O-ring.

4. When 28V DC power source was switched on, amperometer of DC power source oscillated over 5A for an instant and then returned to 1.0 - 1.2A. At that point, DC power source was immediately shut off.

   Cause: Faulty connection of vacuum tank flange connector.

   Action taken: No ill effects on hardware found. Pin assignment of cable changed and testing resumed.

5. In the appearance check of final AT, black binding band was off in two places.

   Cause: Presumably, faulty knots which had come loose.

   Action taken: Re-binding requested to Mitsubishi Electric by NASDA.

Table A2.6 Record of Problems (System QT)

1. During IES/EEO compatibility test, TLM9406(cathode keeper current) dropped from 2.98 TMV(295.28mA) to 0.74 TMV(80.769mA).

   Cause: Due to a design mistake, surge current exceeding the standard was sent to diodes CR4 and CR6(NASDA TX1S 2204) when power was supplied. Because of the stress, diodes opened, lowering the main cathode keeper current telemetry.

   Action taken: Diodes replaced by JANTXV1N645-1. Same treatment given to FM.

2. Gas leak was found in the connecting part of secondary pressure adjuster and primary pressure meter.
   Cause: Presumably, piping to the primary side was touching the lower part of the frame, and due to vibration, strain/stress was conducted to the connecting part, damaging sealing.

   Action taken: The area which caused the gas leak was resealed with sealing tape.

Table A2.7 Record of Problems (System AT)

1. In N_2 gas purge of engine unit(PM), purity of N_2 gas measured did not satisfy the value required by the "Handling Manual for Nitrogen Gas Purge System."

   Cause: While particle counter was adjusted with no pressure, N_2 gas particles were measured with the same amount of flow as in actual use.

   Action taken: Measurement procedure established and remeasured. No problem observed.

A3 Symbols and Formulas

A3.1 Symbols

Ion engine-related sybmols and abbreviations used in this report are summarized in Fig. A3.1(electrical). Temperature measurement points in the engine unit and symbols are shown in Fig. A3.2.

A3.2 Formulas

Formulas for some parameters used in evaluating ion engine are given below.

i) Thrust

Provided that ion beam is univalent and there is no diffusion of beam radius and misalignment,

$$F = \sqrt{\frac{2M}{q}}\, J_b \sqrt{V_a}$$ where M: mass flow of ion
q: electric load

ii) Utilization efficiency of propellant

$$\eta_u = \left(\frac{M}{q} J_b\right) / \dot{m}$$ where $\dot{m}$: amount of propellant flow

iii) Efficiency of propeller

$$\eta_e = J_b V_a / P_e$$ where P_e: input power of engine

iv) Specific impulse

$$I_{sp} = \eta_u \sqrt{\frac{2qV_a}{M}} / g$$ where g: gravity acceleration rate

v) Ion production cost

$$D = I_d V_d / J_b$$

Fig. A3.1 Symbols (electrical)

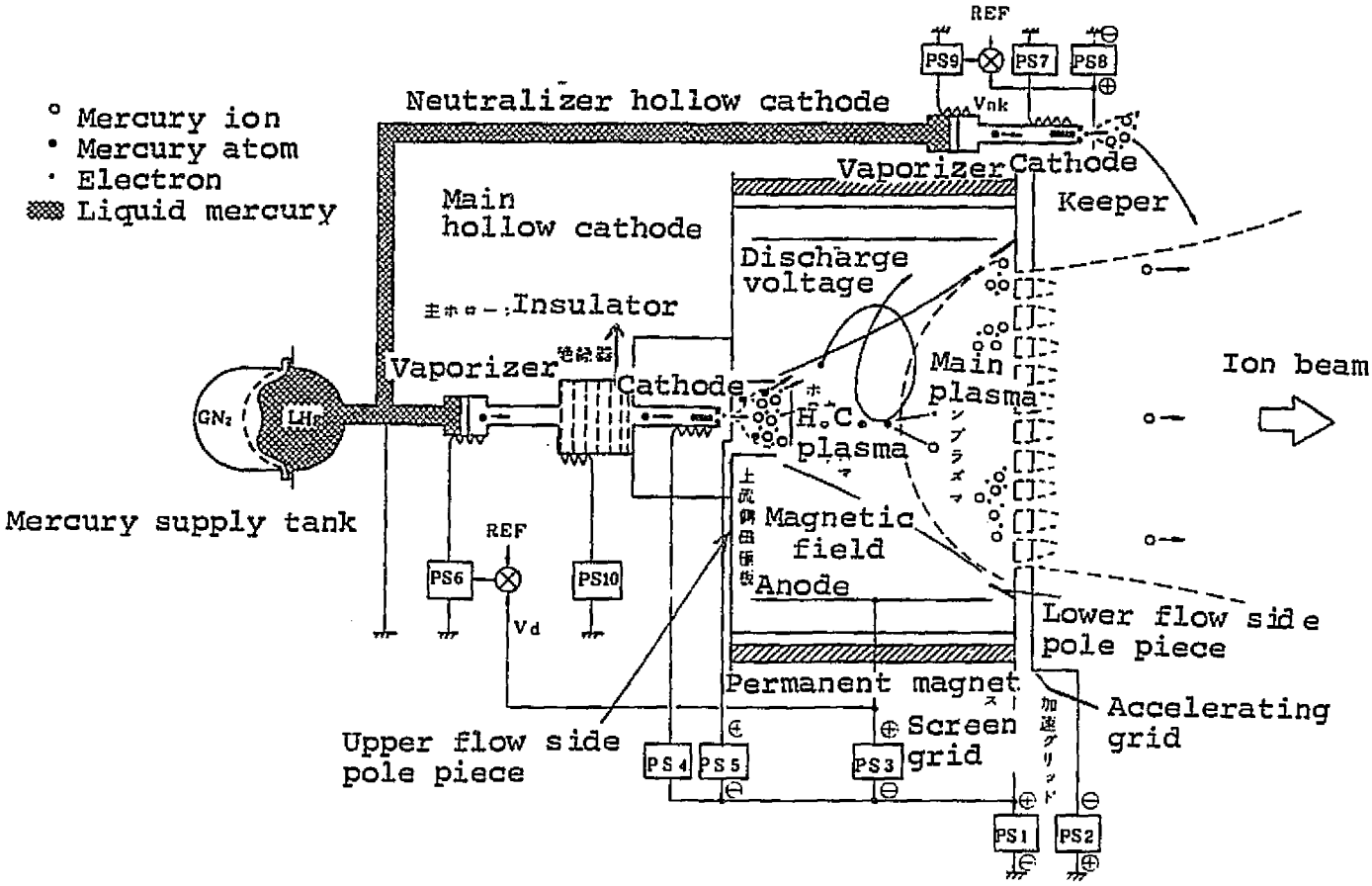

		Voltage	Current
PS1	Screen grid power source	Vn	Jb
	or beam power source	Vb	
PS2	Accelerator grid power source	Va	Ia
PS3	Discharge(anode) power source	Vd	Id
PS4	Main cathode heater power source	Vch	Ich
PS5	Main cathode keeper power source	Vck	Ick
PS6	Main cathode vaporizer power source	Vcv	Icv
	or main vaporizer power source		
PS7	Neutralizer heater power source	Vnh	Inh
PS8	Neutralizer keeper power source	Vnk	Ink
PS9	Neutralizer vaporizer power source	Vnv	Inv
PS10	Insulator heater power source	Vis	Iis

Fig. A3.2 Symbols (temperature)

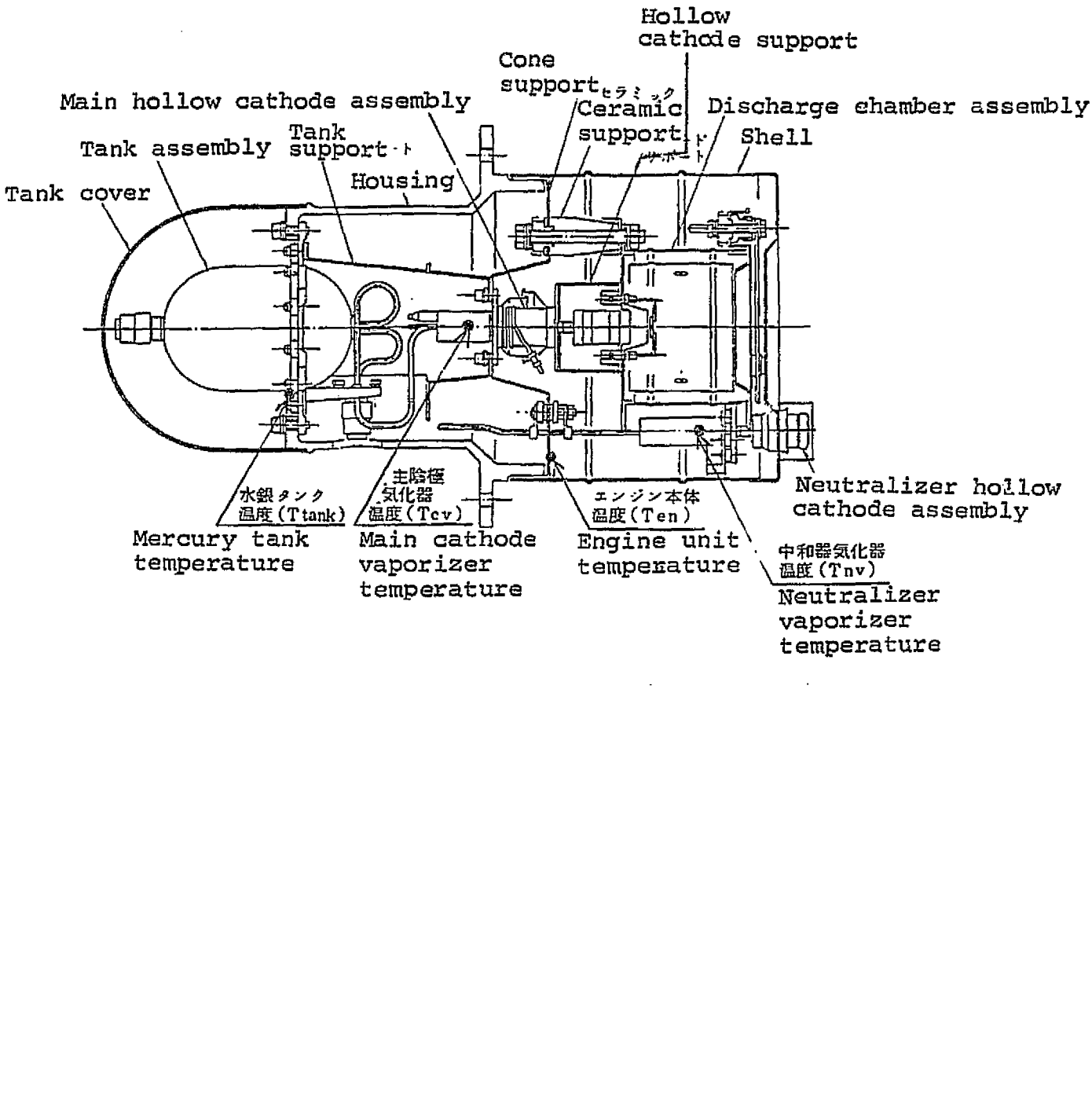

A4 Literature and Reference

A4.1 Specifications

(1) NASDA-ESPC-35 "ETS-III Development Specifications"

(2) NASDA-ESPC-41 "Ion Engine System Development Specifications"

(3) NASDA-ESPC-74 "Ion Engine System/Engineering Test Satellite III Interface Management Specifications"

A4.2 Reference Materials from Satellite Design First Group

(1) DS-114008 "Management Manual for the Ion Engine Development Communication Committee" May 1978

(2) DS-114077 "Handling of Engine Unit in the Ion Engine System (from completion of AT to satellite launching)" Sept. 1981

(3) DS-114098 "Method of Formulating Ion Engine Simulation Program" Jan. 1982

(4) DS-114101 "Development of ETS-III-boarded Ion Engine System" Jan. 1982

(5) DS-114104 "Outline for Formulating Ion Engine System Data Analysis Program(I)" March 1982

(6) DS-114127 "Pre- and Post-transporting Inspections of Ion Engine and Spare Hollow Cathodes" June 1982

(7) DS-114153 "Study of 10mN-class Ion Engine System" Dec. 1982

A4.3 Reports on the Results of Joint Research

(1) NAL/NASDA "Study on Testing and Evaluating Ion Engine System(I): Thermal Vacuum Test of Ion Engine System(1978); Heat Dummy Ion Engine and Thermal Vacuum Test(1979)" Mar. 1981

(2) ETL/NASDA "Study on Testing Evaluating Ion Engine System(II): Analysis of Active Characteristics of Ion Engine System(1978); Control Functions of Power Conditioner(1979)" March 1981

(3) NAL/NASDA "Study on Ground Simulation of Ion Engine System (I): Simulation of Ion Engine Operation(1980); Optical Characteristic Changes of the Satellite Surface by Ion Engine Operation(1981)" Mar. 1982

(4) ETL/NASDA "Study on Ground Simulation of Ion Engine System (II): Reverse Characteristics of Hollow Characteristics and Power Source Coupling(1980); Establishing Operation Commands for Ion Engine Operation" Mar. 1982.

A4.4 Published Materials

Some of the published materials on the development results of ion engine system boarded on ETS-III are listed below. There are also several joint research papers not listed.

(1) Azuma, Nakamura, Kudo, Shimada and Yoshikawa "Electron Bombardment Type Mercury Ion Engine for Boarding on Artificial Satellite" Mitsubishi Electric Tech. Journal, Vol. 54, No. 4, 1980

(2) H. Azuma, Y. Nakamura, S. Kitamura, S. Kaneko, I. Kudo, K. Machida and Y. Toda "Development of Ion Engine" AIAA81-0757, 1981

(3) H. Azuma, Y. Nakamura, S. Kitamura, I. Kudo, K. Machida and Y. Toda "Experimental Plan for Electron Bombardment Ion Thruster on Engineering Test Satellite-Ⅲ" AIAA81-0662, 1981

(4) S. Shimada, K. Yoshikawa, T. Ishii, T. Yamada and H. Azuma "Performance Design of 5 cm Electron Bombardment Mercury Ion Engine" AIAA81-0756, 1981

(5) M. Kubo, T. Sasaki, H. Azuma, Y. Nakamura, I. Kubo "EMI Test Chamber for Ion Thruster" AIAA81-0725, 1981

(6) Ito, Machida, Nakamura, Azuma, Kudo and Toda "Development of Ion Engine System" Academy of Elec. Commun. Research Committee, SANE81-23, 1981

(7) K. Nitta, K. Machida, Y. Nakamura, K. Kushida, H. Koizumi and Y. Kuriyama "The Development of Ion Engine Thruster Thermal Dummy" 13th ISTS, 1982